Alma Mater Studiorum – Università di Bologna
in cotutela con Norwegian University of Science and Technology

DOTTORATO DI RICERCA IN

Ingegneria Civile e Ambientale

Ciclo 32

Settore Concorsuale: 08/A1

Settore Scientifico Disciplinare: ICAR/01

Bedload Monitoring by means of Hydro-Acoustic Techniques

Presentata da: Slaven Conevski

Coordinatore Dottorato

Prof. Luca Vittuari

Supervisore

Prof. Nils Ruther (NTNU)

Supervisore

Prof. Massimo Guerrero (UNIBO)

Esame finale anno 2019

Slaven Conevski

Bedload Monitoring by means of Hydro - Acoustic Techniques

Thesis for the degree of Philosophiae Doctor

Trondheim, January 2020

Norwegian University of Science and Technology
Department of Civil and Environmental Engineering
Hydraulic Engineering

Alma Mater Studiorum, Università di Bologna
Department of Civil, Chemical, Environmental and Materials Engineering

NTNU
Norwegian University of
Science and Technology

ALMA MATER STUDIORUM
UNIVERSITÀ DI BOLOGNA
DEPARTMENT OF CIVIL, CHEMICAL, ENVIRONMENTAL
AND MATERIALS ENGINEERING

Doctoral degree program at both institutions is regulated under the cotutelle agreement between NTNU and UNIBO. The candidate Slaven Conevski has been admitted to PhD programs at NTNU and UNIBO by decision on 6/10/2015 and 01/2/2016, respectively.

Advisor for NTNU: **Prof. Nils Ruther**

Advisor for UNIBO: **Assistant Prof. Massimo Guerrero**

NTNU

Norwegian University of Science and Technology

Doctoral thesis
for the degree of Philosophiae Doctor

Hydraulic Engineering
Department of Civil and Environmental Engineering

© 2020 Slaven Conevski. All rights reserved

ISBN 978-82-326-4448-3 (printed version)
ISBN 978-82-326-4449-0 (electronic version)
ISSN 1503-8181

Doctoral theses at NTNU, 2020:47

Printed by Skipnes Komunikasjon AS

Preface

This thesis is submitted to the Norwegian University of Science and Technology (NTNU) in Trondheim for partial fulfillment of the requirements for the degree of "*Philosophiae Doctor (PhD)*".
This dissertation is a result of a three-years and half PhD programme, which was conducted as a joint degree between the Norwegian University of Science and Technology (NTNU) and the University of Bologna (UNIBO). The research has been supervised by Professor Nils Ruther and Assistant Professor Massimo Guerrero. The PhD position was allocated to 40% at the Department of Civil, Chemical, Environmental and Materials Engineering, UNIBO, and 60% at the Department of Civil and Environmental Engineering, NTNU.
The PhD research program of Slaven Conevski was developed under SediPass project WP1 funded by the Norwegian Research Council and Statkraft.
In accordance with the guidelines of the two departments, this thesis comprises a summary to the research that has resulted in more than five scientific papers.

Acknowledgments

I would like to express my deep gratitude to my supervisors Prof. Nils Ruther and Prof. Massimo Guerrero for guiding me with their valuable and constructive suggestions, motivation and knowledge during the entire work of this research work.
I would like to extend my special gratitude to Prof. Colin Rennie for his collaboration in all our articles, his patience, motivation, and for sharing his immense knowledge of this research matter. My sincere thanks again to Prof. Rennie and Prof. Guerrero for the experimental campaign conducted in the Hydraulc Laboratory at UOttawa, funded by grant of the Erasmus Mundus Novadomus program.
Many thanks to Axel Wintersheid and BfG (German Institute of Hydrology) for the excellent collaboration and the opportunity for conducting ADCP measurements at Oder and Elbe river as part of their regular hydrological campaigns. Beside my advisors I would like to thank the Laboratory technical staff at NTNU and UNIBO: Alberto Boninsegni, Mai Thai, Geir Tesaker, Erik N., as well as to the students Wolfgang Szentkereszty and Sanjoy Saha who worked nights with me in the Laboratory.
I would also like extend my gratitude to the administrative staff at the department at NTNU.
Sincere gratitude to UBERTONE and Marie Burckbuchler for the joint experiments at the NTNU laboratory with their ultrasound velocity profiles.
My special thanks to my parents, my sister Tijana (for graphical design advices), my grandmother, my cousins and my friends for their patience and moral support over the years. It would not be full picture if I do not express my special gratitude to my loving girlfriend Natasha for tolerating me and loving me over the last two years.

Abstract

The bedload distribution through the alluvial streams contributes in shaping of the river morphology. Therefore, bedload transport data are fundamental requirement for proper management of engineering practices in complex river systems. However, measurement series of bedload transport are seldom available and therefore statistically unreliable. The conventional methods can be notoriously hard and labor-intensive, entailing significant stochastic and systematic uncertainties mostly due to the spatio-temporal variability of the bedload as well as the instrument direct disturbance of the riverbed. Thus, the use of non-intrusive surrogate techniques could significantly reduce that uncertainty.

Recently, many studies have demonstrated that the hydro-acoustics instruments are promising technique for bedload measurement. These sensors do not disturb the riverbed and are easy-to-deploy for long and frequent measurements. Some studies have reported strong correlations between the acoustic Doppler current profilers (ADCP) bedload measurements and the conventional bedload samplers. However, most of these methods are site-specific and require detailed calibration.

This study investigates the capability of different ADCPs to measure the bedload velocity and bedload concentration. For those purposes, two laboratory and several field campaigns were conducted. The first series of laboratory experiments were performed in the hydraulic laboratories at UNIBO and UOttawa, focusing on evaluation of the apparent bedload velocity and the scattering processes occurring at the riverbed. The second campaign was conducted at NTNU laboratory aiming to validate the previous results and to further examine the acoustic parameters and signal processing configurations. At the same time the backscattering strength sensitivity towards the bedload concentration was fully examined. Two ADCPs were deployed at the same time on 0.7 m mutual distance (M9 Sontek, 1 MHz and 3 MHz and Stream Pro RDI, 2 MHz). Side and planar looking camera were deployed to measure the bedload velocity, active layer thickness and surface bedload concentration and a bedload trap was installed at the end of the flume to monitor the bedload transport rate. Different bedload transport conditions were reached by

utilizing various sediment materials, (e.g., sand and gravel) and by adjusting the hydraulic conditions. De-spiking and filtering were applied to the raw data, and the temporal average of the apparent bedload velocity was spatially normalized.
The percentage of filtered erroneous velocity data from the ADCP time series demonstrated a strong correlation with the surface concentration of mobile particles. In all experiments the normalized apparent velocities measured by the M9 corresponded well to the bedload velocity of the imagery data, better than those measured by the StreamPro, which appeared to underestimate the bedload velocity by a factor of 2-22. These deviations resulted from the different signal processing configurations, the acoustic geometry, and the immobile sediment bed. The backscattering (BS) strength was de-spiked and corrected by adapting the basic sonar equation for riverbed scattering. For the M9 the BS strength decreased as the bedload concentration increased, independently of the particle velocities and sizes. The BS strength registered by the StreamPro resulted in almost constant values for all transport conditions. Additional tests were performed using ultrasound velocity profilers developed by Ubertone. These results confirmed that the internal pressing and echo profiling resolution are crucial in the determination of the correct bedload velocity.
The field experiments were conducted in two relatively large rivers in Germany (Oder and Elbe River) and in one small river in Albania (Tommorice River). Stationary measurements were performed using four different ADCPs (M9 Sontek, Rio Grande RDI 0.6 MHz and 1.2 MHz, RiverPro RDI 1.2 MHz) working at four different frequencies. The raw apparent bedload velocities were de-spiked and filtered in a stream-wise direction. Then, functional correlations were observed between the magnitudes of the apparent velocities and the bedload transport rates measured by pressure-difference bedload sampler. Each ADCP yielded different results because of the different frequency, backscatter sensitivity and acoustic penetration in the active bedload layer. In addition to the frequency, other acoustic parameters such as the percentage of the filtered data, transducers width, beam-opening and grazing angle, the pulse length, contributed to the different acoustic bedload sampling. More precisely, the lower apparent bedload velocity was obtained when lower acoustic frequency, longer pulse lengths and larger beam focusing were used. The kinematic model was successfully applied for the middle frequencies (1.2 MHz and 1 MHz), which gave the best correspondence to the empirical estimation of the bedload active layer thickness and concentration. The field data helped to understand the influence of the riverbed deformation as well as the acoustic sampling problems.
The future research should focus on a more extensive examination of the internal processing algorithms to eventually clarify the best processing configuration and use of the ADCPs. Therefore, closer cooperation between the researchers and the

manufacturers of the ADCPs is fundamental for better understanding and possible adaptation of the ADCPs to measure even more accurately the bedload velocity and BS strength. A complete model of bedload transport rate based on apparent velocity and BS strength should be fully developed in addition to further testing of the BS strength.

Contents

Preface iii

Acknowledgments v

Abstract vii

Contents xii

List of Tables xiii

List of Figures xvii

List of Symbols xix

List of Publications xxiii

1 Introduction 1

1.1 Sediments in fluvial environment 1

1.2 Bedload (dis)balance and the environment 3

1.3 Bedload Transport Measurements 3

1.4 Motivation and State of Art 7

1.5 Scope of work 8

2 Research Methodologies **11**

2.1 Kinematic transport model and the ADCP outputs 11

2.2 ADCP working principle 12

2.3 Laboratory research methods and techniques 18

2.4 Field Methodology 30

3 Results and Discussions **37**

3.1 Laboratory Results 37

3.2 Field Results 49

4 Conclusions and Future Research **55**

4.1 Final Conclusions 55

4.2 Future work 58

References **61**

Paper *I* **67**

Paper *II* **125**

Paper *III* **179**

Paper IV **189**

Paper V **199**

Paper *VI* **241**

Appendix **251**

List of Tables

2.1 ADCPs basic characteristics and location. Note: The experiment in Ottawa was run using only the 3 MHz with the default RS configuration 13

2.2 Laboratory Hydraulic Parameters. Note that names of the experiments refer to the partition of sand and gravel in the mixture, gravel%15sand = 85%gravel +15%sand 21

2.3 Ubertone transducers properties 27

2.4 Field Characteristics and hydraulic parameters 32

3.1 Average not valid data (ND) observed during the NTNU experimental campaign 42

List of Figures

1.1 Sediment transport modes. 2

1.2 Shileds diagram 3

2.1 Bedload flux 12

2.2 ADCP beam configuration and homogeneity assumption 13

2.3 Riverbed scattering pattern 14

2.4 Acoustic beam geometry for one transducer 15

2.5 Experimental-set up 19

2.6 Theoretical values of the backscattering coefficient K_v), for the sediment material used ion the laboratory tests 22

2.7 Steps of the image velocimetry determination 24

2.8 Active layer estimation using side-looking camera for sand (a) and for gravel (b) 25

2.9 Bedload trap and a load cell 26

2.10 Ubertone set-up scheme 27

2.11 ADCP raw data and the filtered outliers of v_a 29

2.12 Filed Study Locations 31

2.13 Measurement set-up. Boat Scheme 33

2.14 Bedload Sampling in Albania 34

2.15 Bedload Sampling in Germany 34

2.16 Example of vector direction plot at one measurement position of the RDI 0.6 MHz: only water velocity (U, red symbols); the accepted apparent bedload velocity (v_a blue symbols) and discarded apparent bedload velocity (grey-faint symbols). Note that the blue and the faint-grey symbols give the raw apparent velocity measured by the BT mode of the ADCP. The red error represents the mean direction of the water velocity. 35

3.1 *a*) The apparent bedload velocity and the camera data; *b*) Normalized apparent bedload velocity $v_{na} = \frac{v_a}{K}$ and the camera measured velocity. 38

3.2 Apparent bedload velocity measured by different instrument and configuration correlated with the bedload velocity (v_c) estimated by imagery data 39

3.3 Apparent bedload velocity measured by different instrument and configuration correlated with the normalized bedload velocity ($K * v_c$) estimated by imagery data 40

3.4 *a*) The apparent bedload velocity and dimensionless bedload surface concentration (K); *b*) Dimensionless bedload surface concentration (K) and the percentage of the filtered data. Note: the symbols are the same as in Fig. 3.1 41

3.5 *a*) The apparent bedload velocity the camera velocity and the water velocity profile (conditions identical to sandEXP1, U $\sim$ 0.3 m/s); *b*) The apparent bedload velocity the camera velocity and the water velocity profile (conditions identical to sandEXP2, U $\sim$ 0.45 m/s) 43

3.6 An example of shallow sampling due to coarse echo profiling resolution. 44

3.7 BS strength (*Bs*) measured by different instrument and the transport rate (Qs). 45

3.8 The BS strength versus the normalized bed-load thickness (d_t/D_{50}) and the surface concentration (K_{act}). 47

3.9 *a*) The averaged echo amplitudes for five repetitions given for each frequency and grazing angle (90-θ) (conditions identical to sandEXP1, U $\sim$ 0.3 m/s); *b*) The averaged echo amplitudes for five repetitions given for each frequency and grazing angle (90-θ) (conditions identical to sandEXP2, U $\sim$ 0.45 m/s) 48

3.10 The apparent bedload velocity vs the bedload transport rate measured by the bedload sampler: *a*) 0.6 MHz; *b*) 1.2 MHz RioGrande *c*) 3 MHz RS; *d*); 1 MHz IC; *e*) 1 MHz PC; *f*) 3 MHz IC; *g*) 3 MHz PC; *h*) 1.2 MHz RiverPro, Albania 50

3.11 PCA analyses of the ADCP parameters. Some parameters are given in Table 2.1, while *FD*, v_a and z_c are calculated as average values from all point measurments out of all four campaigns; a) explains the importance of the principal components in the analysis and the total captured variance; b) The importance of each variable regarding the PC c) shows how the observations (instruments and configurations) are describing the components and it demonstrates the correlation between the analysed parameters. 52

3.12 The bedload transport rate measured by the bedload sampler (Q_s^m and the ADCP moddeled bedload transport rate (Q_s^{ADCP}) : *a*) 0.6 MHz; *b*) 1.2 MHz RioGrande; *c*) 3 MHz RS; *d*) 1 MHz IC; *e*) 1.2 MHz RiverPro, Albania; *f*) 3 MHz IC; 53

List of Symbols

a	=	mean particle radius (m) ;
A_r	=	variance of the riverbed surface roughness (m^2);
A_f	=	Acoustic footprint scattering surface (m^2);
b	=	beam pattern ;
c	=	speed of sound (m/s);
c_v	=	coefficient of variation ;
$D*$	=	particle dimensionless size;
$D10$	=	particle diameter bigger than 10% (m);
$D50$	=	particle median diameter (m)
$D84$	=	particle diameter larger than 84% (m);
$D90$	=	particle diameter larger than 90% (m);
d_t	=	bedload active layer thickness
D_t	=	transducers diameter
e	=	Eulers number;
E_r	=	beam noise level (dB);
EI	=	BT echo intensity (dB);
f	=	ADCP working frequency (MHz);
f_o	=	particles form factor;
f_d	=	Doppler frequency (Hz);
FD	=	percentage of the discarded velocity samples after the filtering (%);
F_r	=	Froude Number (-);
g	=	gravitational constant (m/s^2);
H	=	water depth in the flume (m);
H^{ADCP}	=	water level meassured by the ADCPs (m)
I_0	=	amplitude of the emitted signal (dB);
I_r	=	amplitude of the returned signal (dB);
I_i	=	image at instance *i*;
K_p	=	instrument coefficient;
K_s	=	surface backscattering coefficient (m/kg$^{0.5}$);

K_v = volume backscattering coefficient (m/kg$^{0.5}$)
k_1 = surface concentration (%);
$1/k_1$ = spatial velocity normalization coefficient;
k_2 = instrument normalization velocity coefficient;
m = pixel position in vertical direction;
M = total number of pixels in vertical direction;
M_{at} = active bedload concentration (kg/m^3);
n = pixel position in horizontal direction;
N = total number of pixels in horizontal direction;
N/A = fraction of bad samples before filtering
ND = total filtered data including the filtered values and zeros ND=FD+N/A
Q = river discharge (m^3/s);
${Q_s}^m$ = physically measured transport rate (kg/m/s)
${Q_s}^A DCP$ = ADCP modeled transport rate (kg/m/s)
R = slant spreading distance from the ADCPs beams (m);
R_e = boundary Reynolds number;
R_{e_p} = Particle Reynolds number;
R_f = predicting coefficient for the settling velocity Dietrich (1982);
s_s = surface backscattering strength (dB);
s_v = volume backscattering strength (dB) ;
U = average-depth water velocity (m/s);
$u*$ = shear(friction) velocity (m/s);
$u*_{cr}$ = critical shear(friction) velocity (m/s);
v_a = apparent velocity (m/s);
v_{bt} = bottom tracking vessel velocity (m/s);
v_{gps} = GPS vessel velocity (m/s);
v_{na} = normalized apparent velocity (m/s) ;
v_s = settling velocity (m/s);
v_p = average particle velocity ;
z_c = *beam focusing*, distance to the inner side of the central lobe (m);
z_s = distance of the side-lobe contaminated region (m);
Z_i = image changes at instance *i*;
α_{at} = attenuation in the active layer (dB);
α_{wc} = attenuation in the water column (dB);
λ = wavelength (mm) ;
π = mathematical constant;
ρ = water density (kg/m^3);
ρ_s = sediment particles density (kg/m^3);
τ = Shear stress (N/m^2);
$\tau*$ = Shields parameter (dimensionless shear stress);

$\tau*_{cr}$ = critical Shields parameter (critical shear stress);
τ_{pl} = pulse time length (s)
θ = acoustic beam incident angle (^{o});
φ = acoustic beam spreading angle (^{o}).

List of Publications

The present thesis is based on four scientific peer-reviewed papers and one conference paper. The thesis context they will be referred with their roman numbers as following:

Paper *I* : Laboratory investigation of the apparent bedload velocity measured by ADCPs under different transport conditions
Slaven Conevski, Massimo Guerrero, Nils Ruther, Colin D. Rennie
Journal of Hydraulic Engineering, 2019

Paper *II* : Acoustic sampling effects on bedload quantification using acoustic Doppler current profilers
Slaven Conevski, Massimo Guerrero, Colin D. Rennie, Nils Ruther
Journal of Hydraulic Research, under review

Paper *III* : Evaluation of an acoustic Doppler technique for bed-load transport measurements in sand-bed Rivers
Slaven Conevski, Massimo Guerrero, Colin D. Rennie, Nils Ruther
RiverFlow, Lyon, 2018

Paper IV : Laboratory monitoring of bedload transport rates using hydro-acoustic techniques (ADCP)
Slaven Conevski, Massimo Guerrero, Colin D. Rennie, Nils Ruther
IAHR, World Congress 2019

Paper V : Towards evaluation of bedload transport characteristics by using velocity and backscatter outputs from ADCPs
Slaven Conevski, Massimo Guerrero, Colin D. Rennie, Nils Ruther
Journal of Hydraulic Research, under review

Paper *VI* : Bedload measurements using ultrasound Velocity profilers (UVP) in controlled laboratory conditions

Slaven Conevski, Massimo Guerrero, Marie Burckbuchler, Nils Ruther
Particles in Europe, Lisbon, 2018

Chapter 1

Introduction

This chapter gives an overview of the main topic in this thesis. It consists of a general information about the fluvial sediments and the techniques typically applied for bedload transport measurements.

1.1 Sediments in fluvial environment

Sediment usually refers to a conglomerate of materials, organic and inorganic, that can be carried out by water, wind, or ice. The sediments in the fluvial environments mostly consist of soil-based mineral matter (e.g., clay, sand, etc.), but sometimes the organic substances can be a significant partition.
Sediment transport can be characterized by its origin, transport mode, or operationally by the collection measurement method. In an aquatic environment, sediment can be either transported as suspended load (in the water column) or bedload (moving at the bottom on the riverbed), depending on where the advection of the particles occurs (Bagnold, 1956; Parker, 2004).

1.1.1 Bedload

The sediments transported in aquatic environment, which involves rolling, sliding and saltating (see, Fig. 1.1) of the particles close to the bed, is called bedload. In addition, Shields (1936) definition, later analytically developed by Bagnold (1956), suggests that a particle will go in suspension if the bed-shear velocity ($u*$) exceeds the, the settling velocity of the particle (v_s), thus the saltation and rolling modes of transport are dominant if $u*/v_s<1$ (see also Shields diagram, Fig. 1.2). The motion consists of successive contacts of the particles with the bed that is strictly limited by the effect of gravity. These particles form a thin layer of mobile

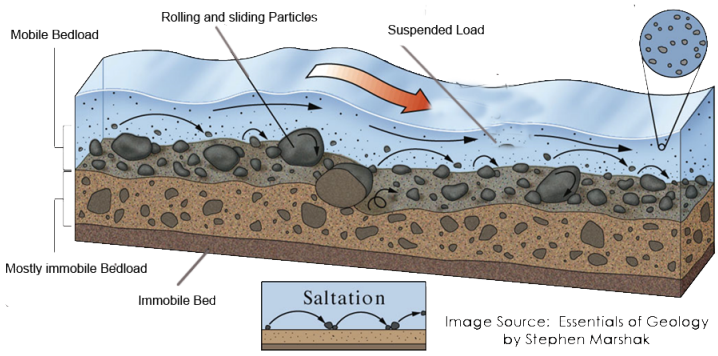

Figure 1.1: Sediment transport modes.

particles, which is defined as the active bedload layer (Einstein, 1950; Bagnold, 1980). The thickness of this layer is typically a few particle diameters (Van Rijn, 1984). The mean height of the active layer can be assumed as the mean saltation height of the particles (Van Rijn, 1984). Please note that the definition of the active layer refers to instantaneously, mobile particles at the riverbed and has nothing to do with erosion and deposition processes throughout the riverbed.

Empirical formulation of bedload transport

The notoriously difficult description of the heterogeneous motion of particles in the fluvial environment was a research goal of many scientists in the previous century. Du Boys initially developed the first theoretical and rational approaches for sediment transport (Hager, 2005). Later, Einstein (1950), Bagnold (1956), and Engelund, Fredsøe (1976) worked on grain scale theoretical analysis of the bed-load. Another group of scientists were focused on the experimental approach based on fitting the data from the laboratory flume or a field data (Fernandez-Luque, Beek, 1976; Bagnold, 1980). Both approaches involve the same dependence on the shear stress ($\tau*$) and the critical shear stress (τ_c*) (Shields, 1936), the characteristics of the particles or the particle Reynold Number (Re_p), and the hydraulic conditions. Depending on the study site, the bedload transport equations can demonstrate a reliable estimation of the bedload transport rate and the bedload velocity, but still, there are large uncertainties between the values yielded from the equations and the observed values.

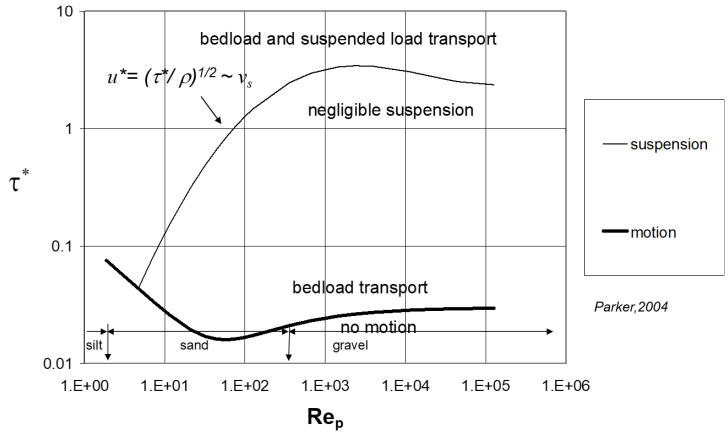

Figure 1.2: Shileds diagram

1.2 Bedload (dis)balance and the environment

The excessive sediment fluxes generated by extreme flows can destabilize river channels. Consequently, the bedload provokes damages to any structures in the flooded area and narrows down the quality of water. Also, the bedload depositions significantly influence the large hydraulic schemes by decreasing the reservoir volume, changing the velocity flow near the inlet structures, disabling normal functioning of the hydraulic structures and sometimes even entering in the turbines and damaging the vanes of a hydro-power plant (HPP).
From a sustainability point of view, trapping of the sediments within the artificial reservoirs can severely impact the eco-systems and the river morphology downstream.
Excessive deposited sediment can smother animals directly and/or motivate them to leave. It can also smother and lower the nutritional quality of fish food and significantly impact the aquatic eco-system.
In that manner the accurate and frequent measurements of the sediment flux are crucial component in any river or reservoir engineering practices.

1.3 Bedload Transport Measurements

To properly sample bed material for interpretation, it is first necessary to establish what constitutes bed material and understand its relation to transported load. No single instrument allows the direct determination of bedload transport rates for the entire range of sediment sizes and concentrations. The bedload transport rate

can be measured directly or indirectly. The direct measurements assume physical catching of the bedlaod material at the riverbed, whereas the indirect measurement methods are based on indicators, parameters that are closely correlated with the sediment concentration, velocity, particles interaction, etc.

1.3.1 Conventional, direct methods

The conventional approach involves physical collection of the mobile bedload sediments, using different types of direct-collecting samplers. The conventional bedload samplers can be grouped into four categories: i.) box or basket, ii.) pan or tray, iii.) pressure-difference, and iv.) slot or pit samplers (Hubbell, 1964).
The most used physical traps are the pressure-difference samplers (such as Helly Smith or BL-84). Pressure-difference samplers are designed to create a pressure drop at the sampler's exit and thus maintain entrance velocities approximately equal to the ambient stream velocity. Sampling efficiencies may be higher with this type of sampler than with others, and the deposition of sediments at the sampler entrance, inherent with basket or tray samplers, is eliminated. Nevertheless, any physical method suffer from systematic (e.g., operation, equipment) and random uncertainties (e.g., environmental conditions, natural variability).

Calibration of the sampling efficiency

The accuracy of the bedload transport measured by use of a mechanical sampler depends on its sampling efficiency (instrumental errors), on the sampling location with respect to the bed-form geometry (spatial variability) and on the near-bed turbulence structure (temporal variability). Most common difficulties and problems during the sampling procedure are: i.) disturbance of the bed when the sampler lands on the riverbed; ii.) gap effect (sampler mouth is not in contact with the bed) iii.) sampling time; iv.) positioning above bedforms; v.) clogging due to fine sediments or organic matter; vi.) mash size; vii.) Loss of material while raising the sampler; (Gaweesh, Van Rijn, 1994; Banhold et al., 2016). This is particularly exacerbated when the bed transport rate is very intensive. It is well known that these samplers mechanically may not catch the material at the actual rate. To overcome the problems of the physical sampler, the sampling efficiencies need to be calibrated and often are dependent on the particle size distribution (PSD) and the mass of the caught bed material.

1.3.2 Surrogate techniques

In light of the often substantial expense, labor-intensive, and insufficient temporal and spatial resolution associated with physical bedload measurements, efforts to

develop new approaches for monitoring bedload have expanded. Development of bedload-surrogate technologies-instruments and methodologies for continuously monitoring bedload transport at dense time and (or) spatial scales without the routine need for collection and analyses of physical bedload samples (except for calibration purposes), has been enabled by advances in computing and sensing capabilities. The bedload-surrogate technologies involve videography, active and passive acoustic sensing, seismic registering mechanisms, etc.

In the last few decades, various videography techniques have been developed to investigate the behavior of the bedload particles, mostly on a small scale and in controlled conditions. Some of them involve particle tracking velocimetry (PTV) techniques where the moving particles can be easily identified and their movement can be analyzed, most (Drake et al., 1988; Lee, Hsu, 1994; Nino et al., 1994; Hu, Hui, 1996; Hergault et al., 2010; Lajeunesse et al., 2015). These technique are usually applied for very weak transports and mostly to examine the incipient motion of the particles. Besides, most of these experiments are applied to a fixed sediment bed with colored particles. The image processing techniques such as optical flow and image differencing have been successfully applied to calculate the mobile bed velocity, the surface concentration of mobile particles and the shape of the particles in the cases of gravel transport (Papanicolaou et al., 1999; Keshavarzy, Ball, 1999; Radice et al., 2006; Blanckaert et al., 2017).

Continuous seismic records near river channels may also be a satisfying technique for monitoring bedload transport in steep channels (Hsu et al., 2011; Gimbert et al., 2014). They have the advantage of being noninvasive as the sensor is located outside of the river, but they are sensitive towards any other processes that produce noise, such as turbulence, massive rain events, road traffic, etc.

The most applied technique in steep streams are the steel plates that register the impact of the gravel particles (Rickenmann, McArdell, 2007; Rickenmann et al., 2012). Successful calibrations were performed over several magnitudes of bedload fluxes (Rickenmann et al., 2012). Nevertheless, the installment of these devices can be expensive and it requires some intensive civil works and stable terrain.

The acoustic techniques that are based on recording the sound backscattered or produced by the bedload particles are an interesting alternative, because of the non-intrusive character and easy field-deployment. These acoustic techniques can be passive and active. Passive methods involve hydrophones that record the acoustic noise of the bedload particle collisions, while the active techniques analyze the effect of the bedload motion on the scattered acoustic signal from the riverbed (Urick, 1983).

The deployment of the hydrophones is easy, but the calibration procedure is challenging because it is hard to isolate the noise generated by the bedload particles from the other ambient noise such as turbulence or an eventual seismic activity

(Geay et al., 2017). In general, the passive methods appear feasible only for small gravel bed streams where hydrophones can be easily deployed, and the noise generated from collision of the particles can be efficiently distinguished .
The active acoustic systems emit acoustic waves at a particular carrying frequency and process the echoes reflected from the riverbed. These acoustic systems can be monostatic, which have a transducer that emits and receives the signal and bistatic when the transmitter and the receivers are reasonably separated. The bistatic sonars are limited to laboratory use of small streams because the distance between the transducer and receiver should be comparable to the distance to the sediment bed. Several studies have demonstrated the capability of these devices (i.e., acoustic Doppler velocity profilers) to measure sediment transport processes, the thickness of the active bedload layer and the water velocities in the near−bed region (Hurther, Thorne, 2011; Blanckaert et al., 2017).

Acoustic Doppler Current Profilers (ADCP) - Application

The acoustic Doppler current profilers (ADCPs) are the most widely used acoustic instruments among the professionals dealing with hydrological measurements. The ADCP transmits an acoustic signal at a known frequency and measures the change in frequency (i.e., the time delay) of the reflected signal from the particles in the water column. The ADCPs are active sonars in which the emitter and the receiver are coincident and the acoustic signal returns to the source. An ADCP is a range-gated monostatic acoustic sensor that employs Doppler shift of backscattered sound to measure water velocity components along multiple beams.
These instruments were originally designed to measure water velocities and discharge, but have also been applied for measurements of suspended sediment fluxes based on backscattered sound intensity (Dinehart, Burau, 2005; Rennie, Church, 2010; Guerrero, Di Federico, 2018). The backscattering echo intensity and the attenuation of the emitted ADCP pulse have also been used to estimate the suspended load and the grain size (Guerrero et al., 2013; Moore et al., 2013).
Measurements of the bedload velocity using the bottom tracking (BT) feature of commercially available ADCPs were initially introduced by Rennie et al. (2002). This technique utilizes the BT bias, defined as the difference between the true GPS boat velocity and the BT velocity ($v_a = v_{gps} - v_{bt}$) delivered by the acoustic pulse backscattered from the river bed. This velocity is denoted as the apparent bedload velocity (v_a). Several studies have reported a significant correlation between the averaged apparent velocity and the bedload transport, attempting to derive a site-specific calibration by correlation with physical samples. The apparent velocity was successfully used for mapping the bedload transport velocity in sand and gravel environments, using some smoothing and interpolating techniques (Rennie, Millar, 2004). Recently, some other site-specific studies (Jamieson, 2008;

Williams et al., 2015; Rennie et al., 2017) have utilized the v_a signal to evaluate morphodynamic processes. An attempt to derive an analytical relation between the real bedload particle velocity and the apparent velocity was reported by Gaeuman, Jacobson (2006). This study also showed that the signal backscattered from the riverbed is unequally weighted by the mobile and immobile particles, considering the acoustic properties of the different particle sizes.
More detailed tests were performed in the St. Anthony Falls Laboratory at University of Minnesota using video cameras, bedload samplers, dune tracking and automatic weigh pans to compare the results with two ADCPs (0.6 MHz and 1.2 MHz) deployed simultaneously (Ramooz, Rennie, 2008; Jamieson, 2008). These studies have shown that the sand data gave better correlation between the apparent bedload velocity and the transport rate measured by all other techniques, whereas the gravel data was more scattered with relatively high standard deviation of the v_a. As expected, the surface bedload concentration obtained from the image processing also showed promising correlations with the apparent bedload velocity measured by the higher frequency ADCP (Jamieson, 2008). In addition, the utilization of the shorter pulses yielded a better correlation with the physically measured transport rate and that lower frequency ADCPs give lower magnitudes of the apparent velocities (Ramooz, Rennie, 2008; Latosinski et al., 2017).

1.4 Motivation and State of Art

The need of easy-to-deploy instruments that can perform continuous and statistically valid bedload measurements is univocal. One possible alternative are the hydro-acoustic techniques or the ADCPs because of their robustness and the possibility to measure few hydraulic variables at the same time, including the bedload transport characteristics.
The previous studies have shown that the ADCPs BT signal is biased towards bedload transport rate, resulting in significant correlations with the physically sampled transport rates. It was also hypothesized that the measured velocity is spatially averaged, but unevenly weighted by the different acoustic properties of the particles. The relation between the bedload true velocity and the apparent velocity was analytically analyzed, but there are no laboratory experimental proofs of the exact correlation. Also, the influence of different instruments or signal processing modulation on the Doppler velocity estimation has not been examined. At the same time most of the studies showed that site-specific calibration is compulsory for bedload transport rate calculations. It is well known that the acoustic signal is well related with the particle size and that the surface scattering has much stronger impact on the total backscattering strength Urick (1983), but no study has examined the details of the scattering processes occurring at the riverbed. Similarly, the backscattering strength from the riverbed has not been examined in details and

no correlation with the bedload transport rate has been reported, yet. In addition, very few studies have correlated the PSD of the riverbed with the acoustic signal (Shields, 2010).
The above-mentioned studies showed that there is a research gap in the application of the hydro-acoustic instruments into bedload transport measurements. Although there is a strong theoretical background and practical evidence of the correlation between the bedload transport characteristics and acoustic signal, there is a lack of experimental study and detailed analysis of the relation between the basic kinematic properties of the bedload and the instrument parameters, as well as between the signal modulation and acoustic data post processing.

1.5 Scope of work

This study aims to test some of the findings and hypothesis defined in the previous studies by performing controlled laboratory filed experiments. The overall goal is to move towards a more comprehensive interpretation of the ADCP signal reflected from a mobile riverbed and fully describe the bedload characteristics through the prism of acoustic theory. The main research objectives of this dissertation are :

- Understanding the apparent bedload velocity by comparison with the true particle velocity.
- Finding laboratory and filed techniques that can be used as comparison in the evaluation of the apparent velocity and the backscattered signal from the bottom.
- Identifying the influence of the carrying frequency and other instrument-specific acoustic characteristics (e.g., scattering pattern, acoustic geometry, signal processing).
- Understanding the backscattered signal from particles with different sizes, including the mobile and immobile partition of the riverbed.
- Evaluating the different scattering processes that occur at the riverbed (i.e., volume and surface scattering).
- Analyzing the backscattering sensitivity of the BT mode towards different PSD and different bedload transport conditions (i.e., various thickness of the bedload active layer and concentration of mobile particles in the bedload).
- Post-processing of the collected ADCP data for bedload quantification.
- Delivering recommendations and guidelines for the application of the ADCPs in different riverine environments for bedload measurements.

- Giving recommendations for correct integration of the apparent bedload velocity, the empirically estimated bedload concentrations and active layer thickness into the kinematic bedload transport model.
- Developing a bedload transport rate model based on a simple kinematics and the ADCP data.
- Developing a methodology for bedload transport rate measurements that is independent of specific site calibrations.

To achieve these goals three series of laboratory experiments and several filed campaigns were performed. In the next chapter 2 the research methodology is explained. The results and discussions are given in chapter 3. The chapter 4 includes the conclusions, recommendations and future research.

Chapter 2

Research Methodologies

This chapter describes the methods and the measurement techniques used in the laboratory and on the field. This chapter incorporates brief overview the experimental set-ups, instrumentation and data post-processing performed during the entire study. More details are given in the papers and the papers will be referred to as given in the list of publications.

2.1 Kinematic transport model and the ADCP outputs

An alternative approach to determine transport rates (Einstein, 1950; Hubbell, 1964) uses information about the virtual velocity of particle movement, dimensions of the active layer of the streambed, and the porosity and density of the bed material. (see, Fig. 2.1). The bedload flux per unit width can be expressed as :

$$q_s = \int_{z_b}^{z_a} v_s c_s dz, \tag{2.1}$$

where z_b is the immobile bed boundary and the z_a is the top of the active layer thickness, v_s is the averaged velocity of the mobile beload (i.e., virtual velocity) and c_s is the bedload concentration. If the integration is simplified, the average quantities can be used as the most common engineering practice. The fundamental equation for the mass rate of transport of bed material, can be obtained if 2.1 is integrated thorough the active layer (z_a to z_b).
The ADCP provides an apparent bedload velocity (v_a), whereas a bedload transport rate often is required. If we assume that (v_a) is an unbiased measure of the actual spatially averaged bedload velocity (e.g., v_s), then the local bedload transport rate per unit width (Q_s^{ADCP}) can be calculated if the depth (nD_50) and the

bedload concentration (c_s) of the active transport layer have to be estimated additionally.

$$Q_s^{ADCP} = \sum n_k D_{50} v_a c_s \rho_s, \tag{2.2}$$

The bedload concentration (c_s) can be estimated empirically by using the equation given by 1984 and the thickness of the active layer can be assumed to be equal as the mean saltation height of the bedload particles (Bagnold, 1956; Fernandez-Luque, Beek, 1976; Van Rijn, 1984; Nino et al., 1994). To apply these empirical equations, the shear stress ($\tau*$) must be known. The shear stress could be estimated by fitting the log-law to the water velocity profiles measured by the ADCPs or to use a semi-empirical approach based on the mean water velocity again obtained from the ADCPs. This is one approach to calculate the total bedload transport rate and its uncertainty come mostly from empirical estimations of the bedload concentration and active layer thickness.
On the other hand, the backscattering strength is sensitive to different PSD of the bed material and high intensity of the bedload transport can attenuate the backscattered signal. These justifications clearly show that the ADCPs can be used to fully estimate the bedload transport rate by knowing only a few information related to the specific field site. This approach should result in reduced uncertainty, because the bedload concentration and active layer can be directly assessed by estimating the attenuation (e.g., change in the BS strength) and the amplitude range of the backscattered acoustic signal.

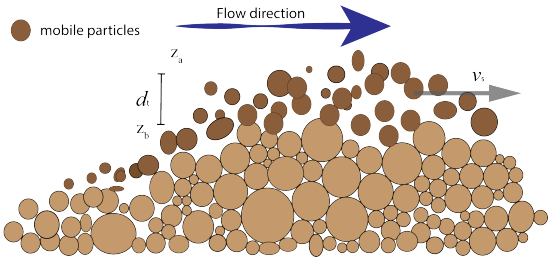

Figure 2.1: Bedload flux

2.2 ADCP working principle

Six different ADCPs were used in this study, depending on the availability at the specific place. Four of the ADCPs are produced by the Teledyne Marine RDI and one by Xylem Sontek. Table 2.1 gives an overview of the instruments, the location where they were deployed, and some of the acoustic characteristics of each ADCP.

Table 2.1: ADCPs basic characteristics and location.
Note: The experiment in Ottawa was run using only the 3 MHz with the default RS configuration

ADCP	f (MHz)	λ (mm)	D_t (cm)	θ °	φ °	*Config*	*Laboratory*	*Field*
Sontek M9	1.00	1.46	4.30	25	2.00	PC,IC,RS	UOttawa, NTNU	Germany
Sontek M9	3.00	0.49	2.70	25	1.06	PC,IC,RS	UOttawa, NTNU	Germany
Sontek M9	0.50	2.91	4.50	90	3.82	PC,IC,RS	UOttawa, NTNU	Germany
RDI StreamPro	2.00	0.73	1.60	20	2.68	BB	UniBo, NTNU	/
RDI Rio Grande 600	0.60	2.43	8.95	20	3.97	BB	/	Germany
RDI Rio Grande 1200	1.20	1.21	6.99	20	1.83	BB	/	Germany
RDI RiverPro	1.20	1.21	6.99	20	1.83	BB	/	Albania

ADCPs are configured as an assembly of four transducers spaced at 90° azimuth intervals (i.e., Janus configuration). The Sontek M9 has two pairs of transducers working at two different frequencies and one vertical in the middle (see, Table 2.1) These transducers form acoustic beams angle of incidence, θ, 20-30° (see Table 2.1), that permit measurements of three velocity components (v_x, v_y, v_z, note that they can be given in earth coordinates v_N and v_E) under the assumption that velocity is homogeneous in the plane defined by equal ranging distances from each of the transducers (see, Fig. 2.2). The assumption of homogeneity in all four beams restrict the bedload measurements if the bedload transport is highly heterogeneous or the riverbed deformed.

This study focuses on the bottom tracking (BT) mode of ADCPs, which is a separ-

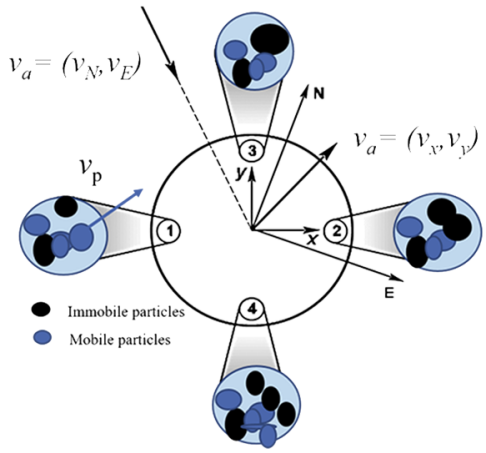

Figure 2.2: ADCP beam configuration and homogeneity assumption

ate signal, used for detection of the riverbed and the vessel velocity, v_{bt}. Compared with water profiling, the BT signal involves emitting longer acoustic pulses (contain more energy) to identify the riverbed, but with the same carrying frequency. For stationary deployment, the BT signal is biased by the riverbed mobility, therefore it can be hypothesized that the apparent bedload velocity is equal to the BT velocity: $v_a = v_{BT}$.

Acoustic current measuring devices operate on the principle that a pulse of sound energy (commonly referred to as a ping) transmitted thorough the water will be scattered/reflected by particles in the water or at the very bottom of the river. The pulses scattered from a particle moving forward generate a drop down in the emitted frequency. This change of the frequency in the echoes is called Doppler shift and it is used to determine the velocity given by the ADCPs. To apply the Doppler shift velocity calculation the pulse coming from the same ranged distance (the riverbed in this case) have to identified, by correlating the returned sound intensities (i.e., echo, EI). This entails spectral analysis, complex covariance or autocorrelation methods that correlates these pulses.

The redistribution of the echo from the BT pulse is quite complex because of variable intensity across the insonified beam width and the bed heterogeneity; therefore the intensity threshold for the bottom cannot be easily detected, especially during moving bed conditions. The pulse passes through the active layer or it is reflected from the surface layer of the bed load.

In underwater acoustics, the bottom scattering can be categorized in two types:

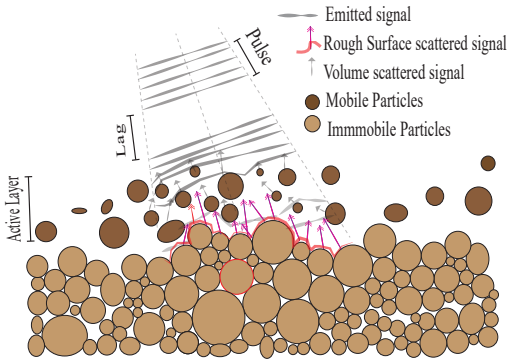

Figure 2.3: Riverbed scattering pattern

surface scattering (S_s) and *volume scattering* S_v, each involving its own mechanism of reflecting the ultrasound wave (Jackson, Richardson, 2007). Accordingly, it can be assumed that the mobile volume of the bed, or the active layer could be associated with volume scattering, while the immobile or potentially mobile with rough surface scattering (Fig. 2.3).

2.2.1 Acoustic Geometry and scattering pattern

The sampling area depends on the transducers width (D_t), the opening angle (φ), the grazing angle (90 - θ) and the distance to the bottom (R), given in Table 2.1 for each ADCP. If the non-linearity is simplified and we consider a rectangular uniform pulse, the sampling areas would be quasi-ellipses centered at a horizontal distance R tan(90 - θ)+ $D_t/2$. The total sampling volume is actually the sum of the four independent volumes located at the impingement points of the beams. To determine the height of sampling above the bed it is assumed that the receiving window occurs only from a reflection that includes the leading and the trailing edge of the pulse (Rennie et al., 2017).

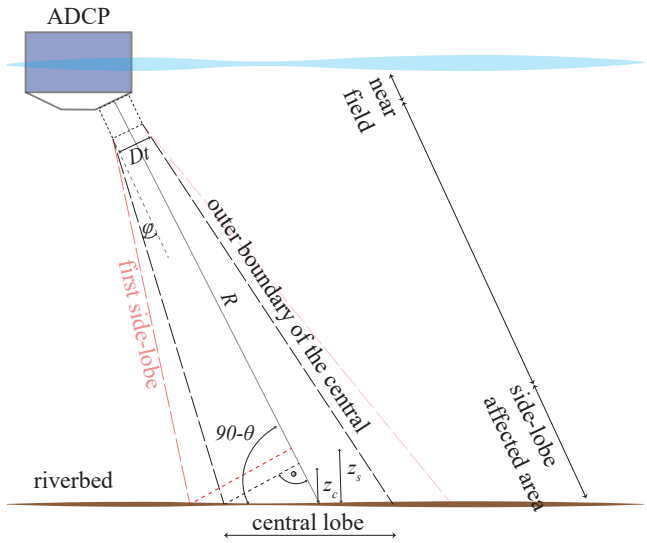

Figure 2.4: Acoustic beam geometry for one transducer

At larger angles than φ small magnitudes of sound intensity are still observed, denoted as side-lobe intensity. The first side-lobe opening angle (i.e., ω, Fig.2.4) defines the so-called side-lobe contaminated area that extends to z_s distance perpendicular of the bed (see, Fig. 2.4). In addition, z_c is the distance from the riverbed to a line perpendicular to the inner side of the central lobe. Note that this is the first side lobe angle, but it is also common to find side-lobes on 15° and even 40° from the main lobe and these can be the dominant source of error. Besides, the ADCPs cannot measure the region near the transducers (near field, Fig. 2.4) due to the ringing effect (RDInstruments, 2011). These regions are denoted as blanking distances, and the water velocity data from these areas is automatically discarded in the final data delivered by the ADCP. By knowing the fact that the observed

D50 in these campaigns is between 0.5-1.5 mm, Fig. 2.4 bears out that the bed-load measurements are always into the side-lobe and central-lobe contaminated area

2.2.2 Signal Processing

The default signal-processing configuration for the newest ADCPs, both RDI and Sontek, usually deploy the Broadband (BB) technology. The standard configuration (RS) by Sontek involves a feature denoted as SmartHD Pulse that changes the processing according to the hydraulic conditions based on some internal parameters. Therefore, besides the BB technology, the M9 can automatically switch to an incoherent (IC) Doppler sonar and pulse-to-pulse coherent (PC) Doppler sonar. A collaboration with Xylem Sontek enabled the M9 to work with all nine beams at the same time and to run all three signal processing configurations separately (IC, PC, RS, Table 2.1). The data from all these configurations was collected for each repetition using the Sontek non-commercial software ADPviewer.
The IC configuration (narrow-band incoherent signal processing) estimates the Doppler shift from the echoes of single pulse ping. On the other hand, the PC configurations transmit a series of short pulses and the phase changes are observed at each cell distance.
Broadband (BB) ADCP transmits two or more sets pulse sequence; each pulse sequence consists of many encoded pulses. The coded pulses are trains of smaller, codded sub-pulses that form long pulse, but Doppler shift measurements remain the same as the basic BB systems because it is calculated between the pseudo-coded elements of the pulse. The longer pulses increase the echo intensity and decrease the decorrelation of the echoes (Brumley et al., 1991).

2.2.3 The BT sonar equation

The basic sonar equation presented in most of the books about ultrasound Urick (1983); Medwin, Clay (1998) can be adapted for the ADCP BT signal emitted from the river bed, by incorporating the specific characteristics of the ADCP transducers and acoustic properties of a mobile riverbed (e.g., including both surface and volume scattering). The active layer of the bedload, including mostly the saltating particles Drake et al. (1988); Nino et al. (1994); Lajeunesse et al. (2010), can be assumed as the main contributor for the volume scattering. In the same manner, the scattering from the immobile particles below the active layer, that are forming the bed surface can determine the surface scattering. If it is assumed that the registered BT signal cannot penetrate within the pores of the immobile sediment bed, the basic sonar equation, adapted for the riverbed could be expressed through

the intensity of the reflected signal as follows:

$$I_r = \frac{I_0 K_p (s_v + s_s)}{R^4} R^2 \frac{c\tau_{pl}}{2} b(\theta, \varphi) e^{-4R(\alpha_{wc}+\alpha_{at})}, \tag{2.3}$$

where I_r is the received signal intensity (the recived echo intensity), I_0 is the transmitted intensity, K_p is an instrument constant, s_v and s_s are volume and surface backscattering (BS) strengths. The τ_{pl} is the pulse duration, c is the speed of sound, R is the slant range to the bottom, $b(\theta,\varphi)$ is a beam coefficient that includes the grazing angle 90- θ , the beam spreading angle (φ) and the beam width. The term $R^2 \frac{c\tau_{pl}}{2} b(\theta, \varphi)$ represents the insonified volume (Urick, 1983; Medwin, Clay, 1998) and it can be precisely calculated (Rennie et al., 2002; Rennie, Millar, 2004). In the above relation, α_{at} is the attenuation coefficient that depends on the acoustic frequency and the particle size distribution and concentration (M_{at}) of the mobile bedload. Additionally, α_{wc} is the attenuation in the water column, usually related to the water viscosity and suspended sediment attenuation. The latter depends on the particle size and concentration in the water column, but in this case it is negligible. The range $4R$ is the squared two-way path of the attenuated sound pressure. The surface scattering will be dependent only on the sampled area, assuming that no energy is transmitted to the solid medium below (Urick, 1983).
The volume scattering coefficient K_v depends on the frequency and the particle size distribution and it can be expressed as:

$$\langle K_v \rangle = \frac{3\langle f_o \rangle^2}{16\pi\rho_s \left\langle \frac{D_{num}}{2} \right\rangle}, \tag{2.4}$$

where f_o is the mean normalized form factor (Thorne, Meral, 2008; Moate, Thorne, 2009), $\frac{D_{num}}{2}$ is the mean radius of the particles taken from the number based PSD, ρ_s is the particle density, taken to be the value for quartz 2.65 cm^3/g. The form factor depends on the shape and size of the particles and the acoustic wavelength (Medwin, Clay, 1998; Thorne, Meral, 2008). The angular brackets denote the mean expected value of the variables. The scattering coefficients calculated for the specific sediment size and specific frequency characterize the scattering domain of the particles moving in the active bedload layer. The scattering domains are: i) Rayleigh for particles smaller than the wavelength ($D_{num} << \lambda$); ii) Mie for particles in the range of the wavelength($D_{num} \sim \lambda$) and iii) Geometric for particles larger than the wavelength ($D_{num} >> \lambda$) emitted by the ADCPs.

2.3 Laboratory research methods and techniques

The experiments were carried out in three different hydraulic laboratories with very similar experimental set-up, but a rather different PSD and bedload transport conditions. The first series of experiments were performed at the University of Ottawa (UOttawa), second at University of Bologna (UNIBO) and finally the last round at the Norwegian University of Science and Technology(NTNU). The experiments conducted at UOttawa and UNIBO are presented in Paper *I*, whereas the experiments performed at NTNU are given in *Paper IV*, *Paper V* and Paper *VI*.

2.3.1 Experimental set-up

The experimental set-up was very similar for all three laboratory campaigns but the instrumentation was limited according to the availability. The basic instrumentation involved high-speed camera with planar view (C1 on Fig. 2.5) and an ADCP (e.g., the first two campaigns UNIBO - A1 and UOttawa - A2 sections in Fig. 2.5). The last laboratory campaign at NTNU included a bedload transport measurements). The ADCPs were fixed in all experimental campaigns and the position of each beam was not changed during the experiments.
The water levels varied between 0.26 m - 0.47 m. depending on the water velocity required to entrain and move the bedload particles (see Table 2.2). The slope at UNIBO and UOttawa was 0%, whereas the tilting flume at NTNU permitted slopes between 0.1% for the sand experiments and 0.8% for the gravel experiments. The dischrages varied between 80-360 l/s and were kept constant during each repetition of an experiment. Different bedload transport conditions were reached by changing the the water velocity at NTNU and UNIBO (e.g., the EXP1 refers to the weakest transport, EXP3 for the most intensive transport conditions), where as at UOttawa different mixtures of sand and gravel were prepared. Table 2.2 gives more details about the other hydraulic parameters. Five repetitions of each experiment type were conducted, in total 65 repetitions were done in all three laboratories.

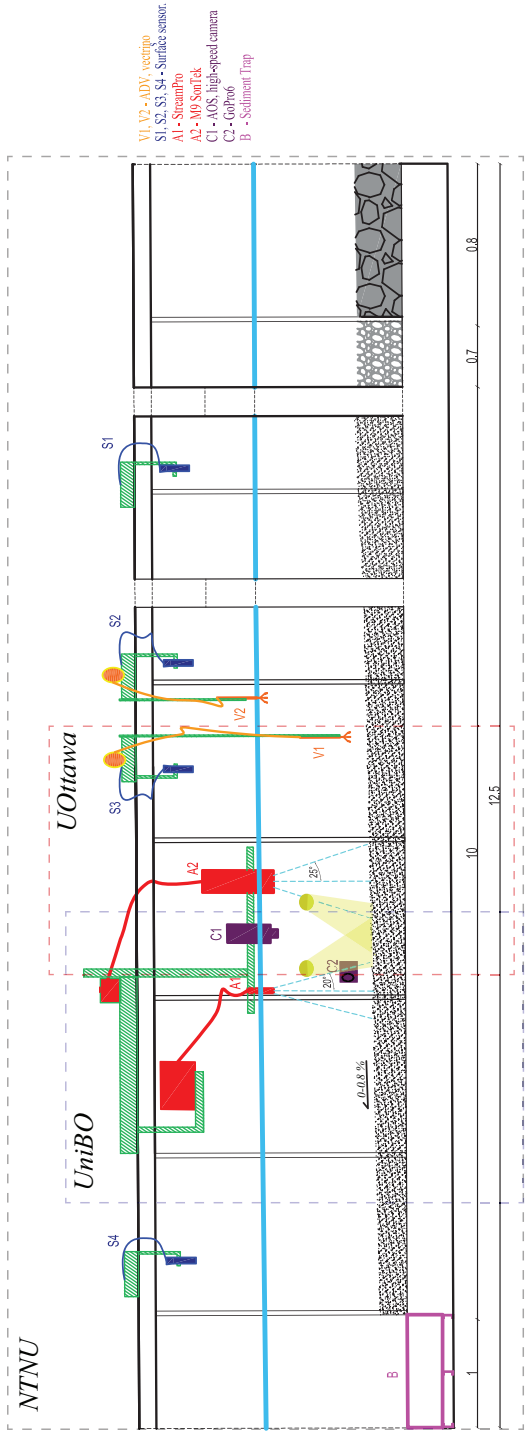

Figure 2.5: Experimental-set up

2.3.2 Hydraulic parameters - Measurement and Calculation

Water depth measurements

The distance from the ADCP to the mobile sediment bed was continuously registered by the ADCPs and the water depths were calculated by adding the submerged distance of the ADCP, which was measured during each repetition. In the NTNU measurement campaign, acoustic surface sensors (see, S1, S2, S3, S4 on Fig. 2.5) registered the surface levels at 50Hz and contributed for even more accurate estimation of the water depths.

Water velocity

The water velocity was measured by the ADCPs, but due to blank zones (see section, 2.2) only several cells in the middle of the profile were available. Due to the lack of instrumentation and attempting to avoid disturbance of the flow and the sediment motion, a convenient solution to calculate the mean velocity was applying the continuum equation $U = \frac{Q}{A}$, where Q is the discharge continuously measured by the flow-meters, $A = BH$ is the cross-section surface assuming rectangular cross section with known width (B) and water level calculated as given in the previous paragraph (only at UNIBO and UOttawa).
At NTNU, two Vectrino ADVs were mounted, one on the surface (see V2, 2.5) and another close to the sediment bed (see V1, 2.5, the measurement point was 1-4 cm above the mobile bed). These two point velocity measurements and the velocity profiles from the ADCPs were used to calculate the mean velocity of the flow, assuming that the velocity flow is the same through the entire width of the flume.

The shear velocity

The shear velocity was calcualted by implementing a semi-empirical approach for rough flows. The formula was suggested initially by Keulegan (1938) and later analytically developed by Van Rijn (1984).

$$u* = \frac{U}{5.75\log_{10}(\frac{12H}{3D_{90}})}, \tag{2.5}$$

where U is the mean water velocity, H is the water levels measured, both calculated as given in the previous paragraphs. D_{90} is the diameter larger than 90% of the particles in the sediment bed. Note that due to he blank zone and relatively large cells of the ADCP water velocity profile, fitting the log-law in the region close to the sediment bed was not possible.

Other parameters that describe the flow and bedload transport conditions

The critical shear velocity (i.e., the shear stress) and the particle Reynolds number, R_{e_p}, are parameters typically used to describe initiation of the particle motion and the conditions of the sediment transport (see, Fig. 1.1). On the other hand, the Reynolds number R_e and the Froude number (*Fr*) are used to describe the flow conditions and the turbulence. The critical shear velocity is calculated using the critical mobility parameter ($\tau*_{cr}$, Shields parameter), defined by Shields and analytically presented by VanRijn (Shields, 1936; Van Rijn, 1984). It should be noted that the formulas for $u*_{cr}$ and v_s do not contain correction for the shape of the particles. The parameters given in Table 2.2, show that there was a bedload motion in all experiments ($u*>u*_{cr}$), but no suspension was initiated (see, Fig. 1.2). The *Fr* and *Re* demonstrate that the flow was turbulent and sub-critical in all experiments.

Table 2.2: Laboratory Hydraulic Parameters.
Note that names of the experiments refer to the partition of sand and gravel in the mixture, gravel%15sand = 85%gravel +15%sand

	EXP	S	U	$u*$	$u*_{cr}$	Fr	Re	H	D_{90}	D_{50}	D_{num}	Re_p
		%	m/s	m/s	m/s			m	mm	mm	mm	
NTNU	sandEXP1	0.100	0.302	0.015	0.015	0.149	10355.3	0.420	0.56	0.39	0.13	25
	sandEXP2	0.100	0.432	0.022	0.015	0.213	14813.2	0.420	0.56	0.39	0.13	25
	sandEXP3	0.100	0.571	0.028	0.015	0.281	19549.7	0.420	0.56	0.39	0.13	25
	sandOVER	0.100	0.478	0.020	0.015	0.228	17550.9	0.450	0.56	0.39	0.13	25
	gavelEXP1	0.800	1.197	0.091	0.082	0.576	42939.6	0.440	10.45	7.55	5.45	2019
	gavelEXP2	0.800	1.321	0.101	0.082	0.636	47395.2	0.440	10.45	7.55	5.45	2019
	gavelEXP3	0.800	1.424	0.107	0.082	0.670	53421.6	0.460	10.45	7.55	5.45	2019
UOttawa	gravel	0.000	0.783	0.059	0.054	0.231	22040.4	0.345	6.00	4.00	3.75	767
	gravel%15sand	0.000	0.827	0.056	0.050	0.258	22040.4	0.327	5.60	3.50	1.13	641
	gravel%25sand	0.000	0.819	0.054	0.048	0.253	22040.4	0.330	5.40	3.30	1.02	574
	gravel%50sand	0.000	0.831	0.049	0.032	0.260	22040.4	0.325	5.00	1.80	0.93	232
	sand	0.000	0.872	0.046	0.023	0.287	22040.4	0.310	1.50	1.10	0.85	111
	sand15%gravel	0.000	0.910	0.046	0.028	0.312	22040.4	0.297	2.40	1.30	0.90	159
UniBo	EXP1sand	0.000	0.407	0.023	0.021	0.115	11960.6	0.360	1.40	1.00	0.82	97
	EXP2sand	0.000	0.473	0.027	0.021	0.156	11960.6	0.310	1.40	1.00	0.82	97
	EXP3sand	0.000	0.564	0.029	0.021	0.221	11960.6	0.260	1.40	1.00	0.82	97

2.3.3 Sediment materials and the acoustic properties

Different sediment materials were used in all Laboratory campaigns. The PSD of the sediment material was poorly distributed with D_{50} that ranged from 0.39 mm to 7.55 mm. At UOttawa, the different bedload transport conditions were reached by preparing six sediment mixtures by different portioning of sand (D_{50} = 1 mm) and

gravel (D_{50} = 4 mm). Fig. 2.6 presents the theoretical mono-granular scattering coefficient (K_v, see eq. 2.4) calculated for all used frequencies (both on field and laboratory) are shown in Table 2.2. Note that in acoustic theory, the mean particle diameter (D_{num}) is derived from the number PSD (Urick, 1983). The D_{num} in the experiments was ranging from 0.113 to 5.5 mm, which permitted examination of K_v for both Rayleigh and geometrical scattering regime for all the frequencies. Moreover, K_v for each (D_{num}) was calculated for the frequency which was used t the related experiment (e.g., for D_{num}= 113 μm, *Kv* was calculated for 0.5MHz, 1 MHz, 2MHz and 3MHz, faint gray symbols in Fig. 2.6).
The left sloped lines of the mono-granular scattering coefficient, K_v, represent the Rayleigh scattering regime, which is characterized with significant change of the scattering for sa rather small change in the particle diameter. The *Kv* calculated for the medium-fine sand belongs to the Rayleigh scattering regime for all frequencies (see gray symbols, Fig. 2.6). On the contrary the *Kv* calculated for the rest of the sediments is in the transitional or the geometrical scattering regime (right side of Fig. 2.6), which is characterized with a constant scattering properties.

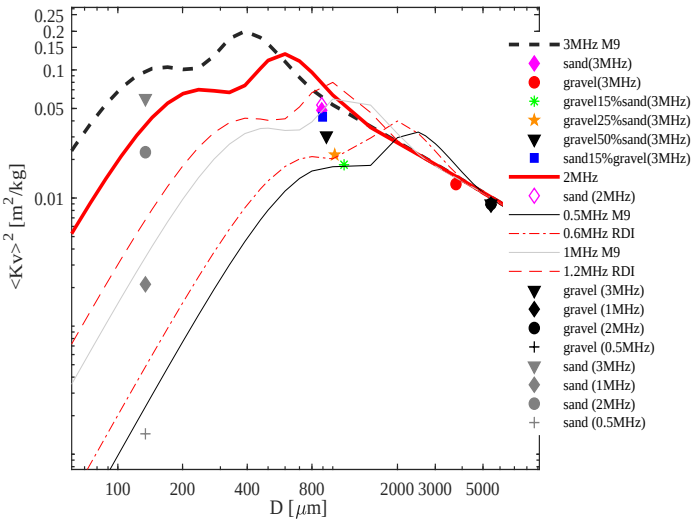

Figure 2.6: Theoretical values of the backscattering coefficient K_v), for the sediment material used ion the laboratory tests

2.3.4 Videography

The primary purpose of the imagery data was to calculate the average surface velocity (v_c) of the particles and the average surface concentration of the mobile particles (K or K_{act}). These variables were compared and analyzed together with the ADCP data. IOI FLARE-2M360MCL (2200 x 1800 pixels, 70fps) and AOS

U1000 (1980 x 1264 pixels, 139 fps) high-speed cameras were used at UOttawa and NTNU, whereas at UnNiBO and for the side-look camera at NTNU an action camera GoPro Hero Black (4k, 30-60 fps) was used. The high - speed cameras did not have any distortion, but the GoPro typically has the fish-eye or barrel effect on its lenses,thus require undistortion of the images. The undistortion was performed on images taken underwater, using the Matlab camera calibration toolbox and checkerboard. Note the angle of the field of view due to the underwater refraction decreases (e.g., for GoPro from 150° to 95°) due to the change of the angle of refraction, which also decreases the distortion. The conversion from pixels to meters involved taking checkerboard pictures at the recording area before and after each repetition.

Image pre-processing

The water impurities and not perfectly distributed light conditions introdued uncertanity in the imagery data, which had to be minimized by depolying image pre-processing algorithms. The image pre-processing was done in Matlab and involved application of light enhancement algorithms (e.g., CLAHE, Zuiderveld (1994)), deblurring filters and high-pass unsharp mask filtering (see, Fig. 2.7).

Image change detection

The pre-processing procedure was followed by a technique called two-frame change detection, or just image change detection. These algorithms assume detection of "meaningful" changes occurring in a scene by the processing of images captured at different time instants. The final outputs are shapes of the objects that appeared, moved or changed in the considered time instant. Moreover, the specific algorithm that was applied in our case is called background subtraction with a 2-frame background update. The image changes denoted as $Z_{i_{m,n}}$ (Fig. 2.7) are subtracted between the sequential frames I_{i-1} and I_i, where (m, n) is the pixel indexing.
The detected changes using background subtraction methods typically suffer from false foreground or background pixels in addition to the noise. Therefore median, Gaussian and local standard deviation filters are applied to eliminate these errors. These filters successfully eliminated the pixels that have lower intensities of the real particles and are usually the false foreground pixels, changes detected because of the water impurities that disturbed the camera view. In the experiments with larger particles, morphological image operations (image opening, closing, and fill-flood operations) were applied to recover the original shape of the particle. In the NTNU gravel experiments, local threshold binarization was applied to identify the single particles. The scripts and functions were developed in Matlab, all the references should be found the description of the Matlab Image processing toolbox (https://se.mathworks.com/products/image.html).

Image velocimetry

To calculate the displacements, cross-correlation algorithms (CC) were applied between the sequences of the image subtractions, similarly to any PIV methodology. Before, the original imaged were divided into smaller regions of interest (ROI), and then the CC was applied between the corresponding ROIs. In the experiments with abundant particle movements and bed forms development, this technique calculates not the displacement of the single particles, but the displacement of the particle fluxes. However, the weak transport experiments permitted full identification of the particles and their displacements. The final camera velocities (v_c) were calculated using the corresponding fps and the conversion factor from from pixels to meters.

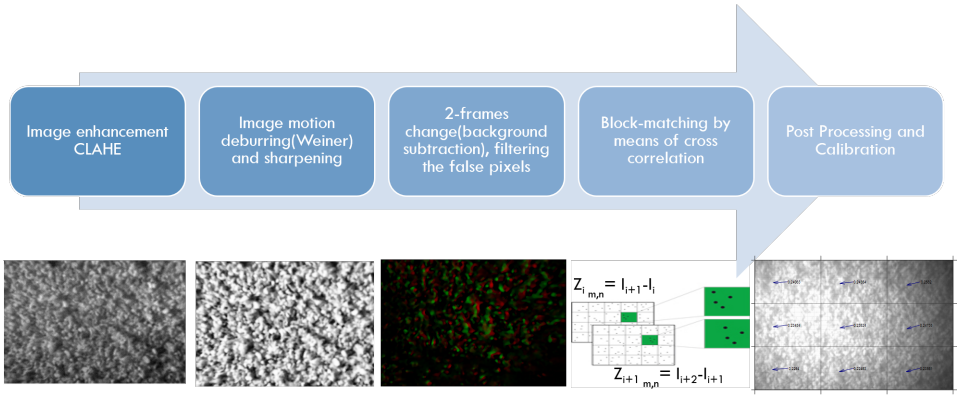

Figure 2.7: Steps of the image velocimetry determination

Side-view videography

The side-looking camera was used only in the NTNU experimental campaign and only to approximatively to evaluate the active layer thickness. The active layer thickness of the bedload can be reasonably estimated as the mean height of the saltation of the mobile particles. (Van Rijn, 1984). Thus, the saltation height of the particles observed by a camera mounted next to side glass wall aiming directly above the sediment bed (see, 2.3).

For the sand experiment, the same image change detection algorithm and image pre-processing was performed, but only in few cases where the dune was passing right on the glass wall of the flume (see, Fig. 2.8). After the detection of the particles, the centroid of each particle was calculated and its perpendicular distance to the bedform boundary calculated. The bedform boundary was defined us-

ing image segmentation algorithms and local binary thresholding, and then pixel coordinates were assigned to the line. The calibration was performed using two checkerboard planes: one right next to the glass wall and another 2 cm towards the other flume wall but on the same height. The final estimation of the height included the uncertainty due to the z-coordinate.
In the gravel experiments, the particles were identified through the entire width of the flume again using the image change detection algorithms. However, this time the immobile boundary was chosen arbitrary, and the distance from the centroid to the immobile bed was estimated semi-manually by running and stopping the video, simultaneously overlaying the results of the image change algorithm (see, Fig. 2.8). The calibration was performed relative to the particle size diameter assuming that is known appriori.
The final results are given as N times the median diameter D_{50}.

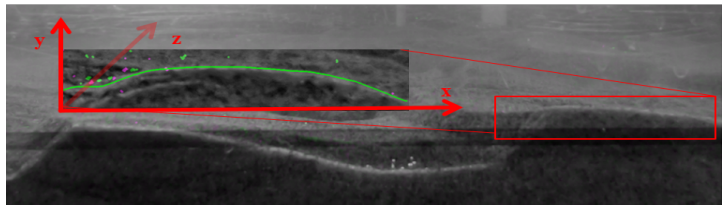

(a)

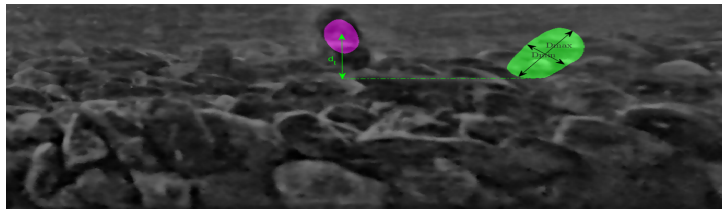

(b)

Figure 2.8: Active layer estimation using side-looking camera for sand (a) and for gravel (b)

2.3.5 Other Techniques

Bedload Trap

The bedload transport rate was measured only during the experiments run at NTNU. The bedload trap is in-house made box that lays on six load cells, at the end of the sediment bed under the level of the flume, enabling free fall of the sediments during the experiment. (Fig 2.9). Load cells are highly accurate devices that are used to measure weight or force in compression, tension, bending or shear. They were used to register the changes in the weight of the box every 1/50s.

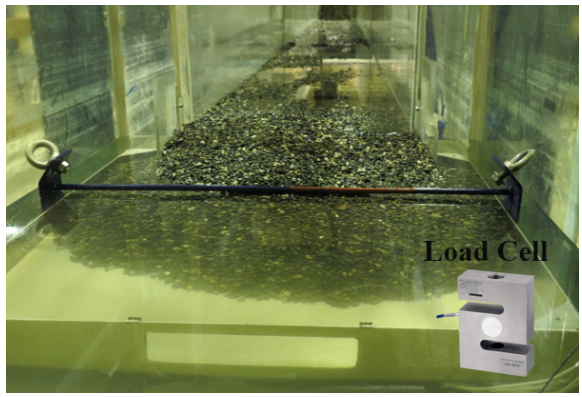

Figure 2.9: Bedload trap and a load cell

The zero values were re-calibrated at the beginning of each test which permitted to eliminate the influence of water dynamic pressure assuming that it is constant during the test. The results were converted from N/s to g/s, using the submerged weight of the sediments.

Experiment with single-beam ultrasound velocity profilers - The Ubertone experiment

To eliminate the uncertainty related to some internal processing parameters, the pulse length and the grazing angle of the ADCPs, several tests of the sand-bed experiment (i.e., sandEXP) at NTNU were run with mono-static transducers and the UB-Lab profiler manufactured by Ubertone. It is an ultrasonic velocity profiler (UVP), designed to measure flow velocities in the direction of the acoustic beam, based on the Doppler effect.
The experiment set-up was the same as the measurement campaign at NTNU, and five separate repetitions were performed only for two conditions of the sand experiment (sandEXP1, sandEXP2, see Table 2.2). Six transducers were working simultaneously at three different frequencies similar to the ADCPs (3 MHz, 1.5 MHz, and 0.5 MHz). Three transducers were declined to form the bottom for 25°

and other three were vertically mounted on the same position as the ADCPs (see, Table 2.3 and Fig. 2.10).

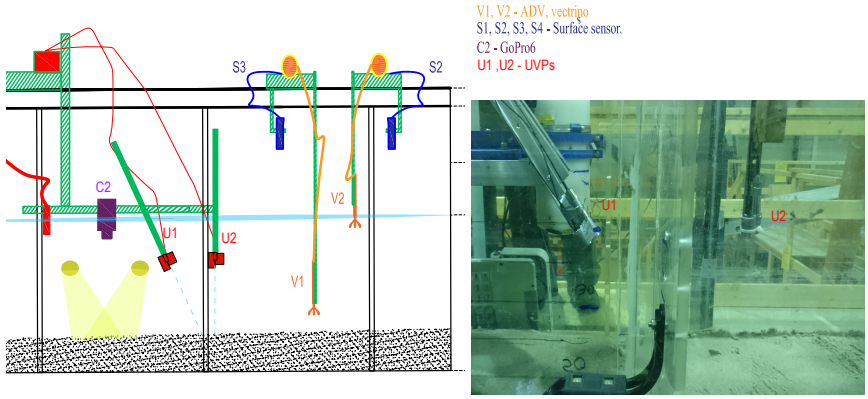

Figure 2.10: Ubertone set-up scheme

The UVP use monostatic Doppler probes that emit a burst of acoustic pulses at a specified pulse repetition frequency (PRF). This pulse incorporates several periods at a given transducer working frequency (UBERTONE, 2016). Moreover, it employs the PC signal processing similar to the one used by the M9. The UVP system permitted choosing different size of the pulse length, that defined the minimum cell sizes (see, Table 2.3) (UBERTONE, 2016). The UVPs are range-gaged

Table 2.3: Ubertone transducers properties

	f	D_t	λ	ω	φ	Near field	$90\text{-}\theta$	R	Cell size	PRF
	MHz	m	m	°	°	m	°	m	m	
inclined	3.0	0.007	0.0005	6.62	2.08	6.62	65	0.39	0.005	1000
	1.5	0.020	0.0010	4.64	1.46	4.64	65	0.39	0.005	500
	0.5	0.015	0.0030	18.54	5.82	18.54	65	0.39	0.011	900
vertical	3.0	0.007	0.0005	6.62	2.08	6.62	90	0.35	0.005	1000
	1.5	0.020	0.0010	4.64	1.46	4.64	90	0.35	0.005	500
	0.5	0.015	0.0030	18.54	5.82	18.54	90	0.35	0.011	900

profilers and do not have an internal processing algorithm to define the bottom and use those values as representative cells of the sediment bed. The processing of the UVP data consisted of:

a) Identifying the cells from the immobile sediment bed and the few cells above. This procedure includes analyzing the echoes through the entire velocity profile. Typically one cell after and one cell before the first maximum of the echo profile, were chosen as representatives of the sediment bed. The distance from these cells to the transducer can be easily determined and controlled with the simultaneous measurements of the water level.

b) The manufacturer of the UVP system, Ubertone claimed that their internal processing algorithms assign zero Doppler velocities to the cells which center reaches the immobile bed. Assuming this is true, all the zero velocities were discarded.

c) The velocities from these cells were averaged in time and the filtering procedure given in the previous section was applied.

d) The echoes from the cells close to the maximum value were also averaged and de-spiked. No correction of the backscattering strength was performed, neither the conversion from μV to dB was performed. The echoes from the inclined beams that were corresponding to zero velocities were deleted. The echoes from the vertical beams were fully considered.

Note that for the bottom identification (BT mode) RDInstruments (2011) uses similar method to identify the echo of interest.That incorporates search trough the depth cells to find the strongest echo amplitude, even searching backward from beyond the echo to actually identify the echo's trailing edge (inner side of the central lobe in Fig. 2.4).

2.3.6 Data post-processing

Apparent velocity

The physical interpretation of the apparent bedload velocity (v_a) measured by the ADCP assumed that v_a is equal to the spatial average velocity of the bed surface, including mobile and immobile particles (Rennie et al., 2002). However, the bedload velocity is typically very noisy and in some other studies have shown that the weighting depends on the instrument frequency and the particle size distribution (Gaeuman, Jacobson, 2006).
This study suggests filtering out of all velocities that have direction opposite of the water and that exceed three times the standard deviation. In the laboratory experiments, this filtering was easily done by knowing the geometry of the flume and the exact position of the ADCP beams. A simple example of filtered v_a is given Fig 2.11.

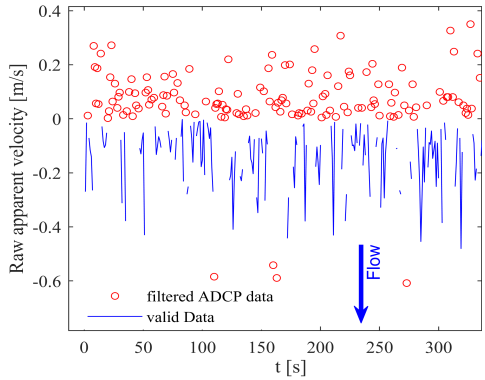

Figure 2.11: ADCP raw data and the filtered outliers of v_a

After the filtering, the apparent velocity data were averaged in time. For the first two experimental campaigns, only the beams in water flow direction were considered in order to eliminate any influence of the side-walls, but at NTNU all beams were considered.
To test the spatial averaging assumption, the apparent velocity was normalized by *K*, (i.e., percentage of the surface bedload concentration) and compared with the velocities messured by the camera. For example, in Paper II , v_a is normalized, giving a new variable $v_{na} = \frac{v_a}{K}$; in Paper III, v_c is multiplied by *K*.

Backscattering strength

The superimposed BS strength ($B_s = 10\log(S_v + S_s)$) was derived from the sonar equation 2.3 in a log form:

$$B_s = -SL + k_{dB}(EI - E_r) - 10\log(A_f) + 2\alpha R + 20\log(R) - P_{dB}, \quad (2.6)$$

where $SL = 10log(I_0 K_p) = 10log(\frac{P}{P0})$ is the source level calculated using the transmit voltage and current present in the RDI output files or the transducers pressure (*P*) in the Sontek output file, as suggested by Shields (2010) and RDInstruments (2011). *EI* is the echo strength converted from "counts" to dB using a factor k_{dB} , which is typically$\sim$ 0.45 for the StreamPro, and $\sim$ 0.1 for M9 (personal communication with Sontek). The noise level (E_r) may vary for each ping and it was available only in the M9 output; for the StreamPro (SPro) it was tentatively assumed as constant $\sim$ 40 dB (RDInstruments, 2011). The transmission losses in two directions include beam spreading (*20logR*) and the attenuation in the water column that accounts only for the water absorption because there is very low or no suspended sediment concentration. *R* is the slant distance to the sedi-

ment bed. P_{dB} is the transmit voltage, that depends of the power supply (12 V for StreamPro and M9) and it was adapted from the tables given in Mulison (2017). The battery voltage changed over the deployment and it was approximately corrected $20\log(\frac{V_b}{12})$, where V_b is the voltage of the battery given at each ping for both ADCPs. Finally, the A_f is the area of the surface scattering strength which can be calculated as the sampling area (based on a perfectly flat floor) of the acoustic beam defined by Rennie et al. (2002) and then corrected for the local slopes of the surface.

Videography data

The similarity of the sediment shape, size and color as well as the impurities in the flume water, contributed for certain percentage of outliers. These outliers were easy-detectable. Eliminating the negative values and de-spiking of the data was applied. No more than 15% of the detected particle velocities were outliers. In some cases, due to the water impurities, the number of outliers was up to 50%. To secure the final results threshold de-spiking was applied using cut-off velocities delivered by the ADV (e.g., close to the bottom, V1, 2.5) or an extrapolated velocity from the ADCP profile.
Besides the velocity (v_c), the bedload surface concentration (K) was also calculated by using the ratio between the number of pixels detected and the total number of pixels in the ROI. K was calculated only for the ROI that match with the sampling area of the ADCP also attempting to reach a temporal synchronization.
The NTNU experiments, only the mean values of all ROI were considered because of the relatively small FOV of the camera and the deployment of the two ADCPs at the same time. This resulted in low values of K (or K_m, in Paper III) for the gravel experiments, due to the sporadic motion of the gravel particles. ADCPs are typically registering the moments when there is transport; thus the sequences with K equal to zero and zero were discarded. The bedload surface velocity where the zero velocities were eliminated is denoted as (K_{act}). The experiments with larger particles (i.e, gravel experiments) permitted labeling of the particles and confirming the percentage of mobile data (K_{act}).

2.4 Field Methodology

The field measurements were conducted in Albania, Devoll on the Tomorrice river and on two large lowland rivers in Germany (Elbe and Oder). In total, five campaigns are included in this study and will be denoted as Alb (two campaigns on the same place with similar discharge), Oder, Elbe1 and Elbe2 (Fig. 2.12). The data from Albania and Oder is presented in Paper *III* and all campaigns in Germany are given in Paper *II*.

The ADCP bedload measurements were performed in fixed stationary positions. The physical samples were taken at the same time and position in Albania, whereas in Germany the exact position of each ADCP and the bedload sampler is depicted in Fig. 2.13.

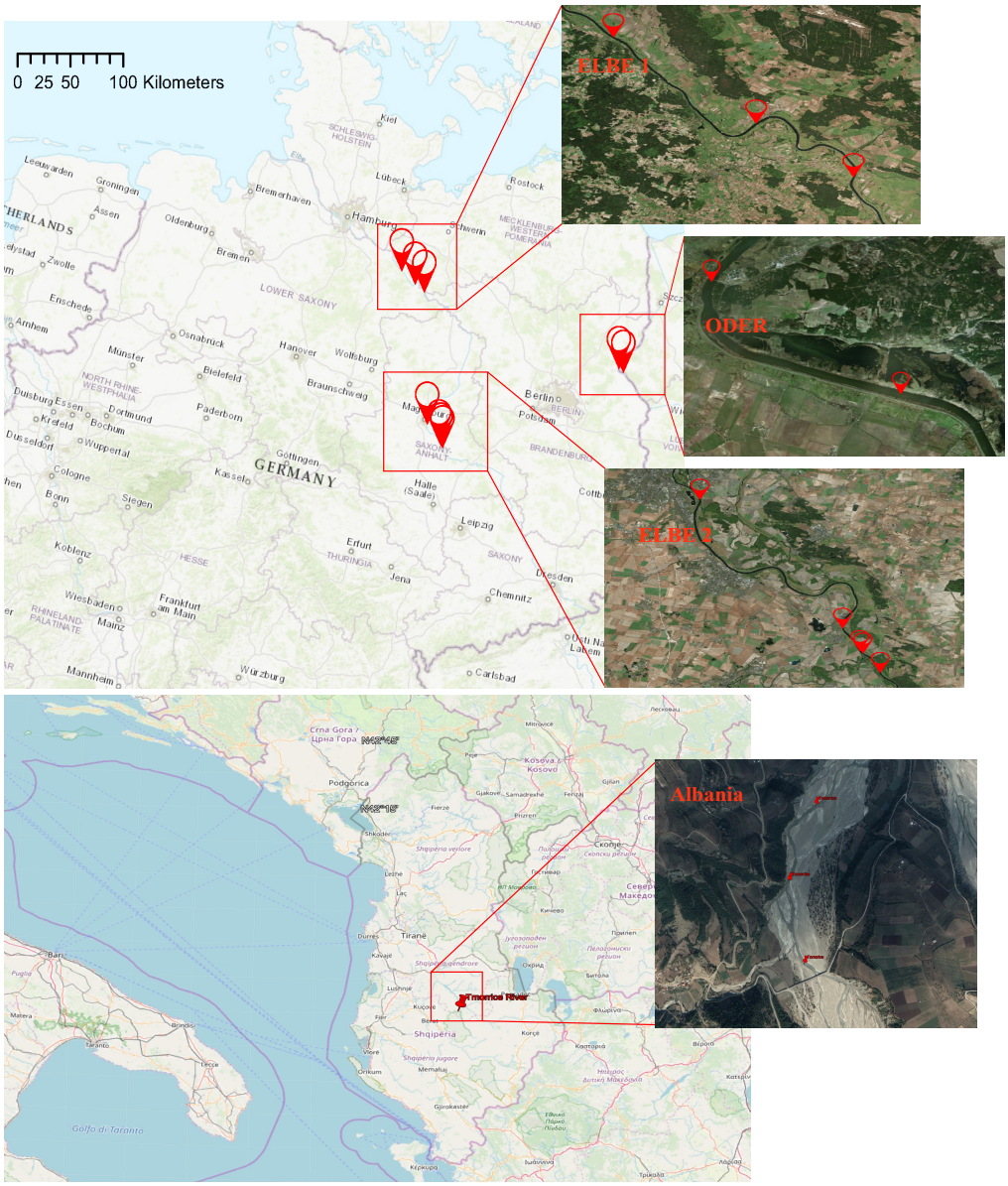

Figure 2.12: Filed Study Locations

2.4.1 Albania- Field characteristics and measurements

The measurements in Albania were conducted on the river Tomorrice, which is characterized with annual discharges varying between 2.7 and 3.3 m^3/s. The Tomorrice river is a tributary of the Devoll River flowing from the Tomorri peak to the 1-km-wide alluvial valley of the Devoll with typical braid morphology. The catchment is characterized with a high coefficient of variation of the discharge; thus, the sediment transport occurs very randomly, consisting of rocks, cobbles, and gravel during the floods and sand during the annual flow discharges (see, Table 2.4). The water velocity (U) was calculated locally by averaging the ADCP water profile and shear velocities were calculated fitting the log-law equation over the entire water velocity profile measured by the ADCP (Rennie, Villard, 2004); thus the values represent the local shear velocity which varied for different positions between 0.06 - 0.11 m/s.
The bedload sampling was performed over three cross sections, manually collecting minimum two physical samples per position. The ADCP (RiverPro, see Table 2.1) was maneuvered manually, trying to keep it as stable as possible. In total, 25 bedload measurements were included in this study from two campaigns obtained in December 2016 and March 2017 in the same are given in Fig. 2.12.

Table 2.4: Field Characteristics and hydraulic parameters

Campaign	Cross-section	Num Of points	Coordinats		Q	B	U [1]	H	S	$D90$	$D50$	Cz	$\tau*$	$u*_{cr}$	$u*$
			LONG	LAT	(m^3s^{-1})	(m)	(m s^{-1})	(m)	‰	(mm)	(mm)	/	/	(m s^{-1})	(m s^{-1})
ODER	1	7	14.195	52.820	748	280.9	1.03	2.6	0.15	1.75	0.67	16.69	0.351	0.018	0.062
	2	8	14.123	52.842	721	228.2	1.01	3.1	0.15	1.81	0.71	14.89	0.399	0.019	0.068
ELBE 1	3	5	10.897	53.234	697	212.1	0.91	3.6	0.13	2.24	0.51	13.43	0.556	0.016	0.068
	4	5	11.119	53.157	691	304.1	0.91	2.6	0.11	2.50	0.76	17.51	0.225	0.019	0.052
	5	5	11.269	53.111	702	219.3	0.98	3.3	0.13	2.64	0.56	15.16	0.460	0.017	0.065
ELBE 2	6	6	11.885	51.978	276	160.4	0.73	2.4	0.19	3.57	1.10	11.03	0.246	0.024	0.066
	7	5	11.917	51.954	323	200.3	0.72	2.2	0.2	3.38	1.05	10.90	0.256	0.023	0.066
	8	5	11.912	51.956	246	166.7	0.69	2.1	0.2	3.03	1.11	10.66	0.234	0.024	0.065
	9	6	11.943	51.936	221	139.8	0.83	1.9	0.19	3.45	1.04	13.91	0.211	0.023	0.060
	10	5	11.677	52.093	296	147.0	0.90	2.3	0.2	2.79	0.98	13.43	0.284	0.022	0.067
ALB[1]	1-3	25	20.186	40.827	3	15	0.71	0.5	/	13.00	0.80	6.80	0.8514	0.020	0.105

[1] The measurment in Albania consist of two campaignas at the same position

2.4.2 Germany- Field characteristics and measurements

The field sites in Germany were ten different reaches of navigable lowland rivers with dominating sandy riverbed in the downstream parts (e.g., ODER and ELBE1) and fine gravel mixed with coarse sand in the upstream part of Elbe (e.g., ELBE2). Note that the values are given in Table 2.4 are average values, calculated for entire cross-section. The discharges varied between 220 - 750 m^3/s, but the water velocities were in the same range for all the campaigns in Germany (see, Table 2.4). The distance between the cross sections varied from 2 to 15 km; thus, each cross-section can be considered as a separate reach. The river surface slope (S) data was

estimated from the local hydrometers that were available for all the reaches, and it was assumed that the flow is uniform (i.e., the riverbed slope and the surface slope are parallel). Due to the presence of dunes (0.08 m to 0.16 m in height, and 10 - 22 m long) and secondary currents, it was most convenient to calculate the bankfull (i.e., mean cross-section) shear stress (τ) by applying the standard equation, $\tau = gHS$, where g is the gravitational constant and $u*$ is the shear velocity calculated as $(\frac{\tau}{\rho})^{0.5}$.

The water depths (H), discharges (Q) and the velocities (U) given in Table 2.4 are the mean values obtained from the moving boat ADCP measurements performed for each cross-section for all campaigns. The Chezzy parameter was calculated for each cross-section using the expression $Cz = \frac{U}{u*}$ and the critical shear velocity in Table 2.4 is calculated only for D_{50} using the Shields mobility parameter (Shields, 1936).

The bedload measurements were performed on pre-selected locations and followed a well-established monitoring program, annually conducted by the German Water authorities and BfG (German hydrological institute). Sediment data were collected in stationary positions from a fully anchored boat (see Fig. 2.13) in 5 - 8 equally spaced points over a cross-section. On each position of the cross-section, three samples were collected with a sampling time of five minutes as soon as the sampler is fully positioned on the riverbed. In total, 171 samples through 10 cross sections were collected during the three campaigns.

Three ADCPs worked at the same time of the physical sampling, on each position spaced as shown in Fig 2.13). The three ADCPs worked with four different frequencies at the same time and positions (see, Table 2.3)

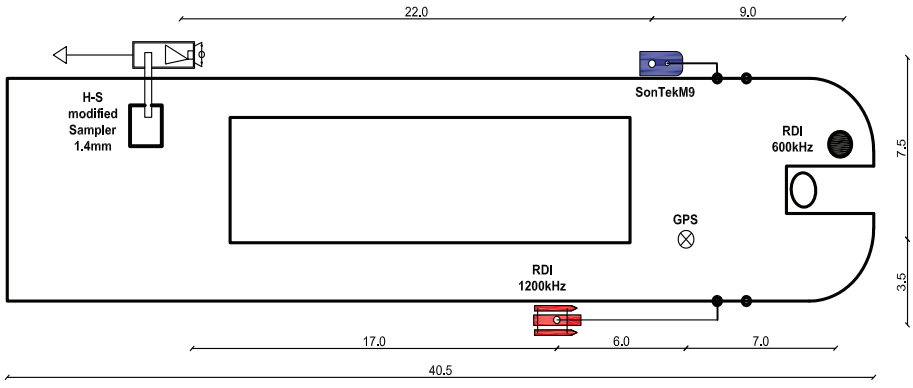

Figure 2.13: Measurement set-up. Boat Scheme



Figure 2.14: Bedload Sampling in Albania



Figure 2.15: Bedload Sampling in Germany

2.4.3 Instrumentation and post-processing

Pressure-Difference Samplers

The physical samples in Abania were collected manually using small Helly-Smith sampler (B = 7.65 cm), as shown in Fig. 2.14. The transport rate per unit width was calculated and data collected at the same position was averaged without any efficiency correction on the estimated rates. The sampler used in the campaigns was a customized pressure-difference sampler, operated with a crane installed in the backside of the boat (see, Fig. 2.13). BfG designed the sampler in the 1970s and it has been further developed ever since. In its basic design, the BfG-sampler are very similar to the Helly-Smith type. However, they are modified and adapted for the German rivers. The mesh size of the collecting steel basket was 1.4 mm and the nozzle had dimensions 8/16 m. The length of the sampler was 91 cm, without the landing structure (Fig. 2.15).To facilitate the landing and to ensure the contact with the riverbed, the samplers are mounted on a still frame. The bedload samplers had mounted cameras and lights above the nozzle giving the live-stream video for each sample. The simultaneous observation of the camera footage helped into the selection of reliable samples and eventually repeating the sampling procedure during the campaign.

The efficiency of the sampler was examined in several laboratory tests performed by BfG (Banhold et al., 2016). The tests were conducted using different bed sediments ranging from sand to coarse gravel. Material smaller than the mesh size used may pass through the collecting steel basket; thus, there is an inevitable loss of bedload material, which means a distortion especially of the actual amount of sandy bedload. To better quantify this amount of sand lost a series of experiments was conducted in the flume at Aachen University. In addition to the actual sand loss, the study also considered the influence of the mesh size, the sand content and the filling level of the collecting steel basket (Banhold et al., 2016). Accordingly, the applied correction factors in this study varied between 1.1 - 1.6, depending on the content of sand in the bedload material and total collected bedload mass. Fi-

nally, an average out of the three samples was considered in the calculations of the transport rate.

ADCP field data post-processing

The ADCPs were collecting data for at least 5 - 7 minutes per configuration at the same position (for the M9, see Table 2.1). Longer sampling was performed by the RDI instruments run with their default configuration during all campaigns.
The raw apparent velocity obtained from the ADCPs was filtered by discarding the velocities in the opposite direction of the water flow, as explained in section 2.3.6. The filtering procedure used the water velocity vectors obtained from the lower part of the water profiles of each ADCP to identify the average direction of the water flow. These vectors determined the reference direction to discard the BT velocity vectors with more than $\pm$ 90 degrees mutual angle difference (see, Fig 2.16). In addition, the measurements close to the steep riverbanks or close to the

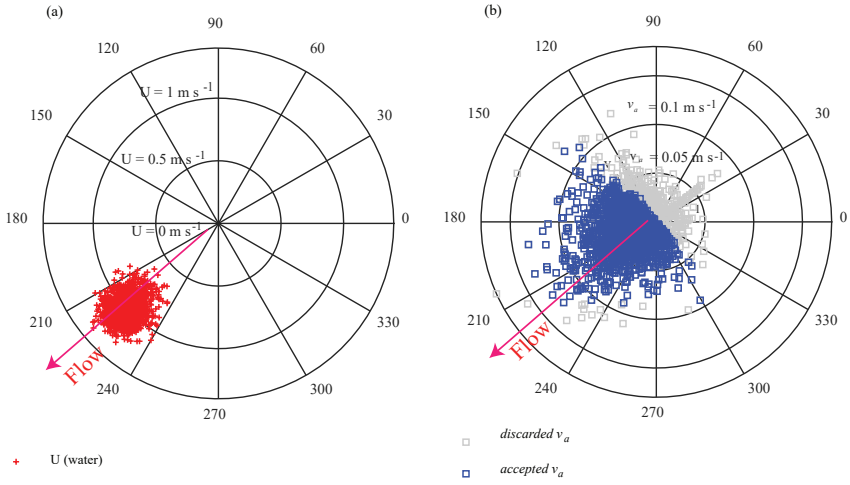

Figure 2.16: Example of vector direction plot at one measurement position of the RDI 0.6 MHz: only water velocity (U, red symbols); the accepted apparent bedload velocity (v_a blue symbols) and discarded apparent bedload velocity (grey-faint symbols). Note that the blue and the faint-grey symbols give the raw apparent velocity measured by the BT mode of the ADCP. The red error represents the mean direction of the water velocity.

groins violated the homogeneity assumption (see, section 2.2). These disturbances led to the estimation of erroneous apparent bedload velocities, mostly due to the different Doppler shift in each beam, but also due to the significantly changed grazing angle (θ). The filtered velocity data were averaged through all the sampling period and later compared with the average transport rates from physical samples taken at the same location.

Chapter 3

Results and Discussions

This chapter is a summary of the main results obtained during this research. The presentation of the results will be divided into two sections, Laboratory and Field data. The figures do not differ from the ones presented in the papers, and each section will include a reference to the paper where these results are presented. Please note that Paper *II* elaborate slightly different dataset Paper *III*, but deliver similar information research objective. The same stands for the *Paper IV* and *Paper V*.

3.1 Laboratory Results

3.1.1 The apparent bedload velocity

(*Paper I and Paper V*)
Initially, the apparent bedload velocities (v_a) measured by the SPro at UniBO and the M9 at UOttawa were compared to the velocity from the imagery data. Considering the planar view of the cameras and chosen hydraulic conditions, the velocity measurements of the videography (v_c) are assumed to be the average velocity of the bedload particles in most of the experiments. Fig. 3.1a compares the velocity measured by the cameras and the filtered apparent velocity from the ADCPs (see, Ch. 2). It demonstrates that there is a significant correlation, but the apparent velocity underestimates the data. Once the surface concentration coefficient K is applied (Fig. 3.1b), the ADCP and camera data match well, especially for the experiment results measured by 3MHz M9 ADCP RS (Fig. 3.1, filled markers). This suggests that K is necessarily present in the acoustic footprint and that 3 MHz RS corresponded well with the homogeneity assumption because it most probably scatters only the surface of the mobile particles. On the other hand, the

SPro (empty markers on Fig. 3.1b) gave a good correlation, but the data showed 2-5 times difference between the v_c and v_{na}. The factor of difference increases for the higher v_a, meaning that SPro is penetrating the active layer of particles and it is strongly influenced by the immobile surface beneath.

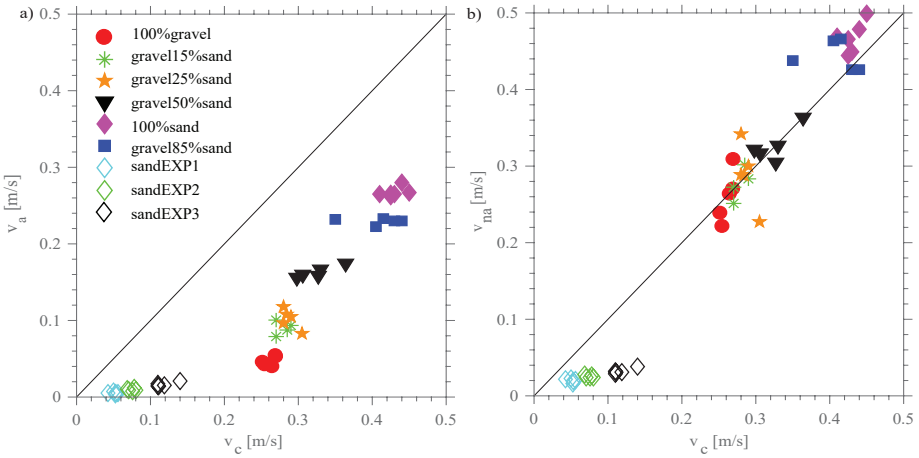

Figure 3.1: *a*) The apparent bedload velocity and the camera data; *b*) Normalized apparent bedload velocity $v_{na} = \frac{v_a}{K}$ and the camera measured velocity.

In the NTNU experimental campaign, both M9 (all frequencies and configurations, see Table 2.2) and SPro were deployed at the same time and the camera recording installed between them. Similarly as reported in Fig. 3.1a-b the 3MHz (PC and RS) and 1MHz (PC, Fig. 3.2d) underestimated the true particle velocities, but followed the spatial averaging assumption. The latter is shown on Fig. 3.3b-c where the filtered apparent velocities of 3 MHz PC and RS matched well with the normalized camera velocity ($v_a * K$). The deviation of v_a in some experiments (e.g., gravelEXP1, black symbols low velocities) is expected and it is associated with the uncertainty in the estimation of *K* coefficient and the sporadic gravel transport. The 3MHz IC measurements did not fully comply with spatial averaging assumption giving slightly higher apparent velocities than the 3MHz PC (Fig. 3.2a). This is related to the internal processing of the longer BT pulses for the IC signal modulation and the shallower acoustic sampling. The 1MHz IC (Fig. 3.2d, squared symbols) actually performed even shallower sampling and measured almost the same as the camera velocity for all experiments.
The shallower sampling is most likely combined effect echo identification and coarser resolution of the cell gating; or only superficial acoustic coverage of the mobile sediment bed.

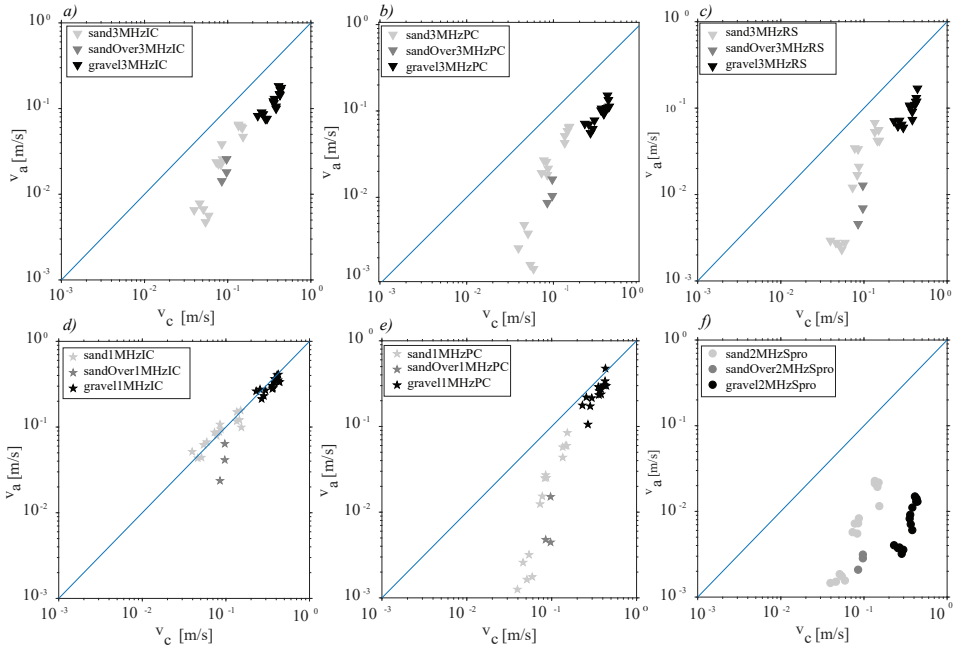

Figure 3.2: Apparent bedload velocity measured by different instrument and configuration correlated with the bedload velocity (v_c) estimated by imagery data

An overestimation of the spatially averaged apparent velocity was also observed for the gravel experiments measured by the 1 MHZ IC and PC (i.e., $v_a \simeq v_c$ in Fig. 3.2d-e corresponding to $v_a > K{*}v_c$ in Fig. 3.3 d-e). Beside the shallower sampling and the different acoustic profiling, the acoustic geometry also contributed for obtaining higher velocities; z_c height shown in Fig. 2.4 for relatively small water depth is very low (z_c = 1-10 mm, see Fig. 2.2), which makes the active layer thickness of the gravel particles ($d_t \sim 8-25$ mm) higher. Having $d_t > z_c$, the acoustic sampling improves because the pulse insonifies equally in the region above z_c and the influence of the surface scattering is diminished. The gravel particles have $D_{50} > \lambda$, which makes them scattering in the geometric regime; and this also contributes to dominant scattering and estimation of Doppler velocities closer to the real particle velocities.

SPro (2 MHz) underestimated the normalized camera velocity in a range between 2-5 times for the sand experiments (grey symbols, Fig. 3.3f), whereas for the gravel measurements (black symbols, Fig. 3.3f) the difference is up to 20 times higher velocities. It confirmed that SPro is strongly affected by surface scattering of the fixed flume bed beneath the active layer of mobile particle.

This confirms that the key component in the determination of the Doppler are the internal signal processing and the pulse length (i.e., ultrasound energy), leading to

a stronger influence of the immobile surface and severe underestimation of the true bedload velocity.

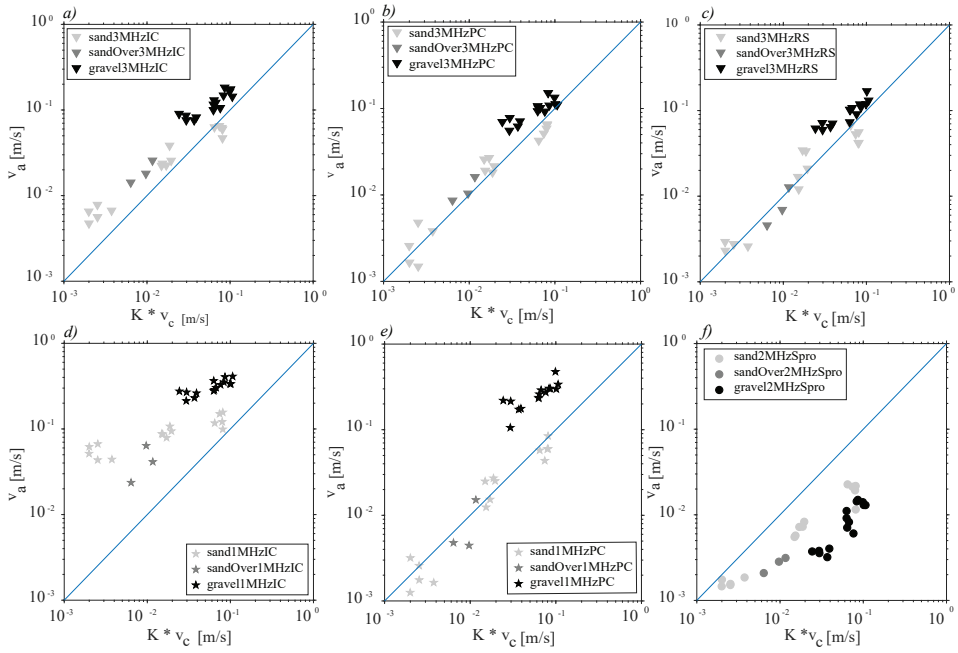

Figure 3.3: Apparent bedload velocity measured by different instrument and configuration correlated with the normalized bedload velocity ($K * v_c$) estimated by imagery data

The filtered data

(*Paper I* and *Paper V*)

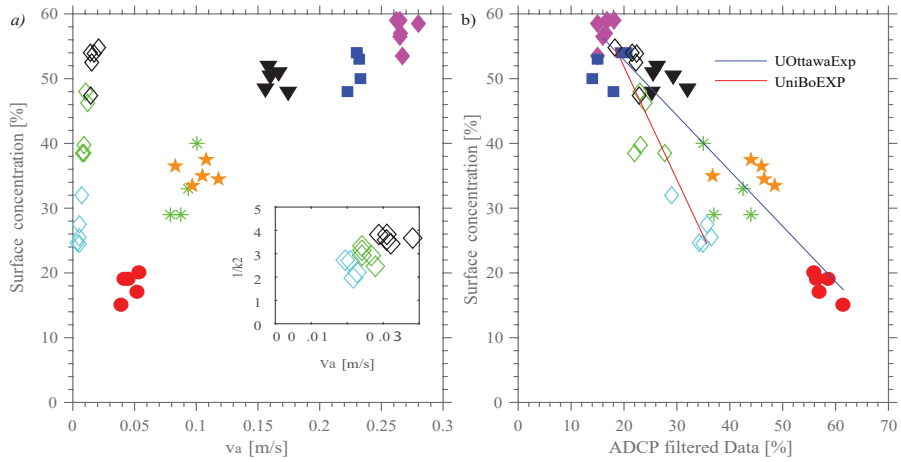

Figure 3.4: *a*) The apparent bedload velocity and dimensionless bedload surface concentration (K); *b*) Dimensionless bedload surface concentration (K) and the percentage of the filtered data.
Note: the symbols are the same as in Fig. 3.1

The raw BT velocity obtained from the ADCPs typically contains many erroneous data that could not be smoothed out only by averaging of the time series. The extreme values were de-spiked, and the velocities with direction opposite of the flow were filtered out. Moreover, the percentage of the filtered data (FD), gave a reasonable correlation with bedload transport intensity. Fig. 3.4 shows that the FD is negatively correlated with the surface bedload concentration, which is a direct measurement of the bedload intensity. This demonstrates that the more abundant the bedload transport contributes to a better sampling of the ADCPs. High percentage of FD can be explained with the strong influence of the immobile bedload surface and the small-scale roughness, but it is also strongly related to the internal processing of the instrument.
To better understand the influence of the internal processing to the total percentage of bad data *(ND = FD + N/A)*, the not valid data (i.e., *N/A*, the data automatically discarded by the internal firmware of ADCPs) is added. The ND average values fo the 1 MHz IC did not give a negative correlation with the increase of the velocity (Table 3.1), showing that there were some internal limitations in the processing of the data. The same positive correlation with the transport rate intensity was also noticed for the *FD* values in the gravel experiments by the M9. The high *ND* values bore out that the instrument is susceptible on turbulent flows and high *Fr* number

(vibrating particles, bubbles, etc.). Besides, the sporadic transport of the bedload and the micro-roughness of the large gravel particles *($D_{50} > \lambda$)* contributed to a higher degree of error. The percentage of the erroneous data and the std in Table 3.1 are highest for the IC configuration; that complies with the limitations of the IC signal processing (Brumley et al., 1991).

Table 3.1: Average not valid data (ND) observed during the NTNU experimental campaign

EXP	3MHz IC		1MHz IC		3MHz PC		1MHz PC		3MHz RS		SPro				
	STDva m/s	ND %	STDva m/s	ND %	STDva m/s	ND %	STDva m/s	ND %	STDva m/s	ND %	STDva m/s	ND %	STDvc m/s	stdKm	stdKact
sandEXP1	0.0038	44%	0.0272	31%	0.0007	48%	0.0011	57%	0.0017	64%	0.0004	80%	0.006	0.022	0.022
sandEXP2	0.0156	38%	0.0601	37%	0.0139	40%	0.0233	53%	0.0166	44%	0.0040	43%	0.007	0.016	0.016
sandEXP3	0.0408	29%	0.0760	41%	0.0336	35%	0.0677	50%	0.0297	37%	0.0123	30%	0.009	0.009	0.009
sandOVER	0.0106	37%	0.0245	40%	0.0058	43%	0.0017	44%	0.0084	46%	0.0016	64%	0.023	0.011	0.050
gavelEXP1	0.0508	71%	0.1472	74%	0.0436	59%	0.1744	83%	0.0489	51%	0.0022	62%	0.190	0.035	0.190
gavelEXP2	0.0590	83%	0.1744	84%	0.0652	74%	0.1991	87%	0.0768	54%	0.0084	57%	0.450	0.125	0.298
gavelEXP3	0.0689	91%	0.1924	89%	0.0912	89%	0.1778	91%	0.1228	56%	0.0129	56%	0.480	0.200	0.302

The apparent velocity - The Ubertone experiment

(*Paper VI*)

Another experiment was conducted in the laboratory of NTNU in collaboration with UBERTONE. Only sand-bed was used and two hydraulic conditions (e.g., sandEXP1 and sandEXP2, see Table 2.2). The main objective was to test different manufacture, different transducers and internal processing techniques.

Note that the apparent velocity was estimated as an average of two to three cells above the first maximum echo of the velocity profile (see, Ch. 2). By doing this, the influence of the immobile bed surface is minimized and the cells are mostly scattering the mobile particles. The second condition (Fig. 3.5b) resulted in higher deviation due to the development of bedforms. The bed irregularities challenged the automatic detection and imposed strong influence of the water velocities above the actual bedload motion (Fig. 3.5b).

The raw apparent velocity also needed to be filtered, and after the filtering, it gave the lowest values for the lowest frequency (0.5 MHz) and similar, comparable values for the 3 MHz and 1.5MHz. The 0.5 MHz had the largest cell and the smallest PRF, which means that the pulses were longer; thus it gave higher values for z_c and larger influence of the immobile bed surface, confirming the strong influence of the acoustic geometry over the estimation of the Doppler velocity.

On the contrary, the higher frequencies in both conditions gave velocities similar to the surface bedload velocities measured by the camera. This has proven that the technique of identifying the bottom and controlled selection of the acoustic cells

used in the estimation of the apparent velocity plays a significant role. In addition, the shorter pulses contributed to more accurate data. In comparison, the internal processing of the BT mode of the ADCPs uses much longer pulses which contribute to have larger cells and the longer contact with the sediment bed contributes for larger influence of the immobile bed. Besides, the lower frequencies use larger cells and longer pulses (see, Table 2.3) that additionally complicates the bedload velocity calculations, but helps the identification of the immobile bed.

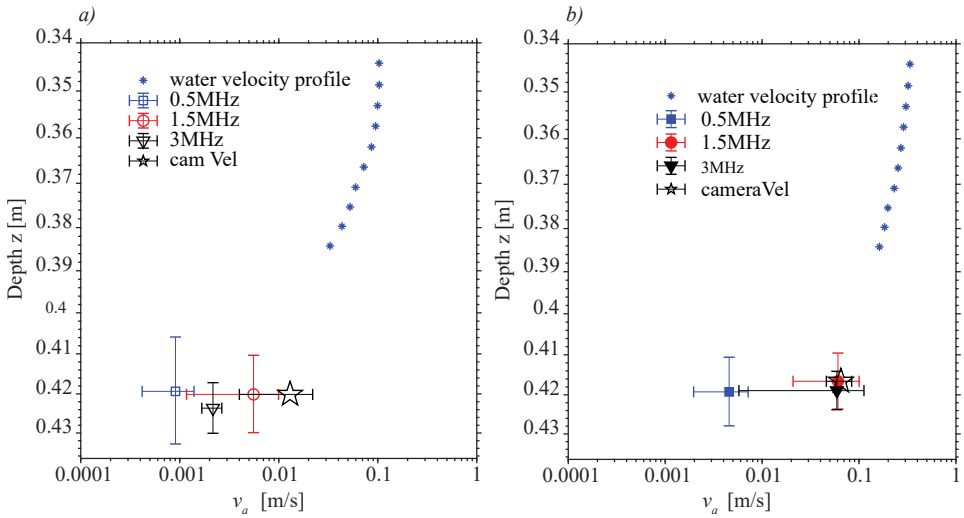

Figure 3.5: *a*) The apparent bedload velocity the camera velocity and the water velocity profile (conditions identical to sandEXP1, U $\sim$ 0.3 m/s); *b*) The apparent bedload velocity the camera velocity and the water velocity profile (conditions identical to sandEXP2, U $\sim$ 0.45 m/s)

The echo profiling (gating) influence to the apparent bedload velocity determination

(*Paper V and Paper VI*)

In acoustics, a typical approach for identifying a solid boundary is to search of the strongest echo in range-gated echo profile (RDInstruments, 2011). These gates (i.e., bins) are pre-determined by the pulse length (IC signal processing) and/or the distance between two pulses/sub-pulses/codded elements (e.g., BB signal processing).

The previous section clearly showed that the correct determination of the bottom echo plays important role into identification of the apparent velocities. For example, the correspondence of the 1 MHz IC values for the sand experiments to the camera velocities in Fig. 3.2 is a clear evidence of this issue. In laboratory scaled conditions the center of the bin used for identification of the bottom most likely

was positioned slightly above the immobile bed. The shallower acoustic sampling is most likely due to longer pulses, larger cells and blank distance that contributed for coincidental shallower sampling and less impact of the surface scattering for the 1 MHz IC configuration than the 3 MHz IC (e.g., Fig. 3.6).

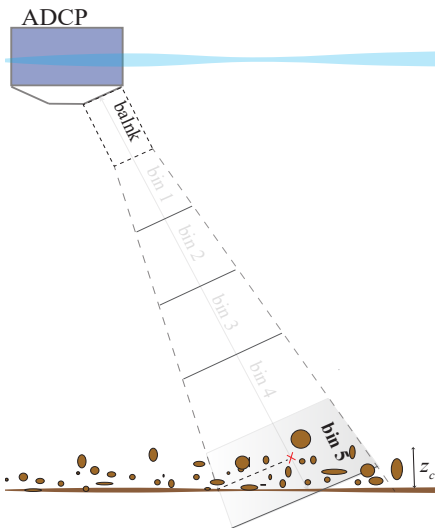

Figure 3.6: An example of shallow sampling due to coarse echo profiling resolution.

Similarly, the BB instruments can reach much finer resolution of the echo profile, defining a cell size thinner than the active layer which contributes to even more accurate determination of the riverbed; thus stronger impact of the immobile surface scattering.

3.1.2 The backscattering strength

Paper IV and *Paper V*

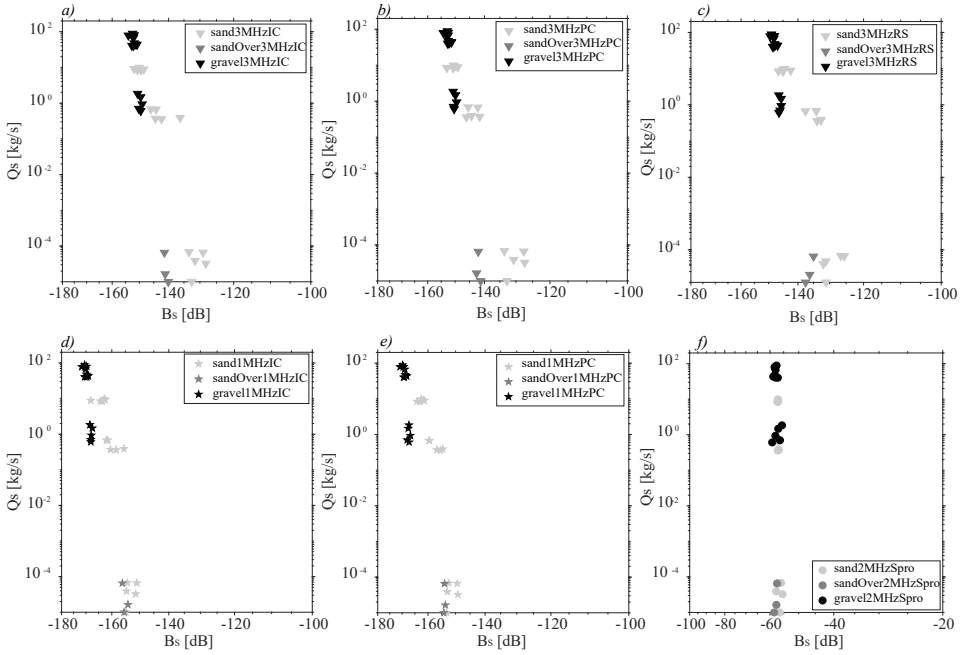

Figure 3.7: BS strength (*Bs*) measured by different instrument and the transport rate (Qs).

The transport rates measured by the bedload trap in the experiments at NTNU were correlated with the corrected BS strength (B_s, see also Eq. 2.6) obtained by the SPro and the M9. The results of the sand and gravel experiments are presented in this section.

A decline of the BS strength was observed for all instruments and configurations as the bedload transport intensity increased, resulting in a negative correlation (Fig. 3.7). For example, the rate of change ΔB_s / ΔQ_s was equal to -250 in case of 3MHz PC and sand experiments, whereas this rate changed to -50 for gravel (e.g., 3MHz PC, Fig. 3.7b). The higher absolute value of ΔB_s / ΔQ_s for sand tests represents a noticeable effect of the active layer on sound propagation at the sediment bed. This demonstrated that the BS signal is much more attenuated for the sand experiments rather than the gravel experiments, even though the bedload transport and apparent velocities were much higher for the gravel experiments. ΔB_s / ΔQ_s absolute value was larger for IC (Fig. 3.7a and Fig. 3.7d) rather than for PC (Fig. 3.7b and Fig. 3.7e). In the same context, higher deviations were observed in the

corresponding apparent velocities (Fig. 3.2a-d and 3.2b-e for IC and PC respectively). This shows that IC performed a shallower sampling within the active layer than PC, giving lower BS strength values, which came along with a higher deviations of the apparent bedload velocity measurements.
On the contrary, SPro registered almost constant backscatter for the three hydraulic conditions (Fig. 3.7f). It corresponds to an acoustic return that is poorly affected by the active layer, and mostly reflected by the immobile sediment. It is consistent with the fact that SPro continuously underestimated the bedload velocity as shown in Fig. 3.2f. In addition, the SPro has longer pulses, the smallest transducers, larger beam opening angle, and smaller grazing angle (see, Table 3.1) and much stronger emitting power that contributes for a stronger effect of the surface scattering by the immobile bed. The z_c value is also highest for the SPro (see, Table 2.1), giving less focused acoustic beams.
The RS configuration in Fig 3.7c follows the same trend as the PC configuration, but the data is more scattered. However, the BS strengths are slightly higher, especially for the gravel data (black triangles, Fig 3.7c) than PC and IC and the ND values (see, Table 3.1) are also in a range expected for turbulence conditions and gravel bedload transport. Note that, greater turbulence in the flow accompanied with a sporadic gravel transport induced more errors in the acoustic measurements.

The BS strength correspondence with the bedload active layer and concentration

In the previous section it was demonstrated that BS strength is well correlated with the physically measured transport rate. In this section the bedload concentration and the active layer measured by the planar-view and side-looking camera, respectively (see Ch.2). Therefore, the average values of the BS strength values and the apparent velocities are correlated with K_{act} (i.e., bedload surface concentration) and d_t/D_{50} (i.e., active layer thickness). In Fig. 3.8 K_{act} is an implicit measurement of the dimensionless bedload concentration and d_t/D_{50} adjusted the thickness to the number of particles, instead of the size, which is a more crucial acoustic indicator. Fig. 3.8a-b and Fig. 3.8d-e show similar trends for the B_s data observed for the sand and gravel experiments pointing out that the BS strength is proportional to the bedload concentration regardless the particle size and mass transport. Moreover, the flatter trends observed for the sand experiments (grey stars and triangles, dashed lines) in Fig. 3.8c and Fig. 3.8f validate that the inverse correlation between the active layer features and B_s, could be described as a sensitivity of the BS strength towards bedload concentration (i.e., number of particles) increases.

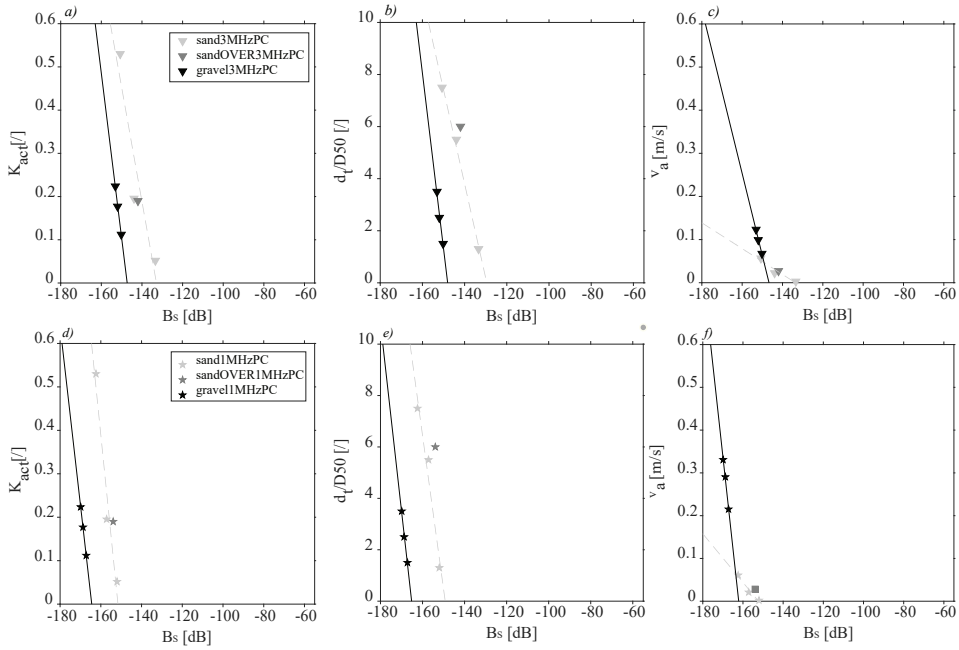

Figure 3.8: The BS strength versus the normalized bed-load thickness (d_t/D_{50}) and the surface concentration (K_{act}).

The echo amplitudes - Ubertone

(*Paper VI*)

The echo amplitudes given in μV, were extracted form the corresponding cells (i.e., gates) of the UVP echo-profiles (see, Ch. 2. The time series of the echo amplitudes were de-spiked using simple threshold approach. Then the average amplitudes per each frequency were compraed for the two two bedload conditions considering both the vertical ($\theta = 0^o$) and inclined ($\theta = 25^o$) transducers (see, 2.3.5). Figure 3.9 shows that when the bedload transport conditions change (e.g., passing from Fig. 3.9a to Fig. 3.9b) the echo amplitudes of the inclined transducers increase and the vertical remain the same or slightly decrease (e.g., black empty symbols, 3MHz). The increase of the amplitudes for the inclined beams is due to the increase of the volume backscattering strength, which is proportional with the concentration of the bedload. The change is most obvious for 3 MHz, because the sand ($D_{50} \sim 0.39$ mm) particles acoustically scatter in the geometric regime (see, Fig. 2.6). The attenuation present in the 3 MHz data, because the only cells above the bed were considered, which showed that the scattering of the immobile surface is present only if the filtering performed unsuccessfully or there was internal error in the data. The amplitudes for the vertical beams gave larger amplitudes, because

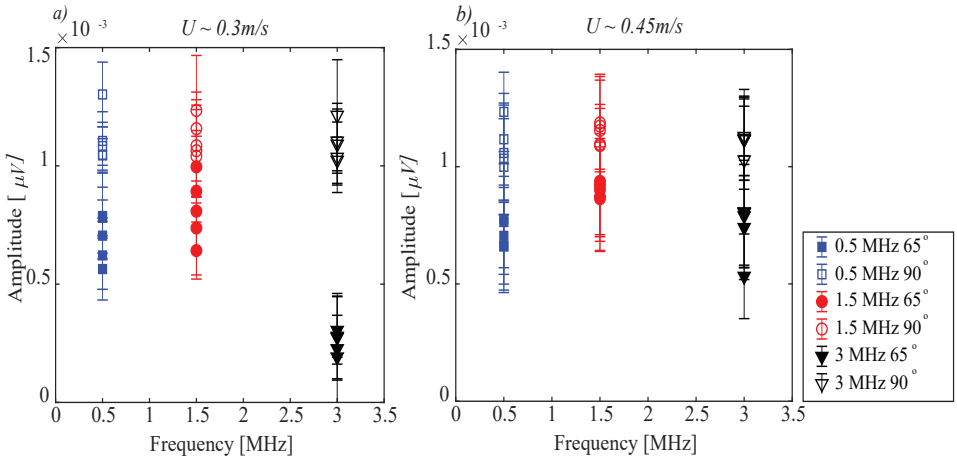

Figure 3.9: *a*) The averaged echo amplitudes for five repetitions given for each frequency and grazing angle (90-θ) (conditions identical to sandEXP1, U $\sim$ 0.3 m/s); *b*) The averaged echo amplitudes for five repetitions given for each frequency and grazing angle (90-θ) (conditions identical to sandEXP2, U $\sim$ 0.45 m/s)

the vertical beams are theoretically more biased towards surface scattering (Urick, 1983), but more importantly because the cells that actually scattered the immobile bed were considered. The slight decline when passing from one to another condition is due to the attenuation of the echoes from the cells below the active layer, that was a result of the thickening of the active layer and deformation of the immobile bed. The largest cell-size and largest pulses of the 0.5 MHz leaded to least sensitive amplitudes towards the bedload concentration and active layer change. In addition, the lower frequencies penetrate easier the active bedload layer and got more influence by the surface scattering of the immobile bed.
Unfortunately the data acquisition in high resolution (e.g., extracting the cells right above the immobile sediment bed) using UVPs and PC signal modulation, is only possible only in laboratory conditions. In field application, the higher water depths require larger pulses and lower resolution, that in theory will always over-sample the active beload layer (e.g., in Fig. 3.5a).

3.1.3 The bedload particle size distribution and the backscattering strength

(*Paper V*)
An interesting results observed in the NTNU experiments was the difference in the magnitudes BS strength related to the gravel and sand (see, Fig. 3.7). This permits rough characterization of the bedload materials, similarly, as suggested by Shields (2010).
On the other hand, B_s is very different in calm (empty symbols) and mobile (filled symbols) conditions. This difference in the scattering strengths indicated the dom-

inance of the surface scattering in calm conditions which depends only of the bed roughness and the micro-roughness of each particle, especially relevant for the highest frequency instruments (i.e., smaller wavelength of the particle size). It also bore out that the BS strength cannot be only associated with the type of the material, but also with the mobility conditions, due to the presence of different types of scattering and different ambient noise.
Furthermore, Table 3 shows that the 0.5 MHz (vertical beam) gave the most considerable difference in the magnitudes of the gravel and sand experiments. The vertical beams (e.g., $\theta = 90^o$) are generally less responsive to a volume scattering (Medwin, 2005), which implies that the vertical beam is less sensitive to concentration changes at the sediment bed. The vertical beam also has 0.5 MHz, which makes the scattering of fine sand and gravel in different regimes contributing to even easier distinction of the materials.

3.2 Field Results

3.2.1 Evaluation of the apparent bedload velocity

(*Paper II* and *Paper III*)
To examine the existence of an effective relationship between the physically measured bedload transport rates (Q_m^s) and the apparent bedload velocity (v_a), a simple linear regression analysis was performed. The (Q_m^s) values used in the analysis are average values of minimum three samples taken at the very same position, and (v_a) are time averaged velocities (minimum 5 - 7 min) of different ADCPs, measured in same position. The apparent bedload velocities were de-spiked, and the velocities with direction opposite of the flow were filtered out, similarly as presented in Ch. 2.4.3. Note that some points were discarded both due to a failure of the bedload sampler (e.g., bad contact with the riverbed, clogging, etc.) or the ADCP (e.g., bead positioning of the beams, such as close to the river banks where the cross-section slope increases rapidly from one side).
The apparent bedload velocity measured by all instruments and configuration showed good correlation with the bedload transport rates (r = 0.55 - 0.85). As expected the lowest measured velocities and the lowest correlation coefficient (r) were measured by the lowest frequency (0.6 MHz, Fig. 3.1a). The highest velocities and the best correlations were observed by 3MHz, similarly, as presented in Fig. 3.1c and Fig. 3.2f-g. However, the 1 MHz for all configuration measured velocities higher than the 1.2 MHz and a little bit lower than 3 MHz.
Regarding the different configurations used, the PC configuration (Fig. 3.10e and Fig. 3.10g) demonstrated the best correlation with the physical transport rates (Q_m^s) for both frequencies (Fig. 3.10g and Fig. 3.10e), but there was no significant difference among IC, RS, PC and def. IC resulted in higher deviations among

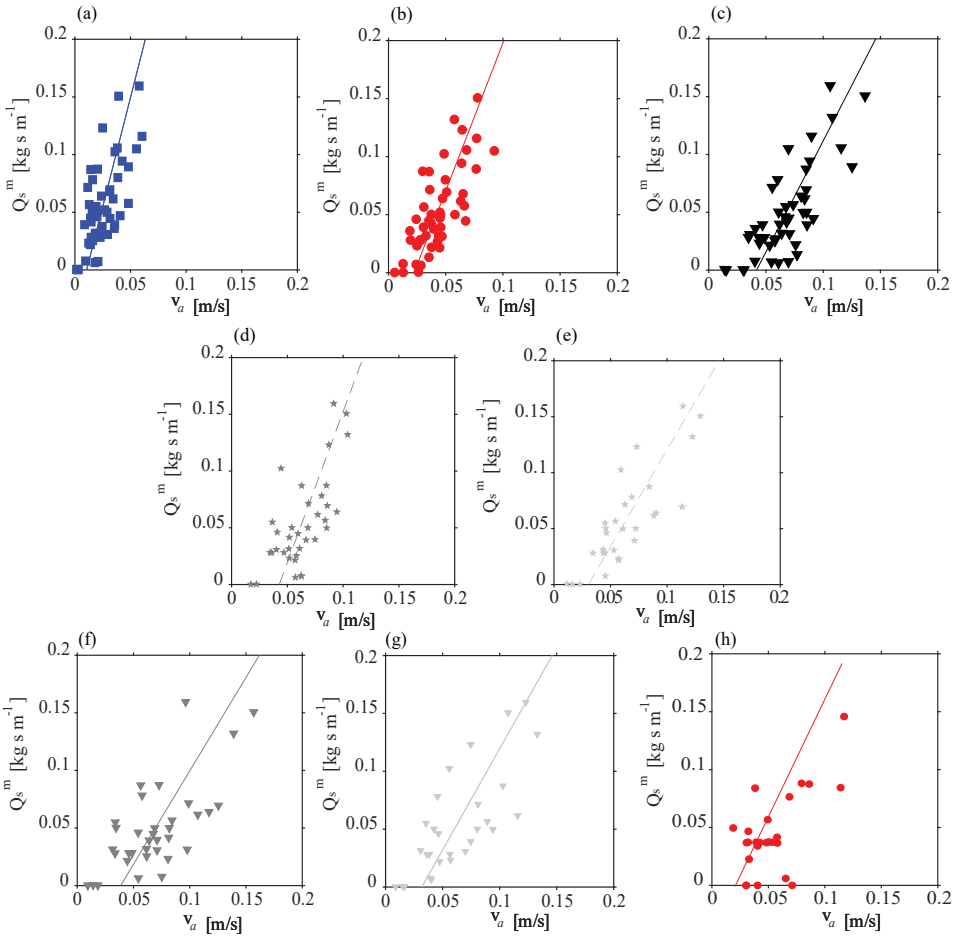

Figure 3.10: The apparent bedload velocity vs the bedload transport rate measured by the bedload sampler: *a*) 0.6 MHz; *b*) 1.2 MHz RioGrande *c*) 3 MHz RS; *d*); 1 MHz IC; *e*) 1 MHz PC; *f*) 3 MHz IC; *g*) 3 MHz PC; *h*) 1.2 MHz RiverPro, Albania

the measurements but also with higher std of the raw velocities. The major difference in the results was observed generally between different instruments (e.g., M9 and RioGrande), but not among the different configurations. A combination of different factors contributed for obtaining different apparent velocities by each instrument:

- Working frequency (f). It is one of the most important factors because the lower frequency is less attenuated (Medwin, Clay, 1998) and fully penetrates through the active layer which leads to a larger disturbance by the immobile particles (i.e., surface scattering) beneath the active bedload layer.

- Internal processing mechanism. It may be the the most important component that can influence the results independently from the frequency. Identification of the bottom related with the cell size can lead to different results, as seen in the UBERTONE experiment.

- Immobile sediment surface that lays beneath the mobile active layer. This includes eventual deformations of the riverbed that can deteriorate the signal. Beside the penetration of the lower frequencies each pulse portions (e.g., if BB configuration is used) arrive at the bottom at different instances due to the grazing angle and the inner edge (see, Fig.2.4) of the pulse spends more time in contact with the immobile surface. Logically longer pulses have a stronger contact with the immobile bed surface.

- The acoustic geometry and acoustic sampling. These are represented through the: pulse length (*Pl*), the wavelength (λ), beam focusing (z_c), grazing angle and the beam opening angle. All given and shown in Table 2.1 and Fig 2.4.

- Backscattering properties of the particles (e.g., see Fig. 2.6)

All these factors are mutually depended and various combinations contribute differently to the estimation of the Doppler velocity.
The results obtained in Albania (Fig. 3.10h) have the same characteristics as the 1.2 MHz in Germany, but the filtering procedure was heavier, resulting in more erroneous data due to the highly heterogeneous bedload transport and the wider PSD (see, Table 2.4). Besides, these measurements were not done in a fully fixed position, and the water depths and velocities varied from position to position, which also led to improper positioning of the sampler and potential human error.
A final interesting observation is the non-zero intersection of all linear regressions created in Fig 3.10. It is obvious that some times the ADCP registered velocity for deficient transport and this is in cases when the physical sampler failed to measure properly, or there was an armored layer, and the sand particles were moving fast on the top (e.g., similar to sandOver experiment in the lab results above).

3.2.2 The acoustic sampling effects

(*Paper II*)
The influence of the acoustic parameters (i.e, acoustic sampling) was analyzed through a simple principal component analysis (PCA). The main concept of PCA is to create new uncorrelated variables that successively maximize variance. The PCA was performed for the averaged parameters of the corresponding instrument used in the field campaigns in Germany. Five variables that are describing the acoustic geometry and explained in Ch.2 (*BP*, *FD*, v_a, λ, z_c) are included in the

analysis. Fig 3.11a shows that more than 60% of the variance is captured by the first principal component (PC1), and more than 20 % by the PC1. The third PC3 gives around 10% of the variance and will be excluded from the analysis. The second plot (Fig. 3.11b) explains that most of the observations related to each instrument/configuration are almost equally describing the PC1. On the other hand, the wavelength (λ), the pulse length (*Pl*), the beam focusing (z_c) and the apparent velocity (v_a) are the major contributors to the variance of the PC1 (Fig. 3.11b). The biplot (Fig.3.11c) shows a positive correlation among *Pl*, z_c and λ and a negative correlation with v_a. This explains the combined effect of the instrument geometric characteristic used to calculate z_c (i.e., ϕ, θ and D_t) and the acoustic instrument parameters (λ and *Pl*) towards the estimation of the apparent velocity. The *FD* appears also negatively correlated with the apparent velocity and contributes equally to both PC1 and PC2. *BP* and *FD* seem to contribute most to the formation of PC2, but they are negatively correlated, which means that using more pings would produce fewer errors. The *BP* contribution to the total variance is small and does not significantly influence the bedload velocity measurements.

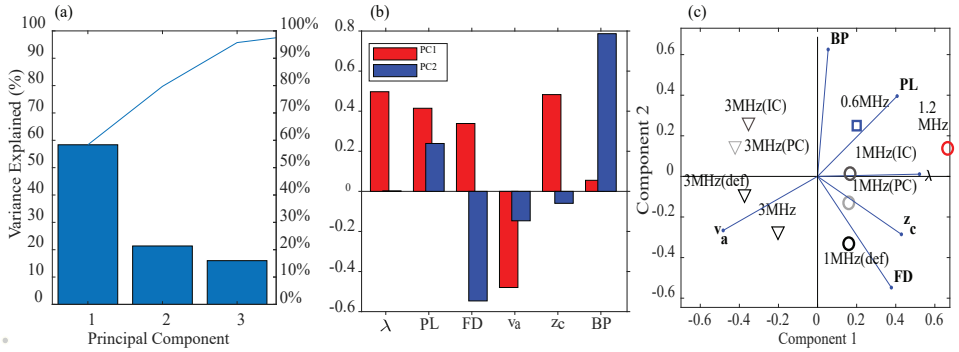

Figure 3.11: PCA analyses of the ADCP parameters. Some parameters are given in Table 2.1, while *FD*, v_a and z_c are calculated as average values from all point measurments out of all four campaigns; a) explains the importance of the principal components in the analysis and the total captured variance; b) The importance of each variable regarding the PC c) shows how the observations (instruments and configurations) are describing the components and it demonstrates the correlation between the analysed parameters.

3.2.3 The modeled transport rate

(*Paper II and Paper III*)

The ultimate goal of utilizing surrogate acoustic techniques in bedload measurements is to estimate the total transport rate. Given the apparent bedload velocity, the most convenient approach is applying the simple kinematic model (Eq. 2.2). The active layer thickness and the bedload porosity remain the most significant uncertainty, but in this study, the estimated kinematic model (Q_s^{ADCP})

is only used to qualitatively evaluate the apparent velocity measured by different instruments/configurations and at the same time to show the potential of future applications. The bedload concentration was calculated using the Van Rijn (1984) equation and the skin shear velocity related to the grain size (note that the total shear velocity given in Table 2.4 consists of the grain related shear and the drag force due to the bedforms). The n_k given in Eq. 2.2 was obtained by optimizing the minimum squared differences between the model and the physically measured transport rate.

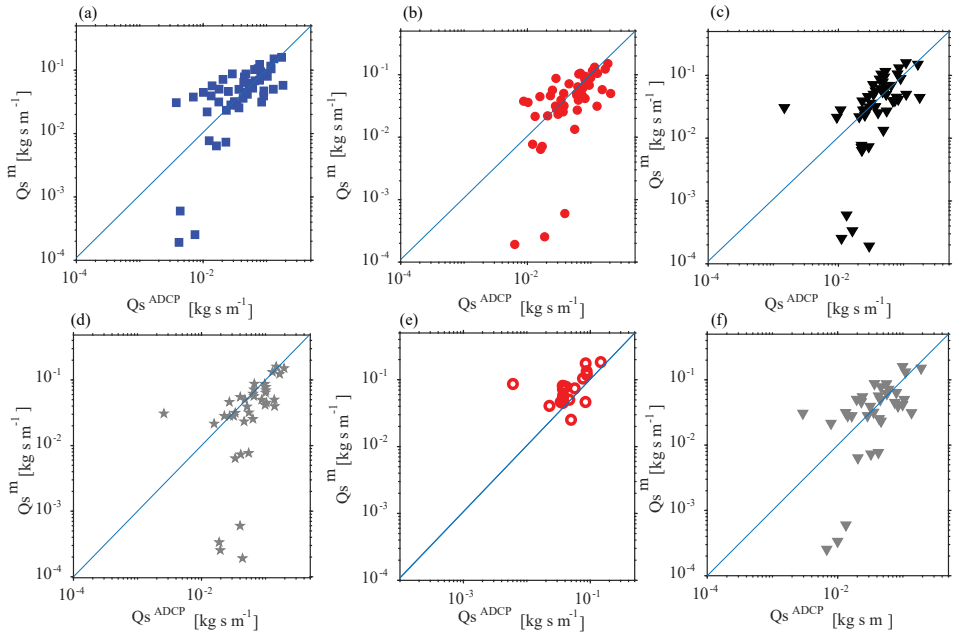

Figure 3.12: The bedload transport rate measured by the bedload sampler (Q_s^m and the ADCP moddeled bedload transport rate (Q_s^{ADCP}) : *a*) 0.6 MHz; *b*) 1.2 MHz RioGrande; *c*) 3 MHz RS; *d*) 1 MHz IC; *e*) 1.2 MHz RiverPro, Albania; *f*) 3 MHz IC;

After the optimization, the modeled bedload transport rate matched very good the physically measured transport rate for all instruments and configurations, yielding correlation coefficients above 0.7 (Fig. 3.12). The worst matching was obtained for the 0.6 MHz (Fig. 3.12a) and the best fitting was obtained for the 1 MHz and 3 MHz (Fig. 3.12d and Fig. 3.12f). Fig. 3.12e shows that the Q_s^{ADCP} overestimated the Q_s^m, which was not the case for Fig. 3.12e, although the same frequency is used. The results estimated from the measurements conducted in Albania slightly differed because the bedload concentration (c_s) was calculated using the shear velocity obtained from the the local log-law fitting, which could overestimate the

grain-related shear stress due to presence of bedforms and bed irregularities. Besides, the captured transport rate in Albania resulted in wider PSD that additionally complicated the bedload concentration assumption. In the previous sections, it was explained that apparent velocity measurements of each instrument depend on the acoustic geometry and acoustic sampling. The optimized coefficient (n_k), gave the highest values for the 0.6 MHz ($n_k \approx 18$) and the lowest for the 3 MHz ($n_k \approx 3$). This implies that the sampling was much shallower for the 3 MHz and scattered mostly from the top of the active layer; whereas the 0.6 MHz fully penetrated the active layer and gave rather unrealistic values for the thickness of the bedload active layer.

The outliers that correspond to a significant overestimation of the Q_s^{ADCP} (see, Fig. 3.12) are associated with measurement positions where the riverbed was artificially armored (e.g., close to the banks and bridges). At these positions it was observed on the cameras that there was not a significant bedload transport except a very thin layer of sand and organic material passing over the armored bed. In this case the ADCPs most likely measured the velocity of that rather dilute sand layer. The armored layer prevented the formation of dunes, resulting in lower transport rates (i.e., low bedload concentration) and relatively high particle velocities, corresponding to the flow strength. The laboratory experiments denoted as sandOver (see, Fig. 3.2) confirmed the same.

Chapter 4

Conclusions and Future Research

4.1 Final Conclusions

This study verified that ADCPs are able to measure the bedload velocity and that the corrected BS strength is sensitive to the bedload concentration and the PSD. The laboratory investigations confirmed that the 3 MHz frequency (M9, Sontek, all configurations) delivered a spatially averaged bedload velocity (including both the mobile particles in the active layer and the immobile particles beneath). The spatial averaging assumption was also validated for the 1 MHz (M9), but only for the PC configuration. On the other hand, the 1 MHz IC demonstrated rather different results for various bedlaod transport conditions, performing shallower sampling and yielding higher velocities in the laboratory tests. On the contrary, in the field experiments the IC and PC resulted in spatially averaged velocity for both frequencies. This bore out the limitations of the IC configuration such as the cell-size, gate profiling, pulse length, distance to bed, etc.
The RDI SPro showed high correlation with transport rates, but it underestimated the spatially averaged apparent velocity by 2-5 times for the sand experiments and up to 20 times for the gravel data. This underestimation was assigned to the stronger impact of the immobile bedload surface, which is more dominant in the RDI configurations due to the specific signal processing (i.e., BB and the possibility of high-resolution gate-ranging).
In general, by filtering out the extreme velocities and velocities in the opposite direction of the water flow, the uncertainty of the apparent bedload velocity decreased from 10% to 30%, depending on the instrument, hydraulic conditions and bedload material. The filtered data was negatively correlated with transport rate intensity, or more precisely with the number of mobile particles. Higher filtering percentage was also noticed for the highly sporadic transport conditions (e.g., gravel experi-

ments) and measurements where the surface scattering had a dominant influence in the echoes (lower frequencies, longer pulses, etc.). Thus, the high percentage of discarded data (60-95 %) could be understood as an indicator of low data quality and weak bedload transport conditions. The oppsote stands for lower percentage of discarded data (10-50 %).

The mono-static sonar system and their specific acoustic geometry (i.e., pules length, transducers diameter, beam opening, distance to the bed, grazing angle, etc.) significantly influenced the acoustic sampling of the bedload material. The beam focusing or z_c was derived from these parameters to describe the acoustic sampling effect. Larger z_c and longer pulses indicated more influence of the immobile bed and underestimated the apparent bedload velocities.

In general, the lower frequency instruments gave lower apparent bedload velocities, because they are less attenuated, penetrate the active bedload material and induce more surface scattering in the echoes. Also, the lower frequencies have longer wavelengths that produce coarser cell-resolution, thus more deviations in the data. However, the M9 1 MHz gave higher velocities and less filtered data than the 2 MHz and 1.2 MHz RDI, which pointed out that the internal processing of the instruments is a key factor for the diversity in the results. Moreover, the IC configuration of the M9, in laboratory conditions, measured velocities similar to the camera velocities (i.e., mean surface velocities of the bedload) because the center of the cell that identifies the sediment bed (i.e., the cell where bedload velocities are actually measured) coincided with the top of the active layer and had very low impact from the immobile bed beneath. This exclusively depends on the pulse length and the profiling resolution (e.g., echo-gating). The other signal processing methods (BB and PC) can produce finer resolution (e.g., smaller cells and shorter pulses) which permits deeper acoustic sampling. Nevertheless, many parameters and thresholds remained unknown to fully examine the influence of internal instrument processing.

The BS strength derived from the sonar equation and adapted for riverbed conditions was tested, only in laboratory condition. The corrected BS strength values observed by the M9 showed high correlations with the bedload transport rate, but the SPro was almost insensitive towards any changes in the bedload transport conditions. The SPro also yielded the highest BS strengths, which complies with the strong surface scattering effect and underestimation of the apparent velocities.

The BS strength measured by all three frequencies (3 MHz, 1 MHz, and one vertical 0.5 MHz) of the M9 declined as the bedload transport rate increased. The BS strength gave similar trends to the bedload concentration, despite the used material and the apparent velocity, which actually affirmed that the ADCPs could deliver additional information about the bedload transport transport conditions.

The BS strength also gave different magnitudes for the gravel and the sand data,

accompanied by a slightly different probability distribution of the echoes. The BS strengths were more distinguishable for the vertical beam and could contribute for a rough characterization of the bedload material.
Finally, the ADCP data from gravel experiments gave larger deviations and outliers due to the highly heterogeneous motion of particles, as well as the more intensive hydraulic conditions, that produced more turbulence and bubbles in the water. The data from the sand experiments was more consistent, but the risk of water bias be present in the signal (note that in this study the water bias was not an issue).

4.1.1 Recommendations and Guidelines

The following recommendations and guidelines should be considered for stationary bedload measurements using acoustic Doppler devices:

- The total sampling time could be adjusted to less than five minutes if the bedload is abundant (e.g., sandy riverbed). When dealing with wide PSD and gravel bedload material, it is recommended longer sampling time, more than ten minutes. Moreover, if the hydraulic conditions are extreme (high Fr or Re number), longer sampling times are recommended (e.g., more than 10 minutes).

- The higher frequencies (3 MHz) should be used in cases of lower depths than five meters and low suspended sediment concentrations.

- It is recommended the raw data to be filtered and de-spiked, independently of the used instrument.

- The RDI instruments have internal processing technique that can yield finer resolutions, but it also uses longer pulses for the BT mode; thus RDI always underestimates the spatially average velocities.

- Coarser cell resolution (i.e., echo profiling) is expected for the IC configuration; thus a more uncertain identification of the riverbed. Therefore it is not recommended for any measurements of the bedload, and if it is the only option it should be used for water levels higher than 1 m.

- In the field campaigns, it is crucial to avoid sampling of the beams in regions with different bedload transport conditions. For example, ADCP BT measurement of the bedload should be carefully conducted in rivers with severely deformed bed and/or steep slopes. Measuring close to the river banks should be carefully done, due to the low transport and possible immediate change of the cross-sectional slope.

- The particles moving above an armored or immobile bed are registered by the ADCPs. Such an environment has very low bedload concentration and the velocity does not correspond to the transported masses. It is especially problematic when sand moves on the top of gravel bed; in this case, the concentration is similar to the one of the sand moving on the crest of the dune, but the transported material in bedforms has much higher yield.
- If the BS strength values are used, they should be corrected following the modified sonar equation (e.g., Eq. 2.6). If some variables are not available, reasonable assumptions should be done according the field conditions and following the instrument manuals. Users should pay attention to the local slopes of the bed and apply the slope corrections in the sonar equation. The ambient noise could influence the results; thus, it should be considered in the derivation of the BS strength.
- The BS strength might be used for identification of the D_{50}, but only after testing the instrument in laboratory and identifying reference BS strength values. The results from the vertical beam (e.g., 0,5 MHz) delivered most distinguishable values between different sediment materials.
- The BS strength obtained from the M9 is sensitive to the bedload concentration. It can be used to indicate the bedload concentration additionally to the apparent bedload velocity. It is crucial to define the reference values of the BS strength in calm conditions without any bedload transport, which would act as a calibration of the transducers sensitivity if the manufacturer does not supply one. Nevertheless, this correlation between the bedload concentration and the BS strength should used carefully before further evaluation tests are performed in field conditions.

4.2 Future work

In this study, the apparent bedload velocity measured by different commercially available ADCPs was examined in details. The BS strength sensitivity towards different bedload transport conditions was tested, and affirmed an evident correlation with the bedload concentration.
Future research should focus on developing functional relations between the BS strength and the apparent bedload velocity to determine the bedload transport rate efficiently (e.g., $Q_s = f(v_a, B_s)$). In addition, more analysis should be performed on the BS strength data obtained from the field and laboratory campaigns to validate the correlations with the bedload PSD and concentration.
Full-step methodology should be defined on the basis of the methods and concepts given in this study, which should enable accurate estimation of the bedload masses

passing through an entire river cross-section.
The internal processing of each instrument was pointed out as the major source of uncertainty in the ADCP data. This implies the necessity of closer collaboration with the manufactures of the ADCPs. In fact, the internal instrument processing of the raw echoes and Doppler velocities should be adjusted for bedload transport rate estimation (i.e.,accurate apparent bedload velocity and BS strengths from the active bedload layer). In addition, experiments for echo calibration of the transducers should be performed in collaboration with the developers of the instruments in order to avoid the uncertainty from the unknown parameters. Note that the ambient noise should also be taken into consideration for the BS strength estimations and transducers calibration.
Furthermore, the concept of bi-static acoustic transducers could overcome numerous problems of the mono-static geometry, such as the side-lobe effect, acoustic sampling, higher echo profile resolution. Therefore, it should be examined in details and the possibility of deploying the bi-static system in field applications for bedload measurements should be also considered as new concept for even more accurate data.

Bibliography

Bagnold F. R. S. R.A. The flow of cohesionless grains in fluids // Philosophical Transactions of the Royal Society of London A: Mathematical, Physical and Engineering Sciences. 1956. 249, 964. 235–297.

Bagnold R. A. An empirical correlation of bedload transport rates in flumes and natural rivers // Proceedings of the Royal Society of London A: Mathematical, Physical and Engineering Sciences. 1980. 372, 1751. 453–473.

Underestimation of sand loads during bed-load measurementsâĂŤa laboratory examination. // . 06 2016. 1036–1041.

Blanckaert Koen, Heyman Joris, Rennie Colin. Measuring Bedload Sediment Transport with an Acoustic Doppler Velocity Profiler // Journal of Hydraulic Engineering. 2017. 143, 6. 04017008.

Brumley B. H., Cabrera R. G., Deines K. L., Terray E. A. Performance of a broadband acoustic Doppler current profiler // IEEE Journal of Oceanic Engineering. Oct 1991. 16, 4. 402–407.

Dietrich William E. Settling velocity of natural particles // Water Resources Research. 1982. 18, 6. 1615–1626.

Dinehart R.L., Burau J.R. Repeated surveys by acoustic Doppler current profiler for flow and sediment dynamics in a tidal river // Journal of Hydrology. 2005. 314, 1. 1 – 21.

Drake Thomas G., Shreve Ronald L., Dietrich William E., Whiting Peter J., Leopold Luna B. Bedload transport of fine gravel observed by motion-picture photography // Journal of Fluid Mechanics. 1988. 192. 193âĂŞ217.

Einstein H.A. The Bed-load Function for Sediment Transportation in Open Channel Flows. 1950. (Technical bulletin (United States. Dept. of Agriculture)).

Engelund Frank, Fredsøe Jørgen. A Sediment Transport Model for Straight Alluvial Channels // Hydrology Research. 1976. 7, 5. 293–306.

Fernandez-Luque R., Beek R. Van. Erosion And Transport Of Bed-Load Sediment // Journal of Hydraulic Research. 1976. 14, 2. 127–144.

Frings Roy M., Vollmer Stefan. Guidelines for sampling bedload transport with minimum uncertainty // Sedimentology. 2017. 64, 6. 1630–1645.

Gaeuman David, Jacobson Robert B. Acoustic bed velocity and bed load dynamics in a large sand bed river // Journal of Geophysical Research: Earth Surface. 2006. 111, F2.

Gaweesh Moustafa, Van Rijn Leo. Bed-Load Sampling in Sand-Bed Rivers // Journal of Hydraulic Engineering-asce - J HYDRAUL ENG-ASCE. 12 1994. 120.

Geay T., Belleudy P., Gervaise C., Habersack H., Aigner J., Kreisler A., Seitz H., Laronne J. B. Passive acoustic monitoring of bed load discharge in a large gravel bed river // Journal of Geophysical Research: Earth Surface. 2017. 122, 2. 528–545.

Gimbert Florent, Tsai Victor C., Lamb Michael P. A physical model for seismic noise generation by turbulent flow in rivers // Journal of Geophysical Research: Earth Surface. 2014. 119, 10. 2209–2238.

Guerrero M., Di Federico V. Suspended sediment assessment by combining sound attenuation and backscatter measurements - analytical method and experimental validation // Advances in Water Resources. III 2018. 113. 167–179.

Guerrero Massimo, Szupiany Ricardo N., Latosinski Francisco. Multi-frequency acoustics for suspended sediment studies: an application in the Parana River // Journal of Hydraulic Research. 2013. 51, 6. 696–707.

Hager W.H. Du Boys and sediment transport // Journal of Hydraulic Research. 2005. 43, 3. 227–233.

Hergault Virginie, Frey Philippe, Métivier François, Barat Cécile, Ducottet Christophe, Böhm Tobias, Ancey Christophe. Image processing for the study of bedload transport of two-size spherical particles in a supercritical flow // Experiments in Fluids. Nov 2010. 49, 5. 1095–1107.

Hsu Leslie, Finnegan Noah J., Brodsky Emily E. A seismic signature of river bedload transport during storm events // Geophysical Research Letters. 2011. 38, 13.

Hu Chunhong, Hui Yujia. Bed-Load Transport. I: Mechanical Characteristics // Journal of Hydraulic Engineering. 1996. 122, 5. 245–254.

Hubbell D. W. Apparatus and Techniques for Measuring Bedload. 1964. Paper 1748.

Hurther D., Thorne Peter D. Suspension and near-bed load sediment transport processes above a migrating, sand-rippled bed under shoaling waves // Journal of Geophysical Research: Oceans. 2011. 116, C7.

Jackson Darrell, Richardson Michael. High-Frequency Seafloor Acoustics. 2007.

Jamieson Rennie C. D. Ramooz R. E. C. Validation of aDcp bedload transport measurements. // Proc. 2008 River Flow Conf. KUBABA Congress Dept. and Travel Services Cesme, Turkey, 2008. 2343âĂŞ2351.

Keshavarzy A., Ball Je. An application of image processing in the study of sediment motion // Journal of Hydraulic Research. 1999. 37, 4. 559–576.

Keulegan Garbis H. LAWS OF TURBULENT FLOW IN OPEN CHANNELS // Part of Journal of Research of the National Bureau of Standard. 1938. 21. 707–741.

Lajeunesse E., Malverti L., Charru F. Bed load transport in turbulent flow at the grain scale: Experiments and modeling // Journal of Geophysical Research: Earth Surface. 2010. 115, F4.

Lajeunesse Eric, Devauchelle Olivier, Lachaussée F., Claudin P. Bedload Transport in Laboratory Rivers: the Erosion-Deposition Model // Gravel Bed Rivers 8 - Gravel Bed Rivers and Disasters. Kyoto and Takayama, Japan, IX 2015.

Latosinski Francisco Guillermo, Szupiany Ricardo NicolÃąs, Guerrero Massimo, Amsler Mario Luis, Vionnet Carlos. The ADCP's bottom track capability for bedload prediction: Evidence on method reliability from sandy river applications // Flow Measurement and Instrumentation. 2017. 54. 124 – 135.

Lee HongâĂŘYuan, Hsu InâĂŘSong. Investigation of Saltating Particle Motions // Journal of Hydraulic Engineering. 1994. 120, 7. 831–845.

Medwin Herman. Sounds in the sea : from ocean acoustics to acoustical oceanography. Cambridge: Cambridge University Press, 2005.

Medwin Herman, Clay Clarence S. Chapter 2 - Sound Propagation // Fundamentals of Acoustical Oceanography. San Diego: Academic Press, 1998. 17 – 69. (Applications of Modern Acoustics).

Moate Benjamin D., Thorne Peter D. Measurements and inversion of acoustic scattering from suspensions having broad size distributions // The Journal of the Acoustical Society of America. 2009. 126, 6. 2905–2917.

Moore Stephanie A., Dramais Guillaume, Dussouillez Philippe, Coz Jerome Le, Rennie Colin, Camenen Benoit. Acoustic measurements of the spatial distribution of suspended sediment at a site on the Lower Mekong River // Proceedings of Meetings on Acoustics. 2013. 19, 1. 005003.

Backscatter Estimation Using Broadband Acoustic Doppler Current profilers-Updated. // . 1. July 2017.

Nino Yarko, Garcna Marcelo, Ayala Luis. Gravel saltation: 1. Experiments // Water Resources Research. 1 1994. 30, 6. 1907–1914.

Papanicolaou Athanasios N., Diplas Panayiotis, Balakrishnan Mahesh, Dancey Clinton L. Computer Vision Technique for Tracking Bed Load Movement // Journal of Computing in Civil Engineering. 1999. 13, 2. 71–79.

Parker Gary. 1D SEDIMENT TRANSPORT MORPHODYNAMICS. 2004. (Morphodynamics Web Page).

RDInstruments . Acoustic Doppler Current Profiler Principles of Operation A Practical Primer. 14020 Stowe Drive Poway, California 92064, 2011.

Radice A., Malavasi S., Ballio F. Solid transport measurements through image processing // Experiments in Fluids. Nov 2006. 41, 5. 721–734.

Ramooz R., Rennie C. D. Laboratory measurement of bedload with an ADCP. Reston, VA, 2008.

Rennie Colin D., Church Michael. Mapping spatial distributions and uncertainty of water and sediment flux in a large gravel bed river reach using an acoustic Doppler current profiler // Journal of Geophysical Research: Earth Surface. 2010. 115, F3.

Rennie Colin D., Millar Robert G. Measurement of the spatial distribution of fluvial bedload transport velocity in both sand and gravel // Earth Surface Processes and Landforms. 2004. 29, 10. 1173–1193.

Rennie Colin D., Millar Robert G., Church Michael A. Measurement of Bed Load Velocity using an Acoustic Doppler Current Profiler // Journal of Hydraulic Engineering. 2002. 128, 5. 473–483.

Rennie Colin D., Villard Paul V. Site specificity of bed load measurement using an acoustic Doppler current profiler // Journal of Geophysical Research: Earth Surface. 2004. 109, F3.

Rennie Vericat D. C., Williams Richard. D., Brasington James, Hicks Murray. Calibration of Acoustic Doppler Current Profiler Apparent Bedload Velocity to Bedload Transport Rate // Gravel-Bed Rivers: Process and Disasters. 2017. 8, 209–231.

Rickenmann D., McArdell B. W. Continuous measurement of sediment transport in the Erlenbach stream using piezoelectric bedload impact sensors // Earth Surface Processes and Landforms. 2007. 32, 9. 1362–1378.

Rickenmann Dieter, Turowski Jens M., Fritschi Bruno, Klaiber Angela, Ludwig Andreas. Bedload transport measurements at the Erlenbach stream with geophones and automated basket samplers // Earth Surface Processes and Landforms. 2012. 37, 9. 1000–1011.

Shields A. Application of similarity principles and turbulence research to bedload movement. Berlin, 1936.

Shields F. Douglas. Aquatic Habitat Bottom Classification Using ADCP // Journal of Hydraulic Engineering. 2010. 136, 5. 336–342.

Thorne Peter D., Meral Ramazan. Formulations for the scattering properties of suspended sandy sediments for use in the application of acoustics to sediment transport processes // Continental Shelf Research. 2008. 28, 2. 309 – 317.

UBERTONE . UB-Lab - The versatile ultrasonic profiler. 2016.

Urick R.J. Principles of Underwater Sound. 1983.

Van Rijn Leo. Sediment Transport, Part I: Bed Load Transport // Journal of Hydraulic Engineering. 1984. 110, 10. 1431–1456.

Williams R. D., Rennie C. D., Brasington J., Hicks D. M., Vericat D. Linking the spatial distribution of bed load transport to morphological change during highâĂŘflow events in a shallow braided river // Journal of Geophysical Research: Earth Surface. 2015. 120, 3. 604–622.

Graphics Gems IV. // . San Diego, CA, USA: Academic Press Professional, Inc., 1994. Contrast Limited Adaptive Histogram Equalization, 474–485.

Paper *I*

Laboratory investigation of the apparent bedload velocity measured by ADCPs under different transport conditions

Slaven Conevski, Massimo Guererro, Nils Ruther, Colin D. Rennie

Journal of Hydraulic Engineering, 2019

Laboratory investigation of the apparent bedload velocity measured by ADCPs under different transport conditions

Slaven Conevski[1], Massimo Guererro[2], Nils Ruther[3], and Colin D. Rennie[4]

[1]Department of Civil and Environmental Engineering, Norwegian University of Science and Technology,SP Andersens veg 5, 7491, Trondheim, Norway. E-mail: slaven.conevski@ntnu.no, slaven.conevski2@unibo.it

[2]Department of Civil, Chemical, Environmental, and Materials Engineering, University of Bologna, Via Terracini 28, 40131, Bologna Italy. E-mail: massimo.guerrero@unibo.it

[3]Department of Civil and Environmental Engineering, Norwegian University of Science and Technology,SP Andersens veg 5, 7491, Trondheim, Norway. E-mail:, nils.ruther@ntnu.no

[4]Department of Civil Engineering, University of Ottawa, 161 Louis Pasteur St. Colonel By building, office A, ON, K1N 6N5,Ottawa, CANADA. E-mail:Colin.Rennie@uottawa.ca

ABSTRACT

Several studies have investigated the use of the bottom tracking (BT) mode of acoustic current Doppler profilers (ADCPs) for evaluating bedload transport. The raw apparent bedload velocity is usually noisy and contains erroneous data. This study investigates how bedload dynamics influence acoustic processes occurring at the riverbed (i.e., volume and roughness scattering). The accuracy of ADCPs apparent bedload velocity measurements is analyzed in two sets of laboratory experiments using two ADCPs working at different frequencies (2MHz RDI StreamPro and 3MHz SonTek M9), with a variety of sediment materials and different hydraulic conditions. Simultaneously, the velocity and surface concentration of the mobile sediments are measured using high-resolution cameras. De-spiking and filtering are applied to the raw data and the temporal average of the apparent bedload velocity is spatially normalized. The percentage of filtered erroneous velocity data from the ADCP

time series demonstrates a strong correlation with the surface concentration of the mobile particles. Velocities measured with the M9 matched the particle velocities measured by image velocimetry better than those measured with the StreamPro, which appeared to underestimate the bedload velocity by a factor of 2-4. This suggests that instruments with different acoustic frequency yield a different interpretation of the apparent velocity; instruments with lower acoustic frequency and larger acoustic sampling length are more affected by the fixed surface beneath the layer of moving particles. These results bear out that the filtered apparent bedload velocity can be used to estimate the spatial velocity of the bedload, but its dependence on a set of acoustic properties has to be further investigated.

INTRODUCTION

The notoriously difficult description of bedload transport in a fluvial environment was a research goal of many scientists in the previous century. Du Boys initially developed the first theoretical and rational approaches for sediment transport in the 19th century (Hager 2005). Later, many scientists worked on estimating the transport rate by developing an equation that would describe the sediment flux (Einstein 1950; Bagnold 1956; Engelund and Fredsøe 1976; Fernandez-Luque and Beek 1976; Bagnold 1980). All of the equations involve a similar dependence on the forcing flow (usually shear stress or the Shields number and its threshold value), as well as characteristics of the particles or the particle Reynold Number (R_{e_p}). There are many bedload transport equations, but still, there are large uncertainties and differences between the values yielded from the equations and the observed values. Bedload transport is mostly a site-specific problem and if an empirically or physically based equation is used it is recommended to be confirmed with observed data. On the other hand, the traditional measuring approach deploys bedload samplers at some point of the river reach. The bedload samplers disturb the original hydraulic conditions once they are laid on the riverbed and require hard manual labor and organization effort. Also, due to spatial variation and the temporal fluctuations inherent in bedload transport, a large number of bedload samples is required to characterize the mean transport at a section (Frings and Vollmer 2017). Based on the preceding discussion, it can also be seen that the traditional physical sampling techniques cannot

collect continuous and statistically sound data of bedload transport rates.

One proposed option is the use of hydroacoustic instruments, which provide non-intrusive measurements, are easily deployable, and offer detailed data. ADCPs (acoustic Doppler current profilers) are range-gated monostatic-coherent acoustic sensors that employ Doppler shift of backscattered sound to measure water velocity components along multiple beams. These instruments were originally designed to measure water velocities and discharge, but have also been applied for measurements of suspended sediment fluxes based on backscattered sound intensity (Dinehart and Burau 2005; Guerrero and Lamberti 2011; Guerrero et al. 2016; Guerrero and Di Federico 2018). The backscattering echo intensity and the attenuation of the emitted ADCP pulse have also been used to estimate the suspended load and the grain size (Simmons et al. 2010; Sassi et al. 2011; Guerrero et al. 2013; Moore et al. 2013).

The measurements of the riverbed velocity using the ADCP bottom tracking (BT) mode was initially introduced in Rennie et al. (2002), using a commercial ADCP. This technique utilizes the BT bias, defined as ($v_a = v_{gps} - v_{bt}$) the difference between the true GPS boat velocity v_{gps} and the BT velocity v_{bt} delivered by the acoustic pulse backscattered from the river bed. This velocity is usually denoted as the apparent bedload velocity. Several studies have demonstrated a significant site-specific correlation between the averaged apparent velocity and the bedload transport from physical samples (Rennie and Villard 2004; Gaeuman and Jacobson 2006; Rennie et al. 2017). The apparent bedload velocity was successfully used for mapping the bedload transport velocity in sand and gravel environments, using some smoothing and interpolating techniques (Rennie and Millar 2004). Recently, some other site-specific studies (Rennie and Church 2010; Jamieson et al. 2011; Williams et al. 2015; Rennie et al. 2017) have utilized the BT signal to evaluate the reliability of ADCP bed velocity measurements for a range of sediment transport environments. In some of the studies, the analysis of the BT signal considers the effect of the instrument frequency and the pulse length (Ramooz and Rennie 2008). Shorter pulses give more accurate velocity data due to reduced influence of "water bias" associated with near-bed suspended load (Rennie and Villard 2004). In an ADCP comparison study on the Parana River, Latosinski et al. (2017) found that the

lower frequency ADCP consistently gave smaller apparent bedload velocities due to the frequency dependence of the particles, scattering regime. Others have attempted to derive analytically a relation between the real bedload particle velocity and the apparent bedload velocity (Gaeuman and Jacobson 2006) or to de-convolve the error from the real signal measured in moving bed conditions (Rennie and Millar 2007).

In the St. Anthony Falls Laboratory at the University of Minnesota, several bedload experiments were performed using video cameras, bed load samplers, and automatic weigh pans to test the capabilities of ADCPs for measuring bedload velocity (Jamieson 2008; Ramooz and Rennie 2008). Jamieson (2008) compared the apparent bedload velocity with the concentration of the bed load transport using the videography technique introduced by Papanicolaou et al. (1999) and Keshavarzy and Ball (1999), later advanced by Radice et al. (2006), where the surface concentration of the particles is calculated by image subtraction and the velocity by a particle image velocimetry (PIV) technique. As could be expected, Jamieson (2008) obtained a high correlation between the surface concentration and the apparent velocity. Most recently, Blanckaert et al. (2017) in a study conducted in laboratory conditions found a strong correlation between the near-bed acoustic signal from a custom made acoustic profiler and the particle velocity calculated from video imagery using the optical flow (Lucas and Kanade 1981) and particle tracking velocimetry (PTV) methods. The latter studies show that new camera technology can be efficiently used in measuring the surface velocity and concentration of the bedload in laboratory conditions and that an acoustic Doppler velocity profiler has the potential capability of estimating the bedload velocity.

Nevertheless, it remains unknown whether the ADCP-BT mode is a reliable and accurate way of measuring the bedload velocity. The authors are not aware of an existing study that examines the direct relation between the simultaneous measurements of the actual bedload velocity and the ADCP apparent bedload velocity. Therefore, this study focuses on direct measurement of the average velocity of bedload particles in laboratory conditions using high-resolution cameras and the apparent bedload velocity measured with ADCPs. More precisely, the average bedload velocity of the moving particles and the percentage of the moving particles in a certain region of interest

(ROI) were measured by the cameras.

ADCPs usually have four ultrasound transducers of a high frequency *(f)* and short wavelength (λ). The ultrasound waves are generated in pulses (intermittent trains of pressure) that may consist of 5-20 cycles of the same frequency. One ping comprises the pulse duration, the blanking time, and the processing time. A Broadband ADCP transmits two or more sets of pulses in sequence. The BT signal is a separate acoustic signal, characterized by longer pulses and smaller number of pings than the water profile signal. The broadband principle and the basic sonar equation for the returned BT signal intensity from the riverbed are explained in detail in Appendix I, including all the scattering processes occurring in the water column and the river bottom.

The ADCP pulse insonifies a relatively large area (actually, a volume, see Rennie et al. (2017)) of the flume, covering many particles. The sampling area depends on the transducer width, the beam spreading angle, the grazing angle and the distance to the bottom (Rennie et al. 2002; Rennie et al. 2017). The four-velocity measuring beams from the four transducers are spaced at 90° relative azimuth and projected on vertical angles (θ). If the non-linearity is simplified and considering a rectangular uniform pulse, the sampling areas would be quasi-ellipses centered at a horizontal distance $H_t \tan(\theta) + r_{adcp}$. The r_{adcp} term is the transducer radius, and H_t is the vertical distance between the transducer and the bed. The total sampling volume is actually the sum of the four independent volumes located at the impingement points of the beams. In order to determine the height of the acoustic sampling above the bed, it is assumed that the receiving window results only from a reflection that includes the leading and the trailing edge of the pulse (Rennie and Millar 2004). Each of the incident ultrasound pulses reflects from the riverbed in a different way, depending on the instrument frequency, the particle size distribution (PSD), and the transport conditions. The pulse passes through the active layer and it is reflected from the surface layer of the bed load. In underwater acoustics, the bottom scattering can be categorized in two types: surface scattering and volume scattering, each involving its own mechanism of reflecting the ultrasound wave (Jackson and Richardson 2007). It is not clear if this categorization is useful for gravel-sized riverbeds, but it distinguishes important processing of the scattering phenomena. Usually, the riverbed is

highly irregular with different sediment dynamics. The bed scattering most likely depends on those irregularities, sediment characteristics and water-sediment interference. Accordingly, it can be assumed that the mobile volume of the bed (i.e. the active layer) could be associated with *volume scattering,* while the immobile or potentially mobile with *rough surface scattering* (Fig. 1).

Low suspended sediments concentration (SSC) and low and constant water depth for each experiment repetition permit the assumptions of constant losses in the water column and no water bias in the Doppler shift frequency (Rennie et al. 2002). Additionally, assuming that the surface of the immobile particles is acoustically impermeable, the sonar equation of the returned signal (see Appendix I, Eq.7) can be modified for the bottom track signal intensity (Ir_{BT}). Given the low water depths and minimal SSC, the spreading losses and attenuation in the water column are considered to be negligible. Furthermore, the active layer thickness (R_{at}), which varies between experiments, is conveniently substituted for the slant range to the bottom (R).This is because volume scattering is due to sediment particles saltating within the active layer (M_{at}). The sound attenuation coefficient α_{at} should incorporate the active layer concentration, similarly as it is described for the suspended sediment in the water column (Thorne et al. 1991). The final logarithmic form of the equations is:

$$Ir_{BT} = 10log(I_0K_p) + 10log(K_sA_r{}^2 + K_v{}^2M_{at}) + 10\log(\frac{c\tau_{pl}}{2}) - 40R_{at}\alpha_{at}log(e), \qquad (1)$$

where Ir_{BT} is the received signal intensity(the received echo from the riverbed), I_0 is the transmitted intensity, K_p is an instrument constant, τ_{pl} is the pulse duration and c is the speed of sound. The coefficient K_v is the volume scattering coefficient that depends on the frequency and the particle size distribution. M_{at} is the concentration of particles (Thorne et al. 1991) and K_s accounts for the surface reflection depending on the surface roughness, acoustic frequency and surface to beam inclination. The A_r^2 term is the variance of the surface of the rough bed which accounts for the phase reinforcement (i.e., Marsh (1963)'s theory), depending on the acoustic and bottom wavelength irregularities. K_v is described in several studies by the following equation:

$$\langle K_v \rangle = \frac{3\langle f_o \rangle^2}{16\pi\rho_s \langle a \rangle}\,, \tag{2}$$

where f_o is the mean normalized form factor (Thorne and Meral 2008; Moate and Thorne 2009), a is the mean radius of the particles taken from the number based PSD, ρ_s is the particle density, taken to be the value for quartz 2.65 cm^3/g. The form factor depends on the shape and size of the particles and the acoustic wavelength (Medwin and Clay 1998; Thorne and Meral 2008). The angular brackets denote the mean expected value of the variables. The neglected variables of the basic sonar equation (Eq.7, Appendix I) are taken as constant and included in the instrument coefficient K_p.

Equation 1 is essential for interpreting the influence of the immobile and the mobile particles in the insonified sampling volume. Theoretically, pulse reflection from immobile surface should not induce any Doppler shift in the BT backscattered signal. However, the measured apparent bedload velocity cannot be directly related to the backscattering sensitivity towards a certain PSD or bed morphology; in other words, the volume and surface scattering combine, eventually yielding unpredictable sensitivity to the actual moving particles. This study attempts to evaluate how the BT signal is changed in different sediment and hydraulic conditions that produce varying combinations of volume and surface scattering. Moreover, a relation is defined between the apparent velocities measured with different frequency ADCPs and the actual average bed load particle velocity. In the experiments, different particle size distributions (PSD) were used, attempting to produce different transport modes for a different acoustic response. The main objective is to analyze the ADCP BT velocity in different transport conditions. The following methods and results aim to explain the capability of the BT mode to measure the average bedload particle velocity; this includes distinguishing the influence in the returned signal of the immobile particles associated with the rough sediment surface scattering versus the mobile particles in the active layer that produce volume scattering.

METHODOLOGY

Experimental set up

The experimental campaign was divided into two experimental sets. The first experimental set was performed at the University of Ottawa (UOttawa) using a Sontek M9 ADCP (Sontek 2017), working on 3MHz. The aim was to test the high frequency ADCP response to different modes of bedload transport. The second experimental set was performed at the University of Bologna (UniBo) using a lower frequency, 2MHz StreamPro RDI (RDInstruments 2015), to test the lower frequency response towards different bedload velocities and concentrations. In the interpretation of the apparent velocity, it is important to mention that these instruments have different beam geometry, therefore different sampling areas. The beam slant angle is 20 degrees for StreamPro and 25 degrees for the M9, which has a larger diameter of the transducers (2.5 cm) comparing to the StreamPro (1.5 cm), but smaller half-beam spreading angle (1.3 degrees for M9 and 3.4 degrees for StreamPro). The pulse length for RDI is typically 20% of the water depth and for Sontek is variable between 5-20 cm depending on the water depth, which most likely resulted in the lower limit for about 40 cm of water depth in the UOttawa tests. Instrumental parameters are reported in Table 1.

The different bedload transport conditions were reached by using sediments with different particle size distribution (PSD) and by changing the water depth. In the first set of experiments, the 0.75 m wide flume had an active bedload length of 10m, the average water velocity above the sampling area varied between 0.75−0.9 m/s as the bed configuration changed during the experiments. Two poorly sorted materials with median diameters ($D50$) of 1 mm (sand) and 4 mm (gravel) were used to create six different test mixtures. The particle Reynolds number (Re_p) of the different mixtures ranged between 110 and 770 (Table 2). The dimensionless critical shear stress ($\tau*_{cr}$) for all the PSD was between 0.03-0.045. The second set of experiments had a discharge of 110 l/s and single PSD, having $D50$=1 mm and $D84/D10$ = 1.2. In this case, three different transport conditions were reached by simply emptying the flume, decreasing the water depth and increasing the water velocity (0.41 m/s for EXP1, 0.47 m/s for EXP2, 0.56 m/s for EXP3). At UOttawa six experiments were

repeated five times using the same hydraulic conditions and six different particle size distributions. At UniBo three experiments with different hydraulic conditions and the same PSD were repeated five times (Table 2). The preliminary calculation of the mean Shields number ($\tau*$) and the particle Reynolds number (Re_p) suggest that there is not any resuspension of the bedload material in the chosen hydraulic conditions (e.g Shields diagram, see Parker (2004)). Table 2 gives an overview of the hydraulic conditions and the mentioned parameters. The parameters were calculated with the equations given in Appendix II.

The scientific camera, IOI FLARE-2M360MCL, having a resolution of 2200x1080 pixels and an acquisition rate of 70 frames per seconds (fps), was suitable for measuring particles velocity in the first set of experiments characterized with high velocities. The cameras and the ADCPs were aimed at the same region, which later enabled a comparison of the two measurements. A GoPro4 action camera with 4k (3840x2160 pixels) resolution, maximum underwater field of view (FOV) of 94° and acquisition rate of 30 frames per second (fps) was used in the second set of experiments with lower velocity. Additionally, a special INON underwater wide close-up lens was mounted on the GoPro camera, and the light was enhanced in order to produce equal lighting throughout the sampling area. The light projectors were mounted underwater downstream, upstream, and from the sides in order to enhance the light from all the positions, while ensuring minimal flow disturbance in the test region. The ADCPs were installed looking downwards from a height of 25-35 cm above the sediment bed, and with 3-7cm^3 sampling area for each beam. The cameras were mounted slightly higher than the ADCP transducers, but still submerged under the water depth. A sketch of the experimental set-ups is given in Fig.2.

The apparent bedload velocity

The BT velocity in this study is calculated using only the downstream and upstream beams. The data for each beam were separately evaluated and it was concluded that the velocities from the beams perpendicular to the flow direction have negligible values close to zero, thus they were excluded for the final bedload velocity estimation. The noise in the ADCP measurements is present as bias and random errors (RDInstruments 2011). The bias is usually due to parameter

and system uncertainty, such as the speed of sound in water, the grazing angle of each beam, and transducer characteristics. The bias is always present and it cannot be filtered, thus the estimated ADCP velocity will always differ from the bedload velocity. Nevertheless, this bias does not affect significantly the apparent velocity measurements, particularly in stationary laboratory conditions (RDInstruments 2011). On the other hand, the heterogeneous motion of the bed load particles influences the random error. The wide velocity range and highly unsteady dynamics of rolling, sliding, vibrating and saltating particles cause uncorrelated echoes that burden the procedure of the post-processing. The uncorrelated backscattered signals give a wide spectrum of frequency that hinders the assessment of Doppler frequency shift (f_d). The possible aliasing of the signal can also lead to erroneous calculation of the apparent bedload velocity (e.g., internally processed Doppler velocity). Additionally, the backscattered signal depends on the immobile rough surface and on the thickness of the active layer. This variability of the reflected pulse train may result in bias and random errors in the apparent velocity calculation. The Doppler velocity is affected by the limitations of the instrument, the natural variability of the bedload transport and the scattering from the immobile bed surface. In its simplest form, it can be expressed as:

$$v_a = k_1 k_2 v_p \,, \tag{3}$$

where k_1 is the coefficient that accounts for the sparseness of the mobile sediments, and k_2 is a coefficient that depends on all of the above-mentioned instrument properties and the sediment transport variability, and v_p is the average velocity of the mobile particles. The simplest assumption is that k_1 is equal to the percentage of the mobile bed surface. In other words, the ADCP measurement of the apparent velocity signal also incorporates scatter from the immobile bed surface. The additional deviation between the bedload velocity and the apparent velocity was parameterized with the coefficient k_2, determined by fitting the ADCP versus videography data. Once k_1 is defined, k_2 is expected to be constant for certain hydraulic conditions, depending only on the bedload PSD and the instrument related parameters.

Image pre-processing

The unequal light sources, the water impurity and the requirements of the algorithm used for bedload velocity estimation necessitated pre-processing of the images (Fig.3a). The gray-level intensity histogram of the images was equalized using an algorithm that locally adapts the values and limits the contrast to a certain level in order to prevent an over-amplification of the intensity of some particles (Fig.3b). Specifically, the Contrast Limited Adaptive Histogram Equalization (CLAHE) (Zuiderveld 1994) algorithm was used to equally distributes the pixel intensities on locally chosen tiles of the image. Next, when an image is blurred, it means that a low-pass filter has corrupted the image. Thus, the second preprocessing technique removed the blurring effects due to the particle motion by means of a Wiener filter (Fig.3c) (Jin et al. 2003). Additionally, the Wiener filter reduced the noise that was introduced by CLAHE, particularly in the experiments where the light was very low (e.g. Fig.3). These effects were more visible for GoPro images due to the lower fps and bit rate. The last step in the pre-processing procedure was applied to enhance the edges of the particles and better define their shape for the subsequent analysis. This was accomplished by using a highpass unsharp mask filtering (Fig.3d). The parameters for the used techniques were optimized for the specific conditions of each experiment. In general, the sharpening and Wiener filter kernels did not exceed the minimum size of the particles in pixels and the sharpening method was only applied in cases where the motion of individual particles was identifiable.

Image change detection

The pre-processing procedure was followed by a technique called two-frame change detection, or simply image change detection. These algorithms assume detection of "meaningful" changes occurring in a scene by processing of images captured at different time instants. The final outputs are shapes of the objects that appeared, moved or changed in the considered time interval. Having the camera in a static position the algorithm assumes pixel-by-pixel comparison. The specific algorithm that was applied in our case is called background subtraction with a 2-frame background update. The procedure follows similar steps as the technique applied by Stefano et al. (2003). A very similar approach was used by Keshavarzy and Ball (1999), wherein after the change detections

the authors, manually estimated the bedload surface concentration and applied a similar FFT (Fast Fourier Transformation) cross-correlation method to define the velocity and direction of the particles. Radice et al. (2006) improved this technique by introducing some limiting parameters for detection of individual particles; specifically, automatic detection of the bedload concentration was achieved by defining an arbitrary intensity threshold. In the present study identification of individual particles was out of the scope and no labeling was performed. It was also noticed that in high-intensity transport the preprocessing of the images improved the quality of the velocity estimation. The main assumption is that after the pre-processing, the moving particles are the first visible layer of sediments, and they reflect the highest pixel intensities (Radice et al. 2006). Greater intensity is expected for moving particles because they are higher in the flow and therefore closer to the light source. This assumption was confirmed for the present analysis by manual counting of moving particles in some of the images. In each sequence of two frames, the particles had starting position in the first frame and end position in the second frame, thus the first one was considered as a background for the subsequent image:

$$Z_{i_{m,n}} = \begin{cases} I_{i_{m,n}} - I_{i-1_{m,n}} \; if \; I_{i_{m,n}} > I_{i-1_{m,n}} \\ 0 \qquad\qquad\qquad if \; I_{i_{m,n}} < I_{i-1_{m,n}} \end{cases} \tag{4}$$

The procedure was extended to the entire sequence of images to isolate the moving particles in each frame. The image changes denoted as $Z_{im,n}$ (see Fig.4, Eq.4) are derived from the subtraction of the frames $I_{i-1}$and I_i, where m, n are the pixel indexing. This technique was chosen to be the core of the velocity measurements for several reasons. Firstly, in all performed experiments more than 10% of the particles were mobile, thus no single particle tracking was theoretically possible. Second, no particle tracers were used and no uniform background conditions were applied, in order not to disturb the nature of the phenomena. Nevertheless, this technique suffers from some weaknesses, especially in the experiments with intensive movement and finer particles. In these cases, the change detection was not performed over single particle displacements, but over the

collective displacements of particles entrained as fluxes. These fluxes are characterized by brief, frequent and random patches of particles traveling over the flume bed (Drake et al. 1988), and have been associated with turbulent fluctuations in bed shear stress induced by sweep events. They contained many diffused particles, and were observed particularly at dune crests where the mean bed shear stress would also have been higher due to convective acceleration.

After obtaining the changes, two filters were applied to reduce the random pixel noise. Firstly, a median filter and then a Gaussian filter with standard deviation equal to one were slid through the image matrices. The median filter was applied in a neighborhood comparable with the minimum particle diameter *D10* (5-20 pixels).

Image velocity calculation

To calculate the displacements, different cross-correlation algorithms (CC) were applied between the sequences of the image subtractions. Discrete Fourier Transformations were performed over the large image matrices. The image differences were divided into smaller tiles and accordingly the CC was calculated for each tile (from 25 to 64 tiles per image depending on the abundance of moving particles detected). The tiles are called Regions of Interest (ROI) and in the final calculation, only the ones covering the ADCP sampling area were used. Finally, the zero mean cross correlation (ZCC) and the sub-pixel algorithm (Guizar-Sicairos et al. 2008) were applied for assessing the final displacements of each tile. The videography velocities (v_c) were calibrated using underwater checkboard images and calculating the homography matrices for a known distance (Zhang 2000). The computational burden increased exponentially as the number of ROI was increased. Therefore, the ROI was chosen, following two criteria: i.) the ROI dimension in the flow direction did not exceed the maximum saltation length of the particles (e.g., 10*D50); ii.) the number of the ROI was the minimum possible while maintaining stable mean velocity values. In most of the experiments, the camera measured velocity was assumed as equal to the average velocity of the mobile particles ($v_c \cong v_p$), because the active layer did not exceed $2*D50$. In the experiments with abundant transport (prevailing content of sand), v_c represented only the average surface velocity of the bedload.

Surface bedload concentration

The percentage of moving particles, or active bedload surface, was also extracted from the videography. The calculation of this coefficient utilized the total number of pixels visible after the change detection and the total pixel size of the ROI.

$$ZZ_{m,n} = \begin{cases} 1 \quad if \quad Z_{i_{m,n}} > 0 \\ 0 \quad if \quad Z_{i_{m,n}} = 0 \end{cases} \qquad (5)$$
$$k_1 = \frac{\sum_{m=1}^{M-1} \sum_{n=1}^{N-1} ZZ_{m,n}}{MN}$$

where N and M are the pixel dimensions of one cell (ROI), and the numerator is the total number of pixels where intensity changes were identified between the frames (i.e., the mobile particles). The coefficient k_1 gave the instantaneous percentage of the acoustic footprint covered by mobile particles and it represents the *surface concentration*. Similarly as Gaeuman and Jacobson (2006) suggested in their analysis of the apparent velocity, k_1 was applied for the spatial weighting of the ADCP BT footprint (see Eq.3).

Post-processing data

ADCP data post-processing

The analysis and post-processing were performed directly on the available apparent bedload velocity data. The available velocity data are internally averaged depending on the pinging time and the number of pulses per ping, thus the Doppler velocity from each pair of pulses and their amplitudes are not available for the users. Consequently, it is not possible to perform detailed analysis of the bottom tracking signal, especially considering the fact that it is designed only to calculate the boat speed, based on reading the strongest echoes reflected from the static bottom. In addition, some technical limitations constrained the data analysis: i.) the inability to conduct an experiment with intense gravel transport; ii.) the inability to establish a uniform and steady flow in moving-bed conditions.

The parameters of the post-processing filtering procedure were adapted to each experiment accord-

ing to the PSD and the hydraulic conditions. Even though most of the laboratory experiments had 5-10 min long series of 1 Hz sampling, the random errors could not be eliminated by only averaging. Firstly, the ADCP apparent bedload velocities with negative streamwise velocity components were discarded. This included the unreasonably small velocities that are corresponding to noise and instrument uncertainty. These values were zeros or close to zero. The minimum cut-off velocity was arbitrarily chosen to be 0.001m/s, as it is the velocity resolution of the ADCPs and velocity that might be associated with random Doppler noise. Excessively large values were also eliminated; a maximum cutoff velocity served to eliminate all the instantaneous values that exceeded three times of the total standard deviation (std). The std of the raw data was particularly high, especially for the experiments with scarce transport and many erroneous data (e.g., v_a reached 18-19 times the mean value of the raw data). Thus, the cut off threshold was limited to one std. for some experiments; the performed sensitivity analysis showed that three times std was not applicable to the scarce bedload transport (e.g. only gravel and gravel85% in UOttawa, and EXP1sand in UniBo).

The filtered velocities were fitted to gamma or Poisson-gamma distributions, which are the most commonly reported bedload velocity distributions (Einstein 1950; Rennie and Millar 2007; Lajeunesse et al. 2010). Finally, the time series of each experiment were averaged in time and space, considering only the streamwise components calculated from the two beams in the flow direction (see Fig.2). These time series showed that 3-4 minutes of 1Hz sampling frequency was sufficient to obtain statistically steady mean values for the cases without bed-forms. The total filtered data varied from 60% for gravel to 10% for sand materials in the UOttawa experiments and from 40% for weak to 15% for intensive sand mobility in the UniBO experiments. In the cases where bed-forms developed, only the data registered from the stoss to the crest of dunes were considered, eliminating the reattachment zone below the crest in the trough of dunes (Rennie and Villard 2004).

In the final phase of the data post-processing, the ADCP apparent velocity was normalized with the coefficient $1/k_1$ (Eq.6). Implicitly the use of k_1 embedded the assumption that the apparent velocity represents the average bedload velocity, including the immobile particles. k_1 is not a universal constant; the apparent velocity was multiplied by the weighting factor of $1/k_1$ that is equal to the

388 percentage of the bed surface covered by moving particles (as determined from analysis of the
389 camera images). The corrected apparent velocity is denoted as the *normalized apparent velocity*
390 *(v_{na})*.

391 $$v_{na} = \frac{1}{k_1} v_a \tag{6}$$

392 *Image velocimetry post-processing*

393 Post–processing procedure of the image velocity vectors was also necessary. Due to the
394 similarity of the particles and relatively low sampling frequency (30-70fps), the CC at times
395 matched different particles, rather than the same particles at different positions. This consequently
396 produced outliers. Those outliers were easily detected by eliminating the negative values and
397 simple local threshold de-spiking of the dataset (five times the local mean with a window of length
398 15 elements backward and 15 forward). No more than 15% of the detected particle velocities were
399 outliers. It is worth noting, that the image velocity data is much denser spatially and in time, hence
400 ROI*70 or ROI*30 velocity vectors per second were obtained.

401 **Distributions of the post-processed velocity data**

402 Similar velocity distributions were observed from the videography and the ADCPs and this
403 confirms the validity of the ADCP BT velocities (Blanckaert et al. 2017). Fig.5 gives an overview
404 of the distributions of the filtered apparent velocity and the image velocimetry. Similarity between
405 the distributions of the filtered apparent velocity data *(v_a)* and the camera velocity is clearly present.
406 In fact, gamma probability distribution functions (red lines Fig.5) fitted both data sets. However,
407 perfect fitting of the ADCP data cannot be expected due to the lower sampling frequency. The
408 cameras had sampling frequency between 35-70 Hz (fps) and the ADCPs default was 1Hz. The
409 sand data had fewer samples because it contained only the transport from the dune crest to the dune
410 trough. The UOttawa distributions of the filtered apparent velocity (Fig.5, first row) do not account
411 for the spatial coefficients and the camera velocity distributions clearly demonstrate the shift due to
412 k_1 (Fig.5, second row). On the other hand, the ADCP measurements in Bologna (Fig.5, EXP2sand,

first row) underestimated the results, thus presenting more significant shifting (Fig.5, EXP2sand, second row). The need for another fitting coefficient (e.g., k_2) is obvious and it will be considered in the further analysis.

RESULTS

The average bedload velocity and the apparent velocity

The planar view of the videography can only give the surface velocity of the particles that pass in the field of view. Fig.6*a* compares directly the mean velocity measured by the cameras and the mean apparent velocity from the ADCPs. A significant correlation is demonstrated but the apparent velocity underestimates the particle velocities measured by videography. The ADCP and camera velocities, from the UOttawa experiment (first experimental set using 3MHz M9 ADCP), matched well, after the application of the surface concentration coefficient k_1 (Eq.6, Fig.6*b*, filled markers). This suggests that the ADCP apparent bedload velocity is a spatial average of the surface velocity, including both immobile and mobile portions of the bed surface, and that the spatial normalization (i.e., k_1) corrects for the percentage of the bed that is mobile to yield the mean particle velocity. The time-averaged data from the first experimental set show a good positive correlation between the normalized ADCP velocity and the camera measured velocities (Fig.6*b*) because the pulse emitted by higher frequency instruments most probably scatters only the surface of the mobile particles. The results of the first experimental set also demonstrated an increase in the velocity as the *D50* decreases. The addition of sand particles in the bed sediments contributed to an increase of the mean velocity of the bedload and additionally decreased the friction between gravel particles. For these experiments, the slope of the correlation appears to be slightly greater than one. It is reasonable to suggest the image processing technique is biased to the larger particles because they were more visible, while the ADCP may overestimate the velocity due to the stronger BS properties of the sand particles. In addition, the velocities measured by videography (v_c) corresponded to some empirically calculated bedload velocities (Lee and Hsu 1994; van Rijn 1984; Lajeunesse et al. 2010), given the hydraulic conditions in Table 2.

The empty markers in the lower left corner Fig.6*a* present the second set of only sand experiments

440 measured with a 2MHz ADCP. For these experiments, it was necessary to decrease the water
441 depth to reach the desired sediment velocity, which did not change significantly the bedload
442 transport conditions (see Table 2). The determination of the dune-controlling region in the ADCP
443 signals was more complicated for the 2MHz tests, due to the irregular dunes caused by the facility
444 limitations. Nevertheless, the data were successfully processed albeit with higher deviation of the
445 results among the experiment repetitions in sandEXP2 and sandEXP3. After the normalization
446 with k_1, the normalized apparent velocity of the UniBo experimental set yielded an increasing
447 trend and good correlation between the measuring techniques (Fig.6*b*). However, there is a factor
448 of 2-4 difference between the camera measured surface velocity and the normalized apparent
449 ADCP velocity (v_{na}). Considering the camera velocity as the average surface bedload velocity, the
450 normalized ADCP velocity appears to depend on an additional weighting or calibration coefficient
451 k_2. That underestimation was not caused by the dune formation (Gaeuman and Jacobson 2006;
452 Latosinski et al. 2017), as the reattachment zone and the dune trough have been eliminated from
453 the sampling region. Initially, the main reasons for this negative bias in the Bologna experiments
454 might be assigned to the instrument features such as: i.) the ability of the 2MHz signal to penetrate
455 through the active layer and give higher value to the scattering of the immobile particles (that
456 are forming the rough surface), ii.) different acoustic sampling at the bottom which broadens the
457 spectrum of the returned echo, eventually misleading the phase (Doppler) shift calculation, and
458 iii.) different transducer geometry that resulted in with less focused beams for the StreamPro rather
459 than for the M9 (e.g. side-lobe effect (Urick 1983)).

460 **Measured Velocities and the Flow strength**

461 To examine the results further, in Fig.7 the measured apparent and image velocities are plotted
462 as a function of the excess non-dimensional bed shear stress (see Appendix I, Eq.10-15). The
463 velocities are non-dimensionalized by the settling velocity (v_s, Eq.16) to exclude the influence
464 of the particle size. The first and third plots (Fig.7a and c) present the ADCP apparent velocity
465 and normalized apparent velocity, while the second plot (Fig.7b) presents the particle velocities
466 measured by the cameras. Fig.7 demonstrates a correlation between the measured velocities and

467 the excess shear stress, indicating reasonable particle velocities were observed in response to the
468 particular PSD and water velocity of each experiment.
469 The deviation of the UniBo data from the UOttawa data in the apparent bedload velocity response
470 to the forcing flow (empty markers, Fig.7a and c) demonstrates the influence of using a different
471 ADCP with a different acoustic frequency. On the other hand, the bedload velocities measured
472 using the cameras from the two experiments (Fig.7b) merge to form a more consistent trend of
473 increasing particle velocity with increasing excess shear. A trend of increasing particle velocity
474 with excess shear is consistent with previous literature (Fernandez-Luque and Beek 1976; Engelund
475 and Fredsøe 1976; Abbott 1977; Sekine and Kikkawa 1992; Nino et al. 1994; Lee and Hsu 1994;
476 Lajeunesse et al. 2010). As seen in Fig.7b, non-dimensional particle velocity increased relatively
477 slowly at low excess shear, but more rapidly when excess non-dimensional shear stress exceeded
478 a value of 0.1 s. Fig.7d shows the parameter k_1, i.e., the percentage of the bed surface that is
479 mobile, as a function of excess shear stress. At low excess shear stress, the percentage of mobile
480 bed surface increases rapidly with increasing shear, which is consistent with previous observations
481 of partial bedload transport (Wilcock and McArdell 1997). In particular, the experiments with
482 scarce transport (UOttawa experiments with a majority of gravel, and UniBo sandEXP1) fall
483 into this regime. A break in this trend occurs at $\tau*$-$\tau*_{cr}$= 0.03 when the percentage of the bed
484 surface in transport (i.e., k_1) plateaus at a value between 50-60% during conditions of more general
485 bedload transport. The experiments with highly mobile sand transport (UOttawa experiments with
486 a majority of sand, and UniBo sandEXP3) fall into this plateau. Overall, the percentage of the bed
487 surface in transport as a function of excess shear stress is thus closely related to the properties of
488 more or less erodible bed sediment particles, as described by Lajeunesse et al. (2010). Furthermore,
489 the percentage of the bed surface in motion represents the instantaneously eroded particles, and thus
490 is closely related to erosion-deposition processes driven by particle transport (Drake et al. 1988).
491 The surface concentration of the moving particles did not exceed 60% out of the total number of
492 surface particles in the sampling zone (Fig.7d). It is worth noting that, Jamieson (2008) observed
493 40% to 45% of the bed surface was instantaneously mobile in their sand-bed flume experiments.

Similarly, van Rijn (1984) reported the maximum bed load concentration c=0.65, throughout the depth of the active layer, which is reasonable given that even a static river bed has 30-40% porosity (Frings et al. 2011). Sand transport with considerable excess shear stress occurred for cases in the upper plateau above the break-point in Fig.7d, thus this is likely associated with a maximum percentage of a surface that can be mobile.

In general, the trends shown in Fig.7 are consistent with increasing bedload transport with excess shear stress. At low excess shear stress, a small proportion of the bed surface is mobile, and particle velocities are relatively low, thus the bedload transport is relatively weak. However, transport increases precipitously with increasing excess shear, initially because more of the bed surface becomes mobile, and then because particle velocities increase more rapidly.

Evaluation of the filtering procedure and variation of observed velocities

In this study, the surface velocity and concentration of the bedload enabled the interpretation of ADCP data under the hypothesis that the acoustic beams are completely scattered by the first layer of the bedload and that the signal did not penetrate below. Therefore, the surface concentration (k_1) was used as the $1/k_1$ normalization coefficient mentioned in the previous section (Eq.6).

The surface concentration was positively correlated with the apparent velocity (Fig.8*a*). In both experiments, the percentage of the filtered ADCP data gave a strong correlation with the surface concentration (k_1). However, the 2 MHz ADCP data (open symbols in Fig.8*a*) has a steeper slope due to the above-mentioned velocity underestimation. The coefficient k_2, obtained from the linear fitting of the ADCP data had a different value for each of the UNiBo experiments collected with the 2MHz ADCP (see empty markers inset figure of Fig.8; note that k_2 equals to 1.0 for all the UOttawa experiments). In general, $1/k_2$ increased as the apparent bedload velocity increased and the observed deviations within the individual experiments are due to the temporal and spatial variation of the bedload velocity. The average $1/k_2$ varied among the three experiments as a factor from 2 to 4, and among the tests in each experiment it shows deviation in the range of one.

During low sediment motion when a small percentage of the bed surface was moving the ADCP BT produced many erroneous values that required filtering (Fig.8). The total filtered data reached

a maximum value of 60% for the case with only gravel incipient motion that had 10-15% of the bed surface in motion in the ADCP sampling area. Even though only 40% of the data were reliable in this case, the measured velocity after averaging reasonably well matched the camera results. On the contrary, the experiments with abundant sediment transport had only 10-15% erroneous ADCP data that had to be discarded. As expected, ADCP BT sensitivity and reliability increased for abundant transport that had more uniform surface velocity.

In the second set of experiments, it was necessary to distinguish between the spatial weighting (k_1) and instrument/environment dependent coefficients (i.e., k_2). This occurrence may be ascribed to an effect of both the moving particles and the immobile bed below them. The immobile bed produced velocity values closer to zero (UniBo experiments, EXP, Fig.8*a*). In other words, the StreamPro pulse was penetrating through the active layer; as a consequence the echoes were less influenced by the particle motion. The returned echo cloud is thereby even more complex, containing the signals from the mobile particles and the immobile bed below them with the same PSD, making it even more difficult to auto-correlate the echoes. Interestingly, it appears that higher apparent velocity requires higher $1/k_2$ (Fig.8, nested). This trend implies that the acoustic penetration occurred in all the experiments with 2MHz ADCP and that the signal was less influenced by the bedload velocities from the fast bedload particle velocities at the top of the active layer.

The coefficient of variation (c_v), the ratio between the standard deviation (std) and the mean, was assessed both for the raw data and the filtered data (Fig.9). The c_v of the non-filtered apparent velocity (Fig.9*a*) shows similar behavior as the errors (i.e., data removed by filtering), with maximum values for the scarce transport conditions (red circles, gravel, Fig.9*a*). As the surface concentration increases (i.e., decreasing data removed by filtering in Fig.8b), the c_v decreases (Fig.9*a* and Fig.9*b*). This is expected because the errors corresponded to the observed variability in the BT ADCP velocity measurements. Appropriate filtering of the bedload velocity appears to be crucial for analyzing the sediment transport velocity using ADCPs. Before filtering (Fig.9*a*) the std and the mean values were strongly influenced by the erroneous data. The non-filtered data clearly bears out the limitations of the instrument.

548 The noticeably high values of c_v before filtering in the only-gravel experiments (Fig.9*a*, red circles)
549 is indicative of the inherited uncertainty in ADCP v_a measurement during heterogeneous and
550 sporadic movement of bedload particles. On the contrary, after filtering, c_v was relatively stable
551 among the experiments and more convincingly reflected a physical variability of the observed
552 velocities. At the same time, the variability of the gravel-dominated transport is higher than the
553 sand–dominated transport. This reflects the heterogeneity of the gravel particles motion, the hiding
554 effects of the smaller sand particles and the sudden gravel bursts. It is worth noting that the gravel
555 bedload in Fig.9b does not exhibit the highest coefficient of variation (c_v). In fact, the filtering
556 procedure gave the highest c_v for the mixed sediment (asterisks and stars, Fig.9b) and it decreased as
557 the transport increased. This deviation bore out the wider velocity range in those experiments that
558 reflected the hiding effects and mass dominance (Parker 2004). As for the sand only experiments,
559 the second set of experiments (UniBo sand tests) was characterized with an almost constant c_v after
560 the filtering, but slightly higher compared to the first set of experiments. This is most likely due to
561 the not completely stable hydraulic conditions causing more turbulent and irregular motion of the
562 bed load as well.

563 **DISCUSSION**

564 **Backscattering strength, the attenuation and acoustic geometry**

565 A returned echo from moving sediment at the riverbed entails complex two-phase scattering
566 from the mobile particles moving in the active layer and from the immobile particles that are shaping
567 the surface roughness. This opens a discussion for evaluating the influence of the backscatter
568 strength (BS) echo and the attenuation on the Doppler velocity calculations, as well as the other
569 artifacts that triggered the erroneous data in our tests before the filtering.

570 Regarding the BS ($K_s A_r{}^2 + K_v{}^2 M_{at}$, Eq.1), the surface scattering was denoted as the scattering of
571 the immobile particles and the volume scattering as the scattering of the moving particles. This
572 equation implicitly includes BS dependence on instrumental frequency, the emitted amplitude, the
573 pulse length and the attenuation of the signal. These parameters approximately determine how the
574 signal weights the mobile and immobile particles. The wavelengths of 0.73 mm for 2MHz and 0.48

mm for 3MHz were comparable with the used particles sizes ($D50$ = 1 mm - 4 mm). The scattering processes, described by Rayleigh (1877), are dominantly produced by the particles for which phase reinforcement occurs for scattering back in direction of the incident sound. Thus, the particles with a size comparable to the ADCP wavelength produced the strongest BS signal. The variation of the volume backscattering coefficient (K_v, Eq.2, Fig.10a) bears out that the PSDs used in the experiment are in the geometric scattering regime (Rayleigh 1877). This leads to an almost constant form factor (Thorne and Buckingham 2004), where the particles scatter proportionally with their size. However, the presented results suggested a relevant influence of the surface scattering from the immobile particles and the heterogeneous motion of the gravel made the variation of K_v less relevant.

Regarding the acoustic attenuation, the received amplitude of the bottom track signal decreased as the apparent velocity and the active layer increased (Fig.10b). This resulted in a high amplitude of the received signal (Fig.10b). On the contrary for abundant transport, the active layer was thicker and the acoustic signal most likely did not penetrate completely up to the immobile bed resulting in higher attenuation and lower BT amplitude (Fig.10b).

This analysis confirms the fact that, after the penetration of the signal through the active layer, the rough surface scattering plays an important role in the underestimation of the apparent velocity. This was especially the case for the UniBo experiments conducted with the 2 MHz instrument that underestimated the particle velocities obtained from videography (see Fig.6b, empty markers).

It appears the effective height of the BT sampling volume was greater for the 2 MHz StreamPro than the 3 MHz M9, with surface scattering from the immobile bed as well as volume scattering from the active bedload layer. This could be interpreted as a lower vertical resolution within the layer of moving particles, leading to more signal contribution from the immobile bed. This lower resolution would be due in part to the larger acoustic wavelength for the 2 MHz instrument for the same given pulse length of about 5 cm (Table 1), although the exact pulse encoding (see Appendix II) and resolution are unknown for the two ADCPs. In addition, the lower slant beam angle (20° for the StreamPro versus 25° for the M9) further enlarges the acoustic sampling length (i.e., lowers the

602 resolution) along the vertical for given wave and pulse lengths. This would enhance the ability of
603 2 MHz pulses to reach the immobile surface underneath the active layer. Finally, it is possible that
604 side lobe contamination of the BT signal resulted in contribution of immobile surface scattering
605 received in the same portion of the backscattered pulse as volume scattering from the main lobe.
606 It is worth noting that overlapping of returned signals across the beam width is exacerbated for
607 beams with greater spread opening, which shortens the beam path for the side first lobe (Urick
608 1983; Medwin 2005). Also, the beam opening typically is greater for smaller transducers at a
609 given acoustic frequency (Urick 1983; Medwin 2005). Due to its wider beam opening and smaller
610 transducers (Table 1), the 2 MHz StreamPro instrument used at UniBo may have had less focused
611 beams with greater side lobes than the Sontek M9. These three factors may have increased immobile
612 surface scattering in the received BT signal of the 2 MHz StreamPro data. This would have both
613 biased the BT Doppler shift velocity estimate towards the zero velocity of the immobile layer and
614 broadened the spectrum of the returned echo leading to greater uncertainty in the estimated va.
615 Consequently, deterioration of the spatially normalized apparent bedload velocity occurred for the
616 UniBo data, necessitating the additional filter factor k_2.

617 **Other possible sources of error**

618 As argued above, the existence of the erroneous data in the raw apparent velocity is related
619 with the immobile rough surface scattering. The produced errors likely have something to do
620 with misinterpretation of parts of the signal scattered from the rough immobile bed that causes
621 production of values with false Doppler velocity. In fact, the erroneous data were very well
622 correlated with the measured surface density (Fig.8*b*). Lower surface velocity or scarce transport
623 are associated with more errors (greater influence of the immobile rough surface). Additionally,
624 other artifacts may have contributed to the erroneous data, such as aliasing, de-correlation of the
625 echoes inside the beam (e.g. spectral broadening), false bed surface frequency shift, change of
626 the grazing angle and the internal post-processing algorithm of the instrument. The aliasing is
627 related with the ping rate and the sampling volume. If the particles escape the sampling area during
628 insonification of the pulse on the bed, then the signal may be aliased. In this case, the Doppler

frequency shift is ambiguous and the velocity estimation is erroneous. However, for an individual BT pulse the duration of bed insonification is less than a millisecond, thus aliasing is not likely an issue. On the other hand, signal de-correlation is very likely during bedload transport. The particle mobility of the bedload occurs in three different modes of transport (saltating, rolling, vibrating). During saltation the particles experience some relaxation period. In addition to this, some particles terminate the succession of jumps and rolling due to collisions and hiding, while other particles are initiating a new motion trajectory. All this contributes to relatively de-correlated echoes. The de-correlation means that the internal algorithm cannot identify the echoes from the peak Doppler frequency because the correlation is very low. Similar to the aliasing, erroneous data such as negative values and large spikes may have been produced.

CONCLUSIONS

Simultaneous laboratory measurement of ADCP apparent bedload velocity (v_a) and bedload particle velocities by videography (v_c) have demonstrated that v_a is a measure of the spatially averaged surface velocity of the bedload sediment. For the experiments with a 3 MHz ADCP and sediments ranging from sand to gravel, the data filtering involved removal of all negative, near-zero, and extreme apparent bedload velocities. A spatial normalization coefficient, $1/k_1$, where k_1 is the percentage of bed surface that is mobile, was used to normalize the measured apparent velocity such that it is representative of particle velocities. For the experiments with a 2MHz ADCP and sand bedload material, an additional coefficient (k_2, Eq.3) was required to match observed particle velocities. This accounted for negative bias presumably caused by increased acoustic penetration of the active layer and stronger backscatter from the immobile bed surface.

As the transport rate increased, the signal from the higher frequency instrument was less affected by the immobile bed and the apparent velocity become more accurate. On the other hand, the influence of the beam geometry, the signal penetration and the surface scattering contributed to the signal interpretation even in the more abundant transport rates (i.e., the introduction of k_2 is necessary). A noticeable correlation between filtered data (erroneous data) and the spatially normalizing ($1/k_1$) coefficient was observed in both experimental sets. This correlation was valid for the 3MHz Sontek

ADCP and could be used for the assessment of k_1 from ADCP data in the field where it is difficult to measure k_1 due to the infeasibility of positioning a camera.

This study gave evidence that the active layer of the mobile particles, even in its thinnest form of 2-3$D50$, influences the estimation of the ADCP BT velocities. A thicker active layer increases the ratio between the true surface bedload velocity and the apparent velocity. In case if the acoustic signal penetrates the active layer, the apparent velocity (v_a) decreases because of the scattering of the immobile riverbed layer. On the other hand, the sediment size theoretical volume scattering strength does not significantly influence the Doppler velocity estimation.

With the goal of using the ADCP for measuring bedload transport rate (e.g., by applying the apparent velocity in the transport kinematic model), several recommendations can be derived from this study:

- The ADCP v_a signal provides an estimation of the spatially averaged velocity of the exposed surface, thus a bedload surface concentration factor ($1/k_1$) is required to estimate the mean bedload particle velocity.
- The described filtering procedure is recommended for more accurate bedload velocity data, particularly when measuring low sediment transport rates.
- A linear correlation between the percentage of the filtered data and the bedload concentration can be applied to estimate the bedload concentration and eventually combined with the raw apparent velocity for a reliable estimation of bedload velocity.
- Three minutes averaging of v_a data with 1Hz sampling rate is sufficient to yield a stable estimate of mean velocity in stationary measurements, at least for the range of transport conditions examined during these experiments.
- An additional instrument-related coefficient is necessary for ADCPs with lower working frequency than 3MHz. In the presented tests, using the StreamPro (2MHz) by Teledyne-RDI, the resulting calibration coefficient ($1/k_2$) ranged between two and four.

The influence of the surface scattering and the other sources of errors in the velocity estimation

682 of the ADCP bottom track remain to be further tested with detailed information about the sediment
683 bed and the instrument parameters (k_2). Future studies shall be performed to explore the behavior
684 of the normalizing coefficients (k_1, k_2) by changing the instrument working frequency, the encoding
685 of bottom track signal and the PSD to tailor the acoustic sampling length on the basis of the actual
686 thickness of the active layer.

687 **ACKNOWLEDGMENTS**

688 Authors acknowledge the Erasmus Mundus Novadomus program for funding the research
689 visiting period from 12 June 2016 to 25 July 2017 of Massimo Guerrero in Ottawa University where
690 the first set of tests were conducted under Prof. Colin Rennie supervision. The research equipment
691 utilized at UOttawa was procured through a grant from the Natural Sciences and Engineering
692 Research Council of Canada. In addition, authors acknowledge the Research Center for Building
693 and Constructions (CIRI-EC) of Bologna University that made available the Hydraulic Laboratory
694 for the second set of tests. The PhD research program of Slaven Conevski was developed under
695 SediPass project funded by the Norwegian Research Council and Statkraft.

APPENDIX I. BROADBAND PROCESSING AND RIVERBED SCATTERED SIGNAL

A broadband ADCP transmits an individual ping that consists of many encoded pulses. In coherent signal processing the Doppler shift is not calculated from a single pulse return but rather the return of the sequence of encoded pulses (Brumley et al. 1991). The pulses reflected from particles moving away from the transducer produce a Doppler frequency drop which corresponds to time dilation and phase change in the temporal domain. The ADCP calculates the echo autocorrelation function, the phase difference and then calculates velocity based on phase difference. The RDI Stream Pro and Sontek M9 SmartPulse mode both operate with pulse coherent broadband. This entails (Fast Fourier Transformation) FFT, complex covariance method and other methods, but the manufacturer does not provide the details of the processing algorithm. Most of the broadband ADCPs use the autocorrelation method that correlates the echoes from the scattering of different encoded pulses (Brumley et al. 1991; Brumley and Ramon Cabrera 1993). Then, the phase of the autocorrelation of the complex demodulated signal at a lag corresponding to the pulse spacing is proportional to the velocity (RDInstruments 2011). The broadband instruments usually process more than one pulse in the duration of one ping and deliver the final value depending on the signal processing approach.

The redistribution of the echo from the BT pulse is quite complex, especially during moving bed conditions. The intensity across the insonified beam width is highly variable, thus the threshold for the bottom cannot be easily detected. In addition, it is hard to determine how the received and analyzed signals are affected by the immobile surface and the active layer. In the literature, volume scattering is usually associated with the suspended sediments or scatterers in the water. For the purposes of this study the moving layer of the bottom, including mostly the saltating particles (Drake et al. 1988; Nino et al. 1994; Lajeunesse et al. 2010), can be simplified as volume scattering that occurs slightly above the immobile river bottom. On the other hand, the scattering of the immobile particles forming the bed surface could be denoted as surface scattering. We assume that the registered BT signal cannot penetrate into pores of the immobile sediment bed. The equation, including a weighted sum of volume and surface scattering strength could be expressed through the

intensity of the reflected signal as follows:

$$I_r = \frac{I_0 K_p (s_v + s_s)}{R^4} R^2 \frac{c\tau_{pl}}{2} b(\theta, \varphi) e^{-4R(\alpha_{wc}+\alpha_{at})}, \tag{7}$$

where I_r is the received signal intensity (the recived echo intensity), I_0 is the transmitted intensity, K_p is an instrument constant, s_v and s_s are volume and rough surface backscattering(BS) strengths. The τ_{pl} is the pulse duration, c is the speed of sound, R is the slant range to the bottom, $b(\theta,\varphi)$ is a beam coefficient that includes the grazing angle 90- θ , the beam spreading angle (φ) and the beam width. The term $R^2 \frac{c\tau_{pl}}{2} b(\theta, \varphi)$ represents the insonified volume (Urick 1983; Medwin and Clay 1998) and it can be precisely calculated (Rennie et al. 2002; Rennie and Millar 2004). In the above relation, α_{at} is the attenuation coefficient that depends on the acoustic frequency and the particle size distribution and concentration (M_{at}) of the mobile bedload. Additionally, α_{wc} is the attenuation in the water column, usually related to the water viscosity and suspended sediment attenuation. The latter depends on the particle size and concentration in the water column, but in this case it is negligible. The range $4R$ is the squared two-way path of the attenuated sound pressure. If we assume that the insonified volume on distance R has N mobile particles in the active layer then the concentration of the mobile particles (M_{at}) can be used as a representation of the particles volume scattering (Thorne et al. 1991). The surface scattering will be dependent only on the sampled area, assuming that no energy is transmitted to the solid medium below (Urick 1983).

$$s_v = {K_v}^2 M_{at} \tag{8}$$

$$s_s = K_s {A_r}^2, \tag{9}$$

where the coefficients K_v and K_s are scattering coefficients and are described in the Acoustic theory section. Long pulses ($\frac{c\tau_{pl}}{2}$) are used to improve identification of the pulse edge and to reduce the variance. If there is high suspended sediment concentration (SSC) close to the bottom, additional volume scattering contributes to the final Doppler velocity estimation (Rennie and Millar 2004). Shorter pulses would have higher variance, but smaller impact of the eventual water bias,

748 thus registering better results if they are not attenuated in the SSC layer (Rennie and Millar 2004).

APPENDIX II. SHEAR VELOCITY ASSESSMENT

The equations listed here were used to calculate the parameters given in Table 2. The most common way to define the bedload transport mode is to calculate the shear stress and the Shields number.

$$\tau* = \frac{\tau}{\rho_S(\frac{\rho_s}{\rho} - 1)gD50} = \frac{u*^2}{(\frac{\rho_s}{\rho} - 1)gD50} \tag{10}$$

$$R_{ep} = \frac{\sqrt{g(\frac{\rho_s}{\rho} - 1)D50}D50}{\nu} \tag{11}$$

$$R_e* = \frac{u * D50}{\upsilon} \tag{12}$$

$$D* = D50\left(\frac{(\frac{\rho_s}{\rho} - 1)g}{\nu^2}\right) \tag{13}$$

$$\tau*_{cr} = f(D*) \tag{14}$$

$$u*_{cr} = \sqrt{\tau*_{cr}D50(\frac{\rho_s}{\rho} - 1)g} \tag{15}$$

$$v_s = R_f\sqrt{(\frac{\rho_s}{\rho} - 1)gD50}, \tag{16}$$

where $\tau*$ is the dimensionless shear stress (Shields 1936), $u*$ is the shear velocity, *D50* is the median diameter, ρ is the water density, ρ_s is the sediment density. The main objective of analyzing these parameters is to define the critical shear velocity and the particle Raynolds number R_{ep}. R_e is the boundary Reynolds number that depends on the shear velocity. The critical shear velocity is calculated using the critical mobility parameter ($\tau*_{cr}$, Shields parameter), defined by Shields and analytically presented by VanRijn (Shields 1936; van Rijn 1984). With this, it is confirmed that

bedload motion occurs and the suspension of the sediments is avoided (Parker 2004). Finally, v_s is the settling velocity expressed through R_f. R_f is a coefficient defined by Dietrich (1982) and it is a function of R_{ep}. It should be noted that the formulas for $u*_{cr}$ and v_s do not contain correction for the shape of the particles. Usually, the log law velocity profile is employed to estimate $u*$, particularly for near-bottom velocity data in turbulent flow conditions with irregular bedforms (Afzalimhr and Rennie 2009). However, the low water depth and the limitations of the ADCPs do not comply with the application of the $u*$ log-law equation in the lower part of the velocity profile. These events increased the uncertainty and caused a high standard deviation. In the first set of experiments, only the ADCP velocity profiles were available, which cannot be taken as relevant for calculating the shear velocity or zero-velocity height, due to their incapability to measure near the bed, especially in shallow laboratory flumes. Instead, the shear velocity was estimated using the depth-averaged version of the log law by Keulegan (1938), later adapted by van Rijn (1984) in his bed load transport formulations.

$$u* = \frac{U}{5.75\log_{10}(\frac{12H}{3D90})}, \tag{17}$$

where U is the depth-averaged velocity calculated using the mean flow depth (H) measured by the ADCPs and the flume geometry. $D90$ is the diameter larger than 90% of the particles in the sediment bed.

NOTATION LIST

The following symbols are used in this paper:

a = mean particle radius (m) ;

A_r = variance of the riverbed surface roughness (m^2);

b = beam pattern ;

c = speed of sound (m/s);

c_v = coefficient of variation ;

$D*$ = particle dimensionless size;

$D10$ = particle diameter bigger than 10% (m);

$D50$ = particle median diameter (m)

$D84$ = particle diameter larger than 84% (m);

$D90$ = particle diameter larger than 90% (m);

e = Euler's number;

f = ADCP working frequency (MHz);

f_o = particles form factor;

f_d = Doppler frequency (Hz);

g = gravitational constant (m/s^2);

H = water depth in the flume (m);

I_0 = amplitude of the emitted signal (dB);

I_r = amplitude of the returned signal (dB);

I_i = image at instance i;

K_p = instrument coefficient;

K_s = surface backscattering coefficient (m/kg$^{0.5}$);

K_v = volume backscattering coefficient (m/kg$^{0.5}$)

k_1 = surface concentration (%);

k_2 = instrument normalization velocity coefficient;

m = pixel position in vertical direction;

M = total number of pixels in vertical direction;

M_{at} = bedload concentration (kg/m^3);

n = pixel position in horizontal direction;

N = total number of pixels in horizontal direction;

R = slant spreading distance from the ADCPs beams (m);

R_e = boundary Reynolds number;

R_{e_p} = Particle Reynolds number;

R_f = predicting coefficient for the settling velocity (Dietrich 1982);

s_s = surface backscattering strength (dB);

s_v = volume backscattering strength (dB) ;

U = average-depth water velocity (m/s);

$u*$ = shear(friction) velocity (m/s);

$u*_{cr}$ = critical shear(friction) velocity (m/s);

v_a = apparent velocity (m/s);

v_{bt} = bottom tracking vessel velocity (m/s);

v_{gps} = GPS vessel velocity (m/s);

v_{na} = normalized apparent velocity (m/s) ;

v_s = settling velocity (m/s);

v_p = average particle velocity ;

Z_i = image changes at instance i;

α_{at} = attenuation in the active layer (dB);

α_{wc} = attenuation in the water column (dB);

λ = wavelength (mm) ;

π = mathematical constant;

ρ = water density (kg/m^3);

ρ_s = sediment particles density (kg/m^3);

τ = shear stress (N/m^2);

$\tau*$ = dimensionless shear stress;

$\tau*_{cr}$ = critical shear stress;

τ_{pl} = pulse time length (s)

θ = acoustic beam incident angle (^{o});

φ = acoustic beam spreading angle (^{o}).

787 **REFERENCES**

788 Abbott, J., J. F. (1977). “Saltation and suspension trajectories of solid grains in a water stream.”
789 *Philosophical Transactions of the Royal Society of London A: Mathematical, Physical and*
790 *Engineering Sciences*, 284(1321), 225–254.

791 Afzalimhr, H. and Rennie, C. (2009). “Determination of bed shear stress in gravel-bed rivers using
792 boundary-layer parameters.” *Hydrological Sciences Journal*, 54(1), 147–159.

793 Bagnold, R.A., F. R. S. (1956). “The flow of cohesionless grains in fluids.” *Philosophical Trans-*
794 *actions of the Royal Society of London A: Mathematical, Physical and Engineering Sciences*,
795 249(964), 235–297.

796 Bagnold, R. A. (1980). “An empirical correlation of bedload transport rates in flumes and natural
797 rivers.” *Proceedings of the Royal Society of London A: Mathematical, Physical and Engineering*
798 *Sciences*, 372(1751), 453–473.

799 Blanckaert, K., Heyman, J., and Rennie, C. D. (2017). “Measuring bedload sediment transport with
800 an acoustic doppler velocity profiler.” *Journal of Hydraulic Engineering*, 143(6), 04017008.

801 Brumley, B. H., Cabrera, R. G., Deines, K. L., and Terray, E. A. (1991). “Performance of a
802 broad-band acoustic doppler current profiler.” *IEEE Journal of Oceanic Engineering*, 16(4),
803 402–407.

804 Brumley, B., D. K. and Ramon Cabrera, E. T. (1993). “Device for the treatment of hiccups,
805 <https://patents.google.com/patent/US5208785> (05).

806 Dietrich, W. E. (1982). “Settling velocity of natural particles.” *Water Resources Research*, 18(6),
807 1615–1626.

808 Dinehart, R. and Burau, J. (2005). “Repeated surveys by acoustic doppler current profiler for flow
809 and sediment dynamics in a tidal river.” *Journal of Hydrology*, 314(1), 1 – 21.

810 Drake, T. G., Shreve, R. L., Dietrich, W. E., Whiting, P. J., and Leopold, L. B. (1988). “Bedload
811 transport of fine gravel observed by motion-picture photography.” *Journal of Fluid Mechanics*,
812 192, 193–217.

813 Einstein, H. (1950). *The Bed-load Function for Sediment Transportation in Open Channel Flows*.

Technical bulletin (United States. Dept. of Agriculture). U.S. Department of Agriculture, <https://books.google.no/books?id=xIhtv2wpR9oC>.

Engelund, F. and Fredsøe, J. (1976). "A sediment transport model for straight alluvial channels." *Hydrology Research*, 7(5), 293–306.

Fernandez-Luque, R. and Beek, R. V. (1976). "Erosion and transport of bed-load sediment." *Journal of Hydraulic Research*, 14(2), 127–144.

Frings, R. M., Schüttrumpf, H., and Vollmer, S. (2011). "Verification of porosity predictors for fluvial sand-gravel deposits." *Water Resources Research*, 47(7).

Frings, R. M. and Vollmer, S. (2017). "Guidelines for sampling bedload transport with minimum uncertainty." *Sedimentology*, 64(6), 1630–1645.

Gaeuman, D. and Jacobson, R. B. (2006). "Acoustic bed velocity and bed load dynamics in a large sand bed river." *Journal of Geophysical Research: Earth Surface*, 111(F2).

Guerrero, M. and Di Federico, V. (2018). "Suspended sediment assessment by combining sound attenuation and backscatter measurements - analytical method and experimental validation." *Advances in Water Resources*, 113, 167–179.

Guerrero, M. and Lamberti, A. (2011). "Flow field and morphology mapping using adcp and multibeam techniques: Survey in the po river." *Journal of Hydraulic Engineering*, 137(12), 1576–1587.

Guerrero, M., Rüther, N., Szupiany, R., Haun, S., Baranya, S., and Latosinski, F. (2016). "The acoustic properties of suspended sediment in large rivers: Consequences on adcp methods applicability." *Water*, 8(1).

Guerrero, M., Szupiany, R. N., and Latosinski, F. (2013). "Multi-frequency acoustics for suspended sediment studies: an application in the parana river." *Journal of Hydraulic Research*, 51(6), 696–707.

Guizar-Sicairos, M., Thurman, S. T., and Fienup, J. R. (2008). "Efficient subpixel image registration algorithms." *Opt. Lett.*, 33(2), 156–158.

Hager, W. (2005). "Du boys and sediment transport." *Journal of Hydraulic Research*, 43(3), 227–

841 233.

842 Jackson, D. and Richardson, M. (2007). *High-Frequency Seafloor Acoustics*. Springer-Verlag New
843 York.

844 Jamieson, E. C., Rennie, C. D., Jacobson, R. B., and Townsend, R. D. (2011). "Evaluation of adcp
845 apparent bed load velocity in a large sand-bed river: Moving versus stationary boat conditions."
846 *Journal of Hydraulic Engineering*, 137(9), 1064–1071.

847 Jamieson, E. C., R. C. D. R. R. (2008). "Validation of adcp bedload transport measurements.."
848 *Proc. 2008 River Flow Conf.*, Engineers' Soc. of Western Pennsylvania, KUBABA Congress
849 Dept. and Travel Services Cesme, Turkey, 2343–2351.

850 Jin, F., Fieguth, P., Winger, L., and Jernigan, E. (2003). "Adaptive wiener filtering of noisy images
851 and image sequences." *Proceedings 2003 International Conference on Image Processing (Cat.*
852 *No.03CH37429)*, Vol. 3, III–349–52 vol.2 (Sept).

853 Keshavarzy, A. and Ball, J. (1999). "An application of image processing in the study of sediment
854 motion." *Journal of Hydraulic Research*, 37(4), 559–576.

855 Keulegan, G. H. (1938). "Laws of turbulent flow in open channels." *Part of Journal of Research of*
856 *the National Bureau of Standard*, 21, 707–741.

857 Lajeunesse, E., Malverti, L., and Charru, F. (2010). "Bed load transport in turbulent flow at the grain
858 scale: Experiments and modeling." *Journal of Geophysical Research: Earth Surface*, 115(F4).

859 Latosinski, F. G., Szupiany, R. N., Guerrero, M., Amsler, M. L., and Vionnet, C. (2017). "The
860 adcp's bottom track capability for bedload prediction: Evidence on method reliability from sandy
861 river applications." *Flow Measurement and Instrumentation*, 54, 124 – 135.

862 Lee, H. and Hsu, I. (1994). "Investigation of saltating particle motions." *Journal of Hydraulic*
863 *Engineering*, 120(7), 831–845.

864 Lucas, B. D. and Kanade, T. (1981). "An iterative image registration technique with an application
865 to stereo vision." *Proceedings of the 7th International Joint Conference on Artificial Intelligence*
866 *- Volume 2*, IJCAI'81, San Francisco, CA, USA, Morgan Kaufmann Publishers Inc., 674–679,
867 <http://dl.acm.org/citation.cfm?id=1623264.1623280>.

Marsh, H. W. (1963). “Sound reflection and scattering from the sea surface.” *The Journal of the Acoustical Society of America*, 35(2), 240–244.

Medwin, H. (2005). *Sounds in the sea : from ocean acoustics to acoustical oceanography*. Cambridge University Press, Cambridge.

Medwin, H. and Clay, C. S. (1998). “Chapter 2 - sound propagation.” *Fundamentals of Acoustical Oceanography*, H. Medwin and C. S. Clay, eds., Applications of Modern Acoustics, Academic Press, San Diego, 17 – 69.

Moate, B. D. and Thorne, P. D. (2009). “Measurements and inversion of acoustic scattering from suspensions having broad size distributions.” *The Journal of the Acoustical Society of America*, 126(6), 2905–2917.

Moore, S. A., Dramais, G., Dussouillez, P., Coz, J. L., Rennie, C., and Camenen, B. (2013). “Acoustic measurements of the spatial distribution of suspended sediment at a site on the lower mekong river.” *Proceedings of Meetings on Acoustics*, 19(1), 005003.

Nino, Y., Garcna, M., and Ayala, L. (1994). “Gravel saltation: 1. experiments.” *Water Resources Research*, 30(6), 1907–1914.

Papanicolaou, A. N., Diplas, P., Balakrishnan, M., and Dancey, C. L. (1999). “Computer vision technique for tracking bed load movement.” *Journal of Computing in Civil Engineering*, 13(2), 71–79.

Parker, G. (2004). *1D SEDIMENT TRANSPORT MORPHODYNAMICS*. Morphodynamics Web Page, <http://hydrolab.illinois.edu/people/parkerg/morphodynamics>.

Radice, A., Malavasi, S., and Ballio, F. (2006). “Solid transport measurements through image processing.” *Experiments in Fluids*, 41(5), 721–734.

Ramooz, R. and Rennie, C. D. (2008). “Laboratory measurement of bedload with an adcp..” *In Bedload-surrogate monitoring technologies: United States Geological Survey Scientific Investigations Rep. 2010-5091 Rep. 2010-5091*, USGS, Reston, VA, <http://pubs.usgs.gov/sir/2010/5091/papers/>.

Rayleigh, J. W. S. B. (1877). “On progressive waves.” *Proceedings of the London Mathematical*

Society, s1-9(1), 21–26.

RDInstruments (2011). "Acoustic doppler current profiler principles of operation a practical primer." *Practical primer*, Teledyne RD Instruments, 14020 Stowe Drive Poway, California 92064, <http://www.teledynemarine.com>.

RDInstruments, T. (2015). *StreamPro ADCP Guide*, p/n 95b-6003-00 (september 2015) edition, <http://www.teledynemarine.com/Documents/Brand(September).

Rennie, C. D. and Church, M. (2010). "Mapping spatial distributions and uncertainty of water and sediment flux in a large gravel bed river reach using an acoustic doppler current profiler." *Journal of Geophysical Research: Earth Surface*, 115(F3).

Rennie, C. D. and Millar, R. G. (2004). "Measurement of the spatial distribution of fluvial bedload transport velocity in both sand and gravel." *Earth Surface Processes and Landforms*, 29(10), 1173–1193.

Rennie, C. D. and Millar, R. G. (2007). "Deconvolution technique to separate signal from noise in gravel bedload velocity data." *Journal of Hydraulic Engineering*, 133(8), 845–856.

Rennie, C. D., Millar, R. G., and Church, M. A. (2002). "Measurement of bed load velocity using an acoustic doppler current profiler." *Journal of Hydraulic Engineering*, 128(5), 473–483.

Rennie, C. D. and Villard, P. V. (2004). "Site specificity of bed load measurement using an acoustic doppler current profiler." *Journal of Geophysical Research: Earth Surface*, 109(F3).

Rennie, C., V. D., Williams, R. D., Brasington, J., and Hicks, M. (2017). "Calibration of acoustic doppler current profiler apparent bedload velocity to bedload transport rate." *Gravel-Bed Rivers: Process and Disasters*, Wiley-Blackwell, Chapter 8, 209–231.

Sassi, M. G., Hoitink, A. J. F., and Vermeulen, B. (2011). "Impact of sound attenuation by suspended sediment on adcp backscatter calibrations." *Water Resources Research*, 48(9).

Sekine, M. and Kikkawa, H. (1992). "Mechanics of saltating grains. ii." *Journal of Hydraulic Engineering*, 118(4), 536–558.

Shields, A. (1936). "Application of similarity principles and turbulence research to bed-load movement." *Hydraulic Engineering Reports 167*, Soil Conservation Service, Berlin,

922 <http://resolver.caltech.edu/CaltechKHR:HydroLabpub167>.

923 Simmons, S. M., Parsons, D. R., Best, J. L., Orfeo, O., Lane, S. N., Kostaschuk, R., Hardy,
924 R. J., West, G., Malzone, C., Marcus, J., and Pocwiardowski, P. (2010). "Monitoring suspended
925 sediment dynamics using mbes." *Journal of Hydraulic Engineering*, 136(1), 45–49.

926 Sontek (2017). *RiverSurveyor S5/M9 System Manual, Firmware Version 4.02.*
927 9940 Summers Ridge Road, San Diego, CA 92121-3091 USA, oct2017 edition,
928 <http://ysi.actonsoftware.com/acton/attachment/1253/f-041f/1/-/-/-/-/RiverSurveyor(October).

929 Stefano, L. D., Mattoccia, S., and Mola, M. (2003). "A change-detection algorithm based on
930 structure and colour." *Proceedings of the IEEE Conference on Advanced Video and Signal Based*
931 *Surveillance, 2003.*, 252–259 (July).

932 Thorne, P., Vincent, C., Hardcastle, P., Rehman, S., and Pearson, N. (1991). "Measuring suspended
933 sediment concentrations using acoustic backscatter devices." *Marine Geology*, 98(1), 7 – 16.

934 Thorne, P. D. and Buckingham, M. J. (2004). "Measurements of scattering by suspensions of
935 irregularly shaped sand particles and comparison with a single parameter modified sphere model."
936 *The Journal of the Acoustical Society of America*, 116(5), 2876–2889.

937 Thorne, P. D. and Meral, R. (2008). "Formulations for the scattering properties of suspended sandy
938 sediments for use in the application of acoustics to sediment transport processes." *Continental*
939 *Shelf Research*, 28(2), 309 – 317.

940 Urick, R. (1983). *Principles of Underwater Sound*. Peninsula Publishing,
941 <https://books.google.no/books?id=MBBgQgAACAAJ>.

942 van Rijn, L. C. (1984). "Sediment transport, part i: Bed load transport." *Journal of Hydraulic*
943 *Engineering*, 110(10), 1431–1456.

944 Wilcock, P. R. and McArdell, B. W. (1997). "Partial transport of a sand/gravel sediment." *Water*
945 *Resources Research*, 33(1), 235–245.

946 Williams, R. D., Rennie, C. D., Brasington, J., Hicks, D. M., and Vericat, D. (2015). "Linking the
947 spatial distribution of bed load transport to morphological change during high-flow events in a
948 shallow braided river." *Journal of Geophysical Research: Earth Surface*, 120(3), 604–622.

949 Zhang, Z. (2000). “A flexible new technique for camera calibration.” *IEEE Trans. Pattern Anal.*
950 *Mach. Intell.*, 22(11), 1330–1334.
951 Zuiderveld, K. (1994). “Graphics gems iv.” Academic Press Professional, Inc., San Diego, CA,
952 USA, Chapter Contrast Limited Adaptive Histogram Equalization, 474–485.

953 **List of Tables**

954 1 Basic parameters of the instrument acoustic geometry. 43
955 2 Hydraulic and sedimentologic parameters of the experiments. The experiments
956 conducted in UOttawa are named according the ratio of gravel/sand in the sediment
957 bed; The experiments from UniBo are named according the hydraulic conditions,
958 starting with the slow water velocity. 44

Instrument Type	Instrumental Frequency MHz	Wave length mm	Beam slant angle ^{o}	1/2 beam opening angle ^{o}	Transducers diameter cm	Distance Transducer-Bottom cm	Pulse length cm
Teledyne-RDI StreamPro	2.0	0.73	20	3.4	1.5	25-30	5
Sontek M9	3.0	0.48	25	1.3	2.5	30-35	5

TABLE 1. Basic parameters of the instrument acoustic geometry.

	EXP name	Gravel %	Repeated	Q l/s	H m	$D50$ m	$D90$ m	U m/s	$u*_{cr}$ m/s	$\tau*_{cr}$ /	$\tau*$ /	Re_p /	$Re*$ /	Fr /	v_s m/s	ADCP /	Camera fps/resolution
UOttawa	gravel	100%	5	200	0.35	0.0040	0.0060	0.783	0.054	0.045	0.054	767.0	165.0	0.231	0.45	M9 (3MHz)[1]	70 / 2200x1080
	gravel%15sand	85%	5	200	0.33	0.0035	0.0056	0.827	0.050	0.044	0.055	641.0	127.0	0.258	0.4	M9(3MHz)	70 / 2200x1080
	gravel%25sand	75%	5	200	0.33	0.0033	0.0054	0.819	0.048	0.043	0.055	574.0	120.0	0.253	0.36	M9(3MHz)	70 / 2200x1080
	gravel%50sand	50%	5	200	0.33	0.0018	0.0050	0.831	0.032	0.035	0.082	231.5	65.0	0.260	0.25	M9(3MHz)	70 / 2200x1080
	sand	0%	5	200	0.31	0.0011	0.0015	0.872	0.023	0.030	0.119	110.6	30.0	0.287	0.15	M9(3MHz)	70 / 2200x1080
	sand15%gravel	15%	5	200	0.30	0.0013	0.0024	0.910	0.028	0.036	0.101	158.5	40.0	0.312	0.19	M9(3MHz)	70 / 2200x1080
UniBo	EXP1sand	0%	5	110	0.36	0.0010	0.0014	0.407	0.021	0.027	0.033	97.0	25.0	0.115	0.14	SP(2MHz)[2]	30 / 4k
	EXP2sand	0%	5	110	0.31	0.0010	0.0014	0.473	0.021	0.027	0.045	97.0	20.0	0.156	0.14	SP(2MHz)	30 / 4k
	EXP3sand	0%	5	110	0.26	0.0010	0.0014	0.564	0.021	0.027	0.052	97.0	16.0	0.221	0.14	SP(2MHz)	30 / 4k

[1]M9 Sontek,[2]StreamPro, RDI

TABLE 2. Hydraulic and sedimentologic parameters of the experiments. The experiments conducted in UOttawa are named according the ratio of gravel/sand in the sediment bed; The experiments from UniBo are named according the hydraulic conditions, starting with the slow water velocity.

List of Figures

1 Riverbed scattering scheme. Part of the signal is scattered from the mobile particles of the bedload active layer (gray arrows), another part is scattered the surface formed by the immobile particles below the active layer (red arrows). 47

2 Experimental set-up scheme 48

3 Image Preprocessing. An example of an image with very low light intensity, taken at the end of the experiment (gravel15%sand, UOttawa). Local light enhancement, de-blurring and sharpening were consequently applied to each frame. 49

4 Image change detection. Three consequent frames (from the gravel15%sand experiment) are subtracted, the mobile particles are detected and the changes are matched according the highest cross-correlation coefficient. 50

5 ADCP (first row) and Camera (second row) filtered bed load velocity histograms and gamma fitted probability distribution functions. 51

6 *a)* Apparent bedload velocity (v_a) vs the camera velocity (v_c); *b*) Camera velocity vs normalized apparent velocity (v_{na}) 52

7 *a*) Dimensionless excess shear stress versus the filtered apparent (ADCP) velocity normalized by the settling velocity; *b*) Dimensionless excess shear stress versus the image velocity; *c*) Dimensionless excess shear stress versus the surface normalized (v_a/k_1) apparent velocity; *d*) Dimensionless excess shear stress versus the surface concentration k_1) 53

8 *a*) Surface concentration coefficient (normalization coefficient k_1) versus apparent bedload velocity (v_a); *b*) Surface concentration (k_1) versus the percentage of filtered velocity data in the post-processing. The inset plot shows k_2 coefficient versus the apparent bedload velocity v_a. The symbols are as in Fig.6 54

9 *a*) The STD/MEAN ratio (i.e. correlation fo variation c_v) of the ADCP velocity, before filtering; *b*) After the velocity filtering. The symbols are as in Fig.7 55

10 *a*) Theoretical volume backscattering (BS) coefficient (K_v), the lines represent the mono-granular functions of the BS coefficient and the markers are the mean expected values of the BS coefficient derived from the PSD of the used sediments; *b*) Amplitudes in dB of the ADCP BT echoes, only from UniBo data set. 56

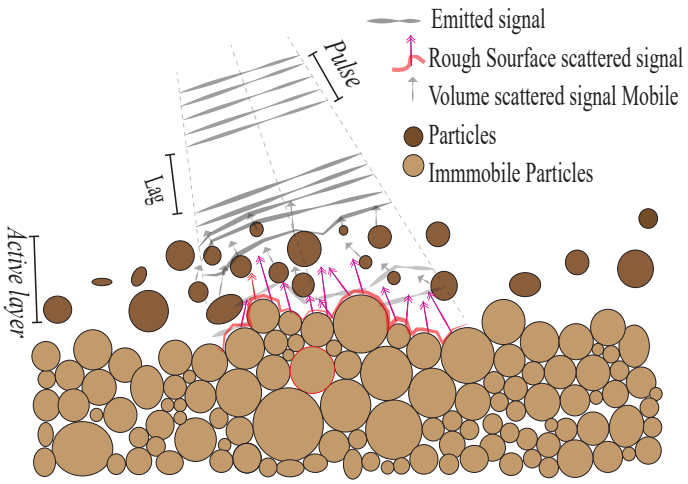

Fig. 1. Riverbed scattering scheme. Part of the signal is scattered from the mobile particles of the bedload active layer (gray arrows), another part is scattered the surface formed by the immobile particles below the active layer (red arrows).

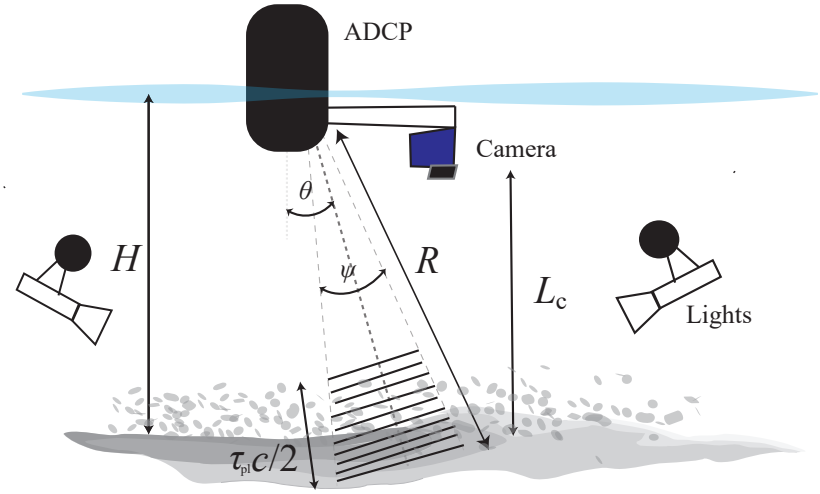

Fig. 2. Experimental set-up scheme

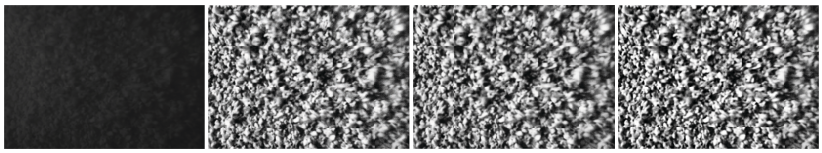

(a) Original **(b)** CLAHE **(c)** Wiener **(d)** Sharpen

Fig. 3. Image Preprocessing. An example of an image with very low light intensity, taken at the end of the experiment (gravel15%sand, UOttawa). Local light enhancement, de-blurring and sharpening were consequently applied to each frame.

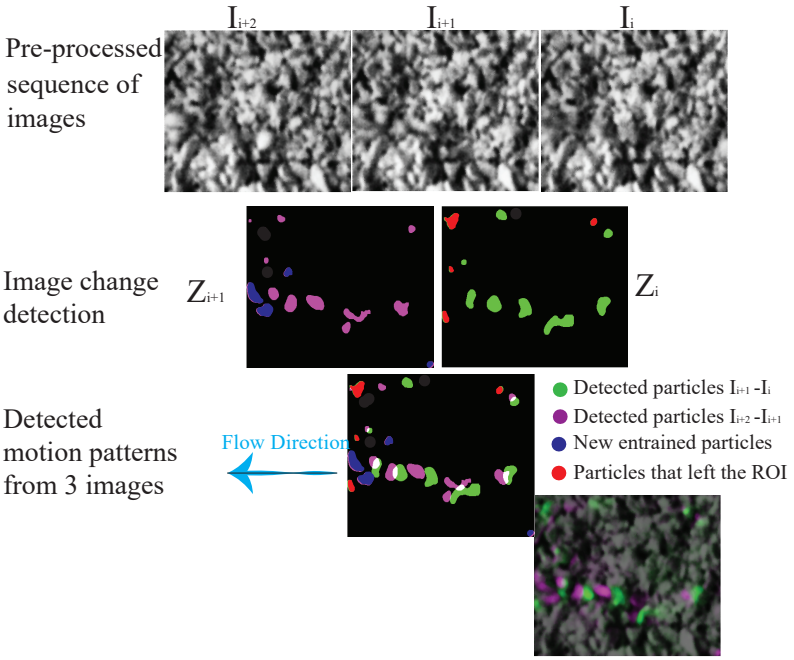

Fig. 4. Image change detection. Three consequent frames (from the gravel15%sand experiment) are subtracted, the mobile particles are detected and the changes are matched according the highest cross-correlation coefficient.

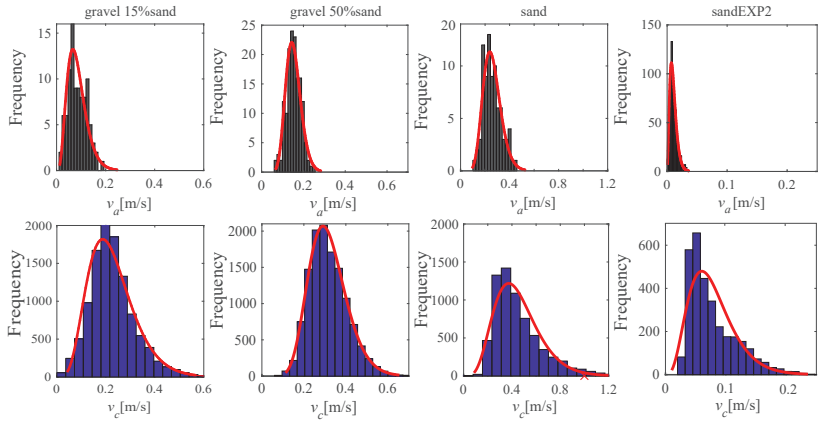

Fig. 5. ADCP (first row) and Camera (second row) filtered bed load velocity histograms and gamma fitted probability distribution functions.

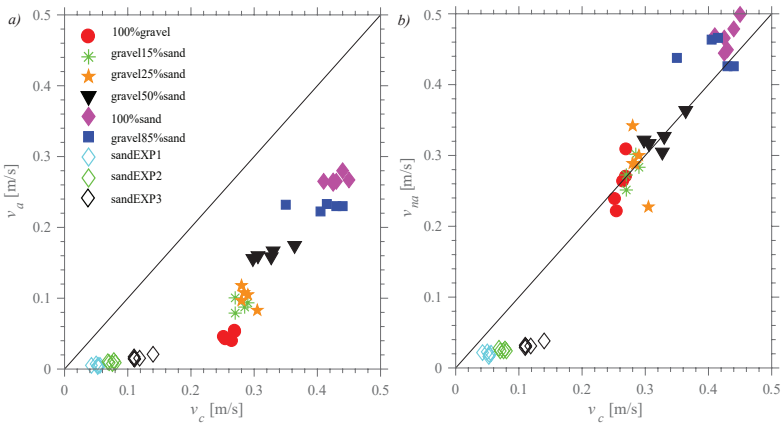

Fig. 6. *a)* Apparent bedload velocity (v_a) vs the camera velocity (v_c); *b)* Camera velocity vs normalized apparent velocity (v_{na})

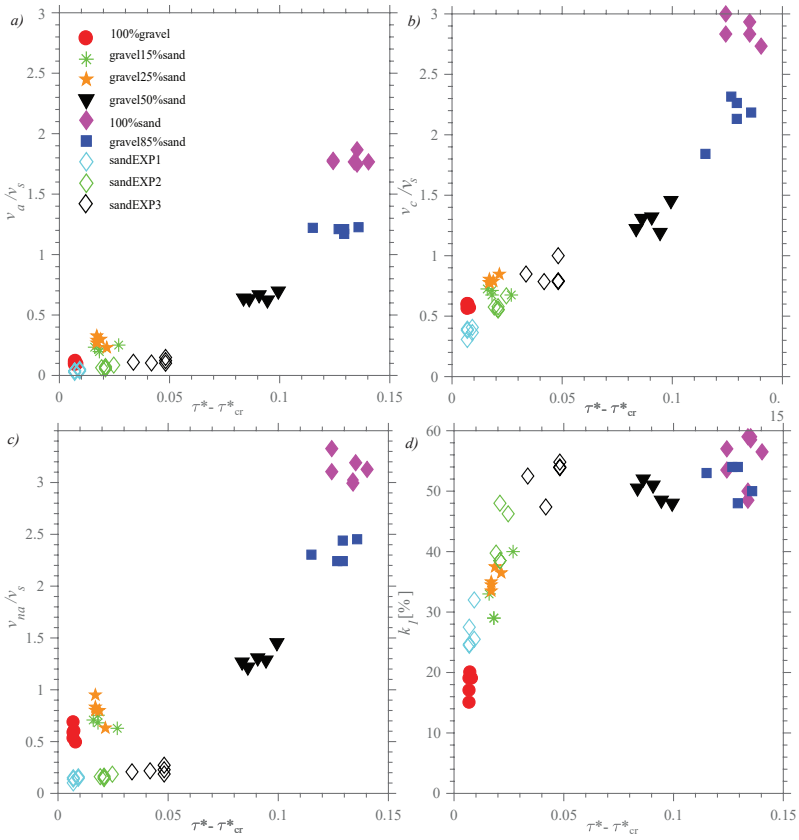

Fig. 7. *a*) Dimensionless excess shear stress versus the filtered apparent (ADCP) velocity normalized by the settling velocity; *b*) Dimensionless excess shear stress versus the image velocity; *c*) Dimensionless excess shear stress versus the surface normalized (v_a/k_1) apparent velocity; *d*) Dimensionless excess shear stress versus the surface concentration k_1)

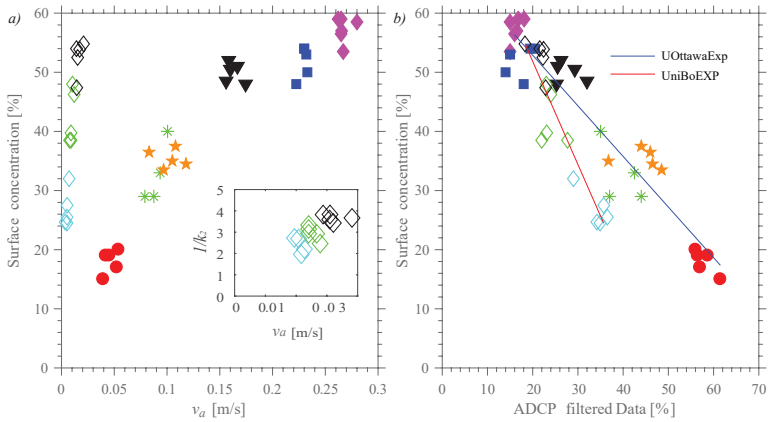

Fig. 8. *a*) Surface concentration coefficient (normalization coefficient k_1) versus apparent bedload velocity (v_a); *b*) Surface concentration (k_1) versus the percentage of filtered velocity data in the post-processing. The inset plot shows k_2 coefficient versus the apparent bedload velocity v_a. The symbols are as in Fig.6

.

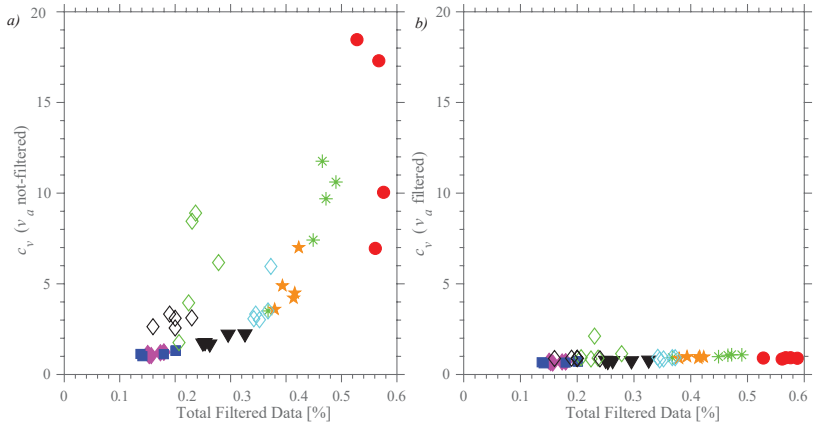

Fig. 9. *a*) The STD/MEAN ratio (i.e. correlation fo variation c_v) of the ADCP velocity, before filtering; *b*) After the velocity filtering. The symbols are as in Fig.7

.

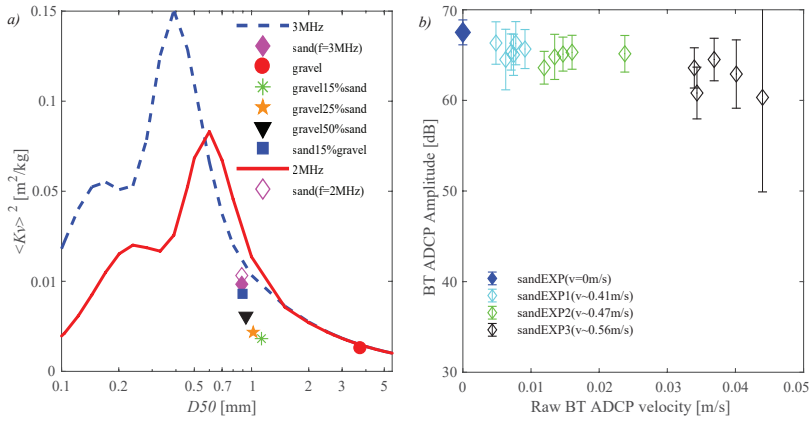

Fig. 10. *a*) Theoretical volume backscattering (BS) coefficient (K_v), the lines represent the monogranular functions of the BS coefficient and the markers are the mean expected values of the BS coefficient derived from the PSD of the used sediments; *b*) Amplitudes in dB of the ADCP BT echoes, only from UniBo data set.

Paper II

Acoustic sampling effects on bedload quantification using acoustic Doppler current profilers

Slaven Conevski, Massimo Guererro, Axel Winterscheid, Colin D. Rennie, Nils Ruther

Journal of Hydraulic Research, under review

Journal of Hydraulic Research

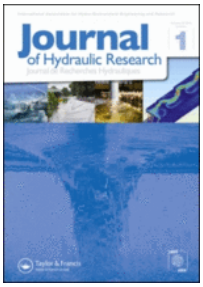

Acoustic sampling effects on bedload quantification using acoustic Doppler current profilers

Journal:	*Journal of Hydraulic Research*
Manuscript ID	TJHR-2019-0123.R2
Manuscript Type:	Research paper
Date Submitted by the Author:	01-Dec-2019
Complete List of Authors:	Conevski, Slaven; Norwegian University of Science and Technology, Department of Civil and Environmental Engineering ; University of Bologna, Department of Civil, Chemical, Environmental, and Materials Engineering Guerrero, Massimo; University of Bologna School of Engineering and Architecture WINTERSCHEID, Axel; German Federal Institute of Hydrology, Fluvial morphology, Sediment dynamics and management Rennie, Colin; University of Ottawa, Department of Civil Engineering Ruther , Nils; Norwegian University of Science and Technology
Keywords:	Acoustic Doppler current profiler, bedload sampler, bedload transport rate, bedload velocity, riverbed
JHR Keywords:	Bedload < Sediment transport, River channels < Fluvial geomorphology, Velocity measurements < Instrumentation, measurements and experimental methods

SCHOLARONE™
Manuscripts

Acoustic sampling effects on bedload quantification using acoustic Doppler current profilers

SLAVEN CONEVSKI, PhD candidate, *Department of Civil and Environmental Engineering, Norwegian University of Science and Technology, Trondheim, Norway*

Email: slaven.conevski@ntnu.no; slaven.conevski2@unibo.it (author for correspondence)

MASSIMO GUERRERO (IAHR Member), Assistant Professor, *Department of Civil, Chemical, Environmental, and Materials Engineering, University of Bologna, Italy*

Email: massimo.guerrero@unibo.it

AXEL WINTERSCHEID, Research Engineer, *Federal Institute of Hydrology, Department Fluvial morphology, Sediment dynamics and management"*

Email: winterscheid@bafg.de

COLIN D RENNIE (IAHR Member), Professor, *Department of Civil Engineering, University of Ottawa, Ottawa, Canada.*

Email: crennie@genie.uOttawa.ca

NILS RUTHER (IAHR Member), Professor, *Department of Civil and Environmental Engineering, Norwegian University of Science and Technology, Trondheim, Norway*

Email: nils.ruther@ntnu.no

Acoustic sampling effects on bedload quantification using acoustic Doppler current profilers

ABSTRACT

This paper provides an evaluation of a hydro-acoustic technique for efficient quantification of the bedload transport in riverine environments. Stationary bedload measurements were conducted simultaneously at different study sites, using three different acoustic Doppler current profilers (ADCP) working at four different frequencies. The raw apparent bedload velocities were de-spiked and filtered in a stream-wise direction. Then, functional correlations were observed between the magnitudes of the apparent velocities and the bedload transport rates measured by the conventional bedload sampler. Each ADCP yielded different results because of the different frequency backscatter sensitivity and acoustic penetration in the active bedload layer. In addition to the frequency, other acoustic parameters such as the percentage of the filtered data, transducers width, beam opening angle, beam-grazing angle and the pulse length, contributed to the acoustic bedload sampling. The influence of these parameters is examined, and recommendations are given for the performance and limitations of each instrument.

Keywords: Acoustic Doppler current profiler; bedload sampler; bedload transport rate; bedload velocity, riverbed.

1 Introduction

Sediment transport can be defined by its origin, transport mode and operationally by the collection measurement method. In an aquatic environment, sediment can either be transported as suspended load (in the water column) or bedload (moving at the bottom of the river). Bedload transport is usually characterized as the portion of the mobile and potentially mobile sediments on the riverbed. Furthermore, the bedload material is typically transported by rolling or saltating within a few particle diameters above the immobile bed (Parker, 2004; Van Rijn, 1984; Lajeunesse, et al., 2010).

The distribution of the bedload through alluvial streams contributes in shaping of the river morphology; thus, it is one of the key components in many branches of river management. Understanding the bed-material mechanics is critical for bedform dynamics and the management of heavily exploited rivers (e.g., ship-navigable waterways). Therefore, bedload transport data are a fundamental requirement for proper management of engineering practices in complex river systems. However, measurement series of bedload transport are seldom available and sometimes considered as statistically unreliable.

The conventional accepted approach of bedload measurements involves physical sampling using different types of bedload traps (Hubbell, 1964). The most used physical traps are the pressure difference samplers such as the USGS Helly - Smith or BL-84. Due to the sporadic

nature of the bedload, all physical sampling techniques suffer from difficulties and problems during the measuring procedure, such as: i.) disturbance of the bed; ii.) gap effect (sampler mouth is not in contact with the bed) iii.) sampling time; iv.) positioning above bedforms; v.) loss of material during sampling and raising the sampler, vi.) clogging of the mesh; etc. (Gaweesh & C. van Rijn, 1994). This is particularly exacerbated in rivers or river sections with sandy bed load material and extremely high or low transport rates. It is well known that these samplers mechanically may not catch the material at the actual rate; thus, they suffer from deterministic (Gomez, 1991) and stochastic (Frings & Vollmer, 2017) uncertainties. The sampling efficiency of the sampler depends on its individual design and the resulting stream conditions as well as the filling level, the mesh size, the particle size distribution (PSD) of the bed load material. Thus, the captured mass is corrected by applying sampling efficiency factors, typically determined in laboratory experiments (Gaweesh & C. van Rijn, 1994).

Due to the above- mentioned reasons, river engineers and scientists are increasingly adopting new surrogate methods that would deliver more accurate and continuous bedload data. The underwater acoustic techniques are an interesting alternative, because of the non-intrusive character and easy field-deployment. The acoustic techniques can be passive and active. Passive methods involve hydrophones (Rickenmann & McArdell, 2007) that record the acoustic noise of the bedload particle collisions, while the active techniques analyse the effect of the bedload motion on the scattered acoustic signal from the bottom (Urick, 1983). Unfortunately, passive methods do not appear feasible for low-land medium to large rivers, mostly due the nature of the bedload transport and the river morphology.

The acoustic Doppler current profilers (ADCPs) are active sonars in which the source and receiving hydrophones are coincident, i.e., monostatic configuration. An ADCP is a type of sonar system that is typically used to measure water velocity over varying ranges. Rennie et al. (2002; 2004) reported a positive correlation between the bedload transport rates (Qs^m) and the Bottom Tracking (BT) signal of the ADCP deployed in stationary, fixed positions. Since then it became a new intriguing approach towards quantifying the bed-load sediment transport. Later, moving-boat ADCP measurements were performed, where the BT mode and the GPS signal were successfully utilized for mapping the bedload velocity in sand/gravel riverbeds and showed the possibility of measuring the spatial distributions of bedload (Rennie & Millar, 2004). The underlying physical interpretation of the apparent bedload velocity (v_a) measured by the ADCP assumed that v_a is equal to the spatial average velocity of the bed surface, including mobile and immobile particles (Rennie, 2002). Another field study presented a complete interpretation of the analytical relation between apparent velocity, the particle velocities and the bedload concentrations (Gaeuman & Jacobson, 2006). Other studies also examined the relationship between the bedload transport rates and the apparent velocities

for a range of particle size distributions (PSD) and sediment transport conditions (Jamieson, et al., 2008; Williams, et al., 2015). Most of these studies confirmed that the ADCP bedload quantification is strictly site-specific and needs calibration for an accurate estimation of the bedload transport rates (Rennie, et al., 2017). Despite the site characteristics and the acoustic backscattering response towards different PSD (Rennie, et al., 2017), some studies demonstrated that instrumental features (i.e., carrying frequency, transducer geometry, the acoustic pulse, etc.) could play an important role into the determination of the apparent velocity. Moreover, it was found that shorter pulses give better correlation with the bedload transport rate due to reduced bias by high close-to-bed suspended load concentrations, and that lower frequency instruments consistently were giving lower apparent bedload velocity both in laboratory and field investigations (Ramooz & Rennie, 2008; Latosinski, et al., 2017). Most recently, laboratory campaigns confirmed that the lower frequency underestimated the mean bedload velocity, by comparing the surface velocities measured by high-speed cameras and the apparent velocities measured by two different ADCPs (Conevski, et al., 2019). The same study bore out the necessity of stream-wise filtering of the apparent velocity for more accurate estimation of the average apparent velocity. The filtered data showed a negative correlation with the bedload surface concentration, which is the number of mobile particles detected by the camera, giving a higher percentage of filtered data for the less abundant sediment transport conditions. These differences between the instruments were tentatively assigned to the strong influence of the surface scattering (i.e., immobile bed particles) as a response of the lower frequency and different acoustic geometry between the ADCPs. The filtering procedure was successfully applied in Conevski et al. (2018) and it was shown that reduced the uncertainty of the kinematic transport model (Rennie & Villard, 2004) and confirmed its application without explicitly fitting parameters. The difference among the velocity magnitudes was registered in Conevski et. al (2018) and part of that data will re-used in this paper.

This paper attempts to apply the recently discovered laboratory results by examining the data of concurrent v_a and Qs^m obtained from three field campaigns with several measurement locations in two large rivers in Germany. The PSD of the bed load ranged from fine to coarse sand and fine gravel depending on the location. This paper analyses the BT signal of three different ADCPs (RDI Rio Grande 1.2 MHz and 0.6 MHz and M9 Sontek) working with four different frequencies (0.6 MHz, 1 MHz, 1.2 MHz and 3 MHz) and all of these have been deployed simultaneously in all campaigns and measuring locations. The focus in the analysis was the acoustic geometry and the acoustic sampling effect on the bedload velocity measurements. By combining the basic principles that govern the ADCP bedload velocity estimation, this paper provides an approach to evaluate the differences among the frequencies

and designs of the acoustic instrument (e.g., acoustic geometry and pulse modulation). In more details, the paper discusses the pulse modulation effect (e.g., broadband - BB) of each ADCP, as well as the importance of acoustic energy focusing at beam axis (i.e., side-lobe and lateral central lobe) for proper acoustic sampling. The discussion is extended towards the usage of each instrument in different transport conditions and pointing out the best practices for sand-bed rivers. Results of this approach are summarized by applying the kinematic transport model (Rennie & Villard, 2004) and empirical formulas for estimating the bedload porosity and active layer thickness. The total error propagation by the ADCP measurements in estimating bedload transport rate is presented in the end.

2 Methodology

2.1 Sampling strategy and instrumentation

The ADCP data in this study were collected in three campaigns in two large low land rivers in Germany. In each campaign, the ADCP measurements were performed on pre-selected locations. At the same time physical samples of the bedload have been taken here, following a well-established monitoring program, which is carried out nationwide along free-flowing waterways by the German Waterway and Shipping authority (WSV) and the Federal Institute of Hydrology (BfG). In addition to the physical sampling bedload data collection, this program includes measurements of the water velocity, discharge and suspended sediment concentration. All bedload data were collected in stationary positions from a fully anchored ship (see Fig.1) in 5 - 8 equally spaced points over a cross-section. On each position of the cross-section, three bedload samples were collected. In total 171 samples from 10 cross sections were collected in three campaigns. In the following sections, some information about the study sites and the data processing are presented. More details of the sediment data and the hydraulic characteristics of the study sites can be found on the SedimentDB database (http://geoportal.bafg.de).

Instrumentation ADCP

Three ADCPs were deployed during the stationary measurements: (i) Sontek M9 1/3 MHz, (ii) RDI RioGrande 1.2 MHz and (iii) 0.6 MHz. The instruments were firmly mounted on the ship (with maximum pitch and roll of 0.5 ^{o}) with a five to ten meters distance between them (see Fig. 1 for the layout of instruments deployed on the ship). Some deviation in the results produced by the different ADCPs may be expected due to their separation distance. In some cases, the ADCPs may have been biased by the heterogeneous sporadic motion of the bedload as well as of the artificial armouring of the riverbed, especially for the positions closer to the

banks. Further details about the bedload sampler and the ADCPs will be given in the next sections. No interferences were observed between ADCPs working at similar frequencies, such the 1 MHz and 1.2 MHz devices which also 11 meters were apart (see Fig. 1).

Instrumentation Physical Samplers

The sampler used in the campaigns was a customized pressure-difference sampler, operated with a crane installed in the backside of the ship (see, Fig.1). The sampler was designed by the BfG in the 1970s and it has been further developed ever since. In its basic design, the BfG-sampler – similar to the Helly-Smith type is based on the "Bed load Transport Meter Arnhem, BTMA" (Brandstetter, et al., 2012). For more than 40 years now, the BfG-sampler has been used for bedload measurements. The mesh size of the collecting steel basket (note that the bottom does not have a mesh, only the sides and the top) is 1.4 mm and the nozzle has dimensions 16 cm width and 10 cm height. The length of the sampler is 91 cm, without the landing structure. To facilitate the landing and to ensure the contact with the riverbed, the sampler is mounted on a steel frame and the nozzle neck is made of flexible plastic material (Fig. 2). The bedload sampler has a camera and lights system mounted above the nozzle giving live-stream video for each sample (Fig. 2). The simultaneous observation of the camera footage helped with the selection of correct samples and identification of samples requiring repetition during the campaign.

The efficiency of the sampler was tested in several laboratory campaigns performed by the BfG, University of Aachen and University of Karlsruhe (Nestmann, et al., 2000; Hillebrand & Frings, 2017). The tests were conducted using different bed sediments ranging from sand to coarse gravel. The total amount captured by the sampler was compared with the total amount of transported sediment that passed behind the sampler. Behind the sampler, a larger mesh box was mounted with smaller mesh size than the material used, able to catch all material passing through the sampler. Using multivariate regression analysis, a correction function dependent on the total collected mass was developed to determine the efficacy calibration factors. Material smaller than the mesh size used may pass through the collecting steel basket, thus there is an inevitable loss of bedload material, which means a distortion especially of the actual amount of sandy bedload. For that purpose, additional series of tests were conducted in a laboratory flume to better quantify this amount of lost sand (Banhold, et al., 2016). In this analysis several other factors were included such as: the size of the sampler, mesh size and the type of bedload material. Accordingly, the applied efficiency calibration factors in this study varied between 1.2 - 1.6, depending on the total collected bedload mass and the hydraulic efficiency related to its design. In addition, these calibration factors are part of standardized

procedure developed by BfG for different samplers.

The sampling time was 5 minutes once the sampler reaches the riverbed. After the campaign the collected samples were sent to a certified contract laboratory to determine the dry mass and the particle size distribution (PSD). To yield the instantaneous transport rate the corrected mass (i.e., using the calibration factors) from each sample was divided by the width of the sampler (10 cm). Finally, the average of three samples per position was used as a representative transport rate per position; thus, 57 data points of the physically measured bedload transport rate were used for the data analysis. It is worth noting that most of the systematic uncertainty is accounted for by applying the efficiency calibration factors; still, some deviation in the samples should be expected. These deviations have a stochastic nature related to human operation errors and the bedload spatial and temporal variability (Frings & Stefan, 2017). Additionally, in the post-processing of the data a few measurements were discarded due to unreliable sampling noticed in the video and those are identified as bad samples. At these positions the large deviation between the three samples was an additional indicator to exclude these samples from further analysis.

2.2 Study Sites

Oder River

The first campaign was conducted in the downstream part of Oder River, along the German-Polish border, in May 2017. Seven positions were chosen in a first cross section near Neurüdnitz and eight positions in the other cross section near Hohenwutzen (see Fig. 3 and Table 1). The positions were chosen to cover the entire active-channel width, avoiding the region between the groins. The average discharge was 800 $m^3 s^{-1}$, with maximum average velocity in the middle of the river of 1 m s^{-1}. The total width of the cross-section was 200-300 m including the groins. The water depth varied from 2.5 m near the banks to 5.2 m in the thalweg. The annual mean discharge is around 500 $m^3 s^{-1}$, and the average annual maximum discharge is around 1200 $m^3 s^{-1}$; thus, the measured flow was high but not a flood event. From the morphological perspective, the Oder River is a typically sandy river with well-characterized slow dune migration. The dunes were 10 - 20.5 m long with a height of 0.09 - 0.15 m. Most likely due to superimposing of the larger dunes some smaller bedforms were also noticed with 1.5 - 5 m length and 0.05 - 0.12 m height (BfG, personal communication). The D_{50} (median diameter) of the bedload in both cross sections was 0.55 mm with a standard deviation (D_{std}) of 1.1 mm. The particle size distribution is relatively homogeneous through both cross-sections. At the Oder River only three frequencies (0.6 MHz, 1.2 MHz and 3 MHz) were used, and the M9 worked only in the default RiverSurveyor configuration.

Elbe River

The other two campaigns (Elbe1 in March 2018 and Elbe2 in May 2018) took place in Elbe River, the third largest river in Germany. The measurement concept implemented was the same as at the Oder. The average annual discharge is 650 m^3 s^{-1} at Neu Darchau close to the estuary (campaign Elbe1) and 320 m^3 s^{-1} upstream at Dresden (campaign, Elbe2). During both campaigns, the discharges were close to the annual average: 700 m^3 s^{-1} during the Elbe1 and 350 m^3 s^{-1} during Elbe2. Measurements were taken at three cross-sections in Elbe1 (Neu Darchau, Wilkenstorf, Langendorf) and 5 cross-sections in Elbe2 (Barby, Saale confluence OH , Saale confluence UH, Breitenhagen, Buckau). The distance between adjacent cross sections varied from 2 to 30 km in these campaigns (see Fig. 3 and Table 1). The Dunes in these two campaigns varied between 13 - 18 m length and 0.16 - 0.23 m height, accompanied by smaller bedforms ranging from 2 - 5 m length and 0.05 - 0.2 m height (BfG, personal communication). The PSD of the captured bedload sediments varied between the campaigns. The bedload material captured in Elbe1 was characterized with fine to coarse sand with D_{50} = 0.75 mm and D_{std} = 0.55 mm, and in Elbe2 coarse sand to fine gravel with D_{50} and D_{std} equal to 0.95 mm and 1.1 mm, respectively. In both campaigns, the PSD showed higher variations from section to section comparing to the rather homogeneous distributions in the Oder campaign.

2.3 Calculation of the hydraulic parameters

The distance between the cross sections was sufficiently large to ensure each cross section can be statistically independent. Table 1 gives an overview of the mean hydraulic parameters for each cross-section, observed during these campaigns. For the energy slope, S, data for all reaches were calculated from the two nearest gauges. The mean water depths, H, discharges, Q, and the depth-averaged water velocities, U, given in Table 1 were obtained from the ADCP measurements performed for each cross-section before starting the bed load measurements. Due to the presence of dunes and groins it was most convenient to calculate the average shear stress of the cross section, τ, by applying the momentum balance equation, from which τ/ρ is given by $g \cdot H \cdot S$, where ρ is the water density and g is the gravitational constant. The total non-dimensional Chezy parameter was calculated for each cross-section using the expression $C_z = U/u_*$, where u_* is the shear velocity calculated as the square root of the shear stress to water density ratio: $\sqrt{\tau/\rho}$. This method gives an estimation of mean shear stress which can be conveniently applied in low land rivers such as these, where the slope was essentially constant over long distances. When bedforms are present the influence of the form drag friction should be eliminated because it does not contribute to the bedload transport. Beside the total shear velocity (u_*), the effective grain-shear velocity (u_*') and Chezy

parameter due to the grain friction (C_z') were calculated using the Van Rijn (1984) formulas. Finally, the critical shear velocity was calculated using the critical mobility parameter, u_{*cr}, defined by Shields and analytically presented by Van Rijn (Shields, 1936; Van Rijn, 1984). Note that all the values given in Table 1 are the average values over a cross section.

2.4 Acoustic theory and ADCPs working principle

The acoustic Doppler current profilers (ADCPs) are active sonar systems that are typically used to measure the water velocity over varying ranges, producing a profile of velocity vectors along the three dimensions. The ADCP transmits an acoustic signal at instrument - specific frequency and measures the change in frequency (e.g., Doppler shift) of the reflected signal from the particles in the water column. The general idea of the Doppler approach assumes that in the water there is a sufficient number of particles to reflect enough acoustic energy and to estimate the Doppler shift (RDInstruments, 2011). ADCPs are generally configured as an assembly of four transducers spaced at 90° azimuth intervals (i.e., Janus configuration). These transducers form acoustic beams with grazing angle of 70 - 60 ° that permit measurements of three velocity components under the assumption that the velocity is homogeneous in the plane defined by equal ranging distances from each of the transducers. This study focuses on the BT mode of ADCPs, which is a separate signal, used for detection of the riverbed and the vessel velocity, v_{BT}. Compared with the water velocity profiling, the BT signal involves emitting longer acoustic pulses with lower sampling frequency to identify the riverbed, but it works with the same carrying frequency. For stationary deployment, the BT signal is affected by the riverbed mobility, particularly, the so-called apparent bedload velocity results: $v_a = v_{bt}$. This bias on the ADCP actual velocity is considered as a measure of the spatially-averaged bedload velocity (Rennie, et al., 2002).

Nevertheless, the apparent bedload velocity is not necessarily spatially averaged, and it is strongly dependent on the instrument frequency, the acoustic geometry and the internal signal processing (Conevski at al. 2019). This is mostly due to the complex two-phase scattering processes that occur at the river bottom. The mobile particles that determine the bedload velocity are responsible for volume scattering, but the signal may also scatter off the rough immobile bed sediment surface underneath the active layer of mobile bedload (Conevski at al., 2019). The surface scattering is typically stronger than the volume scattering and deteriorates signal, which may produce errors in apparent bedload velocity estimation.

Table 2 gives an overview of the used ADCPs and the important acoustic parameters, which will be further explained in the following sections.

Signal Processing

The Rio Grande ADCPs used in this study are designed to process the signal using the coded-pulse Broadband technology (BB) developed by RDI (see, Appendix A). The slant angle of the beams is 20 º, and the pulse length was set to the minimum default value, i.e., 20 % of the water depth at the measuring position. The number of pings differed from measurement to measurement (1 - 5 pings), but no significant difference was noticed (see also, Table 2). On the other hand, four different configurations were used for the M9 by Sontek. The instrument worked with eight beams declined at 25 º from the vertical (Sontek, 2017), four each at 1 MHz and 3 MHz carrying frequencies, able to measure the three-dimensional bedload velocities. An additional 0.5 MHz vertical beam is usually applied for water depth assessment. The first configuration refers to regular use of the commercially available software RiverSurveyor (RS). This software does not permit a change of the signal processing nor any specific parameters. It automatically configures, and this information is only partially available for the user. In these filed studies it only used the 3 MHz transducers, because the water depth did not go over 5.5 m.

The configuration change was enabled because of direct collaboration with Sontek and employing their internal software, ADPviewer, developed exclusively for research purposes. This software permits the use of all nine beams at the same time and change of most of the internal parameters. Moreover, the acoustic beams were enabled only for the BT mode, permitting four transducers to work at 1MHz, the other four to work at 3MHz, and the vertical beam at 0.5 MHz, which does not provide the apparent velocity. In short, two results of the of apparent velocity were available for the M9: at 1 MHz and 3 MHz carrying frequencies. The second configuration involved incoherent (IC) signal processing (see Appendix A) and the third configuration assumed pulse-to-pulse coherent (PC) signal processing. The last configuration refers to the default configuration (def), that gave the raw data (note that the data delivered by the first configuration (RS) go through some internal post-processing steps, not really clear for the users).

The number of pings varied between 1 and 5 and the pulse length was automatically adjusted ranging from 5 to 26 cm length according to the water depth or the sediment concentration. The ADPviewer was not used during the campaign at Oder River, and at the first Elbe campaign several measurement positions were conducted only with the IC configuration. The velocity-ambiguity limitation was not a constraint for this study because the manufacturers (RDInstruments, 2011; Sontek, 2017) claim that have developed a unique signal modulation that avoids the ambiguity.

Acoustic geometry

A typical ADCP beam pattern projected from its monostatic transducer is shown in Fig. 4. The transducers with diameter D_t are typically declined from the vertical by angle θ. The 2φ beam opening angle defines the central lobe, and it depends on the type of the transducer and the instrument working frequency $\varphi = 29.5\lambda / D_t$ (Urick, 1983), where λ is the sound wavelength of the emitted signal. The signal intensity of a reflected pulse is greatest along the central axis and non-linearly diminishes to the outer boundary of the central lobe (i.e., at angle φ), defined to be where intensity is half the central intensity. At larger angles than φ, small magnitudes of sound intensity are still observed, denoted as side-lobe intensity. The first side-lobe opening angle defines the so-called side-lobe contaminated area that extends to distance z_s perpendicular to the bed (see, Fig. 4). Note that this is the first side lobe angle (i.e., ω in Fig. 4) typically appears at 6 % and 14 % of the distance of the ADCP to the riverbed, for $\theta = 20^{\circ}$ and for $\theta = 25^{\circ}$, respectively (RDInstruments, 2011; Sontek, 2017). It usually corresponds to 1.5 - 7 $^{\circ}$ opening from the main lobe, but it is also common to find side-lobes at 15 $^{\circ}$ and even 40 $^{\circ}$ from the main lobe and these could be a dominant source of error in the bottom echo identification. In addition, z_c is the distance from the riverbed to a line perpendicular to the inner side of the central lobe. Furthermore, the ADCPs cannot measure the region near the transducers (near field, Fig. 4) due to the ringing effect (RDInstruments, 2011). These regions are denoted as blanking distances, and the water velocity data from these areas is automatically discarded in the final data delivered by the ADCP. Given that the observed D_{50} in these campaigns is between 0.5 - 1.5 mm, Fig. 4 bears out that the bedload measurements are always into the side-lobe and central-lobe contaminated area. However, the signal emitted to track the bottom is optimized to detect the riverbed and by that to estimate the boat velocity; in this case, the high reflection produced from the bottom at central lobe should overwhelm the side-lobe energy.

The emitted BT pulse by each beam insonifies four independent areas of the riverbed at different bed elevations. The water depth, H, pulse length, Pl, transducer width, D_t, beam opening, φ, and the riverbed surface determine the sampling area. The sampling volume was previously defined for IC configuration with the maximum height occurring at about half pulse length, as explained in detail by Rennie (2002). However, the height of the sampling volume appears also to be related to sub-pulse and coded elements distances in the case of more advanced signal processing.

The beam geometry in Fig. 4 also shows that the sampling of the riverbed occurs in unequal portions of the pulse due to the beam slant and spreading angle (Rennie, et al., 2017). This suggests that the pulse portion closer to the inner boundary of the central lobe has a dominant

effect in the distribution of the scattered energy. Moreover, the surface scattering may amplify both the inner boundary of the central-lobe and the side-lobe intensity, which further complicates the processing of the signal. The acoustic sampling of the bed, as well as the scattering of the BT pulse, will be described in detail in the first part of the discussion in this paper.

2.5 ADCP Data Post-processing

To obtain three samples with the physical sampler at least 25 - 30 min were needed per position; thus, it predetermined the sampling time of the ADCPs. Previous studies demonstrated that a total time of 5 to 7 min is enough for getting a stable average of the BT velocity data (Rennie et al. 2002, Conevski et al. 2019). The RDI ADCPs were run through all the bedload sampling time at a station; hence, no change of the configuration was performed. On the contrary, the measurements of the M9 ranged between 5-7 minutes for each of the four configurations.

The raw apparent velocity obtained from the ADCPs was filtered by discarding the velocities in the opposite direction of the water flow as explained in Conevski et al. (2019). The filtering procedure uses the water velocity vectors obtained from the lower part of the water profiles of each ADCP to identify the average direction of the water flow. These vectors determined the reference direction to discard the BT velocity vectors with more than ± 90 º mutual angle difference. Also, the values that exceed three times the standard deviation of the raw data were discarded. A simple explanation of the filtering procedure from one sampling position is shown in Fig. 5. The water velocities that determine the reference direction are given in plot Fig. 5a, and the BT velocity is plotted in Fig. 5b where the discarded data are presented in faint-grey symbols and the accepted v_a is in blue. The filtering discarded the erroneous data produced internally by the ADCP, and it eventually discarded the velocities measured in the bedforms reattachment zone, where the bed velocities are highly heterogeneous (Rennie & Villard, 2004). Note that large deviations of the bedload vectors in comparison to the water velocity data should be expected (see, Fig. 5), but not negative values (e.g., opposite direction of the flow). Negative values are ascribed to surface scattering and internal data processing which determines the instrumental accuracy (i.e., error in Doppler assessment). These effects were discussed in Conevski et al. (2019) and are further pointed out in Results and Discussion. The unreasonable extremes in the bedload velocity were most likely a result of a water bias and were also filtered out. Similarly, as in Conevski et al. (2019), the fraction of ensembles removed is denoted as *FD* and it is specific for each instrument and configuration and each measurement position.

The filtered velocity data were averaged through all the sampling period and later compared

with the average transport rates from physical samples taken at the same location.

The homogeneity assumption mentioned in the previous section can be a serious disadvantage in highly deformed riverbeds. Riverbed undulations, sediment depositions or large bars can introduce additional uncertainty of the BT data because the four beams sample in regions with significantly different bedload transport conditions (see, Fig. 6). Similarly, the measurements close to the steep riverbanks or close to the groins violated the homogeneity assumption. These disturbances led to estimation of erroneous apparent bedload velocities, mostly due to the different Doppler shift in each beam, but also due to the significantly changed grazing angle (θ). The measurements in this study were on predefined positions which did not account for these disturbances in ADCP performance. Therefore, by observing the direction of the BT velocity and looking at the riverbed bathymetry, these measurements were identified as well as bad samples and fully discarded from the further analysis. Moreover, a high percentage (e.g., $FD > 60\%$) of the filtered data also indicated a problematic measurement position (i.e., bad sample). Note at the same ship position the ADCPs measured in at least 10 m distance, therefore the number of bad samples is specific for each ADCP. The bad samples from the ADCPs and the physical sampler ranged between 5 - 15 % of the total samples for each ADCP.

To evaluate analytically the influence of the acoustic geometry on the apparent bedload velocity estimation, two indicators are offered and will be discussed later in this paper:

- M, denoted as the acoustic sampling. It is the product of the pulse length (Pl) and the wavelength (λ) and the total filtered data (FD) over the number of pings (BP) per sample (i.e., $M = Pl \cdot \lambda \cdot FD / BP$). The pulse length and the wavelength are representing the total energy transmitted to the riverbed by a single pulse/ping. This indicator also equalizes the filtering rate among different modulations, taking into account the sampling time of the bed portion given by the pulse length and the number of pings per sample.

- z_c, also shown in Fig.4, determined as the vertical distance between the inner boundary of the central lobe and its axis, which was calculated by using the average depth (H^{ADCP}) measured by each ADCP. It directly demonstrates the influence of the beam geometry on the acoustic energy spreading within the central lobe, which may affect apparent bedload velocity estimation. z_c is calculated by simple application of trigonometry knowing the grazing and opening angles (θ and φ respectively) and the water depth at the measurement position, assuming a flat riverbed. Note that z_c does not consider the riverbed deformations (i.e., bottom roughness), which would contribute for more uncertainty.

2.6 The kinematic model

Similarly, as reported in Rennie and Villard (2004) the bedload transport rate can be calculated using the ADCP data and some of the hydraulic parameters given in Table 1. The bedload transport rate was estimated using the kinematic model:

$$Q_s^{ADCP} = v_a n_k D_{50} c_b \rho_s , \quad (1)$$

where v_a is the filtered apparent bedload velocity, $d_{tk} = n_k D_{50}$ is the active layer thickness applied in the model wherein n_k is a coefficient, c_b is the bedload concertation, and ρ_s is the dry grain density of the bedload sediment. To apply this model conveniently, it must be assumed that the apparent bedload velocity represents the spatially average bedload velocity. Thus, in the case of full transport it is necessary that the ADCP samples through the entire active layer while having less possible influence of the immobile surface beneath the active layer. The best acoustic sampling must be chosen to give a reliable estimation of the mean bedload velocity. Additionally, the transport rate was assumed to be spatially homogeneous in all the four beams footprints on the riverbed and with constant velocity, thickness and porosity.

The bedload concentration (c_b) was calculated using grain shear friction velocity (u_*'), specific for each measurement position and the empirical formula given by Van Rijn (1984). To calculate the effective grain shear velocity, the Chezy coefficient (C_z') related to the skin roughness was estimated for each position separately utilizing the depth measurements from the ADCPs and the D_{50} estimated form the captured bedload material.

The active layer thickness accounts only for the mobile particles; therefore, the active layer thickness (d_t) was assumed to be equal to the average saltation height of the bedload particles. The saltation height has been a research topic for many years and several empirical equations are offered in the literature. Given the hydraulic conditions and the observed PSDs, four different empirical equations were used to calculate locally the active layer thickness (Van Rijn, 1984; Lee & Hsu, 1994; Borthwick, 2015). These formulas were applied at each sampling position and the results gave maximum and minimum values of about $d_t = 8\ D_{50}$ and $d_t = 3\ D_{50}$, respectively. The results did not deviate significantly for the different positions due to the similar water velocities and PSD (see Table 1). However, the positions very close to the banks demonstrated different results, mostly because of the influence of the groins, the artificially armoured riverbed, as well as the lower water velocity. Note that d_t is the empirically calculated thickness of the active layer used to validate the obtained values of the d_{tk} integrated in the Eq. (1).

3 Results

3.1 The apparent bedload velocities

After the post-processing of the apparent bedload velocity data, the magnitudes were calculated separately for each measurement position and ADCP configuration given in Table 2. Then, to examine the existence of an effective relationship between the bedload transport rates (Qs^m) and the apparent bedload velocity (v_a), a linear regression analysis was performed. Table 3 gives an overview of some of the parameters from the linear analysis (e.g., coefficients of correlation, r), as well as the averaged hydraulic and acoustic parameters from the measurements conducted separately by each ADCP and configuration. For example, v_a in Table 3 is the averaged post-processed apparent velocity measured by the corresponding ADCP and configuration for all three campaigns. Similarly, the filtered data (FD), the water depth (H^{ADCP}), the water velocity (U^{ADCP}), coefficients of variation (CV) are the averaged values given for each ADCP and configuration. Table 3 also gives the total number of positions measured by each instrument, as well as the number of the bad samples discarded before the linear regression analysis. These parameters were explained in the Methodology section and will be further elaborated in the following section. More details of the linear analysis are given in Fig. 7, where the equations and the summed square of the residuals of the fitting (SSE) are presented together with the plots of the v_a versus the Qs^m. Note that the analysis was performed over a broad set of bedload data, at different study sites, with different PSDs, ranging from fine sand to fine gravel (e.g., some positions in the upstream part of Elbe). Also, the number of the data used for each instrument varied depending on the availability at a specific campaign, as well as of the presence of outliers.

Figure 7 shows that each ADCP and configuration delivered velocities that are in relatively good correlation with the physical samples taken at the corresponding positions. However, the lowest frequency, RDI 0.6 MHz, continuously gave the lowest mean apparent velocities resulting with steeper slope and lowest intercept. The data of this instrument gave the lowest r = 0.69 and the highest percentage of filtered data, FD = 0.34 (see Table 3 and Fig. 7a). On the contrary, the 3 MHz configurations reported highest v_a and lowest FD. The RDI 1.2 MHz in comparison with 0.6 MHz observed higher magnitudes of the apparent velocities, giving a slightly lower slope of the fitted line and higher correlation coefficient (see, Fig. 7b). Nonetheless, the 1 MHz Sontek data did not give lower v_a than the 3MHz and 1.2MHz, as it would be expected because of the lower carrying frequency. Indeed, it gave very similar v_a to the 3MHz obtained from the same instrument. In average, all configurations using 1MHz frequency showed almost double higher v_a than the 1.2 MHz and slightly lower v_a than all 3MHz configurations (see Table 3, and Fig. 7d-f). The correlation coefficients are highest for

the 1MHz, showing a small variation among the configurations, partially due to the different sampling positions and the time gap between the two configurations. The small difference between the magnitudes of the apparent velocities for 1 MHz and 3 MHz confirms the influence of the instrument carrying frequency towards underestimation of the v_a, but it appears that the different frequency for M9 did not play the main role in the ADCP BT measurements. In addition, the higher proportion of filtered data (*FD*) for the 1 MHz than 3 MHz corroborates the fact that the lower frequency is more sensitive to noisy data, because of the stronger surface scattering. Noticeable is the difference between the *FD* for the RDI and Sontek (see, Table 3), and it is associated with the unique internal data processing of each instrument (Conevski et al. 2019).

The use of different signal processing modules for the M9 (i.e., ADCP configurations) also did not result in significant divergences among them. Regardless of the different numbers of pings (BP, see Table 2) and different configurations, the Sontek M9 measured similar apparent velocities (see, Fig. 7d-i and Table 3). This corroborates the expectation that range-velocity limitation should not introduce additional deviations in the bedload measurements in most of the riverine environments due to the relatively low bedload velocities and shallow waters. However, the PC configuration demonstrated the best correlation with the physical transport rates (Qs^m) for both frequencies. Note that RS in most of the cases should work with PC, but also it may have switched to IC. In relation, Fig. 7c shows that the slope of the fitted line for the RS configuration is between the PC and IC, which eventually confirms the fact that the instrument may have changed between these two configurations during the measurements. Besides, the information for the used frequency delivered by the RS is only about the water profile measurements; thus, one may rightfully suspect that both frequencies were used during the measurements with RS.

Furthermore, no instrument configuration in Fig. 7 has zero intercept. The intercept is around 0.01 for 0.6 MHz, 0.025 for 1.2 MHz and between 0.04 - 0.05 for both M9 frequencies (1 MHz and 3 MHz). This means that the same bias is present in all measurements; therefore, it can be associated with the inability of the bedload sampler to capture bedload material during weak transport.

The coefficient of variation (*CV*) shown in Table 3, decreased by 10 -15 % comparing the coefficients after (CV_{va}) and before (CV^{*}_{va}) the filtering of the raw apparent velocity, and the proportion of the filtered data (*FD*) differs for each instrumental configuration. The decrease of the *CV* shows that the filtering procedure successfully decreased the uncertainty induced by the instrument measurement errors. The filtered data (FD) of the apparent velocity is different for each instrument/configuration because it strongly depends on the instrument characteristics such as frequency, ambient noise, etc. In general, lower frequencies required

heavier filtering, due to the more substantial impact of the immobile surface enabled by the deeper acoustic penetration including stronger influence of the local deformations and slopes due to the larger sampling area. This also means a lower accuracy of lower frequencies especially when measuring scarce transport.

3.2 Acoustic sampling parameters

To clarify and visualize the influence of the ADCP parameters on the estimation of the BT velocity, a principal component analysis (PCA) was performed for the averaged parameters of the corresponding instrument given in Table 3. Its objective is to extract the important information from Table 3, to represent it as a set of new orthogonal variables called principal components (PC1, PC2 and PC3), and to display the pattern of similarity of the observations and of the instrument-related parameters as points in a plot. Five variables that were previously explained (*BP, FD,* v_a, λ , z_c) are included in the analysis, four of them influence the observed apparent velocity, the fifth variable. The PCA does so by creating new uncorrelated variables that successively maximize variance. The original variables are previously standardized to have zero average and unit standard deviation. Figure 8a shows that more than 60% of the variance is captured by the first principal component (PC1), and more than 20% by the PC2. The third PC3 gives something above 10 % of the variance and will be excluded from the analysis. The second plot (Fig. 8b) explains that most of the observations related to each instrument and configuration are almost equally describing the PC1. The wavelength (λ), the pulse length (*Pl*), the beam focusing (z_c) and the apparent velocity (v_a) are the major contributors to the variance of the PC1. The biplot (Fig. 8b) shows a positive correlation among *Pl*, z_c and λ and a negative correlation with v_a. This explains the combined effect of the instrument geometric characteristic that is used to calculate z_c (i.e., φ, θ and D_t) and the acoustic instrument parameters (λ and *Pl*) towards the estimation of the apparent velocity. The *FD* appears also to be negatively correlated with the apparent velocity and contributes equally to both PC1 and PC2. In the same vein the proximity of the *FD* and z_c is a result of a good correlation which bore out that the instruments with higher z_c have larger percentage of filtered data. *BP* and *FD* seem to contribute most to the formation of PC2, but they are negatively correlated, which means that using more pings would produce fewer, which means more internal data averaging.

The PCA analysis is supported with another figure, that represents the beam focusing z_c and the indicator *M* (explained in the Methodology section) versus the average apparent bedload velocity given for each ADCP and configuration (Fig. 9). The lower z_c (e.g., 3 MHz) might be described as the capability of the acoustic beam to measure close to the riverbed. Figure 9a shows that the highest frequency (e.g., 3MHz) measures the highest apparent

velocity and has the shortest z_c, suggesting that most of the signal is scattered from the top layer of the active bedload. The middle frequencies most probably penetrate the entire active bedload layer and are more influenced by the immobile bed surface. The 0.6 MHz RDI has larger z_c than 1.2 MHz and 3 MHz and gives four times lower apparent bedload velocity than the 3 MHz. It is presently uncertain how the scattering pattern of each instrument (frequency) corresponds at different heights of the active layer. On the other hand, higher z_c (i.e., wider spreading of the acoustic energy across the beam and therefore greater sensitivity to side-lobe effect, see also Fig. 4), is also related with higher variability of the apparent velocity and heavier filtering. Furthermore, the higher z_c corresponds to a wider beam opening (φ) and beam width (D_t), i.e., less focused and larger acoustic beam footprints over the sampling region at the riverbed. Interestingly, the 1 MHz resulted in apparent velocities larger than the 1.2 MHz, but it gave z_c and *FD* almost equal to the 0.6 MHz. Although the less focused beams are more exposed on the surface scattering and require more filtering, the higher frequency and the different signal processing from Sontek most likely enabled the measuring of velocities from the top of the bedlaod active layer. Confirming that, the combined effect of the acoustic and geometrical properties may also be interpreted through the indicator *M* plotted versus v_a in Fig. 9b. The excellent correlation between *M* and v_a shows that the shorter pulse length in combination with the related wavelength and *FD* contributes for higher v_a. Indeed, the 1 MHz (Sontek) frequencies observed higher v_a than the 1.2 MHz (RDI), although z_c is almost equal. In general, with increasing *M* more weight is given to the volume scattering by the mobile bedload particles, resulting in more frequent velocity measurements obtained from the upper portion of the active layer.

3.3 Modelled Transport Rate

The goal of utilizing surrogate acoustic techniques in bedload measurements is to estimate the total transport rate. Given the apparent bedload velocity, the most convenient approach is applying the simple kinematic model (Eq. 1). The active layer thickness and the bedload porosity remain the most significant uncertainty, but in this study, the modelled kinematic model (Qs^{ADCP}) is only used to qualitatively evaluate the apparent velocity measured by different instruments/configurations and in the same time to show the potential of future applications.

The bedload concentration c_b calculated with the formula reported by Van Rijn (1984) gave values ranging from 0.03 to 0.35, which is reasonable assuming that 0.03 refers to the positions with very weak transport conditions (note that Table 1 gives the average values over a cross-section that includes the low transport positions close the banks). Assuming that c_b is appropriately calculated and for a given D_{50}, v_a, ρ_s for each position (see, Eq. 1), the model

was optimized by selecting n_k using the root mean square criterion. The obtained values of n_k are given in Table 3 and the modelled transport rates (Qs^{4DCP}) versus the measured transport rates (Qs^{m}) for four configurations (0.6 MHz, 1.2 MHz, 1 MHz PC and 3 MHz PC) are presented in Fig. 10. For 0.6 MHz the active layer thickness $dt_k = n_k\ D_{50}$, exceeded the empirically calculated average values of $dt \sim 18\ D_{50}$ given in Table 1, and for 3 MHz the values obtained for dt_k were near the minimum empirical values of $d_t = 3$ - $4\ D_{50}$. On the contrary, the $dt_k = 4$ - $6\ D_{50}$ for 1 MHz and $dt_k \sim 7\ D_{50}$ for 1.2 MHz are in the range of the average d_t given in Table 1. In addition, the correlation coefficients did not change significantly (e.g., $r = 0.75$ for 1.2 MHz; $r = 0.65$ for 0.6 MHz; $r = 0.7$ for 1 MHz PC; and $r = 0.69$ for 3 MHz PC), showing that the apparent bedload velocity is the most important variable in the kinematic model.

4 Discussion

4.1 Acoustic scattering pattern and the acoustic sampling

In the interpretation of the results in the previous section it was observed that the lower frequencies underestimate the apparent velocities if all the other acoustic parameters (see, Table 2) are the same or similar. This can be explained with the fact that the lower frequency is less attenuated (Clay & Medwin, 1998) and fully penetrates through the active layer which leads to a larger disturbance by the immobile particles (i.e., surface scattering) beneath the active bedload layer (Conevski et al. 2019). Therefore, it underestimated the correct mean velocity of the bedload particles and gave lower correlation coefficients. If shorter pulses are used in combination with, more focused beams (i.e., lower z_c), the effect of the frequency can be masked and the acoustic sampling for the lower frequencies would be less disturbed by the surface scattering. Differences in BT signal processing among instruments may also have an influence.

Understanding better the scattering pattern might be crucial to explain the influence of the two types of scattering processes that happen at the mobile riverbed (i.e., surface and volume scattering). For those purposes, a simple scattering pattern is given in Fig. 11 to qualitatively describe the influence of the acoustic resolution on the estimation of the apparent velocity. Two consecutive pulse portions are considered to calculate the Doppler velocity. Indeed, it may be the possible scenario for almost all ADCP configurations, except the IC. It can also represent a simplified concept for explaining the scattering of the coded elements (codded sub-pulses that form longer pulses) in the BB technology (Brumley, et al., 1991). The pulses are emitted at time difference T_l, that is called the lag time or dilatation time, mainly used in the BB and PC algorithms by both instruments to calculate the Doppler shift (RDInstruments,

2011; Sontek, 2017). Figure 11 describes one possible scenario of three consecutive time instances of a pulse portion approaching and scattering from the riverbed. It also visualizes that the pulse portions arrive at the bottom at different time instants, mostly due to the slant angle (90 -θ) and the beam opening (φ). Moreover, the pulse spends most time at point 1 (see, Fig. 11a-c), also reported by Rennie et al. (2002). Particularly relevant, the inner edge (point 1 in Fig. 10a) reaches the bottom before the central axis (point 2) and that edge possibly returns first to the monostatic transducer. This is something similar to side lobe effect (RDI report 1996) but occurring at the scale of the radial distribution of central lobe energy. The beam inner edge reflected from the bottom (Fig. 11b, point 1), may produce a large surface scattering therefore masking the lower intensity return from mobile particles in the sediment layer (namely, volume scattering) at the beam axis, besides the fact that due to beamforming the acoustic energy initially concentrates at the central beam axis (Urick ,1983). Depending on the prevailing effect of volume scattering at beam axis and surface scattering at the inner edge, consecutive portions of the acoustic pulse may yield a corrected and biased position of the acoustic return, respectively. In fact, prevalence of volume scattering locates the maximum energy return along the beam axis (point 2 Fig. 11c), whereas on the contrary the surface scattering makes the return shallower (point 1 Fig. 11c) which corresponds to the projection of the inner edge (point 1 in Fig. 11) on the beam axis. Although the beam opening angle (φ) is associated with the half-intensity decrease of the transmitted energy from the central axis (Urick, 1983), the surface scattering, in theory, is much stronger and could prevail over the volume scattering. Besides, the distance between the beam axis and the beam edges (e.g., central lobe width) increases for less focused beams (i.e., higher z_c) that makes more likely the surface scattering bias at a given acoustic sampling time lag T_l. The higher z_c does not necessarily give the lowest apparent velocities (e.g., 1MHz in Fig. 9a); in fact the surface scattering also increases with the grazing angle (Urick, 1983): RDI instruments adopts a larger grazing angle than Sontek which may contribute for stronger surface scattering (Ivakin, 1981) and accounts for the lower apparent velocities in Figure 9a. Furthermore, the other acoustic parameters (e.g., pulse length) have an influence which can force the beam to sample more in the upper region of the bedload layer. However, the larger z_c still implies heavier filtering and longer averaging time.

Summarizing, the higher values of the *FD* may be a consequence of an enhanced surface scattering at the riverbed due to the lower beam resolution (i.e., higher z_c or less beam focusing). This produces a reduction of time delay among consecutive portions of the pulse length that corresponds to an additional underestimation of Doppler and apparent velocities. On the contrary, the more focused beams (i.e., low z_c) are less affected by the surface scattering, delivering less biased values of the apparent bedload velocity.

4.2 Bedload sampler failure and the water bias

The bias of the apparent bedload velocities, mentioned in the result section (Fig .7) may be due to the systematic uncertainty of the bedload sampler, or its failure to measure in weak transport conditions. This was confirmed by the previous experiences of the BfG staff, but also by observing the videos from the mounted camera. It appears that the sampler could not collect the fine sand and some organic material moving on top of the partially armoured bed, but the ADCPs registered it. The intercept in Fig. 7 is not the same for all the frequencies and this difference can be interpreted as less sensitivity of the lower frequencies towards fine materials, additional to the stronger surface scattering. Moreover, the isolated points, in the lower part of all plots in Fig. 10 make this uncertainty even more evident. These values clearly show that the modelled bedload transport rate using the apparent bedload velocity provided reasonable values for weak transport conditions, whereas the bedload sampler was most probably unable to capture any bedload physically.

Nevertheless, this interception may also be associated with the water bias caused by a high suspended sediment concentration (SSC) close to the bed (Rennie et al. 2002). To examine the potential for water bias in the apparent velocity, the water velocity from the last velocity cell was compared to v_a. The water velocity in the bin nearest the bed was twice as large as v_a. Furthermore, an insignificant change of the backscattered signal was observed between the last three cells of the water profile. Most importantly, the SSC measured close to the riverbed was relatively low and varied from 20 mg l^{-1} to 150 mg l^{-1}. It was thus concluded that water bias did not influence the apparent bedload velocity.

4.3 The kinematic model and the acoustic sampling

The fitting of the kinematic model resulted in certain values of the n_k parameter. The n_k is directly correlated with the thickness of the bedload active layer and bedload concentration, but in this study, it is assumed that the bedload concentration is correctly estimated. For the given n_k, the active layer thickness ($d_{tk} \sim 18\ D_{50}$) in most of the points of the modelled transport rate for the 0.6 MHz (Fig. 10a) exceeded the empirically calculated values ($d_t = 3$ - $8\ D_{50}$), showing that this instrument underestimated the apparent bedload velocity. On the other hand, $d_{tk} = 3$ - $4\ D_{50}$ for the 3 MHz confirms that the 3 MHz frequency mostly scatters the surface of the active bedload layer, therefore performing a shallower acoustic sampling within the range of the minimum empirical values of the active layer ($d_t \sim 3\ D_{50}$). The most realistic values of $n_k = 4$ - 6 and $n_k \sim 7$ were calculated for 1 MHz and 1.2 MHz, respectively (Fig. 10d and Fig. 10b). Most likely, these frequencies sampled the entire active layer, measuring an average value of the apparent bedload velocity. It must be noted that c_b and d_{tk} are mutually dependent variables and that this analysis does not give detailed information

about the bedload concentration. Nevertheless, this analysis successfully confirmed the hypothesis about acoustic sampling and apparent velocity estimation.

Finally, Fig. 10 clearly shows that the application of this model, using the empirical formulas, successfully predicted the bedload transport rates giving r higher than 0.8 in all the cases. The configuration 1 MHz (Sontek) and 1.2 MHz (RDI) eventually gave the best correspondence to empirical estimations of the active layer thickness.

5 Conclusions and recommendations

The apparent bedload velocities, measured by three different ADCPs and four different frequencies, have been compared when deployed fixed in the same position. Results from different study sites with different PSDs were merged to examine the capability of each instrument and the corresponding configurations. All the tested ADCP configurations showed a good correlation with the bedload transport rates measured with physical bedload sampling. The filtering procedure of the apparent velocity confirmed a reduction in the total uncertainty which corroborate the need of decimating negative values from the apparent velocity. Lower apparent bedload velocity was obtained when lower acoustic frequency, longer pulse lengths and larger beam focusing were used. The lower acoustic frequency is not necessarily the only reason for underestimation of the mean apparent velocity. The combined effect of few instrumental parameters influences the acoustic sampling of the riverbed and thus the estimation of the apparent bedload velocity. The shorter pulses and the specific signal processing (i.e., riverbed detection and BT velocity estimation) of the Sontek M9 leaded to higher apparent velocities independently of the beam focusing and frequency limitation but requires heavier filtering and showed higher deviations. The PC configurations gave the best correlations and it is recommended for bedload velocity measurements.

The kinematic model was successfully applied for the middle frequencies (1.2 MHz and 1 MHz), which gave the best correspondence to the empirical estimation of the bedload active layer thickness and concentration. Thus, the 1.2 MHz RDI and 1MHz Sontek could be used for calculation of the bedload transport by combining the ADCP data and empirical equations without necessary calibration of the instrument. The relatively good correlation coefficient may also enable the application of the kinematic model with the other frequencies too (i.e., 0.6 MHz RDI and 3 MHz Sontek) but the empirical formulas should be used with caution and a calibration is recommended.

The removal of the bed samples (e.g., inconsistent sampling of the four beams) out of the final data set appears to be crucial for calibration of the instruments as well as for calculation of the cumulative bedload transport rate per one cross section. This removal should be conducted by verifying the layer homogeneity assumption, was achieved by checking a

similar ranging distances at four beams (i.e., the deviation between the beams should not be larger than the approximate dune height) and the maximum amount of filtered data, FD, should be smaller than 60 %.

The fact that different frequencies and instrument configurations sample differently through the active bedload layer calls for a detailed analysis of the corrected backscattering strength obtained with the ADCPs. This could help to better describe the active layer thickness and bedload concentration. Besides, the backscatter strength may contain information about the PSD of the scattered particles at the riverbed. Therefore, further research effort will address the instrumental sensitivity towards different bedload materials in laboratory-controlled conditions, focusing on both the obtained apparent velocity and corresponding backscattering strength.

Acknowledgements

The authors acknowledge the collaboration with Sontek Xylem, that allowed free using of the ADPviewer software permitting a full control of the M9 ADCP.

Funding

This research and the filed measurement campaigns were funded by the Norwegian Research Council and Statkraft as part of the multidisciplinary project SEDIPASS.

Appendix A

Commercial ADCPs commonly use two techniques for signal processing that can be classified as incoherent (narrowband) or pulse coherent (broadband and/or pulse-to-pulse coherent).

The narrowband incoherent (IC) technique estimates the Doppler shift from echoes of a single-pulse (i.e., ping). Profilers utilizing pulse-incoherent processing use the echoes from each pulse independently, measuring the phase change in the returned signal to determine the Doppler frequency shift. The length of the measuring cell depends on the duration of the pulse, and the spectral resolution and signal bandwidth limit the accuracy of the velocity estimation. This requires many seconds of averaging to produce acceptable, statistically robust estimations of the mean velocity (Brumley, et al., 1991). Longer pulses result in more accurate estimation of the velocity but decreases the resolution and the maximal measured velocity without aliasing. Regarding the bedload velocity measurements, the most severe limitation appears in the resolution trade-off, because the bedload has a significantly lower velocity than the water column above, but the thickness of the bedload active layer is usually

shorter than the BT pulse length (see, Fig. 4).

The pulse-to-pulse coherent (PC) system, often called the pulse-coherent, involves transmitting a series of short pulses in a single ping and the phase changes are observed from ping to ping at each cell distance. The time between pings, T_l, is adjusted to minimize the interference between two consecutive pings, and by sampling the echo from each sub-pulse at a fixed range, the samples correspond to the same scatterers. Thus, the Doppler spectral broadening is not dependent on the pulse length, *Pl*, as it was the case with the incoherent systems (Brumley, et al., 1991). This technology improves the accuracy over the incoherent method but is also highly unstable due to decorrelation of the echoes, or equivalently, broadening of the spectral peak. As sampled systems, they are also aliased about the Nyquist frequency of the sampling, leading to the well-known velocity-range ambiguity.

The limitations mentioned above are reduced in the Broadband (BB) systems for which the time between the pulses (T_l) is no longer constrained by the propagation time of the maximum range. The BB system emits two or several very narrow pulses in a burst, which helps to shorten the time between the pulse pairs and increase the maximum unambiguous velocity. The effect of shortening the pulses decreases the correlation time, or equivalently broaden its bandwidth. Consequently, the spacing between the pings (i.e., a set of pulses) also can be adjusted to cover the desired range. However, the energy loss of the narrow pulses is so significant that sometimes useless results are obtained. To overcome this problem, the coded-pulse was introduced by RDI. The Doppler shift measurement in the coded pulse systems is the same as BB, allowing longer pulses to be used without decreasing the bandwidth and decreasing the self-noise associated with use of short pulses. The longer pulses add more energy in the system, the longer distance between the coded elements is inversely proportional to the Doppler error and the resolution is determined by the short-coded elements.

Notation

B	=	width of the river reach	(m)
BP	=	Bottom Tracking pings per ensemble	(-)
c	=	speed of sound	(m s^{-1})
c_b	=	bedload concentration	(-)
CV_{va}	=	coefficient of variation of the apparent velocity after filtering	(-)
CV^b_{va}	=	coefficient of variation of the apparent velocity before filtering	(-)
C_z	=	Chezy dimensionless coefficient	1
C_z'	=	Grain related Chezy dimensionless coefficient	
D_{50}	=	particle median diameter	(m)

D_{90}	=	particle diameter bigger than 90%	(m)
D_{std}	=	standard deviation of the PSD	(m)
d_t	=	empirically calculated active layer thickness	(m)
D_t	=	transducers diameter	(cm)
d_{ik}	=	modelled active layer thickness	(m)
f	=	ADCP working frequency	MHz
FD	=	percentage of the discarded velocity samples after the filtering	(%)
g	=	gravitational constant	(m s^{-2})
H	=	water level	(m)
H^{ADCP}	=	water level measured by the ADCPs	(m)
M	=	indicator for acoustic sampling	(m · mm)
n_k	=	fitting coefficient of the kinematic model	(-)
Pl	=	acoustic pulse length	(mm)
Q	=	river discharge	m^3 s^{-1}
Qs^{ADCP}	=	modelled transport rate based on apparent velocity	(kg s m^{-1})
Qs^m	=	physically measured transport rate	(kg s m^{-1})
r	=	correlation coefficient	(-)
S	=	energy surface slope of the river reach	(-)
Tl	=	time between pings	(s)
U	=	average-depth water velocity	(m s^{-1})
u_*'	=	grain related bed shear (skin friction) velocity	(m s^{-1})
u_*	=	bed shear velocity	(m s^{-1})
u_{*cr}	=	critical shear velocity	(m s^{-1})
U^{ADCP}	=	depth-averaged velocity measured by the ADCPs	(m s^{-1})
v_a	=	the apparent velocity, measured by the ADCP and filtered	(m s^{-1})
v_{bt}	=	Bottom Tracking vessel velocity	(m s^{-1})
v_{gps}	=	GPS vessel velocity	(m s^{-1})
WP	=	Water Profile pings per ensemble	(-)
z_c	=	beam, focusing, distance to the inner side of the central lobe	(m)
z_s	=	distance of the side-lobe contaminated region	(m)
λ	=	wavelength	(mm)
φ	=	acoustic beam opening angle	(°)
θ	=	acoustic beam incident angle	(°)
ρ	=	water density	(kg m^{-3})
ρ_s	=	sediment particles density	(kg m^{-3})
τ	=	bed shear stress	(N m^{-2})
τ_*	=	shields parameter (dimensionless shear stress)	1
τ_{cr}	=	critical Shields parameter (critical shear stress)	(-)

References

Banhold, K., Schüttrumpf, H., Hillebrand, G., & Frings, R. (2016, 6). Underestimation of sand loads during bed-load measurements—a laboratory examination., (ss. 1036-1041). doi:10.1201/9781315644479-165

Borthwick, S. M. (2015). Sensitivity Analysis and Statistical Convergence of a Saltating Particle Mode. *Journal of Hydraulic Engineering, 151*(5). doi:10.1061/(ASCE)HY.1943-7900.0000987

Brandstetter, B., Gehres, N., & S., V. (2012). *Messverfahren des Geschiebetriebs für Wasserstraßen. Bundesanstalt für Gewässerkunde.* Koblenz: BfG-1761.

Brumley, B. H., Cabrera, R. G., Deines, K. L., & Terray, E. A. (1991, 10). Performance of a broad-band acoustic Doppler current profiler. *IEEE Journal of Oceanic Engineering, 16*, 402-407. doi:10.1109/48.90905

Clay, C. S., & Medwin, H. (1998). *Fundamentals of Acoustical Oceanography.* Boston San Diego New York: ACADEMIC PRESS .

Conevski, S., Guerrero, M., Ruther, N., & Rennie, C. (2019). Laboratory investigation of the apparent bedload velocity measured by ADCPs. *Journal of Hydraulic Engineering*. doi:10.1061/(ASCE)HY.1943-7900.0001632

Conevski, S., Winterscheid, A., Ruther, N., Guerrero, M., & Rennie, C. (2018). Evaluation of an acoustic Doppler technique for bed-load transport measurements in sand-bed rivers. *River Flow 2018*. Lyon.

Frings, R. M., & Stefan, V. (2017). Guidelines for sampling bedload transport with minimum uncertainty. *Sedimentology*. doi:10.1111/sed.12366

Frings, R. M., & Vollmer, S. (2017). Guidelines for sampling bedload transport with minimum uncertainty. *Sedimentology, 64*, 1630-1645. doi:10.1111/sed.12366

Gaeuman, D., & Jacobson, R. B. (2006). Acoustic bed velocity and bed load dynamics in a large sand bed river. *Journal of Geophysical Research: Earth Surface, 111*. doi:10.1029/2005JF000411

Gaweesh, M., & C. van Rijn, L. (1994, 12). Bed-Load Sampling in Sand-Bed Rivers. *Journal of Hydraulic Engineering-asce - J HYDRAUL ENG-ASCE, 120*. doi:10.1061/(ASCE)0733-9429(1994)120:12(1364)

Gomez, B. (1991). Bedload transport. *Earth-Science Reviews, 31*, 89-132. doi:https://doi.org/10.1016/0012-8252(91)90017-A

Hubbell, D. W. (1964). *Apparatus and techniques for measuring bedload.* USGS. U. S. Govt. Print. Off.,. doi:10.3133/wsp1748

Jamieson, E. C., Rennie, C. D., & Ramooz, R. (2008). Validation of aDcp bedload transport measurements. *Proc. 2008 River Flow Conf.*, (ss. 2343–2351). KUBABA Congress Dept. and Travel Services Cesme, Turkey.

Lajeunesse, E., Malverti, L., & Charru, F. (2010). Bed load transport in turbulent flow at the grain scale: Experiments and modeling. *Journal of Geophysical Research: Earth Surface, 115*(4). doi:10.1029/2009JF001628

Latosinski, F. G., Szupiany, R. N., Guerrero, M., Amsler, M. L., & Vionnet, C. (2017). The ADCP's bottom track capability for bedload prediction: Evidence on method reliability from sandy river applications. *Flow Measurement and Instrumentation, 54*, 124-135. doi:https://doi.org/10.1016/j.flowmeasinst.2017.01.005

Lee, H., & Hsu, I. (1994). Investigation of saltating particle motions. *Journal of Hydraulic Engineering, 122*, 245–254.

Parker, G. (2004). *ID SEDIMENT TRANSPORT MORPHODYNAMICS with applications to RIVERS AND TURBIDITY CURRENTS.* St. Anthony Falls Laboratory, Mississippi River at 3rd Avenue SE.

Ramooz, R., & Rennie, C. D. (2008). *Laboratory measurement of bedload with an ADCP.* In Bedload-surrogate monitoring technologies: United States Geological Survey Scientific Investigations Rep. 2010-5091, USGS, Reston. Downloaded form: http://pubs.usgs.gov/sir/2010/5091/papers/

RDInstruments. (2011). *Acoustic Doppler Current Profiler Principles of Operation A Practical Primer.* Practical Primer, Teledyne RD Instruments, 14020 Stowe Drive Poway, California 92064. Downloaded form : http://www.teledynemarine.com

Rennie, C. D., & Millar, R. G. (2004). Measurement of the spatial distribution of fluvial bedload transport velocity in both sand and gravel. *Earth Surface Processes and Landforms, 29*, 1173-1193. doi:10.1002/esp.1074

Rennie, C. D., & Villard, P. V. (2004). Site specificity of bed load measurement using an acoustic Doppler current profiler. *Journal of Geophysical Research: Earth Surface, 109*. doi:10.1029/2003JF000106

Rennie, C. D., Millar, R. G., & Church, M. A. (2002). Measurement of bed load velocity using an acoustic doppler current profiler. *Journal of Hydraulic Engineering, 5*(128), 473-483.

Rennie, C. D., Vericat, D., Williams, R., Brasington, J., & Hicks, M. (2017). "Calibration of aDcp apparent bedload velocity to bedload transport rate" in Gravel-Bed Rivers. I *Processes and Disasters.* Tsutsumi, D., and Laronne, J., Wiley.

Rickenmann, D., & McArdell, B. W. (2007). Continuous measurement of sediment transport in the Erlenbach stream using piezoelectric bedload impact sensors. *Earth Surface Processes and Landforms, 32*(9), 1362-1378. doi: 10.1002/esp.1478

Shields, I. (1936). Anwendung der ahnlichkeitmechanik und der turbulenz- forschung auf die gescheibebewegung. *Mitt. Preuss Vers. Wasserbau Schiffbau*.

Sontek. (2017, 10). *RiverSurveyor S5/M9 System Manual, Firmware Version 4.02.* . 9940 Summers Ridge Road, San Diego, CA 92121-3091 USA: Sontek, a Xylem brand. Downloaded form : ysi.actonsoftware.com

Urick, R. J. (1983). *Principles of Underwater Sound.* Peninsula Publishing. Downloaded form: https://books.google.no/books?id=MBBgQgAACAAJ

Van Rijn, L. (1984). Sediment transport, part i: bed load transport. *J. Hydraul. Eng., 110*, 1431–1456.

Williams, R. D., Rennie, C. D., Brasington, J., Hicks, D. M., & Vericat, D. (2015). Linking the spatial distribution of bed load transport to morphological change during high-flow events in a shallow braided river. *Journal of Geophysical Research: Earth Surface, 120*, 604-622. doi:10.1002/2014JF003346

List of tables

Table 1 Average hydraulic parameters given for the entire cross-section.

Table 2 ADCP parameters, configurations and acoustic characteristics. The configuration abbreviations are as follows: RS - RiverSurveyor default start, IC - Incoherent BT signal processing, PC - Pulse Coherent, BB – BroadBand, *WP*- water Pings, *BP*- number of pings per sample, *Pl* - pulse length.

Table 3 Instrument and configuration related parameters. Note that the given parameters are averaged over all three campaigns.

List of figures

Figure 1 Measurement set-up and position of the instruments on the ship. Ship measurement scheme.

Figure 2 BfG Physical Sampler. Camera Set-up in the front.

Figure 3 Study site locations

Figure 4 Acoustic beam scheme (pattern) of one ADCP transducer

Figure 5 Example of vector direction plot at one measurement position of the RDI 0.6 MHz: (a) only water velocity (U, red symbols), (b) the accepted apparent bedload velocity (v_a blue symbols) and discarded apparent bedload velocity (grey-faint symbols). Note that the blue and the faint-grey symbols give the raw apparent velocity measured by the BT mode of the ADCP. The red error represents the mean direction of the water velocity.

Figure 6 Riverbed deformation influence on the ADCP bedload measurements. Note that this is simplified 2D scheme, the beams can be rotated differently with respect to the mean flow direction.

Figure 7 Filtered apparent velocities and the mean transport rate from the physical samples. All configurations given in Table 2 are shown in this figure : (a) 0.6 MHz RDI Rio Grande , blue squares, (b) 1.2 MHz RDI Rio Grande, red circle, (c) 3 MHz M9 Sontek, RS, black triangles (d) 1 MHz Sontek, IC, grey stars, (e) 1 MHz Sontek, PC, faint-grey stars, (f) 1 MHz Sontek, def, black stars, (g) 3 MHz Sontek, IC, grey triangles (h) 3 MHz Sontek, PC, faint-grey triangles, (i) 3 MHz Sontek, def, black triangles. The correlation coefficient r is given on each sub-figure together with linear fitting regression model.

Figure 8 PCA analyses of the ADCP parameters given in Table 3. (a) explains the importance of the principal components in the analysis and the total captured variance, (b) shows how the observations (instruments and configurations) are describing the components and it demonstrates the correlation between the analysed parameters. The symbols are the same as in Fig. 7

Figure 9 The acoustic parameters and the apparent bedload velocity: (a) gives the correlation between the beam focusing z_c, given also in Table 3 and the averaged apparent bedload velocity for each instrument and configuration measured trough all three campaigns, (b) the combined acoustic indicator M is plotted versus the apparent bedload velocity.

Figure 10 Modelled Transport rate Qs^{ADCP} versus the measured transport rate Qs^{m} , calculated for the apparent velocities of four representative configurations: (a) RDI 0.6 MHz, (b) RDI 1.2 MHz, (c) Sontek 1 MHz PC , (d) Sontek 3 MHz PC

Figure 11 A possible scenario of a simplified beam scattering pattern scattering, given at three consecutive instances: (a) the pulse emitted in the water column consisting of two sub-pulses or codded elements, (b) the front of the pulse penetrate through the active layer and reaches the immobile riverbed , where the first sub-pulse (red) starts the reflection, (c) the first sub-pulse is fully reflected of the immobile bed, the second sub-pulse (blue) starts the reflection at the top of the active layer.

.Tables

Table 1 Average hydraulic parameters given for the entire cross-section.

	Cross-section	Num of positions	Coordinates		Q	B	U	H	S	D_{90}	D_{50}	C_z	C_z'	τ	u_{*cr}	u_*	u_*'	c_b	^1d_t	^2d_t	^3d_t
			LONG	LAT	($m^3 s^{-1}$)	(m)	(m s^{-1})	(m)	‰	(mm)	(mm)	1	1	1	(m s^{-1})	(m s^{-1})	(m s^{-1})	%	(mm)	(mm)	(mm)
ODER	1	7	14.195	52.820	748	281	1.03	2.59	0.15	1.75	0.67	16.69	22.51	0.351	0.018	0.062	0.046	0.09	4.16	4.98	2.13
	2	8	14.123	52.842	721	228	1.01	3.12	0.15	1.81	0.71	14.89	22.89	0.399	0.019	0.068	0.044	0.09	4.94	5.73	2.58
ELBE 1	3	5	10.897	53.234	697	212	0.91	3.60	0.13	2.24	0.51	13.43	22.72	0.556	0.016	0.068	0.040	0.18	3.30	5.03	1.99
	4	5	11.119	53.157	691	304	0.91	2.56	0.11	2.50	0.76	17.51	21.60	0.225	0.019	0.052	0.042	0.05	3.98	4.17	1.76
	5	5	11.269	53.111	702	219	0.98	3.27	0.13	2.64	0.56	15.16	22.07	0.460	0.017	0.065	0.044	0.14	3.52	4.93	1.99
ELBE 2	6	6	11.885	51.978	276	160	0.73	2.35	0.19	3.57	1.10	11.03	20.48	0.246	0.024	0.066	0.036	0.03	7.64	6.47	3.17
	7	5	11.917	51.954	323	200	0.72	2.22	0.20	3.38	1.05	10.90	20.48	0.256	0.023	0.066	0.035	0.04	7.32	6.36	3.12
	8	5	11.912	51.956	246	167	0.69	2.14	0.20	3.03	1.11	10.66	20.67	0.234	0.024	0.065	0.033	0.03	7.55	6.30	3.08
	9	6	11.943	51.936	221	140	0.83	1.91	0.19	3.45	1.04	13.91	20.05	0.211	0.023	0.060	0.041	0.03	6.45	5.54	2.61
	10	5	11.677	52.093	296	147	0.90	2.30	0.20	2.79	0.98	13.43	21.04	0.284	0.022	0.067	0.043	0.05	6.96	6.34	3.10

1 - Van Rijn (1984); 2 - Lee & Hsu (1994); 3 - Maldonado & Borthwick (2015)

Table 2 ADCP parameters, configurations and acoustic characteristics. The configuration abbreviations are as follows: RS - RiverSurveyor default start, IC - Incoherent BT signal processing, PC - Pulse Coherent, BB - BroadBand, *WP* - water Pings, *BP*- number of pings per sample, *Pl* - pulse length.

ADCP	*f*	^1D_t	θ	φ	*Config*	*WP*	*BP*	*Pl*
	(MHz)	(cm)	°	°	/	/	/	(cm)
Sontek M9	3.0	2.70	25	0.53	RS	20	2	26
Sontek M9	1.0	4.30	25	0.99	IC	0	4	21
Sontek M9	3.0	2.70	25	0.53	IC	0	4	26
Sontek M9	1.0	4.30	25	0.99	PC	0	3	21
Sontek M9	3.0	2.70	25	0.53	PC	0	3	26
Sontek M9	1.0	4.30	25	0.99	def	10	2	21
Sontek M9	3.0	2.70	25	0.53	def	10	2	26
RDI Rio Grande 600	0.6	8.95	20	0.80	BB	1	3	55
RDI Rio Grande 1200	1.2	6.99	20	0.51	BB	1	3	55

1- Please note the diameter of the transducer is the boundary of the plastic from the outside of the ADCP, the real transducers have slightly smaller diameter which is unknown for the users

Table 3 Instrument and configuration related parameters. Note that the given parameters are averaged over all three campaigns.

ADCP Configuration	Total samples	Bad samples	H^{ADCP}	U^{ADCP}	v_a	*FD*	CV_{va}	CV^2_{va}	λ	z_c	M	r^2	r	n_k
	/	/	(m)	(m s^{-1})	(m s^{-1})	/	/	/	(mm)	(m)	(m)	/	/	/
M9 3MHz RS	53	11%	2.85	1.011	0.069	0.33	0.63	0.73	0.483	0.020	0.150	0.60	0.77	2.35
M9 1MHz IC	42	14%	2.69	N/A	0.063	0.31	0.59	0.71	1.450	0.033	0.062	0.59	0.77	4.10
M9 3MHz IC	42	14%	2.69	N/A	0.071	0.20	0.57	0.67	0.483	0.019	0.017	0.49	0.70	1.90
M9 1MHz HD (PC)	39	13%	2.45	N/A	0.060	0.32	0.58	0.67	1.450	0.031	0.029	0.70	0.84	2.60
M9 3MHz HD (PC)	39	13%	2.55	N/A	0.074	0.18	0.55	0.63	0.483	0.018	0.005	0.59	0.77	3.30
M9 1MHz def	39	15%	2.69	0.890	0.065	0.33	0.55	0.71	1.450	0.033	0.040	0.46	0.68	/
M9 3MHz def	39	15%	2.70	0.930	0.074	0.22	0.59	0.72	0.483	0.019	0.006	0.42	0.65	/
RDI 0.6MHz BB	56	11%	2.90	0.945	0.026	0.34	0.66	0.78	2.417	0.032	0.062	0.47	0.69	8.80
RDI 1.2 MHz BB	56	11%	2.94	0.950	0.045	0.24	0.65	0.72	1.208	0.023	0.011	0.57	0.75	5.10

FIGURES

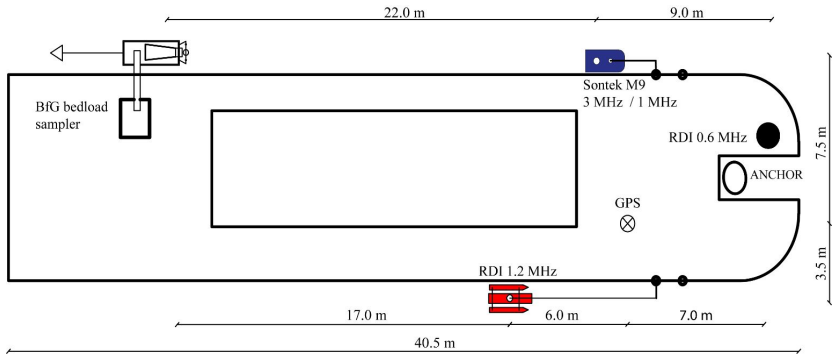

Figure 1 Measurement set-up and position of the instruments on the ship. Ship measurement scheme.



Figure 2 BfG Physical Sampler. Camera Set-up in the front.



Figure 3 Study site locations.

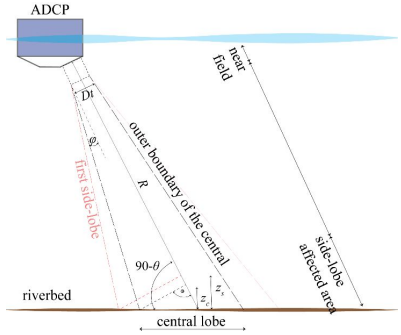

Figure 4 Acoustic beam scheme (pattern) of one ADCP transducer.

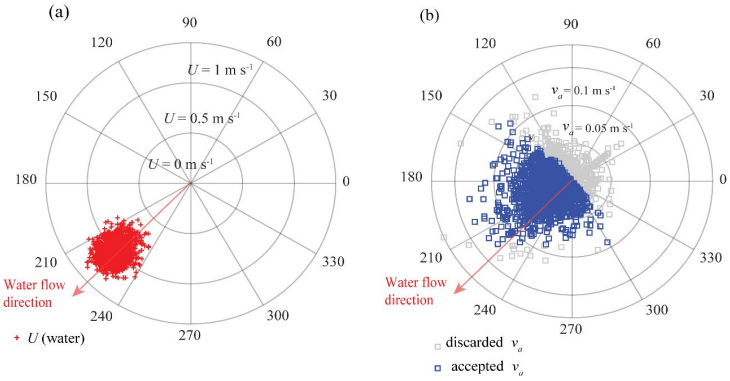

Figure 5 Example of vector direction plot at one measurement position of the RDI 0.6 MHz: (a) only water velocity (U, red symbols), (b) the accepted apparent bedload velocity (v_a, blue symbols) and discarded apparent bedload velocity (grey-faint symbols). Note that the blue and the faint-grey symbols give the raw apparent velocity measured by the BT mode of the ADCP. The red arrow represents the mean direction of the water velocity.

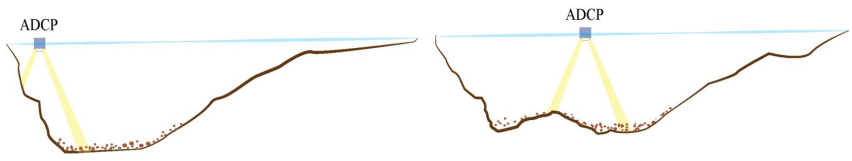

Figure 6 Riverbed deformation influence on the ADCP bedload measurements. Note that this is simplified 2D scheme, the beams can be rotated differently with respect to the mean flow direction.

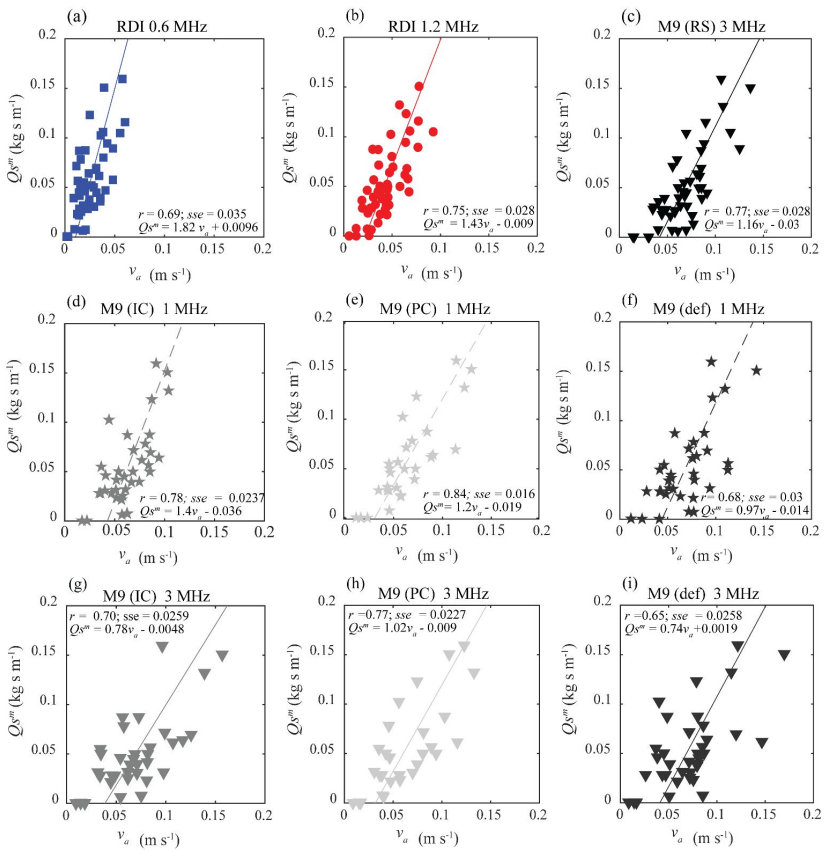

Figure 7 Filtered apparent velocities and the mean transport rate from the physical samples. All configurations given in Table 2 are shown in this figure : (a) 0.6 MHz RDI Rio Grande , blue squares, (b) 1.2 MHz RDI Rio Grande, red circle, (c) 3 MHz M9 Sontek, RS, black triangles (d) 1 MHz Sontek, IC, grey stars, (e) 1 MHz Sontek, PC, faint-grey stars, (f) 1 MHz Sontek, def, black stars, (g) 3 MHz Sontek, IC, grey triangles (h) 3 MHz Sontek, PC, faint-grey triangles, (i) 3 MHz Sontek, def, black triangles. The correlation coefficient *r* is given on each sub-figure together with linear fitting regression model.

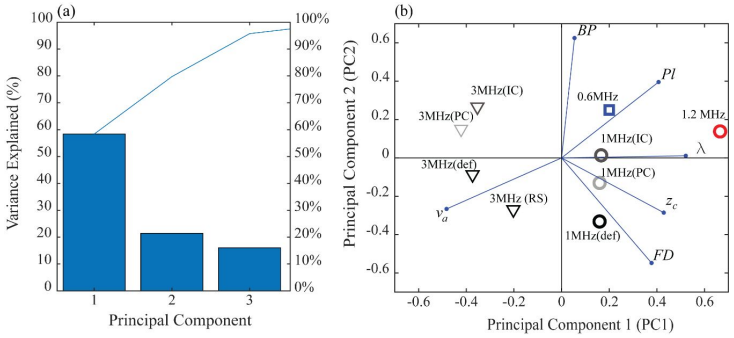

Figure 8 PCA analyses of the ADCP parameters given in Table 3. (a) explains the importance of the principal components in the analysis and the total captured variance, (b) shows how the observations (instruments and configurations) are describing the components and it demonstrates the correlation between the analysed parameters.

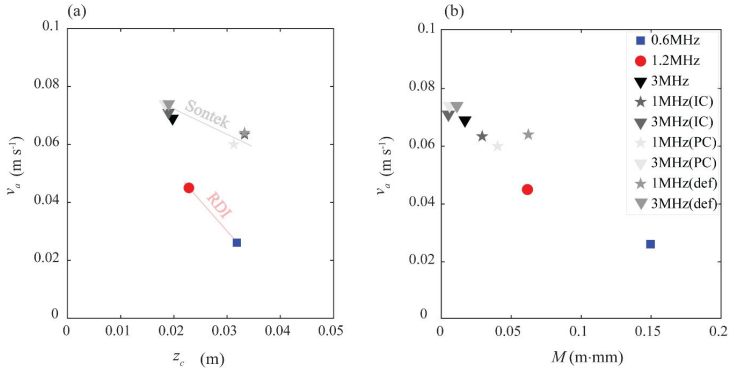

Figure 9 The acoustic parameters and the apparent bedload velocity: (a) gives the correlation between the beam focusing z_c, given also in Table 3 and the averaged apparent bedload velocity for each instrument and configuration measured trough all three campaigns, (b) the combined acoustic indicator M is plotted versus the apparent bedload velocity.

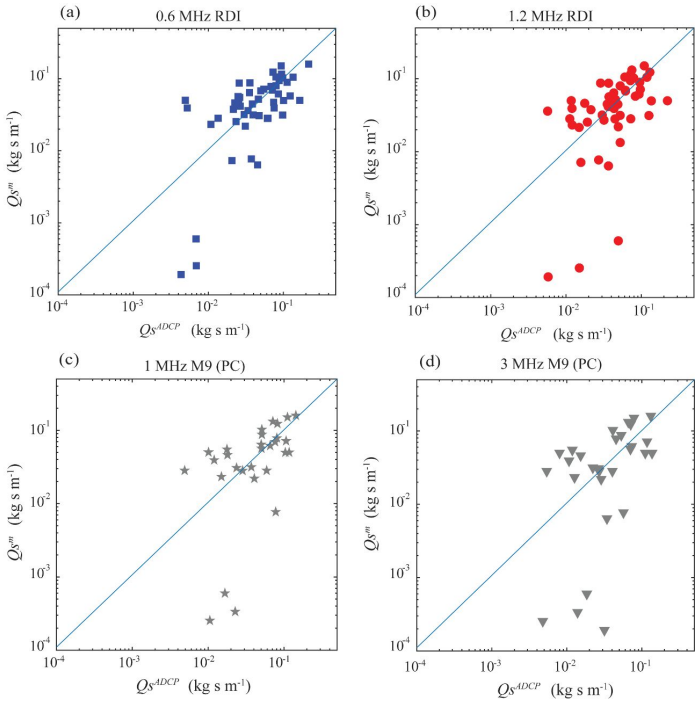

Figure 10 Modelled Transport rate Qs^{ADCP} versus the measured transport rate Qs^m, calculated for the apparent velocities of four representative configurations: (a) RDI 0.6 MHz, (b) RDI 1.2 MHz, (c) Sontek 1MZ PC, (d) Sontek 3MZ PC.

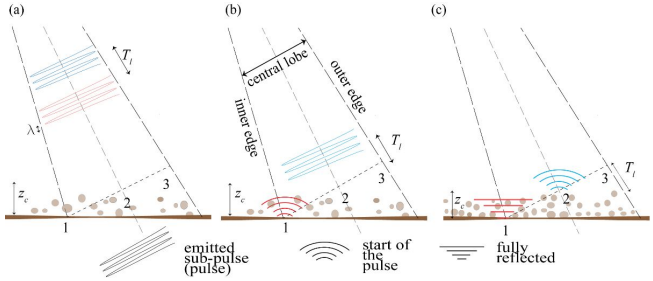

Figure 11 A possible scenario of a simplified beam scattering pattern, given at three consecutive instances: (a) the pulse emitted in the water column consisting of two sub-pulses or codded elements, (b) the front of the pulse penetrate through the active layer and reaches the immobile riverbed , where the first sub-pulse (red) starts the reflection, (c) the first sub-pulse is fully reflected of the immobile bed, the second sub-pulse (blue) starts the reflection at the top of the active layer.

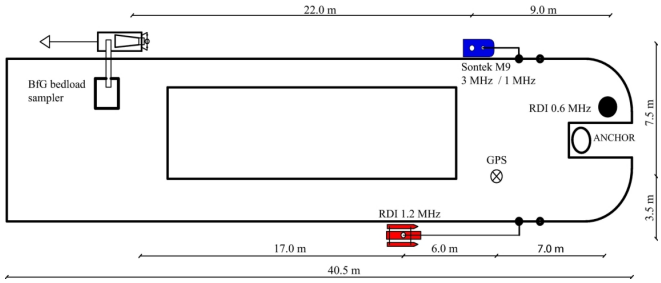

Measurement set-up and position of the instruments on the ship. Ship measurement scheme.

177x74mm (300 x 300 DPI)



(a) BfG Physical Sampler. Camera Set-up in the front.

279x130mm (300 x 300 DPI)



(b) BfG Physical Sampler. Camera Set-up in the front.

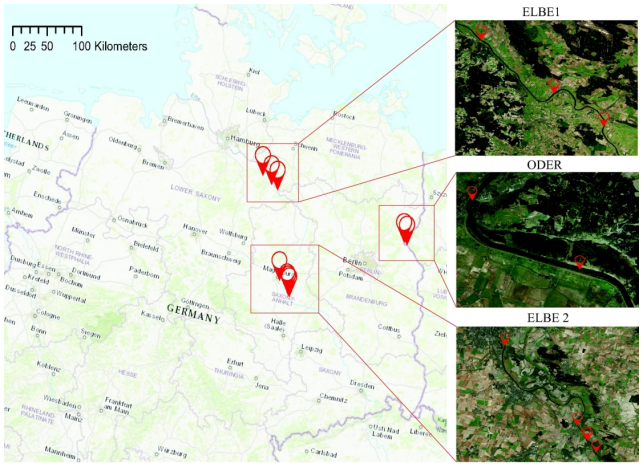

Study site locations.

173x214mm (300 x 300 DPI)

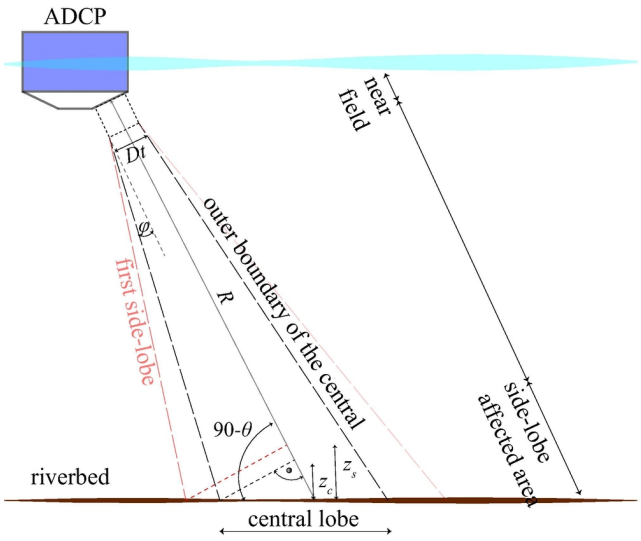

Acoustic beam scheme (pattern) of one ADCP transducer.

86x71mm (300 x 300 DPI)

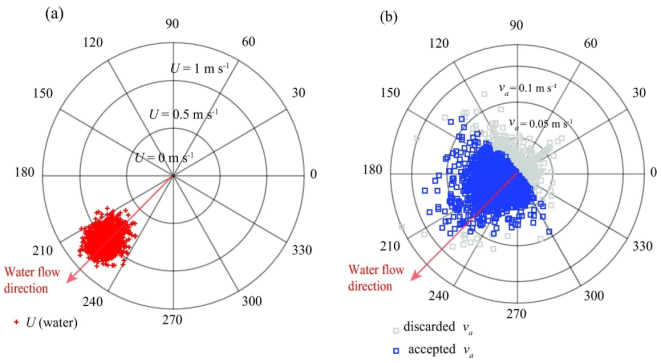

Example of vector direction plot at one measurement position of the RDI 0.6 MHz: (a) only water velocity (U, red symbols), (b) the accepted apparent bedload velocity (va, blue symbols) and discarded apparent bedload velocity (grey-faint symbols). Note that the blue and the faint-grey symbols give the raw apparent velocity measured by the BT mode of the ADCP. The red arrow represents the mean direction of the water velocity.

147x81mm (300 x 300 DPI)



Riverbed deformation influence on the ADCP bedload measurements. Note that this is simplified 2D scheme, the beams can be rotated differently with respect to the mean flow direction

123x18mm (300 x 300 DPI)

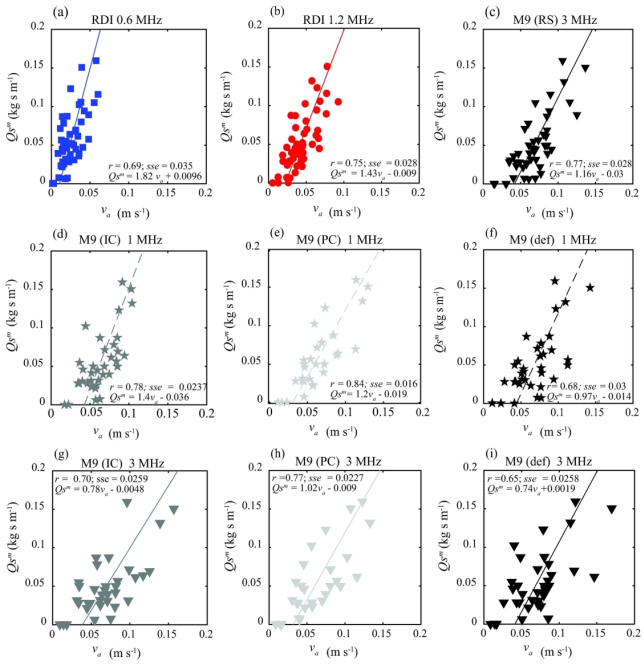

Filtered apparent velocities and the mean transport rate from the physical samples. All configurations given in Table 2 are shown in this figure : (a) 0.6 MHz RDI Rio Grande , blue squares, (b) 1.2 MHz RDI Rio Grande, red circle, (c) 3 MHz M9 Sontek, RS, black triangles (d) 1 MHz Sontek, IC, grey stars, (e) 1 MHz Sontek, PC, faint-grey stars, (f) 1 MHz Sontek, def, black stars, (g) 3 MHz Sontek, IC, grey triangles (h) 3 MHz Sontek, PC, faint-grey triangles, (i) 3 MHz Sontek, def, black triangles. The correlation coefficient r is given on each sub-figure together with linear fitting regression model.

180x181mm (300 x 300 DPI)

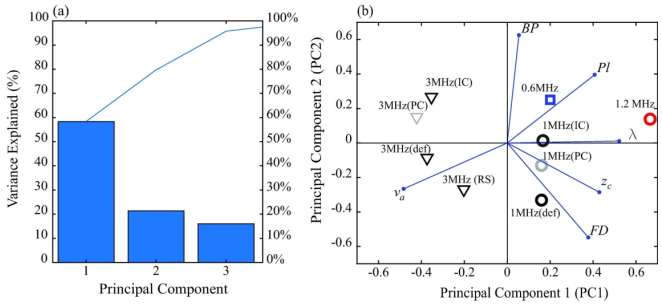

PCA analyses of the ADCP parameters given in Table 3. (a) explains the importance of the principal components in the analysis and the total captured variance, (b) shows how the observations (instruments and configurations) are describing the components and it demonstrates the correlation between the analysed parameters.

155x71mm (300 x 300 DPI)

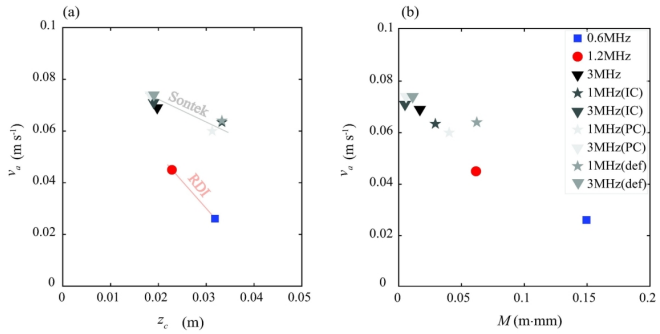

The acoustic parameters and the apparent bedload velocity: (a) gives the correlation between the beam focusing zc, given also in Table 3 and the averaged apparent bedload velocity for each instrument and configuration measured trough all three campaigns, (b) the combined acoustic indicator M is plotted versus the apparent bedload velocity.

156x79mm (300 x 300 DPI)

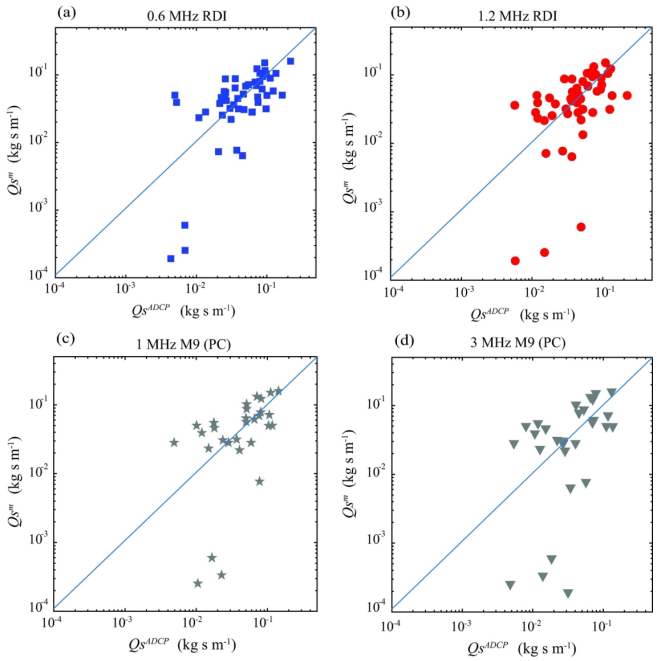

Modelled Transport rate QsADCP versus the measured transport rate Qsm, calculated for the apparent velocities of four representative configurations: (a) RDI 0.6 MHz, (b) RDI 1.2 MHz, (c) Sontek 1MZ PC, (d) Sontek 3MZ PC.

149x149mm (300 x 300 DPI)

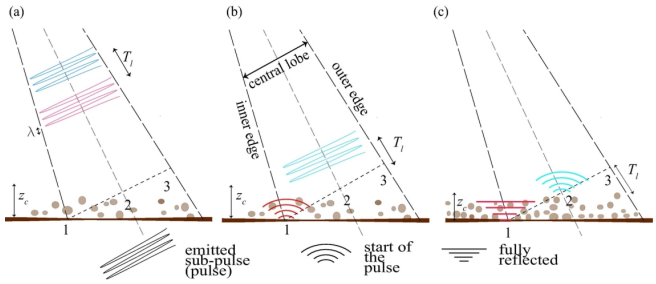

A possible scenario of a simplified beam scattering pattern, given at three consecutive instances: (a) the pulse emitted in the water column consisting of two sub-pulses or codded elements, (b) the front of the pulse penetrate through the active layer and reaches the immobile riverbed , where the first sub-pulse (red) starts the reflection, (c) the first sub-pulse is fully reflected of the immobile bed, the second sub-pulse (blue) starts the reflection at the top of the active layer.

139x59mm (300 x 300 DPI)

Paper *III*

Evaluation of an acoustic Doppler technique for bed-load transport measurements in sand-bed Rivers

Slaven Conevski, Axel Winterscheid, Massimo Guererro, Colin D. Rennie, Nils Ruther

River Flow 2018, Lyon

Evaluation of an acoustic Doppler technique for bed-load transport measurements in sand-bed Rivers

*S.*Conevski[1, 2], *A.* Winterscheid[3], *N.* Ruther[1] , *M.* Guerrero[2], *C.* Rennie[4]
[1]Department of Civil and Environmental Engineering, Norwegian University of Science and Technology, Trondheim, Norway. slaven.conevski@ntnu.no; nils.ruther@ntnu.no
[2] Department of Civil, Chemical, Environmental, and Materials Engineering, University of Bologna, Italy. massimo.guerrero@unibo.it; slaven.conevski2@unibo.it
[3]Federal Institute of Hydrology, Department Groundwater, Geology, River Morphology, Koblenz, Germany winterscheid@bafg.de
[4]Department of Civil Engineering, University of Ottawa, Ottawa, Canada. crennie@genie.uOttawa.ca

Abstract. The bottom tracking (BT) feature of the acoustic Doppler current profilers (ADCP) has emerged as a promising technique in evaluating the bed load. Strong statistical correlations are reported between the ADCP BT velocity and the transport rate obtained by physical sampling or dune tracking; however, these relations are strictly site-specific, and a local calibration is necessary. The direct physical sampling is very labor intensive, and it is prone to high instrument uncertainty. This work aims to develop a methodology for evaluating the bed load transport using commercial ADCPs without calibration with physical samples. Relatively long stationary measurements were performed in a sand-bed and sand gravel rivers, using three different ADCPs working at 3MHz, 1.2MHz and 0.6MHz. Simultaneously, bedload samples were collected with physical samplers, and the riverbed was closely observed with digital cameras mounted on the samplers. It is demonstrated that the kinematic transport model can yield a relatively good estimate of the transport rate by directly using filtered apparent velocity, the knowledge of the hydraulic conditions and instrument-related calibration coefficients. Additionally, the ADCP data can help in the qualitative assessment of the physical sampling. Future investigation of the backscattering echo and further confirmation of the BT apparent velocity should be performed in laboratory-controlled conditions.

1. Introduction

The quantification of the bedload transport in fluvial environments is a notoriously labor-intensive and challenging task. The temporal and spatial variability of the bed load together with the instrument disturbance can induce stochastic and systematic uncertainties. These data are usually considered as unreliable, which complicates the further elaboration of the sediment transport behavior. Statistically valid measurements are crucial for the evaluation of the sediment transport masses, especially in large navigable or heavily exploited rivers. Recently, many studies showed that the measurements with the bottom tracking (BT) feature of the acoustic Doppler current profilers (ADCP) have emerged as a promising technique in evaluating the bed load [1, 2, 3, 4]. The use of these non-intrusive techniques could significantly reduce uncertainty. Firstly, they do not disturb the riverbed and facilitate continuous measurements of the bed load. Secondly, they are easy to deploy and more frequent measurements can be expected. Widespread implementation of the ADCP BT bedload technique would reduce the scarcity and statistical uncertainty of bed load data.
Strong statistical correlations are reported between the ADCP BT velocity and the transport rate obtained by direct physical sampling or dune tracking [5]; however, these relations are strictly site-specific and a local calibration is necessary. Previous laboratory research has demonstrated that with a rather simple filtering and smoothing of the ADCP BT velocity (denoted as the *apparent velocity.* v_a), one can obtain relatively correct spatially averaged

velocity of the bed surface [6]. Deviation in the results is assigned to the coupling between acoustic waves at the given instrumental frequency, the size distribution of mobile particles (i.e., PSD) and the riverbed morphology.
This work aims to develop a methodology for evaluating the bed load transport using commercial ADCPs without specific calibration to the physical samples. However, it is necessary to know the hydraulic conditions and the particle size distribution (PSD) of the riverbed material that could be taken from some previous studies. The necessary hydraulic conditions can be obtained from the ADCPs water velocity column and used for further analysis of the bedload transport. The primary goal of this study is to assess the capability of the ADCP measurements to overcome the already existing problems with the bedload samplers and help the final estimation of the bedload masses.

1.1. Study sites

The measurement campaign in Germany took place in two cross-sections of the lower Oder River along the German-Polish border (52.8743° N, 14.1419° E). Seven positions were chosen in the one cross section and eight positions in the other cross section. The positions were chosen to try to avoid the groynes influence. The average discharge was 800m^3/s, with a maximum average velocity in the middle of the river of 1 m/s. The total width of the cross-section was 200-300m including the groynes. The water depth varied from 2.5m near the banks to 5.2m in the thalweg. The annual mean discharge is around 500m^3/s, and the mean annual maximum discharge is around 1200 m^3/s (http://geoportal.bafg.de); thus the measured flow had elevated discharge but was not a flood event. From the morphological perspective, the Oder River is a typically sandy river with well-characterized slow dune migration. The *D50* (median diameter) of the bedload in the measurement reach was 0.75 mm with standard deviation *(std=D84/D16*) of 1.5 mm. The particle size distribution is relatively homogeneous through the entire cross-section.
The measurements in Albania were performed in the sand-gravel reach of the small river Tomorrica (40.8271° N, 20.18639 ° E) where the average velocity in the sampling area of the ADCP reached 1.1 m/s. The Tomorrica is a tributary of the Devoll River flowing from the Tomorri peak to the 1-km-wide alluvial valley of the Devoll with typical braid morphology. In total 25 measurement positions are included in this study from two campaigns obtained in December 2016 and March 2017. The discharge varied between 2.5-3.5 m^3/s, and the measuring cross section width around 9m with variable depths at a maximum of 0.6m. The sand-gravel bed has *D50* that varied between 0.5-4mm with considerably higher std of 4-6 mm. The catchment is characterized with a high coefficient of variation of the discharge; thus the sediment transport occurs very randomly, consisting of rocks, cobbles, and gravel during the floods and sand during the annual flow discharges. There were fully armored parts of the river with some sand passing over and sand-gravel mixed areas. The measurements were conducted in the sandy parts with 0.45-0.7m average depth of the measurement area.
It has to be mentioned that the PSD distribution analyses were done only on the captured bed material that was sampled during the measurements; therefore the general riverbed characteristics should not be identified with these PSDs. The purpose is to estimate their acoustical footprint of the particles that are forming the active bedload layer.

1.2. ADCP operation

In total four different ADCPs were used in the campaigns. Two Teledyne RDI ADCPs (RioGrande 1.2MHz and 0.6MHz, four beam configuration) and one SonTek(M9 3MHz - working with four slanted-beam Janus configuration and one vertical beam of 0.5MHz) were used in Germany. In Albania, only one RDI (RiverPro 1.2MHz, with four slanted-beam configuration plus additional vertical beam) was used. The ADCP-type instruments are designed to measure the water velocities at several ranges to determine discharge and to give

information about the flow field. These monostatic sonars have usually four beams, i.e., four transducers that emit acoustic pulses and receive back the backscattered echoes intensities (*BsEI*). The signal is scattered from the particles that enter the acoustic beams and from the impermeable acoustical boundary, namely the immobile riverbed. The returned echoes contain information from the acoustical properties of each object they are reflected from and a shift of frequency (e.g. Doppler shift) to the object velocity, thus the object velocity in the direction of the beam can be easily calculated and then transformed in the coordinate system of interest, which is well explained by *Rennie et. al* [1]. The ADCPs have a separate signal called the bottom tracking (BT) mode to identify the bottom and its position. It uses a longer pulse and in case of mobile riverbed, it is significantly biased. The bias(e.g., $v_a=v_{gps}-v_{BT}$) can be exploited to calculate the average velocity of the river bed surface, denoted as the apparent velocity. The apparent velocity in case of fixed stationary measurements is equal to the BT velocity ($v_a= v_{BT}$), since the GPS velocity (v_{gps}) is zero.

Nevertheless, the received echo is not only scattered from the mobile bedload, but it may be also influenced by the suspended particles close to the riverbed, the immobile particles (immobile rough surface) and the riverbed morphology. Considering the complicated transmission of the signal in the active layer of the bedload and the scattering from the highly porous immobile and deformed riverbed the returned signal is noisy and contains erroneous data [7]. Furthermore, the erroneous data in the bedload velocity is more common for the areas with scarce transport. It is also an instrument-related problem related to the interpretation of the multiple two-phase scattering in the riverbed. For example, the working frequency (*f*), the pulse length, the grazing angle, and the instrument specific coefficients can significantly change the results. The returned signal contains backscattered information of the immobile particles (*rough surface scattering*) and the mobile particles (*volume scattering*). For the acoustic simplicity, only the particles in motion are considered as the *active layer* of the riverbed, the vibrating and potentially mobile are considered as the part of the rough surface scattering, thus the immobile particles.

Fig. 1. Acoustic footprint of the riverbed from one ADCP beam and the sonar equation

$$BsEI = SL + SV + K - 2TS - 20\log R \quad , \tag{1}$$

where the *SL* is the emitted source level, *SV* is the backscattering strength, *K* is the instrument related coefficient, *TS* is the transmission loss in the water column and in the active layer of the riverbed. The last component is related to the spreading of the signal at different water depth (*R*). The *SV* and *TS* are varying in different conditions of bedload transport, different PSD and different instrument frequency (*f*) and other instrument related parameters. SV and TS are depending differently from the two types of scattering mentioned above. The variability of the Doppler velocity calculation is strongly related to the variability of the *BsEI*;

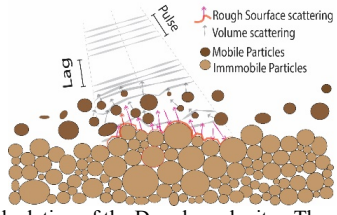

hence it is used into the calculation of the Doppler velocity. The correct interpretation of the components of the returned signal from the riverbed (e.g., *SV* and *TS*) would lead to a better understanding of the velocity information, and it will yield additional information about the thickness of the active layer.

A possible high concentration of suspended sand above the bed can bias the results showing the velocity of the suspended particles moving in the water layer above the bed and not the bedload. It is called the *water bias* [1] and has to be checked before the analysis. In both

campaigns the velocity of the last cell of the water velocity profile is significantly higher than the apparent velocity, thus the water bias is not an issue in this study. It is worth noting that the scattering from the riverbed material is expected to have significantly higher BS strength than the fine suspended sand or silt that would eventually induce the bias.

1.3. Physical Sampling

Three physical samplers were collected on each position at almost the same time interval with the ADCPs. In Tommorice river, small Helley-Smith (H-S) sampler (width of the inlet *b=7.65cm*) was used and in Germany two custom-made samplers were used [8]. The width of each was b=16cm but they had different mesh sizes (0.5mm and 1.4mm) of the collecting bag resulting with slightly different collection efficiency. Physical samplers are disturbing the original hydraulic conditions once they enter the river, and require hard manual labor and organization effort. There is a wide range of uncertainty. First of all the human operation and experience, but the pulsating behavior of the bedload transport that can be caused by the instantaneous variations in movement [9].
Additionally, the uncertainty can be induced by some systematic problems, such as improper sampler design, that may cause clogging of the collecting bag and prevents the entry of bed-load, or the loss of material when lifting up the sampler after each finish of the measurement. The custom-made bedload samplers demonstrate constant uncertainty during sampling in the sandy rivers. Due to the specific design, the typically underestimated the transport rates. The most sensitive part was the mash size of the sampler's bag, where the coarser one loses material while the other one is prone to clogging. The mounted cameras on the samplers (only in Germany) frame also helped to identify the problems of clogging, losing material, debris obstacles, blocking the nozzle and similar. The standard H-S sampler used in Albania is very sensitive to correct positioning in the river. The samplers were not at the same position as the ADCPs; therefore some deviation is expected due to the spatial and temporal natural variability of the river morphology and the transport processes.

2. Methodology

2.1. ADCP data analysis

The collected data from the acoustic instruments cannot be used directly, and there is non-commercial software that acquires instant and accurate estimation of the BT velocity. The ADCP data has to be filtered and the average velocity has to be calculated in a reasonable sampling period. In Germany, the averaging occurred on the entire sampling period where 15-20min were collected from all the three ADCPs with the sampling frequency of 1Hz. In Albania, the samples were shorter, but yet above 3min. If the opposite flow direction is denoted as a negative velocity, then the apparent velocity filtering follows the following simple conditions:

$$\begin{cases} v_{a\,fi} = NaN \;\; if \;\; v_{ai} < 0 \\ v_{a\,fi} = NaN \;\; if \;\; v_{ai} > \overline{v_{a\,i}} + 3\dfrac{1}{N_{raw}-1}\sum_{i}\;(v_{ai} - \overline{v_{a\,i}})^2 \end{cases} \tag{2}$$

where the $\boldsymbol{v_a}$ is the raw apparent velocity, and $\boldsymbol{v_{af}}$ is the filtered apparent velocity. *i* stands for the number of the ADCP sample. N_{raw} is the total number of raw data. The application of this simple filtering is mostly due to the known acoustic artifacts like aliasing, roughness frequency change, grazing angle variation, and high natural variability of the sediment transport causing decorrelation in the Doppler velocity calculation. Finally, to diminish the white noise, simple averaging of the filtered data is applied, considering only the filtered data. This filtering procedure is expected to deliver corrected magnitude and direction of the spatially averaged velocity of the bed. The spatially averaged velocity assumes not only the beam homogeneity but also the fact that each beam is highly influenced by the immobile river rough surface that can change from position to position. The highly dilute active layer

(with porosity of 0.8-0.95) allows the signal to penetrate to the immobile surface for any frequency.

2.2. Physical samples data analysis

The physical samples were analyzed and the transport rates were calculated together with the PSD specific for each sample. No correction of the transport rates (Fig.2 plot *b.)* was applied, even though the study and the report of the BfG (German Institute of Hydrology, responsible for all measurements in Germany) s that the average samples have to be corrected [8]. The potential loss of sandy part of the bed load was analyzed and tested under laboratory conditions in a flume resulting with 1.5-3.5 times less collecting mass than the real transport, due to the issues mentioned above [8]. This order of magnitude was also confirmed by other investigations [10] . The transport rates were compared with the apparent velocities and the ADCPs calculated transport rate (e.g. using the kinematic transport model). All three samples per position are directly included in the analysis, without averaging. The data from Albania was selectively chosen, where some unreasonable samples were discarded and the average of the available samples per position was correlated with the ADCPs.

2.3. Kinematic Transport Model

The riverbed surface explicitly incorporates the footprint of the immobile and mobile particles. Where the apparent velocity ($\boldsymbol{v_a}$) is assumed to be spatially averaged, equal to:

$$v_{af} = \frac{A_i}{A} v_p \,, \tag{3}$$

where $\boldsymbol{v_p}$ is the average particle velocity and A is the total sampling area. A_i is the insonified area of the mobile particles. Rennie et al. [1] pointed out that the transport rate is equal to the product of the average particle velocity and the mass of the particle per unit area. Later, they extend the concept to the kinematic transport model:

$$q_s = \sum_i v_{p_i} \left[\delta(1-\lambda) \frac{A_i}{A} \rho_s \right], \tag{4}$$

where q_s is the transport rate, δ and λ are the thickness and the porosity of the active layer and ρ_s is the density of the sediment (usually quartz 2.65 g/cm^3). It remains unclear how exactly the frequency and the sampling area/volume are influencing the A_i, but it is clear that each frequency penetrates differently through the active layer and that bottom roughness significantly influences the instantaneous values of the apparent velocity. The filtering method is reducing this uncertainty, and it makes the apparent velocity directly applicable in the transport model. However, there is considerable uncertainty of the highly dynamic active layer thickness and porosity. In this study, the variation of active layer thickness is considered as the main model uncertainty varying between two and eight times the median particle diameter (*D50*). The porosity is calculated according to the VanRijn equations [11] for bedload concentration, where $c_b=(1-\lambda)$. The shear velocity used in the VanRijn equations was calculated by using the assumption for log law profile in the lower part of the water velocities column obtained from the ADCPs (typically). It is also known that the log profile tends to fail if the data is not close enough to the boundary layer. It also may not perform well if the ADCP velocities are not processed correctly or if the cell resolution does not fit the assumptions for the log-law region. In these cases, the shear velocity is calculated using the Kalugelan formula for shear velocity for rough boundaries that uses the depth-averaged velocity as an input. The active layer is expected to be much more diluted than the dune and riverbed porosity usually reported in the literature (e.g., higher than 0.35-0.4) [11].

3. Results and discussion

3.1. The filtered apparent velocity

The filtering of the BT velocity or the apparent velocity increased the values from all the frequencies (Fig. 2, (a.)) and produced a vector direction that is more reasonable. The direction improvement is more obvious especially if you deal with shorter time series and the temporal averaging is not sufficient to smooth the data, such as the case of Albania (Fig.2. rhombs, markers). The filtering also deals with the fudge effect of the reattachment dune region where the high turbulent flow confuses the ADCP signal and produces unreasonable data (e.g. Oder River Germany).
The 3Mhz could be partially sensitive to the "*water bias*" if some highly concentrated suspended clouds of sediments pass through the sample volume and produce some spikes of very high velocities. These outliers were also discarded with the filtering procedure.
The variation of the bedload velocities is mostly because the PSD changed from position to position, especially in the data from Albania (Fig 2. (*a.*), rhomb markers) and due to the different sampling positions associated with different water depth and velocity. Therefore, the filtering is much heavier in the Albania data where *D50* varies from 0.7mm to 13.5mm. Additionally, the weaker transport rates are due to the improper positioning of the sampler, clogging, blocked nozzle or human error, that is hard to be noted during the sampling but could be discarded later after the results from the ADCPs are processed and demonstrate some bedload velocity.

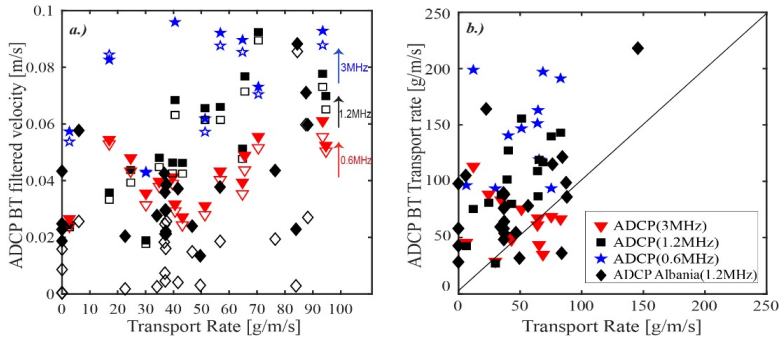

Fig. 2. (*a.*) Filtered (filled markers) and unfiltered (empty markers) apparent ADCP velocity demonstrating correlation with the physical transport rates; (*b.*) Transport rates from the physical sampling on the x-axis and the ADCP kinematic model on the y-axis

Even after filtering and post-processing the data, there is a difference between the velocities measured by ADCPs with different frequencies. Namely, the lowest frequency demonstrates the lowest values especially in the area of higher transport rates (Fig. 2 *(a.)*). M9 SonTek delivered the highest apparent velocities working with 3MHz. There are several factors that cause this effect but the most obvious one is that the lower frequency penetrates the active layer or deeper in the loose immobile bed and the received echo contains more data from the immobile surface than the active layer. The lower velocity is related to the Doppler shift calculation, thus with the echo identification in the range of the lowest part of the active layer where the immobile surface echoes may dominate. This is also related to the internal algorithm of the instrument that identifies the echoes used for calculating the BT velocity. Usually, the algorithm considers the maximum echo of the small searching range. Considering that, the 0.6MHz have longer pulses and less acoustic sensitivity towards sand (as it is the dominant material in both campaigns), it is logical that the signal from the lower frequency would have more considerable input of the immobile surface bottom.

On the other hand, the higher frequency waves contain more information from the mobile particle; hence they are dissipated in the active layer. It has to be noted that the mobile bed load layer has high porosity compared to the immobile riverbed below, therefore any plane acoustic wave will partially contact the immobile surface. The more abounded transport, the less the signal is biased by the immobile particles or surface, meaning less filtered data. The percentage of filtered data is increasing as the transport rate decreases. Finally, it has to be mentioned that the grazing angle of the emitted wave or the slanting angle of the beams in combination with the riverbed inclination and the inundations may contribute to different echo intensity and inaccurate echo identification by the internal algorithm.

3.2. The transport rates

The transport rates are calculated using the different frequencies, filtered apparent velocities and the kinematic model from eq. (3).The ADCP calculated transport rates are directly correlated with the transport rates obtained from direct physical measurements. Assuming that the filtering procedure filtered most of the uncertainty in the data the variation of the transport rates is associated with the thickness of the active layer (δ in eq. 4. The data from Albania results with higher uncertainty due to the wider PSD and larger *D50* of the samples and, thus the sensitivity of the active layer assumption. The values of the ADCP calculated transport rates vary with the ADCP frequency and the Van Rijn calculated concentration of the bedload ($c_b=1-\lambda$) and the thickness is $5D50$ for Oder data and $3D50$ for Tommorice data. The thickness of the active layer is intentionally chosen with smaller variation due to the larger *D50* and higher sorting coefficient of the PSDs in Albania. As it was mentioned before, the highest frequency with its filtered apparent velocity offers the highest transport rates boundaries. The non-corrected transport rates directly measured by the custom-made samplers are expected to underestimate the average bedload transport for sand in accordance with *Hillebrand*, *et al* and *McLean at al* [8, 12].
However, this makes more reasonable the values from the ADCPs, especially the ones with 1.2MHz and 3MHz, complying with the assumptions. Fig 2 (*b.)* shows the uncertainty of th physical sample given by the horizontal bars. It should be noted that the std is out of the mean values, without excluding eventual erroneous data such as zero values or bad positioning recorded on the videos. The videos from the mounted camera also showed that it could dig inside the dune and collect only that material instead of real transport occurring while the dune is migrating. They were also analyzed using velocity estimation algorithms (e.g., Optical Flow). This image analysis suggests that the bedload material was not correctly entering the sampler due to the disturbed hydraulic conditions induced by the clogging of the smaller mesh (0.5mm) in Germany.
The kinematic model data overestimates some of the results, but in general, there is a good matching of the data. The deviation of the physical samplers is not presented because the number of samples per position was not consistent. The too low transport rates in some measurements by the sampler are part of the high physical sampling uncertainty. These data can be excluded from the total estimation of the transport rates and the ADCPs could easily identify these outliers and later to exclude them from the final average of the physical sample rates. One of the drawbacks of this model is the arbitrary chosen constant thickness of the active layer that in reality can vary in the mentioned constraints.
Nevertheless, using two frequencies gives the opportunity of estimating the BsEI from the two frequencies and analyze the dependence of the *SV* and *TS* and the active layer thickness; hence the penetration changes as the thickness increases or a change of the PSD is present. It is an ongoing laboratory study and will be presented in the future work of the authors. Currently, the chosen mean values of the thickness are related to the intensity of the transport and variation of the *BsEI*. In the supplementary material, the deviation of each position is presented as a possible range($2D50$-$8D50$) of the ADCP measured transport rate.
In the end, one can quickly draw a conclusion that even with the considered uncertainty of the ADCP values the transport rates are slightly higher than physical transport rates. This

leads to the fact that the physical sampling has its disadvantages (seen on the recorded videos and laboratory tests) and a correction factor has to be chosen for a proper presentation.

3.3. Conclusions

The limited number of measurements demonstrated that the ADCPs BT velocity could be used for relatively accurate estimation of the bedload transport rate. The filtering procedure decreased the uncertainty of the kinematic model and delivered its application without explicitly fitting parameters. Besides, they could help for a qualitative validation of the physical samples or support the determination of a correction factor if they are conducted together. Excluding the outliers improves the statistical validity of the physical sampling. The ADCP data gives a more comprehensive description of the erosion-deposition process in the rivers and can be reported in shorter periods (longer than 3min averages).
Additionally, with apriori defined PSD of the bed load the kinematic model reported relatively good estimation of the bedload transport rates not just in comparison with the physical samples but also in compliance with the uncertainty of the bedload measurements. Attention should be paid on the frequency used and the predefined hydraulic conditions for estimating the active layer porosity and thickness. These two parameters contribute to the highest uncertainty of the kinematic model. The ADCP parameters settings are also essential in order to have a reasonable resolution of the water velocity data. It remains unknown how the internal processing of the signal and the identification of the echoes influence the Doppler velocity calculation. The future work focuses on identifying the different types of bottom scattering and associating the active layer properties with the acoustic parameters. Additionally, all the sources of Doppler uncertainty should be identified and the procedure of filtering has to be improved and eventual in situ software should be developed for direct evaluation.

References

1. C. Rennie, R. G. Millar and M. A. ,. Church, "Measurement of bed load velocity using an acoustic Doppler current profile," *Journal of Hydraulic Engineering,* vol. **128**(5), p. 473–483, 2002.
2. C. Rennie and P. V. Villard, "Site specificity of bed load measurement using an acoustic Doppler current profiler," *J. Geophys. Res.,* vol. **109**, no. F03003, 2004.
3. D. Gaeuman and R. B. Jacobson, “Acoustic bed velocity and bed load dynamics in a large sand bed river,” *J Geophys Res Earth Surf,* vol. **111**(F2), no. F02005, 2006.
4. F. G. Latosinski, R. N. zupiany, M. Guerrero, M. L. Amsler and C. Vionnet, “The ADCP's bottom track capability for bedload prediction: Evidence on method reliability from sandy river applications,” *Flow Measurement and Instrumentation,* vol. **54**, no. June 2016, pp. 124-135, 2017.
5. C. Rennie, D. Vericat, R. Williams, J. Brasington and M. Hicks, Calibration of aDcp apparent bedload velocity to bedload transport rate, Tsutsumi, D., and Laronne, J., Wiley., 2017
6. S. Conevski, M. Guerrero, N. Ruther and C. Rennie, “ADCP performance of measuring the bedload velocity under changing conditions of particles mobility/bedload transport conditions,” *in submition,* 2018.
7. R. I. R. Lee Gordon, “*Acoustic Doppler Current Profiler Principles of Operation A Practical Primer*,” RD Instruments, San Diego, California, 1996.
8. G. Hillebrand and R. Frings, “Von der Quelle zur Mündung: Die Sedimentbilanz des Rheins im Zeitraum 1991 – 2010.,” Internationale Kommission für die Hydrologie des Rheingebietes, Lelystad, Achen, 2017.
9. R. M. Frings and V. Stefan, “Guidelines for sampling bedload transport with minimum uncertainty,” *Sedimentology,* 2017.
10. D. McLean, M. Church and B. and Tassone, “Sediment transport along the lower Fraser River. 1. Measurements and hydraulic computations,” *Water Resour. Res,* vol. **35**, pp. 2533-2548, 1999.
11. L. Van Rijn, “Sediment transport, part i: bed load transport,” *J. Hydraul. Eng.,* vol. 110, p. 1431–1456, 1984.
12. D. McLean, M. Church and B. Tassone, “Sediment transport along the lower Fraser River. 1. Measurements and hydraulic computations,” *Water Resour. Res.,* no. **35**, pp. 2533-2548, 1999.

Paper IV

Acoustic sampling effects on bedload quantification using acoustic Doppler current profilers

Slaven Conevski, Massimo Guererro, Colin D. Rennie, Nils Ruther

IAHR World Congress, September 1-6, 2019, Panama City, Panama

---

E-proceedings of the 38th IAHR World Congress
September 1-6, 2019, Panama City, Panama

LABORATORY MONITORING OF BEDLOAD TRANSPORT RATES USING HYDRO-ACOUSTIC TECHNIQUES (ADCP)

SLAVEN CONEVSKI[1], MASSIMO GUERRERO[2], NILS RUTHER[3] & COLIN RENNIE[4]

[1,3]Department of Civil and Environmental Engineering, Norwegian University of Science and Technology, Trondheim, Norway. slaven.conevski@ntnu.no; nils.ruther@ntnu.no
[1,2] Department of Civil, Chemical, Environmental, and Materials Engineering, University of Bologna, Italy. massimo.guerrero@unibo.it; slaven.conevski2@unibo.it
[4] Department of Civil Engineering, University of Ottawa, Ottawa, Canada. crennie@genie.uOttawa.ca

ABSTRACT

This study aims to develop a surrogate methodology for quantification of the bedload transport in riverine environments by using acoustic devices. Bedload transport experiments were performed in laboratory conditions to test the capabilities of the acoustic current Doppler profilers (ADCP) to quantify the bedload velocity, concentration, and active layer thickness. Two ADCPs working at four frequencies (0.5MHz, 1MHz, 3MHz M9, by Sontek, and 2MHz StreamPro, by RDI) were deployed at the same time. Simultaneously, the bedload transport was monitored by high-speed cameras, and continuous bedload transport rate measurements were conducted at the end of the measurement section. The apparent bedload velocity was analyzed and compared with the velocity from the imagery data and the transport rates measured by the bedload trap. Besides the apparent bedload velocity, the ADCPs also registered the backscattered (BS) signal from the sediment bed, which appeared to be sensitive to the change of the bedload transport conditions and the type of the sediment particles. The results confirmed the capability of these acoustic instruments to measure the bedload velocity by demonstrating a strong correlation with the physical transport measurements and the velocities from the imagery data. The apparent velocities measured by the 3 MHz and 1 MHz demonstrated similar results; the 2 MHz measurements led to lower values with 2-4.5 times magnitude difference comparing with the spatially normalized image velocity. The corrected BS signal documented a clear correlation with the apparent bedload velocity, more precisely with the change of the bedload transport condition. The variation between the results from the two instruments is assigned to the different acoustic geometry of the instruments, internal processing, and availability of the instrument related parameters needed for correction of the backscattered signal. Future tests should aim towards a better understanding of the internal processing of the signal and extensive analysis of BS strength sensitivity towards a wide range of sediment types and hydraulic conditions.

Keywords: ADCP; bedload velocity; sediment transport; acoustic backscattering

1 INTRODUCTION

Accurate estimation of bedload transport has been an engineering challenge since the previous century. The traditional measurements are highly uncertain and often statistically invalid. Several studies have investigated the use of the bottom tracking (BT) mode of acoustic current Doppler profilers (ADCPs) for evaluating bedload transport. Measuring the bedload transport rate, using direct traditional methods (i.e., pressure difference samplers) is a notoriously labor-intensive and challenging procedure. The temporal and spatial variability of the bedload together with the instrument disturbance, can induce stochastic and systematic uncertainties, which complicates the further elaboration of the sediment transport behavior. Statistically accurate measurements are crucial for correct estimation of sediment transport masses, which is especially important in large navigable or heavily exploited rivers.

Several studies have shown that the measurements with the bottom tracking (BT) feature of the acoustic Doppler current profilers (ADCP) have emerged as a promising technique in evaluating the apparent velocity of the bedload (Rennie, et al., 2002; Rennie & Villard, 2004; Jamieson, et al., 2008). This technique utilizes the BT bias, defined as $v_a = v_{gps} - v_{bt}$, the difference between the actual GPS boat velocity and the BT velocity delivered by the acoustic pulse backscattered from the riverbed. Another field study presented a complete interpretation of the analytical relation between apparent velocities, particle velocities, and the bedload concentrations (Gaeuman & Jacobson, 2006). Some other tests found that shorter pulses give better correlation with the bedload transport rate due to less bias by high close-to-bed suspended load concentrations, and that lower frequency instruments consistently were giving lower apparent bedload velocity both in laboratory and field investigations (Ramooz & Rennie, 2008; Latosinski, et al., 2017).

E-proceedings of the 38th IAHR World Congress
September 1-6, 2019, Panama City, Panama

Most recently, Conevski et al. (2019) conducted a laboratory campaign to compare the surface velocities measured by high-speed cameras to the apparent velocities measured by two different ADCPs (M9 by Sontek, StreamPro by RDI). The instruments were deployed separately in two different laboratories for bed sediments ranging from medium sand to fine gravel. The same study suggests that there is a necessity of stream-wise filtering of the apparent velocity for more accurate estimation of the average apparent velocity. The degree of required filtering increased with the bed transport. Moreover, the lower frequency instrument underestimated the surface bedload velocities in order of magnitude of 2-4 times (Conevski, et al., 2019).

This study aims to confirm the hypothesis and methodologies reported in Conevski et al. (2019), by deploying the two ADCPs simultaneously in the same flume to examine the filtered apparent bedload velocity correlation with the physically measured transport rate. In addition, the sensitivity of the backscattering (BS) strength of both ADCPs (four frequencies) was tested towards different bedload transport conditions. Hence, this work is a further step towards the primary goal of determining the capability of ADCPs to register different characteristics of the bedload transport (velocity, median sediment size, the active layer, etc.) in riverine environments through a detailed and complete investigation of acoustic parameters and identification of the instrument limitations.

2 METHODOLOGY

2.1 Experimental Setup and Instrumentation

The experiments were performed in a 12.5 m long and 0.6 m wide tilting flume at the Hydraulic Laboratory at the Norwegian Institute of Science and Technology. The flume's bottom inclined at 0.1% and it was filled with a sediment layer gradually changing in depth from 13 cm upstream to 10 cm downstream. Additional sediment feeding was not necessary due to the relatively short experiment duration. Attempting to have developed sediment motion the measurement section was located in the last two meters of the flume. Well-sorted fine sand was used having a median diameter (D50) of 0.31 mm and Reynolds particle number (Re_p) of 16.8. The two ADCPs were mounted at the same height (~ 0.35 m) above the sediment bed, but separated longitudinally by 0.7 m, which ensured 0.1-0.2 m distance between the closest beam footprints (see, Fig. 1). A high-speed camera (1980x1350 pixels, 139 frames per second) in an underwater protection box was installed between the ADCPs. It had a planar view towards the sediment bed recording an area of 20x15 cm. On the side of the transparent plastic walls of the flume, a GoPro Hero Black6 camera (2.7K resolution and 60fps) was set to record the bedload formation and the bedload active layer. To obtain efficient velocimetry from images, intense and equalized lightning conditions are necessary, which was arranged by installing four LED lights aiming in the sampling area from outside of the glass walls. At the end of the flume, a weight sensitive box was used to measure at 50Hz the deposited sediment falling into the box. Furthermore, two acoustic Doppler velocimeters (ADV) were mounted upstream to measure the water velocity (U) in two points in the middle of the flume.

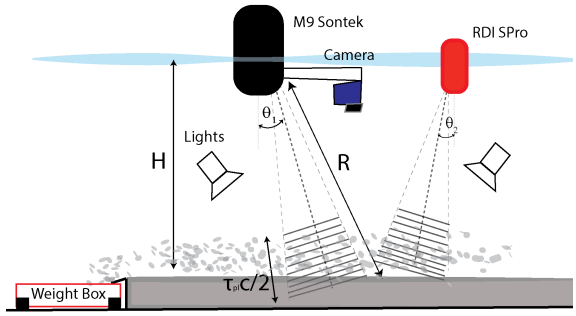

Figure 1. Experimental set-up (*Note: The sketch is scaled for better visualization*)

Three hydraulic conditions were chosen not to induce suspension of the bed sediments, starting from very weak transport at 80 l/s as the first condition (EXP1) to very abundant transport with developed bed forms at 150 l/s, as the third condition (EXP3). The shear velocity was carefully chosen not to exceed the suspension criterion suggested in the Shields diagram (see Table 1). The critical shear velocity (u^*_{cr}) was calculated using the formulation suggested by Dietrich (1982) and the actual shear velocity (u^*) using the semi-empirical log-law equation suggested by Van Rijn (1984). Three repetitions per experiment type were conducted with an average time duration of 20 min each. After each experiment, the sediment bed was distributed back from the sediment box to the flume and the entire surface was flattened again to the initial state of the sediment layer.

Table 1. Basic Hydraulic parameters and experiment characteristics

Name	num rep	Q l/s	H m	Re_p /	U m/s	u^* m/s	u^*_{cr} m/s	$D50$ mm	$D90$ mm
EXP1	3	80	0.4	16.8	0.323	0.016	0.0145	0.31	0.52
EXP2	3	120	0.4	16.8	0.363	0.018	0.0145	0.31	0.52
EXP3	3	150	0.4	16.8	0.412	0.021	0.0145	0.31	0.52

2.2 ADCP working principle

ADCPs are monostatic sonar systems that are typically used for measuring the water velocity, which is calculated internally. Commercial software is available to yield data of the water velocities and discharges over a cross-section. They are deployed in moving or stationary conditions. They are configured with four or more transducers at 90° azimuth intervals, which project diverging beams (Janus configuration). In this study the RDI StreamPro has four transducers (2MHz carrying frequency) in Janus configuration, forming four beams with a slant angle of θ_2=20°. On the other hand, the Sontek M9, has two groups of transducers (four plus four) in Janus configuration with a slant angle of θ_1=25° (1 MHz and 3 MHz carrying frequency), as well as one vertical beam with 0.5 MHz carrying- frequency. The tilted beams permit measurements of the three velocity components under the layer homogeneity assumption, i.e., the velocity field is homogeneous for all beam sampling areas. Besides the water velocity profiling, these instruments have the BT feature, which is used for identifying the water depth and estimating the instrument speed referenced to a fixed bottom. The BT mode involves emitting longer pulses than the water profiling mode but assumes similar signal processing techniques (RDInstruments, 2011). The water depth, pulse length, transducer width, beam opening angle, and the riverbed roughness determine the sampling area. It is a sampling volume with maximum height occurring at about half pulse length, as explained in detail by Rennie (2002). If the riverbed is mobile, then this feature is biased. If the instrument is stationary, this bias is assigned directly to the apparent bedload velocity (v_a=v_{BT}). This bias is considered as a measure of the spatially – averaged bedload velocity (Rennie, et al., 2002). However, it is strongly dependent on the instrument frequency, the acoustic geometry and the internal signal processing (Conevski et al. 2019). The emitted BT pulse by each beam insonifies four independent areas of the riverbed at different positions and elevations, which can challenge the homogeneity assumption.

The bedload exhibits a complex two-phase scattering process. The mobile particles that determine the bedload velocity are responsible for the volume scattering, but the signal may also penetrate through the active layer of mobile bedload and be scattered from the rough immobile bed sediment surface (Conevski 2019). Furthermore, mobile and immobile particles can also be sampled at the bed surface, especially in the case of incipient bedload transport. The details of the internal signal processing and Doppler data modulations are not known for the users; thus, some deviations in the results are expected.

The two ADCPs worked simultaneously during the experiments and registered BT and water profile data. A collaboration with Sontek Xylem enabled the M9 to work and register BT data from all nine beams. Some general parameters related to the acoustic properties of the two instruments are given in Table 2.

Table 2. ADCP acoustic parameters

Instrument Type	Freq.	Wavelength (λ)	Grazing angle (θ)	1/2 beam opening angle (φ)	Transducers diameter (D_t)	Pulse length (Pl)
	MHz	mm	°	°	cm	cm
StreamPro	2.0	0.73	20	1.4	1.5	7.0
M9	3.0	0.48	25	0.6	2.5	5.0
M9	1.0	1.45	25	1.7	3.5	5.0
M9	0.5	2.90	90	3.4	4.5	5.0

2.2.1 Backscattering Strength Correction

The ADCP BT tracking feature also provides information of the echo intensity (EI), which depends on the sediment concentration, the amount of air in the voids, and the geometric non-uniformity of the river bed (the bed roughness). All these qualities are related to the particle size distribution (PSD) of the bed sediments and the transport conditions.
It could be assumed that the volume scattering (Sv) is related to the mobile bed and the surface scattering (*Ss*) with immobile bed grains. It is not clear if this categorization is possible or desirable, but it explains the vital processes of the scattering phenomena. Because it is impossible to distinguish between these scattering processes in this study it is assumed that the backscattering strength derived from the sonar equation is superimposed (*BS=Sv+Ss*), as explained in detail by Conevski et. al (2019).
To analyze the backscattering strength separately, EI was corrected following the sonar equation:

$$BS = -SL - P_{dBW} + kc(EI - EI_r) - Af + 2TL, \quad [1]$$

where the SL is the source level of the transmitted power given in dB, it can be calculated as $10\log(P/P_0)$, if the pressure at the transducer (P) is available and P_0 is the reference pressure, or it is given as the C constant in Mullison (2017). P_{dBW} is the battery voltage given in dB ($20\log(V/V_0)$, where V is the voltage in volts). A_f is the correction due to the transmission loss of the acoustic footprint calculated as $Pl\varphi/\cos(\theta$, where Pl and φ are given in Table 2. k_c is the conversion coefficient from counts to dB (0.45 for StreamPro and 0.1 for M9) and Elr is the ambient noise level. The noise level may vary and it was available only in the M9 output; for the StreamPro it was tentatively assumed as constant ~ 40 dB (RDInstruments, 2015). *TL* is the transmission losses that include beam spreading (*40logRcos(θ)*) and the attenuation in the water column, *R* is the slant distance to the sediment bed. Note that some of the parameters are explained in Table 2.
It should be mentioned that most of these variables are constant due to the known geometry and controlled laboratory conditions. The $EI\text{-}EI_r$ and the P_{dBW}, are the variables that significantly change in time during the measurement procedure. The eventual influence of the high SSC in the region close to the bedload, inducing the so-called water bias to the signal was avoided by adjusting the hydraulic parameters to have very low SSC. Nevertheless, during the extreme conditions (i.e. EXP3), occasional bursts of particles above the crests of the dunes were noticed; thus, in this case, a small influence in the ADCP results is expected.

2.3 Image Processing

The image velocimetry technique involves pre-processing of the images, application of the 2-frames change algorithm, followed by PIV techniques to calculate the velocities detected by the two-frames change method (Radice, et al., 2006; Conevski, et al., 2019). This technique is fully adopted from Conevski at. al (2019) and the same variables are considered in this study:

i. K, the percentage of the mobile particles or the surface bedload concentration calculated as the ratio of the number of pixels of detected image changes and the total number of pixels in the region of interest.
ii. v_c, the image velocimetry, representing the mean velocity of the bedload particles at the top of the active layer (i.e., the layer of mobile particles).

The images recorded by the side-looking camera were used to obtain a qualitative value of the thickness of the active layer formed by the particles moving at the crest of the dune. The intense lights coming from the opposite walls made the sediment particles relatively distinguishable in the water column. Then a simple image

processing technique was applied using threshold binarization to obtain the mean active layer thickness out of several images.
The conversion from pixels to meters was obtained by taking checkerboard calibration images before and after each repetition.

2.4 Physical bedload transport rates

The weight box at the end of the flume was constructed to act as a bedload trap, immediately after the measuring section. After the box, the water recirculation cycle starts, and no sediment transport occurred after this section. It measures the weight changes in N/s at a sampling frequency of 50Hz. The data were converted from N/s to g/s using the submerged density of quartz sediments $\rho_s/\rho = 1.65$ *and* the gravitational constant 9.81 m/s^2.

2.5 Data post-processing

The ADCP data post-processing permitted calculation of the apparent bedload velocity in the stream-wise direction which filtered false direction vectors (i.e., the angle between the water direction vector and the BT did not exceed 90 degrees) and all values higher than three times the standard deviation of the raw apparent velocity. The percentage of the data that were filtered (FD) was also calculated for each ADCP frequency. The data were averaged in time obtaining one value per repetition. The procedure followed the methodology given in Conevski at. al (2019), without deleting measurements from dune troughs, where the recirculation phenomena occur. It was assumed that the filtering procedure discards these values automatically thus some higher percentage of the filtering is expected in these regions.
A similar procedure was performed for the imagery data that resulted in a much lower percentage of filtering. The velocity data was also time averaged. Simple threshold de-spiking was applied on backscattering data because some outliers appeared in the time series.

3 RESULTS AND DISCUSSION

3.1 Filtered apparent bedload velocity and the imagery data

Figure 2 gives an overview of the apparent bedload velocity from the two ADCPs obtained after the filtering procedure, the normalized image velocity ($v_c * K$) and the filtered data. The image velocity (v_c) is calculated from the recorded images by applying an image processing methodology that detects only the mobile particles. To obtain a spatially averaged velocity (i.e., including immobile particles), that is comparable with the apparent velocity; the image velocity is multiplied by the percentage of the bedload surface concentration (i.e., the mobile surface, K).

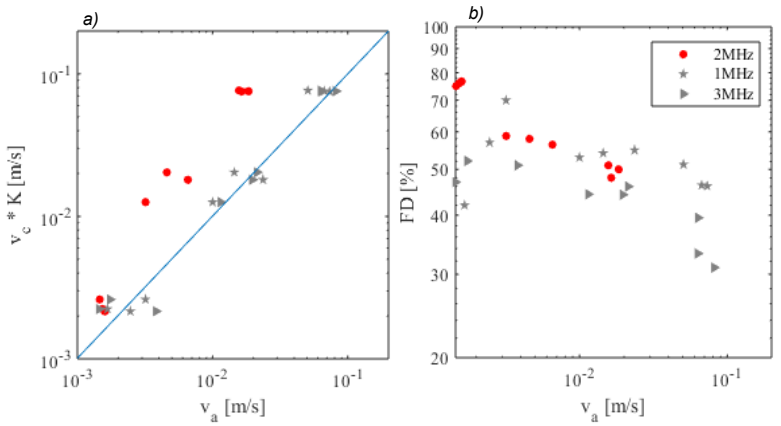

Figure 2. a) The filtered apparent velocity (v_a) and the normalized image velocity ($v_c * K$); b) The percentage of total filtered data vs the apparent bedload velocity

E-proceedings of the 38th IAHR World Congress
September 1-6, 2019, Panama City, Panama

The Stream Pro (Figure 2a, red circles, 2MHz) data gave lower values of the apparent velocity and underestimated the spatially normalized image velocity data (v_c*K) by a factor of (1.7-4.5) times. This is in agreement with Conevski et al. (2019) where the same underestimation was reported concerning camera and the lower frequency ADCP, although the 2 and 3 MHz instruments were deployed in different flumes. On the other hand, after filtering the highest frequency (3MHz M9) apparent velocity values almost match the v_c*K, corroborating the assumption that the higher frequency instrument measures the spatially averaged surface velocity of the mobile bedload. Surprisingly, the lowest frequency measured by the M9 delivered almost the same values as the 3MHz. It leads to a conclusion that acoustic geometry and the internal signal processing play a crucial role in the Doppler velocity estimation (Conevski, et al., 2018) rather than the carrying frequency. The ADCP-filtered data (FD) gives a negative correlation with the surface bedload concentration from the imagery data (see, Figure 2b), similarly as in Conevski et al. (2019). *FD* is decreasing as the transport rate increases (see, Figure 2b), but it seems that saturated at 30 % for the 3MHz and 50% for 2MHz and 1MHz. The filtering percentage has relatively high values because the bedload material is fine sand, acoustically scattering in the Rayleigh regime for all three frequencies. For Rayleigh scattering the wavelength of the acoustic signal is longer than the mean particle size defined from the number probability distribution, resulting with less influence of the mobile particles and more scattering from the immobile surface (Thorne, et al., 1991). The *FD* percentage for the EXP1 is reasonably very high because the thin bedload active layer and the dilute concentration are challenging the measurements of the monostatic slant transducers. Besides, the relatively small acoustic footprints could mostly cover a recirculation region at the dune trough; in this case, the resulting negative velocity is also discarded and included in the filtering percentage.

3.2 Bedload transport and the apparent velocity

To further examine the validity of the apparent velocity measurements, the apparent velocities are correlated with the mass bedload transport rates measured at the end of the flume (Figure 3a) and the surface bedload concentration measured by the cameras (Figure 3a). Figure 3 presents only the data from EXP2 and EXP3 where mass changes were registered in the weight box. In the first condition (EXP1), the transport was very weak such that the box was unable to register any mass changes, but the bedload surface concentration (K) in Figure 3b clearly shows that there was some movement of the particles.

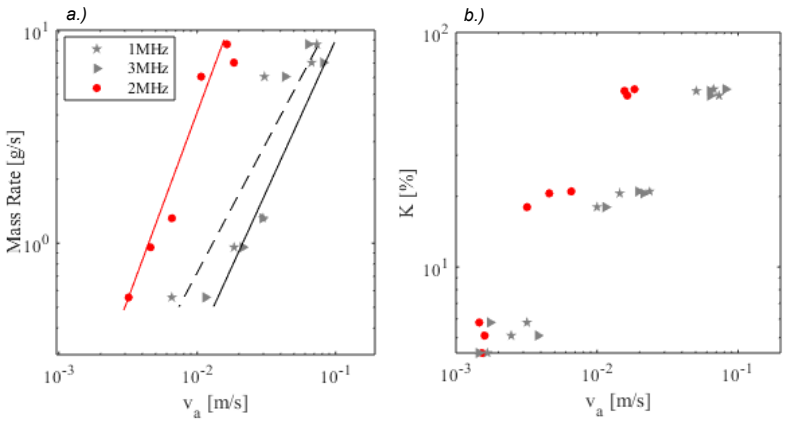

Figure 3. Mass transport rates, the filtered apparent velocity (v_a) and the surface concentration (K) (*Note: the data from the first experiment is not plotted because the measured transport rate was negligible)*

The results in Figure 3a clearly show a strong correlation for both ADCPs with correlation coefficients above 0.8. This indicates that the BT tracking bias is a direct measurement of the bedload velocity and the improved correlation after the filtering procedure of ADCP data confirmed the validity of this method (correlation coefficients changed from 0.6 to 0.8). Figure 3 also bears out that the StreamPro underestimates the spatially averaged bedload velocity and presents a slightly steeper slope than the other two frequencies.

3.3 The apparent bedload velocities and the backscattering strength

The observed values of the BS strength from all four frequencies demonstrated a sensitivity towards different bedload transport conditions, which corroborates the idea that change of the bedload concentration introduces changes in the backscattering strength due to the increase or decrease of the volume scattering. In general, the BS values decreased while the transport rate was intensifying.

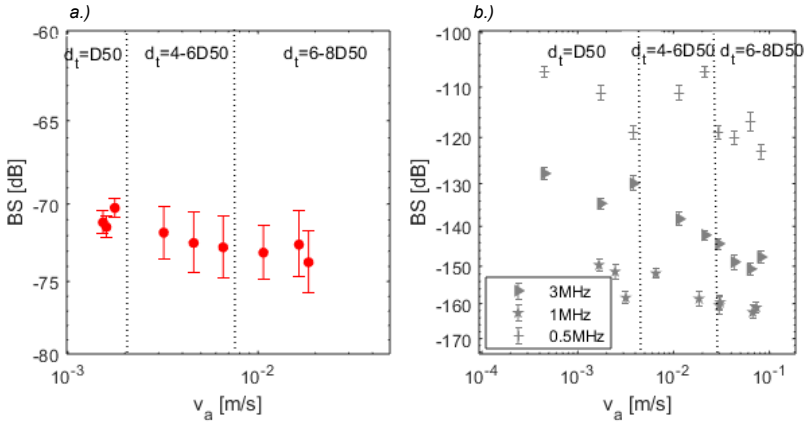

Figure 4. Bedload apparent velocity and the corrected BS strength for 2 MHz StreamPro (a) and the M9 transducers, working at different frequencies (b). Note that the observed backscattering strength, BS, at 0.5 MHz vertical beam is paired with apparent velocity, v_a, from 3 MHz slant beams). The dotted lines show the passage from one to another experiment condition and d_t gives the range of the active layer thickness measured by the side-looking camera.

The absolute differences between the values of BS for each frequency are related to the Source level (SL) and the power intensity distributed to each transducer. Note that the manufacturer does not equalize the EI output leading to an offset among the values from different transducers. However, this does not influence the relative sensitivity of each EI towards the bedload characteristics.

There is a strong correlation of the BS data from the slanted beams (stars and triangles in Figure 4b and circles in Figure 4a, or 1 MH, 3 MHz and 2 MHz, respectively) and a weak correlation with the data from the vertical beam (crosses in Figure 3b). This is due to a higher sensitivity of the inclined beams towards volume scattering (Urick, 1983). The volume scattering increases with the rise of the active layer thickness and the bedload concentration. The surface bedload concentration (K) is also increasing with the thickness of the active layer and the decay of the BS strength (see also, Figure 3b). This decline of the values is more evident for the M9 data (Figure 4b) where the SonTek software delivered more corrected values for EI that account for ambient noise and the beam offset. The availability of these variables resulted in more significant differences between the tested conditions.

On the other hand, the StreamPro data (see Figure3a) showed a worse correlation which is a small change in dB among different experiments. The StreamPro data also emerged with higher deviations and unstable EI values among the experiments with the same hydraulic conditions. It can be explained with the unclear noise level variations and the uneven power distribution to the transducers after each change of the batteries.

Nevertheless, all frequencies proved the hypothesis that changes in the active layer thickness (see d_t in Figure 4) and bedload concertation leads to decay of the BS strength for all frequencies. This decay or attenuation of the BS strength is assigned to the increase of the volume scattering that typically scatters less than the surface scattering. The surface scattering of the immobile particles has less influence on the signal because the signal is exposed to more significant energy losses while penetrating through the increased volume layer of the mobile bedload particles. It should be also noted that gradient of declination among the BS values in different bedload transport conditions may change significantly for different bed materials.

4 CONCLUSIONS

The results in this paper confirmed the validity of the filtering procedure to correct the raw apparent velocity measured by the BT feature of the ADCPs. Apparent velocity measured with the M9 was shown to correspond closely to the spatially normalized surface velocity of the bed. The bed material influences the percentage of the filtered data; for the fine sand used in the present experiments, due to lower sensitivity of the used ADCP frequencies to fine materials, this percentage was greater than for previous experiments with coarse particles (Conevski et al. 2019) . The validity of the apparent velocity was also tested towards physical measurements of the mass transport rate and the high correlation coefficient proved the fact that after the filtering both instruments deliver velocities that correlate with the transport rates.
The assessed backscattering strength at the bed surface bore out the possibility of extracting additional information from the ADCPs about the bedload concentration and the active layer thickness. The inverse correlation (i.e., decline) for the corrected backscatter versus apparent velocity cumulated to around 10dB for 3MHz, 3dB for 1MHz and 0.5 dB for 2MHz, presumably due to decreased surface scattering as volume scattering increased with greater bedload layer thickness. The lower correlation and higher oscillations of corrected backscatter from the vertical beam at 0.5 MHz should not be discouraging since it could be used for identification of the bed sediment type, as the beams with 90 grazing angle are typically more sensitive to the rough surface scattering (Medwin & Clay, 1998).
In further research, it is crucial to correlate the apparent velocity and BS strength and observe their variations. These variations may explain the correlation between the transport rate intensity, bedload concentration, and bedload velocity to eventually approach to a surrogate, non-intrusive measurement of bedload transport rates in riverine environments.

Acknowledgments

This laboratory test was funded by the Norwegian Research Council and Statkraft as part of the multidisciplinary project SEDIPASS. The authors also acknowledge the collaboration with Daniel Waagnar and other people from Sontek Xylem, who made available the software ADPviewer permitting full control of the M9 ADCP.

REFERENCES

Conevski, S., Guerrero, M., Ruther, N., & Rennie, C. (2019). Laboratory investigation of the apparent bedload velocity measured by ADCPs. *Journal of Hydraulic Engineering*. doi:10.1061/(ASCE)HY.1943-7900.0001632

Conevski, S., Winterscheid, A., Ruther, N., Guerrero, M., & Rennie, C. (2018). Evaluation of an acoustic Doppler technique for bed-load transport measurements in sand-bed rivers. *River Flow 2018.* Lyon.

Gaeuman, D., & Jacobson, R. B. (2006). Acoustic bed velocity and bed load dynamics in a large sand bed river. *J Geophys Res Earth Surf, 111(F2)*(F02005).

Jamieson, E. C., Rennie, C. D., & Ramooz, R. (2008). Validation of aDcp bedload transport measurements. *Proc. 2008 River Flow Conf.*, (pp. 2343–2351). KUBABA Congress Dept. and Travel Services Cesme, Turkey.

Latosinski, F. G., Szupiany, R. N., Guerrero, M., Amsler, M. L., & Vionnet, C. (2017). The ADCP's bottom track capability for bedload prediction: Evidence on method reliability from sandy river applications. *Flow Measurement and Instrumentation, 54*, 124-135. doi:https://doi.org/10.1016/j.flowmeasinst.2017.01.005

Medwin, H., & Clay, C. S. (1998). Fundamentals of Acoustical Oceanography. *Academic Press, San Diego, CA.*

Mullison, J. (2017). Backscattering Estimation Using Broadband Acoustic Doppler Current Profilers-Updated. *HMEM.* Durham, USA.

Radice, A., Malavasi, S., & Ballio, F. (2006, 11 01). Solid transport measurements through image processing. *Experiments in Fluids, 41*, 721-734. doi:10.1007/s00348-006-0195-9

Ramooz, R., & Rennie, C. D. (2008). *Laboratory measurement of bedload with an ADCP.* In Bedload-surrogate monitoring technologies: United States Geological Survey Scientific Investigations Rep. 2010-5091, USGS, Reston. Retrieved from http://pubs.usgs.gov/sir/2010/5091/papers/

RDInstruments. (2011). *Acoustic Doppler Current Profiler Principles of Operation A Practical Primer.* Practical Primer, Teledyne RD Instruments, 14020 Stowe Drive Poway, California 92064. Retrieved from http://www.teledynemarine.com

RDInstruments, T. (2015, 9). *StreamPro ADCP Guide.* Teledyne RDInstruments. Retrieved from http://www.teledynemarine.com/Documents/Brand%20Support/RD%20INSTRUMENTS/Technical%20Resources/Manuals%20and%20Guides/StreamPro/StreamPro_ADCP_Guide_Sep15.pdf

Rennie, C. D., Millar, R. G., & Church, M. A. (2002). Measurement of bed load velocity using an acoustic doppler current profiler. *Journal of Hydraulic Engineering, 5*(128), 473-483.

Rennie, C., & Villard, P. V. (2004). Site specificity of bed load measurement using an acoustic Doppler current profiler. *J. Geophys. Res., 109*(F03003).

Rennie, C., Millar, R. G., & Church, M. A. (2002). Measurement of bed load velocity using an acoustic Doppler current profile. *Journal of Hydraulic Engineering, 128(5)*, 473–483.

Thorne, P. D., Vincent, C. E., Hardcastle, P. J., Rehman, S., & Pearson, N. (1991). Measuring suspended sediment concentrations using acoustic backscatter devices. *Marine Geology, 98*, 7-16. doi:https://doi.org/10.1016/0025-3227(91)90031-X

Urick, R. J. (1983). *Principles of Underwater Sound.* Peninsula Publishing. Retrieved from https://books.google.no/books?id=MBBgQgAACAAJ

Paper V

Towards evaluation of bedload transport characteristics by using Doppler and backscatter outputs from ADCPs

Slaven Conevski, Massimo Guererro, Colin D. Rennie, Nils Ruther

Journal of Hydraulic Research, under review

Journal of Hydraulic Research

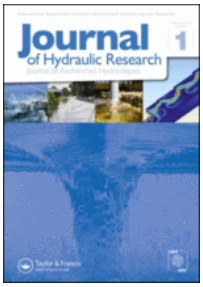

TOWARDS AN EVALUATION OF BEDLOAD TRANSPORT CHARACTERISTICS BY USING DOPPLER AND BACKSCATTER OUTPUTS FROM ADCPS

Journal:	*Journal of Hydraulic Research*
Manuscript ID	Draft
Manuscript Type:	Research paper
Date Submitted by the Author:	n/a
Complete List of Authors:	Conevski, Slaven; Norwegian University of Science and Technology, Department of Civil and Environmental Engineering ; University of Bologna, Department of Civil, Chemical, Environmental, and Materials Engineering Guerrero, Massimo; University of Bologna School of Engineering and Architecture, Department of Civil, Chemical, Environmental, and Materials Engineering – DICAM Rennie, Colin; University of Ottawa, Civil Engineering Ruther , Nils; Norwegian University of Science and Technology, Department of Civil and Environmental Engineering
Keywords:	Bedload transport, Backscattering strength, Bedload apparent velocity, Sediments, ADCP
JHR Keywords:	Laboratory studies < Instrumentation, measurements and experimental methods, Velocity measurements < Instrumentation, measurements and experimental methods, Bedload < Sediment transport, Bed roughness < Environmental Fluid Mechanics, Experimental facilities < Instrumentation, measurements and experimental methods

SCHOLARONE™
Manuscripts

Towards an evaluation of bedload transport characteristics by using Doppler and backscatter outputs from ADCPs

SLAVEN CONEVSKI, PhD candidate, *Department of Civil and Environmental Engineering, Norwegian University of Science and Technology, Trondheim, Norway*

Email: slaven.conevski@ntnu.no; slaven.conevski2@unibo.it (author for correspondence)

MASSIMO GUERRERO, Assistant Professor, *Department of Civil, Chemical, Environmental, and Materials Engineering, University of Bologna, Italy*

Email: massimo.guerrero@unibo.it

COLIN D RENNIE, Professor, *Department of Civil Engineering, University of Ottawa, Ottawa, Canada.*

Email: crennie@genie.uOttawa.ca

NILS RUTHER, Professor, *Department of Civil and Environmental Engineering, Norwegian University of Science and Technology, Trondheim, Norway*

Email: nils.ruther@ntnu.no

TOWARDS AN EVALUATION OF BEDLOAD TRANSPORT CHARACTERISTICS BY USING DOPPLER AND BACKSCATTER OUTPUTS FROM ADCPS

ABSTRACT

Two acoustic Doppler current profilers working at three frequencies (3 MHz and 1MHz by Sontek M9 run at three different configurations and 2 MHz by StreamPro RDI) were deployed simultaneously to measure bedload characteristics in a laboratory flume. Seven different transport conditions were simulated using fine gravel and medium sand as sediment bed materials. The bedload transport was monitored by two high-speed cameras and a bedload trap installed at the end of the flume. The 3 MHz delivered spatially averaged apparent velocity, as well as the 1 MHz for the sand experiments only. The apparent velocity for the 1MHz gravel corresponded to the true mean particle velocities. The 2 MHz severely underestimated the true particle velocities. The backscattering strength measured by the M9 decreased as the bedload concentration increased, independently of the particle's velocities and size; the backscattering strength registered by the StreamPro resulted in almost constant values. An extensive examination of the internal processing algorithms is necessary to clarify the best processing configuration.

Keywords: Bedload transport, Acoustic Doppler Current Profiler, Backscattering strength Bedload apparent velocity, Sediment measurements instrumentation.

1 Introduction

Sediment transport measurements are essential for understanding the river morphology, design of a hydraulic structure, environmental assessment, and flood hazard mapping. The sediment flux in streamflow can be characterized as suspended sediment load and bedload, depending on the advection of the particles occurs as a suspension in the water column or close to the bed (Parker, 2004). The lack of frequent and continuous measurements of these sediment fluxes complicates the accurate prediction of river morphology changes, as well as the development, calibration, and validation of numerical models and analytical formulas. For reliable bedload measurements, it is crucial to understand and characterize the sediment transport mechanisms. The suspended load refers to sediment particles that are transported by the turbulent eddies of the flow and thus are suspended into the water column by following the water velocity streamlines. On the contrary, the bedload transport involves larger particles with high particle Reynolds number (Re_p) that slide, roll, or saltate on the riverbed. They tend to stay close to the riverbed, and the transport mechanism involves collisions and friction of moving particles with the immobile sediment bed that significantly reduces their velocity. The bedload transport mechanism is extremely complicated and therefore, it is challenging to perform accurate and precise measurements of its characteristics and dynamics.
Traditionally the bedload transport is measured using traps and boxes (e.g., pit-traps, basket-type) or pressure-difference samplers (e.g., Helly – Smith). All these conventional techniques

are limited in spatial-temporal resolution, labour-intensive, and when physically placed on the riverbed may disturb the flow and rate of the bedload movement (Hubbell, 1964). Other typical problems of these samplers are related to the instrument design and operation, such as the nozzle height, mash basket size, correct alignment with the flow, sampling time, etc (Gaweesh & Van Rijn, 1994). To overcome the problems of the physical samplers and reduce the uncertainty in measurements, the sampling efficiencies need to be calibrated and often are dependent on the particle size distribution (PSD) of the bed material.

In the last few decades, various videography techniques have been developed to investigate the behaviour of the bedload particles in well-controlled laboratory conditions. Some of those involve particle tracking velocimetry techniques where the moving particles can be easily identified and their movement can be analysed by deploying different particle image recognition algorithms (Drake, et al., 1988; Nifio & Garcia, 1994; Hu & Hiu, 1996; Papanicolaou, et al., 1999; Lajeunesse, et al., 2010). The image processing techniques such as optical flow and image differencing have been successfully applied to calculate the mobile bed velocity and the surface concentration of mobile particles (Keshavarzy & Ball J.E., 1999; Radice, et al., 2006; Blanckaert K., et al., 2017; Conevski, et al., 2019). Nevertheless, these techniques are particularly difficult to deploy in the field, and their usage is limited to laboratory experiments.

On the other hand, the acoustic instruments have shown the potential to be the most attractive surrogate non-invasive technique for measuring the bedload in the field, even during high flow conditions when intense transport occurs. The geophones or hydrophones are known as passive acoustic methods. These techniques involve recording and analysing the acoustic reverberation generated by collisions of the bedload particles (Rickenmann, et al., 2012; Geay, et al., 2017). The required calibration is demanding and is usually performed by trapping bedload sediment during a significant hydrological event to attribute recognized signals to collected sediments. Passive methods are practically limited to small streams where the geophones can be installed on the riverbed during dry periods and the sediment trapping designed at existing or specifically made check dam. The active acoustic systems emit a signal by operating close to the water surface and process the echoes reflected from the riverbed. These acoustic systems can be monostatic, which have a transducer that emits and receives the signal, or bistatic where the transmitter and the receivers are reasonably separated. The bistatic sonars are limited to laboratory use of small streams because the distance between the transducer and receiver should be comparable with the water depth. Several studies have demonstrated the capability of these devices (i.e., acoustic Doppler velocity profilers) to measure near-bed load sediment transport processes, the thickness of the active bedload layer and the flow velocities in the near-bed region (Hurther & Thorne, 2011; Blanckaert K., et al., 2017).

The acoustic Doppler current profilers (ADCP) are monostatic sonars that use four transducers to measure spatial averages of three principal water velocity components in individual beams (RDInstruments, 2011). Although these systems were initially developed for discharge and water velocity measurements (Brumley, et al., 1991), lately they are increasingly used for suspended load estimation, using correlation with the acoustic backscattering strength (B_S) and attenuation (Sassi, et al., 2011; Moore, et al., 2013; Guerrero, et al., 2015; Guerrero, et al., 2017; Szupiany, et al., 2019). The bedload measurements involve the bottom tracking (BT) feature of the ADCP to estimate the apparent bedload velocity (Rennie, et al., 2002). The BT feature is a separate signal emitted along each beam initially designed to estimate the speed of the boat (v_{BT}). The BT velocity is limited to immobile bed conditions and if the bed is mobile, the apparent bedload velocity (v_a) can be determined by subtracting the actual velocity of the boat (i.e., using DGPS). If the measurements are conducted in a fixed stationary position, then it can be assumed that $v_{BT}= v_a$. Rennie (2002; 2004; 2017) reported a good correlation between the apparent bedload velocity and the physically measured transport rate, focusing on calibration towards the samples for different PSD. The primary assumption in these studies is that the apparent velocity is the spatial average of the mobile and immobile bed covered by the acoustic footprint. Besides, an analytical approach towards understanding the relationship between the true particle velocity and the apparent velocity was suggested by Gaeuman (2006). In the same study, it was demonstrated that the BT signal does not scatter equally the mobile bedload particles and the immobile bedload beneath, and it was associated with different acoustic backscattering properties (Gaeuman & Jacobson, 2006). Other studies found out that utilization of shorter pulses yielded a better correlation with transport rate and that lower frequency ADCPs result in apparent velocities of lower magnitudes (Ramooz & Rennie, 2008; Latosinski, et al., 2017). Better correspondence with the true bedload velocity was achieved by filtering the outliers of the apparent bedload velocity signal measured in laboratory conditions (Conevski et al., 2019). The percentage of the filtered data were negatively correlated with transport intensity and the bedload velocity. Moreover, in the same laboratory investigations, it was demonstrated that only the highest frequency ADCPs (e.g., 3MHz) comply with the spatial averaging assumption, whereas the lowest frequency underestimated the true bedload velocity obtained from imagery data (Conevski, et al., 2019). The underestimation of the bedload velocity by some of the ADCPs cannot be associated only to wavelength of the signal and its ability to penetrate deeper in the bedload active layer, but also to the acoustic sampling, the acoustic geometry and the internal signal modulation specific for each ADCP and configuration (Conevski, et al., under review).

Oceanographers have widely used the seabed mapping and analysis using various acoustic systems for many years (Medwin, 2005). Similarly, the riverbed materials scatter differently

depending on the particle's sizes, the intensity of the bedload and the disturbances of the bed surface. Shields (2010) showed that the corrected acoustic backscattering (BS) strength obtained from the BT signal of ADCPs correlates well to different PSD of the riverbed. In addition, the characteristics of the acoustic BS strength measured by a multi-beam sonar were successfully utilized to classify the riverbed sediments (Amiri-Simkooei, et al., 2009).
The main objective of the present paper is an interpretation of the BT signal for different bedload transport conditions. Two ADCPs (Sontek M9 and RDI StreamPro) measured simultaneously at four different frequencies (3 MHz, 1 MHz, 0.5MHz for the M9 and 2MHz for StreamPro) and using different signal processing configurations (incoherent, coherent and broadband). This study analyses the acoustic BS strength and the BT velocity for a set of frequencies and processing configurations tested over different transport conditions and two different PSD (medium sand and fine gravel). The overall aim of our work is to exploit the information embedded in the received BS. This will, in turn, improve the reliability of BT velocity to be used as bedload predictor in the field. The presented work builds upon previous studies, which mostly have relied on the spatial averaging assumption. The specific objective of the laboratory tests, herein presented, is to demonstrate that this hypothesis does not hold for all the configurations. Certainly, the received BS strength reflects different particle sizes and transport intensities, which result in different weights for the averaging of mobile and immobile particles. This is a shortcoming of the previously proposed methods, based on the equal acoustic return from mobile and immobile particles. To this objective, matching techniques were used to monitor the bedload transport. High-speed cameras with a planar view were used to calculate the surface bedload concentration of the mobile particles and the surface bed velocity; together with a side-looking camera for estimation of the active layer thickness; and a bedload trap was installed to measure the transport rate at the end of the flume. Different bedload transport conditions were performed with material characterized by different scattering properties (Medwin & Clay, 1998; Moate & Thorne, 2009).

2 Methodology

2.1 Experimental set-up and procedure

These experiments were conducted in a glass-sided tilting flume channel with a rectangular cross-section and closed hydraulic circuit at the Hydraulic Laboratory of the Norwegian University of Science and Technology (NTNU), Trondheim. The flume is long 12.5 m in total, and the mobile bed section was 10 m long and 0.6 m wide. The bottom was levelled up for 20 cm in order to place the bedload trap at the end of the flume. After the flow distributor,

large stones and coarse gravel were placed to ensure quasi-uniform entrance flow (see, Fig 1). The nominal sediment depths ranged between 10-12 cm with 12 cm at the entrance and 10 cm before the bedload trap. No sediment was fed to the flume or recirculated during the tests. Two types of well-sorted sediments were used: medium sand ($D50$ = 0.39 mm) and fine gravel ($D50$ = 7.55 mm). The sediment PSD characteristics and the critical shear velocity (u^*_{cr}) and the particle Reynolds number (Re_p) calculated for to the $D50$ are given in Table 1, where u^*_{cr} was calculated following the Shields criterion (Parker, 2004).

Three test series with different bedload transport conditions were run for each material separately, attempting to have minimum suspension in the water column. Each series consisted of five repetitions. The sand experiments were run at a slope of 0.1 %, maintaining a constant water level of 42 cm above the sand bed. Due to limitations of the pump capacity and the flume geometry, the gravel tests were conducted at a steeper slope, 0.8% with a water level that varied between 44-46 cm above the gravel bed.

The sand experiments (sandEXP1, sandEXP2, sandEXP3 in Table 1) were conducted with relatively calm hydraulic conditions with mean water velocities ranging within the interval 0.3-0.57 m s^{-1} and Froude numbers between 0.15-0.28. Much larger velocities were required to entrain the gravel particles; thus, the gravel experiments (gravelEXP1, gravelEXP2, gravelEXP31 in Table 1) ranged between 1.2-1.43 m s^{-1}, but still in subcritical flow: Fr = 0.58-0.67. Note that the discharge was kept steady during each repetition, and all three series of experiments: sand, gravel, sand over immobile gravel (i.e., sandOver in Table 1), were conducted with the hydraulic conditions given in Table 1.

The first series of tests (sandEXP1 and gravelEXP1) resulted in an isolated motion of particles, mostly rolling over the immobile particles. During the second and the third test of sand bed (sandEXP2 and sandEXP3) ripples and later dunes were fully developed. The second and the third gravel test (gravelEXP2 and gravelEXP3) showed more intensive transport, and the gravel particles were saltating higher than $D50$, but no sheet flow was formed. In the end, to examine the scattering of the immobile gravel surface influence on the ADCP bedload measurement, three repetitions were conducted with the sand material randomly distributed over the immobile gravel bed (i.e., sandOver) with hydraulic conditions similar to sandEXP2 and sandEXP3. These resulted in patches of sand moving on the top of the gravel particles, but no formation of bedforms was noticed.

The two ADCPs and the camera with a planar view over the sediment bed were placed 1.5 m before the bedload trap, as shown in Fig. 1. The distance between the ADCPs was 70 cm, and the high-speed camera was partially covering the acoustic footprint of one beam of each ADCP. Four lights were installed outside the glass walls focusing at the field of view of the planar camera. They were mounted below the water surface; thus, no shadows of the free surface affected the measurement area. Another camera was mounted outside of the glass

wall, which continuously recorded the changes in the active layer thickness. To measure the water velocity, two acoustic Doppler velocimeters (ADV – Vectrino) were installed upstream of the ADCPs. One measured as close as possible to the sediment bed (5-10 cm), and the other was mounted right below the water surface (V1 and V2, Fig. 1). Four acoustic surface sensors (S1 - S4, see Fig. 1) were placed over the measurement section of the flume to register the change of the water surface. The bedload trap was placed at the end of the flume, which continuously weighed the collected sediment at 50 Hz during each repetition. The trapped sediment was mostly supplied from the entrance reach, where the erosion was visually most intensive at the beginning of each test.

Each repetition lasted 25-30 minutes, enabling to run three processing configurations of the M9 Sontek ADCP that will be explained further in this paper. No perfect synchronization of the measurements was planned, considering that the transport conditions did not change significantly during one repetition.

2.2 ADCP working principle and acoustic properties

Both ADCPs (M9 and StreamPro) are active sonar systems with four monostatic transducers arranged at 90° azimuth intervals. The transducers form acoustic beams at 20° for StreamPro (SPro) and 25° for M9 (see θ, Table 2). The tilted beams permit estimation of the velocity along with three directions under the assumption that the velocity is homogeneous in all four acoustic footprints (RDInstruments, 2011). The M9 has two pairs of four transducers working at 3 MHz and 1MHz, respectively, and another vertical beam in the centre working at 0.5 MHz frequency (Sontek, 2017). The SPro has only four transducers working at 2MHz, but with double smaller diameters (D_t) than the M9. The BT feature of the ADCPs works at the same carrying frequency as the water mode of any ADCP, and it is characterized with longer pulses emitted along these beams. These high energy pulses typically travel the entire water column and might finally penetrate the mobile bedload. However, the longer the pulses, most likely, larger is the resolution that may be thicker than the active layer. The BT pulse is reflected at the bed superposing two different types of scattering:

- Volume scattering (S_v) by mobile bed material and responsible for determination of the bedload velocity
- Surface scattering (S_s) from the surface formed by the immobile particles beneath the active layer that is usually far stronger (Gaeuman & Jacobson, 2006; Conevski, et al., 2018).

Figure 2 shows a typical beam pattern from an ADCP emitted from a transducer with diameter D_t forming a beam declined from the vertical by angle θ. The half beam width φ

(i.e., opening angle) defines the central lobe of the acoustic beam, where the sound intensity is highest in the centre and decreases towards the sides. This opening angle depends on the type of the transducer and the working frequency f (Urick, 1983). At larger angles, the intensity of the returned signal diminishes, and at 6-14% of R from the sediment bed the first side-lobe appears. This intensity could mask the central lobe signal and induce an error in further processing. The distance z_c is related to the central lobe geometry and it is denoted as the beam focusing distance (Conevski et al., under review).

Similarly, z_s determines the so-called blank zone for water velocity profiling or the side lobe contaminated area. These parameters values are given in Table 2 for the ADCPs used in this study. The bedload is typically transported as a moving layer with a thickness of a few *D50*; thus, most of these measurements are conducted in the contaminated area.

Moreover, the acoustic sampling of the bed is not equally distributed at the outer and inner boundaries of the central-lobe, because portions of the emitted pulse reach the bottom first at the inner boundary. It may lead to uneven scattering at different portions of the BT pulse, especially when the bedload motion is highly sporadic.

Summarizing, the sampled volume depends on the pulse length (*Pl*), ADCP distance to the bed, transducer diameter (D_t) and the opening angle (φ), all of these are integrated in the focusing distance z_c. The calculation of sampling volume is explained in Rennie (2002), and more details about the scattering pattern are provided in Conevski (under review). Nevertheless, the exact penetration and extension of the acoustic sampling are unknown, which introduces uncertainty in the estimation of the Doppler velocity registered at the riverbed.

The signal processing configurations

The default signal-processing configuration for the most advanced ADCPs, both RDI and Sontek, usually refer to Broadband (BB) technology. The standard configuration (RS) by Sontek involves a feature denoted as SmartHD Pulse that changes the processing according to the hydraulic conditions based on some internal parameters. Besides the BB technology, the M9 can automatically switch to an incoherent (IC) Doppler sonar and pulse-to-pulse coherent (PC) Doppler sonar. A collaboration with Xylem Sontek enabled the M9 to work with all nine beams at the same time and to run all three signal processing configurations separately (IC, PC, RS). The data from all these configurations was collected for each repetition using the Sontek non-commercial software ADPviewer.

Apparent velocity post-processing

The raw apparent velocities obtained from each ADCP and configuration was filtered by

eliminating all the velocities opposite of the streamflow and all the extreme values (Conevski et al.,2019). The final values were averaged, and the magnitudes of the apparent velocities were calculated (v_a) using all four beams under the assumption of homogeneity. Some configurations during the gravel series of experiments showed 30-40 % empty or bad samples (*N/A*) before filtering the data, most likely due to more turbulent conditions and relatively high-water velocities that restricted the system from acquiring continuous measurements. The filtered data (*FD*), the *N/A* and the zero velocities resulted in the total number of not good data (*ND* = *N/A* + *FD* + ZEROs).

Acoustic backscatter correction and post-processing

The ADPviewer, a software developed by SonTek, beside the configuration change, allowed examining more variables form the ADCP that are not typically available from commercial software, such as the BT echo intensity (*EI*), noise level (E_r), pulse length, acoustic pressure at the transducer and supplied electrical current which determine the power of the emitted signal. This enabled the backscattering strength assessment. Most of these variables are freely available for the SPro in the PD0 binary file and explained in the technical documentation given by RDI (RDInstruments, 2015).

The backscattering strength was derived from the sonar equation (Urick, 1983) and followed the guidelines provided by Deines, (1999), later adapted for the BT signal by Conevski et al. (2019). The corrected backscattering strength (from surface and volume scattering) is given in the logarithmic form:

$$B_S = 10log(S_s + S_v) = -SL + k_{dB}(EI - Er) - A_f + 2\alpha R + 20log(R) - P_{dB}, \quad (1)$$

where SL=10log(P/P$_0$) is the source level calculated using the transmit voltage and currents present in the RDI output files or the pressure at the transducer, P, in the Sontek output file, as suggested by Shields (2010) and RDI (RDInstruments, 2015). *EI* is the echo strength converted from "counts" to dB using a factor k_{dB}, which is typically ~0.45 for the SPro , and ~0.1 for M9 (personal communication with Sontek). The noise level, E_r, may vary for each ping and it was available only in the M9 output; for the SPro it was tentatively assumed as constant ~40dB (RDInstruments, 2015). The transmission losses in two directions include beam spreading (20log$R$) and the attenuation in the water column ($2\alpha R$) that accounts for the absorption due to water viscosity while suspended sediment attenuation in the water column was negligible because of absent or very low concentration of suspended particles. R is the slant distance to the sediment bed. P_{dB} is the transmit voltage, that depends on the power supply (12 V for SPro and M9), and it was adapted from the tables given in Mullison (2017). The battery voltage changed over the deployment and it was approximately corrected using the formula 20log(V_b /12), where V_b is the voltage of the battery given at each ping for both

ADCPs. Finally, the A_f is the area of the surface scattering at flume bed, which is usually applied to normalize the surface backscatter for the unit area. This area corresponds to the acoustic sampling area as defined by Rennie (2002) for an ADCP beam footprint on a perfectly flat floor and then corrected for the local slopes of the surface. Simplified estimation of the A_f can be given as follows (Amiri-Simkooei, et al., 2009):

$$A_f = 20\log\frac{RNG \cdot Pl \cdot \varphi}{\cos(\theta - \alpha_x) \cdot \cos(\alpha_y)}, \quad (2)$$

where RNG is the perpendicular distance from the transducers to the riverbed and α_x, α_y are the angles of the local slopes of the bed in x and y-direction of the instrument coordinate system, repetitively calculated using the registered distances from each transducer to the bed (RNG) and the beam geometry information (Fig. 2). Note that the positive x-direction for M9 and SPro are defined as beam1-beam3, and beam1-beam2, respectively.

The corrected BS strength (B_S) was assessed by considering all the presented parameters although most of them (e.g., A_f, α, R) were constant under controlled conditions and with negligible suspended sediment in the water column. The attenuation within the active bedload layer was implicitly included in the total BS; in other words, B_S in Equation 1 represents the result of surface and volume scattering and attenuation processes at flume bed as detected from ADCP transducers.

De-spiking and low-pass filters were applied to the raw *EI* data from ADCPs that eliminated possible outliers. The corrected B_S values for each repetition were averaged over the testing time and among the transducers characterized with the same frequency and configuration. Nevertheless, detailed specifications for some parameters such as the power distributed to each transducer, their efficiency and offset were not supplied by the manufacturers. Therefore, the values calculated in this study in some manner are relative to the actual BS strength related to the material and the acoustic frequency. Considering that the transducer properties do not change during the experiments, the values presented in this study are an average of all four transducers per instrument and configuration.

2.3 Videography and image data processing

Planar view camera

High-speed camera AOS1000 with HD (1984x1264 pixels) and 139 frames per second, fps,

was used to register the surface velocities of the mobile particles at flume bed. The camera (C1, Fig. 1) was submerged in a water-resistant plastic box. At least three 2-4 minutes, videos were recorded during each repetition. The camera field of view, FOV, covered part of one beam sampling area for each ADCP.

The image data processing followed the same procedure as explained in Conevski et al. (2019), and it involves image enhancement, image de-blurring and applying the background subtraction method (i.e., two–frame change detection). The detected changes are considered as single particles (e. g., gravel) or fluxes of particles movements. These techniques typically suffer from false foreground or background detected pixels in addition to the noise (Radke, et al., 2005). Therefore, median and Gaussian filters are applied to eliminate these errors. In this study, a filter using the local standard deviation of the pixels was applied to the detected changes (Kaushik & Ashraful, 2014). This filter successfully eliminated false foreground pixels and false pixels due to water impurities.

Further, the conventional particle image velocimetry steps were applied: i.) subdivision into the region of interest (ROI), ii.) particles displacement assessment by applying the cross-correlation algorithms. The ROI size and the frame frequency for particles velocity calculation were also taken into consideration following the suggestions given in Radice et al. (2006).

The gravel tests involved the identification of the mobile particles by applying local threshold image binarization (Radice et al., 2006). It permitted calculation of the number and diameter of the particles. To fill the false background pixels, two morphological image operations (imclose and imopen, *Image Toolbox Matlab*) were applied to the detected image changes. Then the elements with connected pixels or the blobs were labelled, and the primary axis lengths were estimated. The conversion of pixels to meters was done by taking several pictures of checkerboards placed on the sediment bed before and after each repetition. The final post-processing of the image velocity data included de-spiking, using the velocity measured by the ADV (V1, Fig 1) as threshold value at each repetition separately. Similarly, D_{max} and D_{min} from PSD were used to eliminate false detection of gravel particles.

Beside the image velocity data (v_c), the mean surface bedload concentration (K_m) were also determined using the planar videography (Conevski et al. 2019). No specific ROI was chosen to calculate K_m, but it was simply determined as an average value of all the available ROI in the FOV. It is well known that the motion of the gravel particles is rather heterogeneous and sporadic, which resulted in no bedload in some parts of the flume and very intense bedload in some others. This heterogeneity affected the K_m. Therefore, the resulting ROIs with zero and close to zero values were discarded, which defined the active bedload surface concentration, K_{acl}, for gravel experiments. The K_{acl} values were verified by calculating the total surface of

the identified particles assuming a circular shape. For the sand experiments, all ROI showed similar values of the bedload surface concentration, resulting in $K_{act} = K_m$. Note that for the ADCP data, the zero velocities were automatically discarded (e.g., *N/A* values) or produced negative values.

Side-look camera

GoPro Black 6 was placed outside of the glass wall to monitor the movement of the bedload during all experiments. The GoPro acquired images at 60 fps, 2.7k resolution with a linear view in order to eliminate the fisheye effect and the distortion of the objects. The Camera perspective was adjusted exactly above the sediment bed before starting each repletion and calibration pictures were taken. Due to the limited vertical length in the field of view which is useful for particles jump detection, this imagery data was utilized only for approximate calculations of the thickness of the active layer given as $d_t = N * D50$.

Again, the core of the image processing involved image light enhancement and two-frame change detection. Different approaches were deployed for sand and gravel videos.

For the sand experiments, only the sequences with a dune passing next to the side glass were considered (Fig. 3). For sandEXP1, any sequence could have been considered, but only a few were analysed. The first step of the procedure is determining the dune crest boundary by using image segmentation tools (i.e., edge detection based on thresholding). Binary morphologic tools (e.g., bwmorph in Matlab) were further used to shape the boundary line correctly and were recalculated every two seconds. It was assumed that the crest line, (given in Fig. 3) represents the immobile surface of the particles at that instant. The image change detection was applied, similarly, as explained in the previous section, with adapted parameters for filtering of the noise and false foreground of the detected changes. The blobs of mobile particles were identified, and their shapes were morphologically corrected, as explained in the previous section. Finally, the image coordinates of the boundary and the particles in motions were determined, and the shortest distances from each particle centroid to the dune crest were calculated. The relatively high resolution resulted in more than 10 pixels per 1 mm, which eventually enabled reasonable identification of the moving particles.

The gravel experiment could neither rely on any calibration nor detection of the immobile boundary because this changed from frame to frame. Thus, the saltation of the particles was estimated interactively by running and stopping the image change detection algorithm. The saltation height of the particles was determined by estimating the perpendicular distance from the centre of the hopping particle to the instantaneously identified immobile bed below (see, Fig. 4). The primary assumption was that the particles were jumping in one vertical plane. This is only consistent for a qualitative measure for the mean active layer thickness. More

than 500 particles were detected, and their hops were calculated for all three series of gravel experiments. The saltation height was also given in *N* x *D50*.
The analysed sequences for both sand and gravel experiments were randomly chosen.

2.4 Other measuring techniques

Bedload trap and sediment transport rate

A bedload trap collected the bedload transported over the measurement section (see, Fig.1). The bedload trap was an aluminium box with dimensions 1 m x 1 m x 0.15 m. The load cells installed underneath the box continuously weighed the collected sediments at a frequency of 50 Hz. In total, six load cells were used, and the cumulative transport rate was calculated as a sum of all six cells. The zero values were re-calibrated at the beginning of each test, which permitted to eliminate zero shifts due to not perfect tare repetition among tests (e.g., the influence of dynamic water pressure) and assuming unchanged zero during the test. To confirm this, the load cells output was tested for all hydraulic conditions without sediment motion. Plastic guides extended from the loose bed to the box facilitated the free fall of sediment the transported material was not perfectly captured during the most intensive send transport condition (i.e., sandEXP3), lost sediments were collected at the end of the flume and were added in the final calculations.

ADV and water velocity calculation

The deployed ADVs (V1 and V2, Fig. 1), were used to measure the mean water velocities at the surface and below the measurement section of the ADCPs as close as possible to the flume bottom. The ADV data was de-spiked and averaged over time. Note that the velocities obtained from the V2 gave more deviations, especially in the sand tests where bedforms were developed at flume bottom. The mean ADV velocities and the mean SPro velocities were used to calculate the depth-averaged water velocities assuming that the flow conditions were almost equal in the entire measurement section. The SPro was used in the water velocity calculations because it functioned without any breaks and delivered a 2-cm resolution of the water velocity profile, whereas the M9 switched among the processing methods and is characterized with a lower resolution. The data from SPro typically ranged between 13 cm below the surface and 10 cm above the sediment bed, whereas the ADVs provided the points above and below this region.

Surface sensors and the water levels

Four acoustic sensors were used to observe the water surface variations and to accurately

estimate the water depth (H) in the measurement section. The sensors registered the surface changes during the entire measurement procedure, showing the distance from the sensor to the water surface. The water depths (H) were calculated by considering the sediment bed changes registered as depths by the ADCPs and the different offset distances of the sensors.

2.5 Shear velocity calculation

Detailed velocity profiles close to flume bed were not available to effectively implement the log-law and to calculate the shear velocity. However, the calculation of the shear stress was performed for each repetition by applying the semi-empirical equation based on the log-law (Van Rijn, 1984):

$$u^* = \frac{U}{5.75\log_{10}(\frac{12H}{3D90})}, \quad (3)$$

where U is the depth-averaged water velocity calculated as given in the previous sections, H is the water level calculated using the surface sensors and the ADCP data, and $3D90$ is from PSD of used sediment which represents the hydraulic roughness.

3 Results

3.1 Bedload Transport rate correlation to ADCP outputs

The assessment of the ADCP bedload measurements was performed by analysing the correlation between the physically measured bedload transport rate (sediment trap at the end of the flume), the post-processed apparent bedload velocity and backscattering strength (Bs) measured by each instrument and configuration.

The bedload transport rate (Q_s) is positively correlated to the apparent bedload velocities (v_a) measured by each configuration. As expected, v_a and Q_s of both gravel and sand gave correlation coefficients, r, higher than 0.8. The sand data resulted in slightly higher coefficients with the highest value equal to 0.93 for 3MHz PC (faint grey, symbols, Fig. 5b) and lowest equal to 0.84 for 1MHz IC (Fig 5d). The gravel tests generally resulted in slightly higher magnitudes of the velocities and much more intensive transport rates, resulting in a steeper trend of increase than the sand data. The highest correlation (r = 0.9) was again obtained for the 3MHz PC (black symbols, Fig. 5b) and the lowest for 1 MHz PC (r = 0.81). The SPro (Fig. 5f) gave the lowest apparent velocities; however, the correlation coefficients were higher than 0.8 for both gravel and sand.

Interestingly, the sandOver experiments delivered negligible transport rate (e.g., similar to the lowest v_a of the sandEXP1 experiments, Fig. 5), but the magnitudes of the velocities were

much higher. The sand transported over armoured bed (e.g., in this experiment the gravel was immobile) moved with similar velocities as the sand moving in bedforms and a significantly lower transport rate. These velocities are not correlated with the negligibly small amount of the captured bedload material and may introduce additional uncertainty in further analysis of the bedload transport rate (Conevski, under review).

When passing from 3 MHz to 1 MHz, the apparent velocity magnitudes increased significantly, especially in the case of gravel experiments (Fig. 5a vs. 5d for IC and Fig. 5b vs. Fig. 5e for PC). This offset appears to be related to some internal processing parameters and different profiling of the acoustic beams used for identification of the riverbed. A more detailed elaboration is given in the discussion.

Fig. 6 presents a correlation between the BS strength and the measured transport rate, which incorporates both the velocity and the bedload concentration (e.g., kinematic model). Differently, from the apparent velocity, the BS strength is negatively correlated to bedload transport rate from sediment trap (see, Fig. 6). The resulting correlation coefficients are above 0.9 for all configurations and instruments. This bears out the corrected BS strength (B_s) is sensitive to the change of the intensity of the bedload transport. An exception is the B_s observed by the SPro, where almost no change is registered when the transport conditions change, i.e., vertically aligned dots in Fig. 6f. Although the BS strength of 1MHz is 20dB smaller than 3MHz outcome, both frequencies gave similar trends for all the configurations shown in Fig. 6. The difference can be observed between the sand data (grey symbols) and gravel data (black symbols). Moreover, the B_s rate of change for unit transport rate (i.e., $\Delta B_S / \Delta Q_s$) increased from 0.03 to 0.9 dB/(kg.s^{-1}) for 3MHz, when passing from gravel to sand tests (see also Table 3). This demonstrated that the BS signal is much more attenuated at the sand bed, even though the bedload transport and apparent velocities were much higher for the gravel experiments. As already mentioned, B_S embeds volume scattering and attenuation through the layer of moving particles at flume bed. These are affected by the number of mobile particles (i.e., near-bed sediment concentration) and their scattering properties (Thorne & Meral, 2008). For example, a thin active layer contains far more particles of sand than of gravel; the higher number of particles contributed to higher attenuation whereas both medium sand and fine gravel, used, where close to geometrical scattering regime for 3MHz. Furthermore, observed sand bedforms resulted in a deformed bed that may have induced additional loss due to the multi-directional surface scattering (Medwin & Clay, 1998).

3.2 Comparison of the apparent velocity and the velocity form the imagery data

The particle's velocities (v_c) given in Fig. 7, were estimated from the planar imagery data. Given the low concentration of the suspended material during all the experiments, the applied

post-processing delivered a reliable estimation of the mean velocity of the bedload particles (Radice et al., 2006; Conevski et al., 2019).

A direct comparison of the velocities obtained from the imagery data and the apparent bedload velocities from ADCPs are presented in Fig. 7. Furthermore, the average velocity of the particles, v_c, was spatially normalized by multiplying it with the bedload surface concentration coefficient, which accounts for the immobile particles. Aforementioned complies with the spatial averaging assumption for the apparent velocity from ADCP (Conevski et al., 2019), and would made the camera output consistent with the ADCP measurements (Fig. 8).

The apparent velocities measured by the 3MHz underestimated the mean particle velocities (Fig. 7a-c). However, after applying the normalization coefficient, K_{act}, the ADCP velocities reached values closer to the camera velocities (Fig. 8a-c). Thus, the 3MHz underestimated the apparent velocities only due to spatial averaging of mobile and immobile particles (Conevski et al., 2019). The apparent velocities measured by the 3MHz PC and RS in the sand experiments matched excellently the spatially normalized camera velocity.

Passing to the 3MHz IC (Fig. 8a), the performed normalization resulted in slightly lower values of the normalized camera velocities, $K_{act} * v_c$, than the apparent velocities measured by the ADCPs. This suggests that the ADCP signal was more sensitive to mobile particles than to the immobile ones. Similarly, v_a values for the gravel experiments were slightly higher than the normalized camera velocities for all frequencies and configurations (Fig. 8a-b-c), showing that the ADCP measurements weighted more the mobile particles.

In Fig. 7c, the apparent velocities measured by 1MHz IC corresponded well with the camera velocities. However, this finding would contradict previous experiences which proved that the apparent velocity from an ADCP is a spatial average of the velocities of the mobile and immobile particles within the acoustic footprint. On the contrary, the spatial averaging by the ADCP, is supported for sand tests in Fig. 7e-b, where the 1MHz PC and 3MHz PC resulted in apparent velocities corresponding the $K_{act} * v_c$ values (Fig. 8e-b). The observed overestimations of the spatially averaged velocity (i.e., $v_a \cong v_c$ in Fig. 7-e corresponding to $v_a > K_{act} * v_c$ in Fig. 8d-e) are assigned to the gravel tests (black symbols) and limited to 1MHz-IC in the sand tests. In those cases, the ADCPs performed a shallower measurement, which enhanced the return from the top layer of the bedload. Besides, the geometric scattering regime of the gravel particles ($D50 > \lambda$) contributed to a stronger gain of the mobile particles in these tests. More importantly, the active layer thickness (d_t , Table 3) in the gravel experiments was thick enough to reach the central lobe region that exceeds z_c in Fig 2 and enables more effective volume scattering (i.e., acoustic sampling within the layer thickness).

The apparent velocity measured by the SPro highly underestimated the particles velocity v_c (Fig. 7f). Besides the normalization of the camera velocity, the underestimation is present again in Fig. 8f. This confirmed that SPro is strongly affected by surface scattering of the fixed flume bed beneath the active layer of mobile particles (Conevski et al. 2019). The underestimation ranged between 2-5 times v_a for the sand experiments, and it reached up to 20 times in case of gravel tests.

ADCP erroneous data

The sediment transport heterogeneity and extreme hydraulic conditions (i.e., high U and $u*$ in Table 1) significantly lowered the performance of the ADCPs, automatically yielding less valid data for the gravel tests. A stable mean was achieved in almost all gravel experiment measured by the M9 (e.g., IC, PC, and RS). However, a fewer number of cumulated good ensembles resulted in higher deviation among repetitions (Fig. 7 and Fig. 8).

As expected, the standard deviation (STD) of the apparent bedload velocity increased with the transport rate (see, Table 4). Mainly, IC gave higher STD than PC and RS (i.e., compare $STDv_a$ in Table 4), which also entailed a higher deviation among experiment repetitions. The filtering procedure decreased the coefficient of variation by 20%, for the weak transport experiments (e.g., gravelEXP1, sandEXP1) and by 10% the experiments with more abundant transport.

The total non-valid data (*ND=FD+N/A,* that is filtered plus not available) was highest for the weak transport experiments and decreased as the transport increases. This negative correlation was present for sand experiments only, except for 1MHz IC, which showed an opposite trend (see Table 4 and Fig. 6d). The not valid data (N/A) was significantly high for the gravel experiments, mostly due to the high turbulence, higher Froud number, higher noise from the pumps and the observed sporadic transport. The trend of *ND* was dominated by the positive trend of not available data (*N/A*) rejected by the ADCPs and it appeared to be similar for all M9 measurement, except the RS. This corresponds to an internal processing failure in identifying the return signal. For the IC and PC processing, a narrowing of the correlation peak is equivalent to a spectral broadening of the Doppler peak, less correlated echoes and erroneous Doppler velocity calculation (Brumley, et al., 1991; Medwin & Clay, 1998). On the contrary, the *ND* for SPro gravel data decreased as the bedload velocity increased, because of fewer *N/A* values.

3.3 The backscattering strength

A negative correlation was observed between the apparent velocity, v_a, and B_s among tests with different hydraulic conditions (Fig. 9). For example, the rate of change $\Delta B_S/\Delta v_a$ was equal to -250 in case of 3MHz PC and sand experiments, whereas this rate changed to -50 for gravel (e.g., 3MHz PC, Fig. 9b). The higher absolute value of $\Delta B_S/\Delta v_a$ for sand tests represents a noticeable effect of the active layer on sound propagation at flume bed.

On the contrary, SPro registered an almost constant backscatter for the three hydraulic conditions (Fig. 9f). It corresponds to an acoustic return that is poorly affected by the active layer, and mostly reflected by the immobile sediment. Besides, SPro is characterized by long pulses, small transducers, large beam opening angle, and small grazing angle (Table 2). These geometrical features and the stronger emitting power contributed to a stronger effect of the surface scattering by the immobile bed. This corroborates with the previous findings (Conevski et al. 2019) and further elucidates the reason for the underestimation of the SPro apparent velocity (Fig. 7f and Fig. 8f). The geometrical parameters result in the less focused beam (i.e., the highest value of z_c), whereas B_S was equal to -50 dB, which was significantly more than -120÷-180 for the M9.

$\Delta B_S/\Delta v_a$ absolute value was more significant for IC (Fig. 9a and Fig. 9d) rather than for PC (Fig. 9b and Fig. 9e). In the same context, the higher deviations were observed in the corresponding apparent velocities (Fig. 7a-d and 7b-e for IC and PC respectively). This shows that IC performed a shallower sampling within the active layer than PC, not producing surface scattering, therefore giving lower BS strength values, larger variation of the latter with changing hydraulic condition and the moving sediment layer thickness (i.e., larger absolute value of $\Delta B_S/\Delta v_a$), and higher deviation in apparent bedload velocity measurements.
The frequency also influenced the acoustic signal to active layer thickness response. Given the same source level for the M9 and for a given instrument configuration, the higher frequency (3MHz, Fig. 9a-b) resulted with an almost double rate of change, $\Delta B_S/\Delta v_a$, in absolute value, than the lower (1MHz, Fig. 9c-d) and with higher *Bs* values in general. The 1MHz is less affected by the active sediment layer, that resulted in a smaller variation of the BS strength among different tests. It's worth nothing that a lower effect of the active layer may result in over and under-estimations of the apparent velocity which, for example, were precisely the case for 1MHz-sand and the SPro, respectively. Furthermore, a low $\Delta B_S/\Delta v_a$ in absolute value may be a consequence of using shallower or deeper acoustic returns in internal processing. In the case of 1MHz sand, the acoustic pulse was most likely reflected from the top of the active layer. On the other hand, the observed echo by the SPro was reflected from beyond the active layer, delivering an apparent velocity that is less affected by the mobile

particles. The difference between these two cases was clearly observed in the BS strength mean value which was low in case of shallower return because of limited backscatter from the bottom (see, Table 3), whereas it reached a maximum value of -55 dB for the deep penetrating signal of SPro. The attenuation among the active layer appears negligible for both these cases.

The RS configuration in Fig. 9c follows the same trend as the PC configuration, but the data is more scattered. However, the *Bs* on average is slightly higher than PC and IC, especially for the gravel data (black triangles). Additionally, the *ND* values of RS (see, Table 4) are also in a range expected for turbulent hydraulic conditions and gravel bedload transport.

The empty symbols in Fig. 9 represent the BS strength measured in calm conditions, with no bedload transport (i.e., no thickness of the active layer) measured before the experiment runs. These measurements further corroborated the observed trends, showing that $\Delta B_S/\Delta v_a$ depends on sound pulse penetration into the active layer thickness. For example, *Bs* for SPro measured in calm conditions (Fig. 9f, empty circles) has almost the same value as the rest of the given values, which points out to a dominant scattering of the immobile bed beneath moving particles.

4 Discussion

4.1 The apparent velocity and the bottom identification

The observed tendencies of the apparent bedload velocities and backscattering strengths measured by different SPro and M9 various configurations is a combination of several factors.

The strongest *Bs* of about -58 dB was estimated for the SPro (BB, 2MHz) which corresponded to the prevailing effect of the immobile surface and resulted in the smallest apparent velocities. This can be attributed to: i.) a complete penetration of the acoustic pulse through the active layer ii.) finer profiling resolution that contributed to a deeper sampling. Regarding the M9, the IC configuration yielded large apparent velocities which were comparable with the camera velocities (i.e., mean particle velocities). This indicates a negligible effect of immobile sediment, that is a shallow acoustic sampling at the surface of the active bedload layer. It is well known that BT mode is a separate signal that uses longer pulses. Moreover, the procedure to locate the bottom and process the Doppler velocity includes the identification of the strongest echo in range-gated echo profile (RDInstruments, 2011). More precisely, the system divides the profile into uniform segments called bins (also, gates or cells). The echo is measured at each bin and the bin with maximum echo identifies the bottom. Finally, the Doppler shift is used to calculate the apparent velocity at that bin.

The profile resolution and gating are, therefore, paramount for the apparent velocity assessment. A coarser-resolution would likely result in contaminated velocity assessment from shallower acoustic sampling at the active layer thickness.

Furthermore, the actual possibility of placing the maximum echo bin close to the flume bed also depends on the instrument distance from the bottom that in turn is very much related to the water depth. For a given cell size (i.e., the profile resolution) shallow water will results in fewer bins than the larger water depth. Thus, coarse resolution reduces the actual possibility of placing a cell close to the bottom in case of shallow water. This was exacerbated in flume experiments where the water depth was limited to less than 0.5 m. The observed deviation among the measured apparent velocities may therefore be attributed to profile gating changes due to bed deformation, which eventually resulted in different positions of the maximum echo cell.

For the IC signal processing the size of the bins is predetermined by the length of the pulse (*Pl*) and the pulse length is automatically adjusted from 5 cm to 26 cm, depending on the water depth. In this experimental set-up, the center of the bin used for the bottom identification and the apparent bedload velocity assessment, most likely coincides with the top of the sediment bed (see, Fig. 11). This resulted in shallower sampling, less contact with the immobile surface, contributing for a more dominant scattering of the mobile particles. The apparent velocities measured by the 3MHz IC partially complied with the spatial averaging assumption and gave lower velocities than the 1MHz. Given the same pulse length for the 2 frequencies, the not-profiled region close to the instrument (namely, the blanking distance) is the only reason for a different gating of the water depth. This was 2cm for 3MHz and 6cm for 1MHz (Fig. 11); a smaller blanking distance eventually resulted in more cells, which may made a bottom-closer acoustic sampling for the higher frequency. It is worth noting that this small change of profile gating in such low water depth eventually gave noticeable deviations of the apparent velocity that maybe not the case in actual rivers (Conevski et al. under review).

The bin size of the PC does not depend anymore on *Pl*, and it is determined by the distance between two consequent pulses. It enables much finer resolution and smaller bins that contributed to more accurate identification of the sediment bed. In this case, the measured apparent velocity was affected both by mobile and immobile particles, which means a bottom-closer acoustic sampling. However, in the gravel tests, the apparent velocities from 1MHz-PC appeared almost equal to moving particles velocities (namely the v_c camera velocity in Fig. 7). In this case, high saltation of the gravel particles, above z_c, enabled an acoustic sampling of the mobile particles without the effect of immobile bed surface. In other words, the gravel particles which are scattered in the geometric regime fully reflected the signal with much less influence of surface scattering from the immobile particles.

4.2 Backscattering strength and the bedload particle concentration

To better examine the BS strength and the bedload particle concentration, the mean B_s of each experiment type for 3 MHz PC and 1MHz PC (see also Table 3) were plotted versus the bedload surface concentration (K_{act}) and the normalized thickness of the active layer ($d_t/D50$). K_{act} is a direct measurement of the dimensionless bedload concentration and $d_t / D50$ represents the active layer thickness with respect to the number of particles, instead of the actual length, in fact the number of particles is a more crucial acoustic indicator. Regardless of the particle velocity and size, the performed experiments made evident an inverse correlation between B_s and the bedload surface concentration, K_{act}, obtained from planar videography (Fig. 10a and 10d for 3MHz-PC and 1MHz-PC, respectively). The same was also observed for B_s and the normalized thickness of the active layer, $d_t / D50$, from side videography (Fig. 10b and Fig. 10e). The inverse correlation between the active layer features and B_s, could be described as a sensitivity of the BS strength towards bedload concentration (i.e., number of particles) increases. Therefore, the backscattering strength embeds information about bedload in addition to apparent velocity. This was particularly relevant in the case of sand tests where a significant variation of the concentration was expected among the three hydraulic conditions. In Fig.10c and Fig. 10f, B_s noticeably changes with a small variation of the apparent velocity (see, the gray line within Fig. 10c and Fig. 10f) giving less steep trend. On the contrary, the same figures give a much steeper trend for the gravel experiments (see, black line with in Fig. 10c and Fig. 10f) B_s, which entailed a small variation of the bedload concentration and thickness among tests characterized with different conditions.

4.3 The backscattering strength and the PSD

Shields (2010) has demonstrated that the BS strengths from 1.2 MHz RioGrande can be utilized to characterize the sediment bed in the rivers and lakes. He distinguished the BS strengths from cohesive and non-cohesive materials, as well as from sand gravel and finer sediment bed.

In this study, Fig. 9 shows that for each frequency, there is a clear difference between the *Bs* values of gravel and sand experiments (see also, Table 3). This permits rough classification of the bedload materials and more detailed analysis of the medium sand and fine gravel scattering in moving or calm conditions. The estimated *Bs* values were higher in the experiments without any sediment transport (empty symbols, Fig. 9) than the experiment with sediment transport (filled symbols, Fig. 9). This difference in the scattering strengths indicated the dominance of the surface scattering in calm conditions which depends only on the bed roughness and the micro-roughness of each particle, especially relevant for the

highest frequency instruments (i.e., a wavelength smaller of the particle size). This also bore out that the BS strength cannot be only associated with the type of the material, but also with the mobility conditions, that is a consequence of surface and volume scattering combination. In addition, B_s for gravel in calm conditions coincided with the B_s measured for the sand in mobile conditions, that potentially hinder the assessment of actual *D50* from measured backscatter in the field (i.e., inverse problem solution).

Furthermore, Table 3 shows that the 0.5 MHz (vertical beam) gave the most considerable difference in the magnitudes of the gravel and sand experiments. The vertical beams are generally less responsive to a volume scattering (Ivakin, 1981), which implies that the vertical beam is less sensitive to concentration changes at the sediment bed, therefore enabling the solution of the inverse problem. In addition, the 0.5 MHz frequency located medium sand and fine gravel in different scattering regimes (i.e., Rayleigh and geometrical) which eventually contributed to a more straightforward distinction of the two materials.

5 Conclusions

5.1 The acoustic sampling

This study examined the apparent bedload velocity and the backscattering strength obtained by two different ADCPs working at four different frequencies, the 0.5/1/3 MHz M9 by Sontek and the 2MHz StreamPro by Teledyne-RDI, and using different signal processing configurations, incoherent (IC), pulse coherent (PC) for the M9 and coded broad-band (BB) for the StreamPro.

The apparent bedload velocity measured by the 3 MHz confirmed the spatial averaging assumption for both gravel and sand experiments, demonstrating an averaged effect of the mobile and immobile particles within the acoustic sampling. Similar results were obtained with 1MHz PC configuration for the sand experiments, but 1MHz IC resulted in higher velocities, in the range of the videography. This is apparently in contrast with previous findings where the apparent velocity usually underestimates the velocity of the mobile particles because of the surface scattering of immobile particles. The deviation of the 1 MHz IC was attributed to the internal profiling resolution of IC configuration, that estimated only the velocities at the top layer of the mobile sediment bed, which is closer to planar sampling of camera velocimetry. For gravel experiments, the apparent velocity was overestimated by 1 MHz-IC and PC too. In this case, the saltation height of the particles further contributed to enhancing the shallower sampling from those moving particles. These superficial returns may also be identified as a laboratory-scale problem that would not happen in the field. In fact, the blanking distance also decreased for 4 cm when passing from 1 to 3 MHz that changed the

cell positions with respect to flume bed. This would not make a significative difference in some meter-deep river.

The 2 MHz SPro underestimated the expected apparent velocity of 2 to 5 times for sand and up to 22 times for gravel. This bore out the intense emitted pulses that penetrate the active layer, and the lower resolution profiling of the BB systems which emphasized the effect of the immobile surface beneath within the acoustic sampling (i.e., surface scattering).

Summarizing the M9 appeared more suited for the measuring of average apparent velocity at the flume bed, provided that the profiling resolution is high enough with respect to water depth.

5.2 Instrumental configuration

A high percentage of not valid data (*ND*) was observed for the M9 PC and IC configurations in case of gravel experiments. This pointed out the limitation of these configurations, especially for extreme hydraulic conditions and the need of averaging time longer than 5 minutes. In this case the SPro provide a more robust measurement although affected by surface scattering.

5.3 Doppler and backscatter outputs

The measured BS strength declined as the observed bedload concentration at flume bed increased, independently of the mass rate. This declination was larger for sand than for gravel tests. M9 gave very similar results regarding the rate of decline of the BS strength whatever the configuration (i.e., internal processing). On the contrary, the SPro appeared to be insensitive of the changes in the bedload concentration, confirming a strong effect of the immobile bed surface. This indicates that M9 provides information regarding the active layer thickness in addition to the apparent velocity. Furthermore, the BS strength measured by the M9 0.5 MHz vertical beam produced the most distinguishable magnitudes, which potentially can be used for riverbed PSD classification. This classification appears important for a correct interpretation of the measured apparent velocity. As a matter of fact the experiments with sand over a flat immobile gravel bed showed apparent velocities and BS strengths from slant beams in the range of sand experiments with the same hydraulic conditions, although the amount of sand trapped was negligible, whereas a deviation was observed among these tests for the BS strength from the 0.5 MHz vertical beam.

These results are the basis towards utilizing both the backscattering strength and apparent velocity in the quantification of the total bedload transport over a cross-section of a river. To this objective, the kinematic model (Rennie et al., 2004) offers an opportunity to physically

combine the B_s as an indicator of the bedload concentration, and v_a as the average bedload velocity.

However, more detailed analysis in collaboration with the ADCP manufacturers is necessary to determine the ambient noise, the rough surface scattering influence, and the echo distribution. Also, more tests should be performed over various PSD in calm and moving conditions. It would help to benchmark BS strength ranges related to different frequencies for more efficient field implementation.

Acknowledgements

The authors acknowledge the collaboration with Sontek Xylem, that allowed free using of the ADPviewer software permitting a full control of the M9 ADCP.

Funding

This research and the filed measurement campaigns were funded by the Norwegian Research Council and Statkraft as part of the multidisciplinary project SEDIPASS.

Notation

A_f	=	area of the surface scattering at flume bed	(dB)
BP	=	Bottom Tracking pings per ensemble	(-)
B_s	=	corrected Backscattering Strength	(dB)
c	=	speed of sound	(m s^{-1})
Cz	=	Chezy coefficient	(-)
$D50$	=	particle median diameter	(m)
$D90$	=	particle diameter bigger than 90%	(m)
D_{num}	=	particle mean diameter derived of the Number Particle Size Distribution	(m)
D_{std}	=	standard deviation of the PSD	(m)
EI	=	BT echo intensity	(dB)
E_r	=	noise level	(dB)
F_r	=	Froude number	(-)
d_t	=	empirically calculated active layer thickness	(m)
D_t	=	transducers diameter	(m)
d_{tk}	=	modelled active layer thickness	(m)
f	=	ADCP working frequency	MHz
FD	=	percentage of the discarded velocity samples after the filtering	(%)
g	=	gravitational constant	(m s^{-2})
H	=	water depth	(m)
K_m	=	mean surface bedload concentration estimated from the imagery data	(%)
K_{act}	=	active surface bedload concentration estimated from the imagery data	(%)
N/A	=	fraction of bad samples before filtering	(-)
ND	=	total filtered data including the filtered values and zeros	(-)
P	=	pressure at the transducer	(Pa)

P_{dB}	=	transmit voltage	(dB)
Pl	=	acoustic pulse length	(mm)
Q_s^m	=	physically measured transport rate at the end of the flume	(kg s m^{-1})
r	=	correlation coefficient	(-)
R	=	slant distance from the transducer to the sediment bed	(m)
r	=	coefficient of correlation	(-)
Re*	=	Reynolds number	(-)
Re_p	=	particle Reynolds number	(-)
S	=	slope of the sediment bed	(%)
SL	=	source level	(dB)
$STDv_a$	=	standard deviation of the raw apparent bedload velocity	(m s^{-1})
$stdK_{act}$		standard deviation of the surface bedload concentration	(%)
$stdK_m$		standard deviation of the active surface bedload concentration	(%)
Ss	=	surface backscattering	(dB)
S_v	=	volume backscattering	(dB)
Tl	=	time between pings	(s)
U	=	average-depth water velocity	(m s^{-1})
$u*$	=	shear(friction) velocity	(m s^{-1})
$u*_{cr}$	=	critical shear(friction) velocity	(m s-1)
U^{ADCP}	=	depth-averaged velocity measured by the ADCPs	(m s^{-1})
v_a	=	the apparent velocity, measured by the ADCP and filtered	(m s^{-1})
V_b	=	voltage of the ADCP battery	(V)
v_{bt}	=	Bottom Tracking velocity	(m s^{-1})
v_c	=	image velocity	(m s^{-1})
v_{gps}	=	GPS vessel velocity	(m s^{-1})
WP	=	Water Profile pings per ensemble	(-)
z_c	=	beam, focusing, distance to the inner side of the central lobe	(m)
z_s	=	distance of the side-lobe contaminated region	(m)
α	=	attenuation coefficient	(-)
α_ξ	=	local slopes of the bed in x - direction	(º)
α_y	=	local slopes of the bed in y - direction	(º)
λ	=	wavelength	(mm)
φ	=	acoustic beam opening angle	(º)
θ	=	acoustic beam incident angle	(º)
ρ	=	water density	(kg m^{-3})
ρs	=	sediment particles density	(kg m^{-3})
τ	=	Shear stress	(N m^{-2})
$\tau*$	=	Shields parameter (dimensionless shear stress)	1
τ_{cr}	=	critical Shields parameter (critical shear stress)	(-)
ω	=	first side-lobe angle	(º)

References

Amiri-Simkooei, A., Snellen, M., & Simons, D. G. (2009). Riverbed sediment classification using multi-beam echo-sounder backscatter data. *The Journal of the Acoustical Society of America, 126*, 1724-1738. doi:10.1121/1.3205397

Bagnold, R. (1956). The flow of cohesionless grains in fluids. *Philos. Trans. R. Soc. London, 249*(A), 235–297.

Blanckaert K., Heyman J., H., & C.D., R. (2017, October). Measurments of bedload sediment transport with an Acoustic Doppler Velocity Profiler(ADVP). *J. Hydraulic Engineering*.

Brumley, B. H., Cabrera, R. G., Deines, K. L., & Terray, E. A. (1991, 10). Performance of a broad-band acoustic Doppler current profiler. *IEEE Journal of Oceanic Engineering, 16*, 402-407. doi:10.1109/48.90905

Conevski, S., Guerrero, M., Colin, R., & Ruther, N. (under review). Acoustic sampling effects on bedload quantification using acoustic Doppler current profilers. *Journal of Hydraulic Research*.

Conevski, S., Guerrero, M., Ruther, N., & Rennie, C. (2019). Laboratory investigation of the apparent bedload velocity measured by ADCPs. *Journal of Hydraulic Engineering*. doi:10.1061/(ASCE)HY.1943-7900.0001632

Conevski, S., Winterscheid, A., Ruther, N., Guerrero, M., & Rennie, C. (2018). Evaluation of an acoustic Doppler technique for bed-load transport measurements in sand-bed rivers. *River Flow 2018.* Lyon: Paper presented at River Flow 2018.

Deines, K. L. (1999, 3). Backscatter estimation using Broadband acoustic Doppler current profilers. *Proceedings of the IEEE Sixth Working Conference on Current Measurement (Cat. No.99CH36331)*, (pp. 249-253). doi:10.1109/CCM.1999.755249

Drake, T. G., Shreve, R. L., Dietrich, W. E., Whiting, P. J., & Leopold, L. B. (1988). Bedload transport of fine gravel observed by motion-picture photography. *Journal of Fluid Mechanics, 192*(1988), 193-216.

Gaeuman, D., & Jacobson, R. B. (2006). Acoustic bed velocity and bed load dynamics in a large sand bed river. *J Geophys Res Earth Surf, 111(F2)*(F02005).

Gaweesh, M., & Van Rijn, L. (1994, 12). Bed-Load Sampling in Sand-Bed Rivers. *Journal of Hydraulic Engineering-asce - J HYDRAUL ENG-ASCE, 120*. doi:10.1061/(ASCE)0733-9429(1994)120:12(1364)

Geay, T., Belleudy, P., Gervaise, C., Habersack, H., Aigner, J., Kreisler, A., . . . Laronne, J. B. (2017). Passive acoustic monitoring of bed load discharge in a large gravel bed river. *Journal of Geophysical Research: Earth Surface, 122*, 528-545. doi:10.1002/2016JF004112

Gomez, B. (1991). Bedload transport. *Earth-Science Reviews, 31*, 89-132. doi:https://doi.org/10.1016/0012-8252(91)90017-A

Guerrero, M., Latosinski, F., Nones, M., Szupiany, R. N., Re, M., & Gaeta, M. G. (2015). A sediment fluxes investigation for the 2-D modelling of large river morphodynamics. *Advances in Water Resources, 81*, 186-198. doi:https://doi.org/10.1016/j.advwatres.2015.01.017

Guerrero, M., Rüther, N., Haun, S., & Baranya, S. (2017). A combined use of acoustic and optical devices to investigate suspende d se diment in rivers. *Advances in Water Resources*, 1–12.

Hu, C., & Hiu, H. (1996). Bed Load Mechanical characteristics. *J Hydr Res, 37*, 559-576.

Hubbell, D. W. (1964). *Apparatus and techniques for measuring bedload.* USGS. U. S. Govt. Print. Off.,. doi:10.3133/wsp1748

Hurther, D., & Thorne, P. D. (2011). Suspension and near-bed load sediment transport processes above a migrating, sand-rippled bed under shoaling waves. *Journal of Geophysical Research: Oceans, 116*. doi:10.1029/2010JC006774

Ivakin, A. N. (1981). Underwater sound scattering by volume inhomogeneities of a bottom medium bounded by a rough surface. *Soviet Physics Acoustics*, 2012-2017.

Kaushik, D., & Ashraful, H. S. (2014). Shadow Detection and. *Smart Computing Review Removal Based on YCbCr Color Space, 4*(1), 23-33.

Keshavarzy, A., & Ball J.E. (1999). An application of image processing in the study of sediment motion. *J Hydr Res, 37*, 559–576.

Lajeunesse, E., Malverti, L., & Charru, F. (2010). Bed load transport in turbulent flow at the grain scale: Experiments and modeling. *Journal of Geophysical Research: Earth Surface, 115*(4). doi:10.1029/2009JF001628

Latosinski, F. G., Szupiany, R. N., Guerrero, M., Amsler, M. L., & Vionnet, C. (2017). The ADCP's bottom track capability for bedload prediction: Evidence on method reliability from sandy river applications. *Flow Measurement and Instrumentation, 54*, 124-135. doi:https://doi.org/10.1016/j.flowmeasinst.2017.01.005

Lee, H. B., Yeo, I. W., & Lee, K.-K. (2014). Fluid flow through rough-walled rock fractures with hydrophobic surfaces. *Geosciences Journal, 18*(4), 375-380. Retrieved 6 22, 2019, from https://link.springer.com/article/10.1007/s12303-014-0028-4

Lee, H. H. (1994). Investigation of saltating particle motions. *J Hydr ENg, 122*, 245–254.

Medwin, H. (2005). *Sounds in the sea : from ocean acoustics to acoustical oceanography.* Cambridge: Cambridge University Press.

Medwin, H., & Clay, C. S. (1998). Chapter 2 - Sound Propagation . In H. Medwin, & C. S. Clay (Eds.), *Fundamentals of Acoustical Oceanography* (pp. 17-69). San Diego: Academic Press. doi:https://doi.org/10.1016/B978-012487570-8/50004-0

Moate, B. D., & Thorne, P. D. (2009). Measurements and inversion of acoustic scattering from suspensions having broad size distributions. *The Journal of the Acoustical Society of America, 126*, 2905-2917. doi:10.1121/1.3242374

Moore, S. A., Dramais, G., Dussouillez, P., Coz, J. L., Rennie, C., & Camenen, B. (2013). Acoustic measurements of the spatial distribution of suspended sediment at a site on the Lower Mekong River. *Proceedings of Meetings on Acoustics, 19*, 005003. doi:10.1121/1.4799128

Mulison, J. (2017). Backscatter Estimation Using Broadband Acoustic Doppler Current profilers-Updated. Druham: HMEM Conference.

Nifio, Y., & Garcia, M. (1994). Gravel saltation. *WATER RESOURCES RESEARCH, 30*(6), 1915-19.

Papanicolaou, A., P., D., M., B., & Dancey. (1999). Computer vision technique for tracking bed load movement. *Journal of Computational Civil Engineering, 13*(2), 71-79.

Parker, G. (2004). *ID SEDIMENT TRANSPORT MORPHODYNAMICS with applications to RIVERS AND TURBIDITY CURRENTS.* St. Anthony Falls Laboratory, Mississippi River at 3rd Avenue SE.

Radice, A., Malavasi, S., & Bailio, F. (2006). Solid transport measurements through image processing. *41*(5), 721-734.

Radke, R. J., Andra, S., Al-Kofahi, O., & Roysam, B. (2005, 3). Image change detection algorithms: a systematic survey. *IEEE Transactions on Image Processing, 14*, 294-307. doi:10.1109/TIP.2004.838698

Ramooz, R., & Rennie, C. D. (2008). *Laboratory measurement of bedload with an ADCP.* In Bedload-surrogate monitoring technologies: United States Geological Survey Scientific Investigations Rep. 2010-5091, USGS, Reston. Retrieved from http://pubs.usgs.gov/sir/2010/5091/papers/

RDInstruments. (2011). *Acoustic Doppler Current Profiler Principles of Operation A Practical Primer.* Practical Primer, Teledyne RD Instruments, 14020 Stowe Drive Poway, California 92064. Retrieved from http://www.teledynemarine.com

RDInstruments, T. (2015, 9). *StreamPro ADCP Guide.* Teledyne RDInstruments. Retrieved from http://www.teledynemarine.com/Documents/Brand%20Support/RD%20INSTRUMENTS/Technical%20Resources/Manuals%20and%20Guides/StreamPro/StreamPro_ADCP_Guide_Sep15.pdf

Rennie, C. D., & Villard, P. V. (2004). Site specificity of bed load measurement using an acoustic Doppler current profiler. *Journal of Geophysical Research: Earth Surface, 109*. doi:10.1029/2003JF000106

Rennie, C. D., Millar, R. G., & and Church, M. A. (2002). Measurement of bed load velocity using an acoustic doppler current profiler. *Journal of Hydraulic Engineering, 5*(128), 473-483.

Rennie, C. D., V. D., Williams, R. D., Brasington, J., & Hicks, M. (2017). Calibration of Acoustic Doppler Current Profiler Apparent Bedload Velocity to Bedload Transport Rate. In *Gravel-Bed Rivers: Process and Disasters* (pp. 209-231). Wiley-Blackwell.

Rennie, D. C. (2002). Measurement of bed load velocity using an acoustic doppler current profiler. *Journal of Hydraulic Engineering, 5*(128), 473-483.

Rickenmann, D., Turowski, J. M., Fritschi, B., Klaiber, A., & Ludwig, A. (2012). Bedload transport measurements at the Erlenbach stream with geophones and automated basket samplers. *Earth Surface Processes and Landforms, 37*, 1000-1011. doi:10.1002/esp.3225

Sassi, M. G., Hoitink, A. J., & Vermeulen, B. (2011). Impact of sound attenuation by suspended sediment on ADCP backscatter calibrations. *Water Resources Research, 48*. doi:10.1029/2012WR012008

Shields, F. D. (2010). Aquatic Habitat Bottom Classification Using ADCP. *Journal of Hydraulic Engineering, 136*, 336-342. doi:10.1061/(ASCE)HY.1943-7900.0000181

Shields, I. (1936). Anwendung der ahnlichkeitmechanik und der turbulenz- forschung auf die gescheibebewegung. *Mitt. Preuss Vers. Wasserbau Schiffbau*.

Sontek. (2017, 10). *RiverSurveyor S5/M9 System Manual, Firmware Version 4.02.* . 9940 Summers Ridge Road, San Diego, CA 92121-3091 USA: SonTek, a Xylem brand. Retrieved from http://ysi.actonsoftware.com/acton/attachment/1253/f-041f/1/-/-/-/-/RiverSurveyor%20Live%20Manual%20v4.0_R.pdf

Szupiany, R. N., Lopez Weibel, C., Guerrero, M., Latosinski, F., Wood, M., Dominguez Ruben, L., & Oberg, K. (2019). Estimating sand concentrations using ADCP-based acoustic inversion in a large fluvial system characterized by bi-modal suspended-sediment distributions. *Earth Surface Processes and Landforms, 44*, 1295-1308. doi:10.1002/esp.4572

Thorne, P. D., & Meral, R. (2008). Formulations for the scattering properties of suspended sandy sediments for use in the application of acoustics to sediment transport processes. *Continental Shelf Research, 28*, 309-317. doi:https://doi.org/10.1016/j.csr.2007.08.002

Urick, R. J. (1983). *Principles of Underwater Sound.* Peninsula Publishing. Retrieved from https://books.google.no/books?id=MBBgQgAACAAJ

Van Rijn, L. (1984). Sediment transport, part i: bed load transport. *J. Hydraul. Eng., 110*, 1431–1456.

List of tables

Table 1 Basic hydraulic parameters and information about the PSD of the bedload material.

Table 2 ADCPs parameters and corresponding signal processing configurations

Table 3 Average values of the most important experimental outputs

Table 4 Average values of the not-valid data (ND=FD+N/A) and the standard deviation of the measured bedload velocities

List of figures

Figure 1 Experimental (flume) Set – Up.

Figure 2 Acoustic beam scheme and parameters.

Figure 3 Detection of the active layer thickness (mean saltation height) above the dune crest. The green coloured particles show the position at time t_1 and the magenta coloured particles at t_2.

Figure 4 Detection of the active layer thickens (mean saltation height) in gravel experiments. The green coloured particle is the first position identified and the magenta coloured particle is approximately the highest jump of the particle.

Figure 5 Apparent bedload velocity measured by different instruments and configurations and the transport rate captured by the bedload trap at the end of the flume.

Figure 6 Corrected backscattering strength measured by different instruments and configurations and the transport rate captured by the bedload trap at the end of the flume.

Figure 7 Apparent bedload velocity measured by different instrument and configuration correlated with the bedload velocity estimated by imagery data.

Figure 8 Apparent bedload velocity measured by different instrument and configuration correlated with the normalized bedload velocity estimated by imagery data.

Figure 9 Apparent bedload velocity and the backscattering strength measured by different instrument and configurations.

Figure 10 Observations of the average backscattering strength calculated form the all experiments for each sediment material and frequency considering only the PC configuration

Figure 11 A possible scheme of the echo range-gaging in the procedure of the identifying the bed. The last bin is the bin that determines the bottom echo.

Tables

Table 1 Basic hydraulic parameters and information about the PSD of the bedload material.

EXP	S	U	u_*	u_{*cr}	Fr	Re_*	H	$D90^1$	$D50$	D_{sed}	D_{num}	Re_{p*}
	%	m s^{-1}	m s^{-1}	m s^{-1}			m	mm	mm	mm	mm	
sandEXP1	0.10	0.302	0.015	0.015	0.15	10355.3	0.42	0.56	0.39	0.42	0.13	25.26
sandEXP2	0.10	0.432	0.022	0.015	0.21	14813.2	0.42	0.56	0.39	0.42	0.13	25.26
sandEXP3	0.10	0.571	0.028	0.015	0.28	19549.7	0.42	0.56	0.39	0.42	0.13	25.26
sandOVER	0.10	0.478	0.020	0.015	0.23	17550.9	0.45	0.56	0.39	0.42	0.13	25.26
gavelEXP1	0.80	1.197	0.091	0.082	0.58	42939.6	0.44	10.45	7.55	3.35	5.45	2019
gavelEXP2	0.80	1.321	0.101	0.082	0.64	47395.2	0.44	10.45	7.55	3.35	5.45	2019
gavelEXP3	0.80	1.424	0.107	0.082	0.67	53421.6	0.46	10.45	7.55	3.35	5.45	2019

1- Note that for sandOVER the sand PSD is considered in the calculations

Table 2 ADCPs parameters and corresponding signal processing configurations

ADCP	f	λ	Dt	θ	φ	*Config*	*WP*	*BP*	*Pl*	z_c[1]
	(MHz)	(mm)	(cm)	°	°				(cm)	mm
Sontek M9	3.0	0.49	2.70	25	1.06	RS	20	2	5	1.57
Sontek M9	1	1.455	4.3	25	2.00	IC	0	4	5	3.99
Sontek M9	3.0	0.485	2.7	25	1.06	IC	0	4	5	1.57
Sontek M9	1	1.455	4.3	25	2.00	PC	0	3	5	3.99
Sontek M9	3.0	0.485	2.7	25	1.06	PC	0	3	5	1.57
Sontek M9	0.5	2.9	4.4	90.0	3.90	PC,IC,RS	0.0	3.0	5.0	0.00
RDI StreamPro	2.0	0.7	1.6	20	2.68	BB	2	2	9	2.24

[1] z_c is an average value of all measurements using the average distance from the ADCP to the sediment bed

Table 3 Average values of the most important experimental outputs

EXP	3MHz IC		1MHz IC		0.5MHz	3MHz PC		1MHz PC		0.5MHz	3MHz RS		0.5MHz	SPro		Camera				
	v_a	B_s	v_a	B_s	B_s	v_a	B_s	v_a	B_s	B_s	v_a	B_s	B_s	v_a	B_s	v_c	Km	$Kact$	d_s	Qs^m
	m s^{-1}	dB	m s^{-1}	dB	dB	m s^{-1}	dB	m s^{-1}	dB	dB	m s^{-1}	dB	dB	m s^{-1}	m s^{-1}	m s^{-1}			mm	g/s
sandEXP1	0.006	-130.9	0.058	-153.2	-108.7	0.003	-133.4	0.002	-152.0	-108.4	0.003	-129.2	-109.1	0.002	-56.5	0.048	0.05	0.05	0.53	0.00
sandEXP2	0.027	-142.6	0.089	-159.6	-116.1	0.022	-143.9	0.021	-157.2	-114.2	0.024	-134.2	-117.1	0.007	-56.8	0.076	0.20	0.20	2.26	0.49
sandEXP3	0.059	-150.1	0.129	-164.3	-120.1	0.057	-150.7	0.061	-162.4	-118.8	0.052	-144.7	-122.7	0.019	-57.1	0.144	0.53	0.53	3.08	8.97
sandOVER	0.031	-140.9	0.092	-155.2	-119.1	0.027	-142.0	0.028	-153.9	-117.7	0.010	-136.2	-119.1	0.009	-57.8	0.091	0.10	0.19	2.46	0.00
gavelEXP1	0.085	-149.8	0.254	-168.0	-128.8	0.067	-150.2	0.215	-167.2	-129.2	0.066	-146.0	-128.4	0.004	-57.2	0.267	0.02	0.12	11.33	1.11
gavelEXP2	0.107	-151.8	0.305	-169.7	-129.7	0.099	-152.0	0.291	-168.8	-129.5	0.095	-147.8	-129.1	0.008	-58.0	0.366	0.07	0.18	18.88	43.27
gavelEXP3	0.163	-152.6	0.368	-170.5	-130.7	0.123	-153.1	0.331	-169.9	-130.6	0.128	-148.6	-129.3	0.014	-58.0	0.410	0.09	0.22	26.43	78.52

Table 4 Average values of the not-valid data (*ND=FD+N/A*) and the standard deviation of the measured bedload velocities

EXP	3MHz IC		1MHz IC		3MHz PC		1MHz PC		3MHz RS		SPro				
	$STDv_a$	ND	$STDv_a$	ND	$STDv_a$	ND	$STDv_a$	ND	$STDv_a$	ND	$STDv_a$	ND	$STDv_c$	$stdK_m$	$stdK_{act}$
	m s^{-1}	%	m s^{-1}	%	m s^{-1}	%	m s^{-1}	%	m s^{-1}	%	m s^{-1}	%	m s^{-1}		
sandEXP1	0.0038	44%	0.0272	31%	0.0007	48%	0.0011	57%	0.0017	64%	0.0004	80%	0.006	0.022	0.022
sandEXP2	0.0156	38%	0.0601	37%	0.0139	40%	0.0233	53%	0.0166	44%	0.0040	43%	0.007	0.016	0.016
sandEXP3	0.0408	29%	0.0760	41%	0.0336	35%	0.0677	50%	0.0297	37%	0.0123	30%	0.009	0.009	0.009
sandOVER	0.0106	37%	0.0245	40%	0.0058	43%	0.0017	44%	0.0084	46%	0.0016	64%	0.023	0.011	0.050
gavelEXP1	0.0508	71%	0.1472	74%	0.0436	59%	0.1744	83%	0.0489	51%	0.0022	62%	0.190	0.035	0.190
gavelEXP2	0.0590	83%	0.1744	84%	0.0652	74%	0.1991	87%	0.0768	54%	0.0084	57%	0.450	0.125	0.298
gavelEXP3	0.0689	91%	0.1924	89%	0.0912	89%	0.1778	89%	0.1228	56%	0.0129	56%	0.480	0.200	0.302

FIGURES

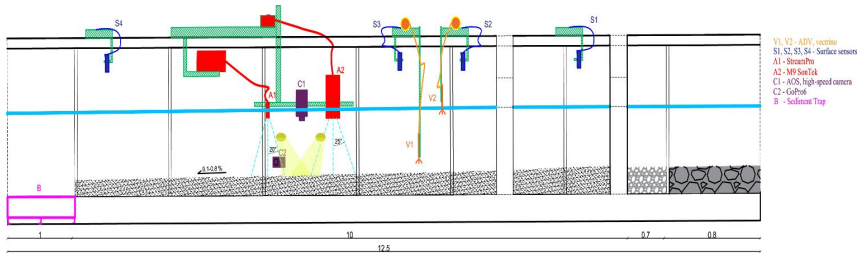

Figure 1 Experimental (flume) Set – Up.

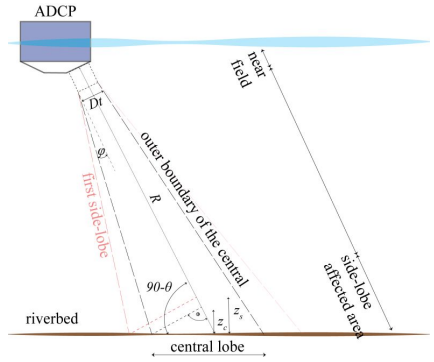

Figure 2 Acoustic beam scheme and parameters.

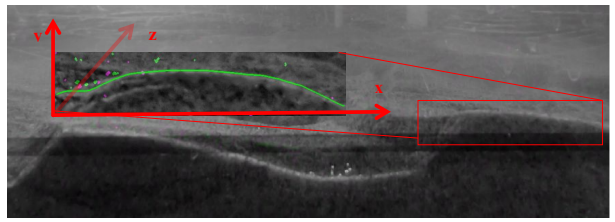

Figure 3 Detection of the active layer thickens thickness (mean saltation height) above the dune crest. The green coloured particles show the position at time t1 and the magenta coloured particles at t2.

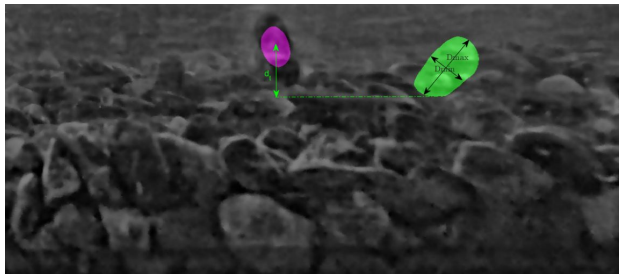

Figure 4 Detection of the active layer thickens (mean saltation height) in gravel experiments. The green coloured particle is the first position identified and the magenta coloured particle is approximately the highest jump of the particle.

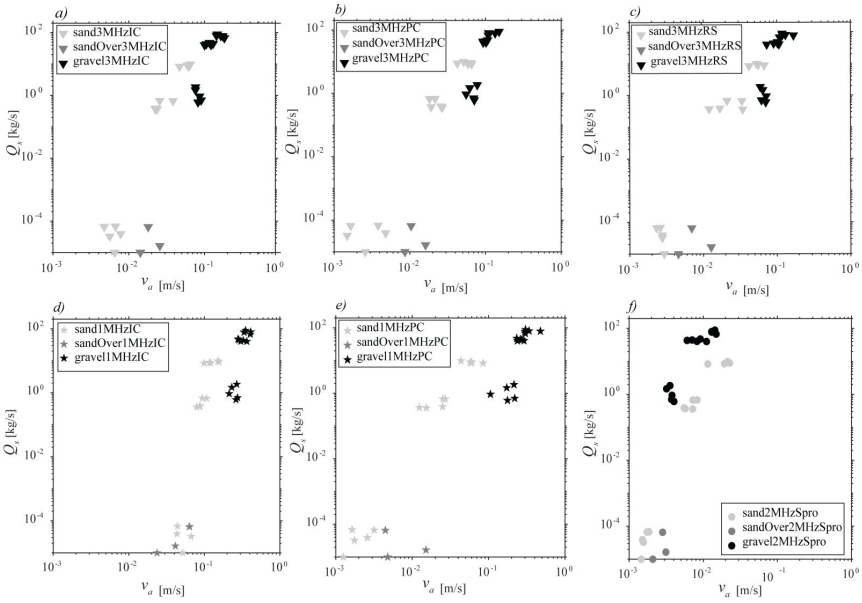

Figure 5 Apparent bedload velocity measured by different instruments and configurations and the transport rate captured by the bedload trap at the end of the flume.

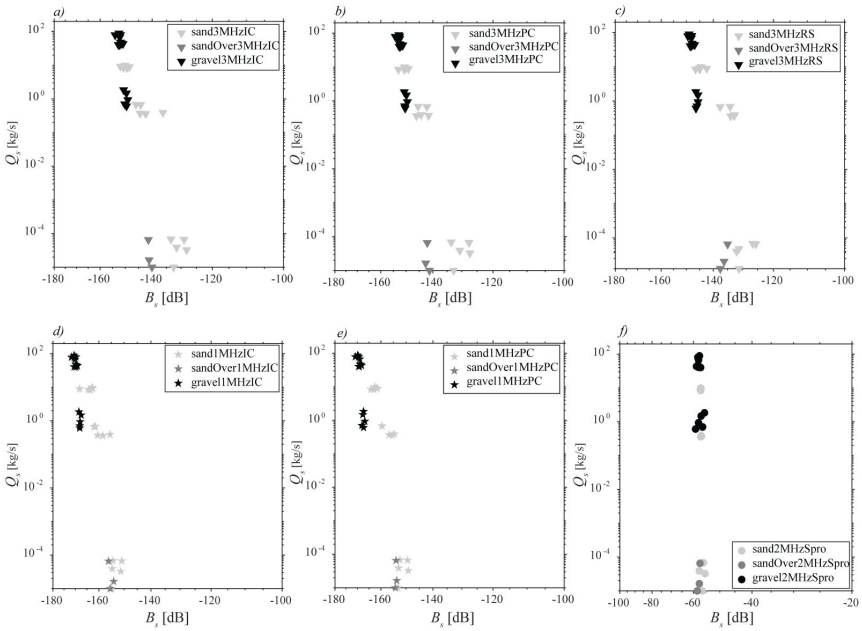

Figure 6 Corrected backscattering strength measured by different instruments and configurations and the transport rate captured by the bedload trap at the end of the flume.

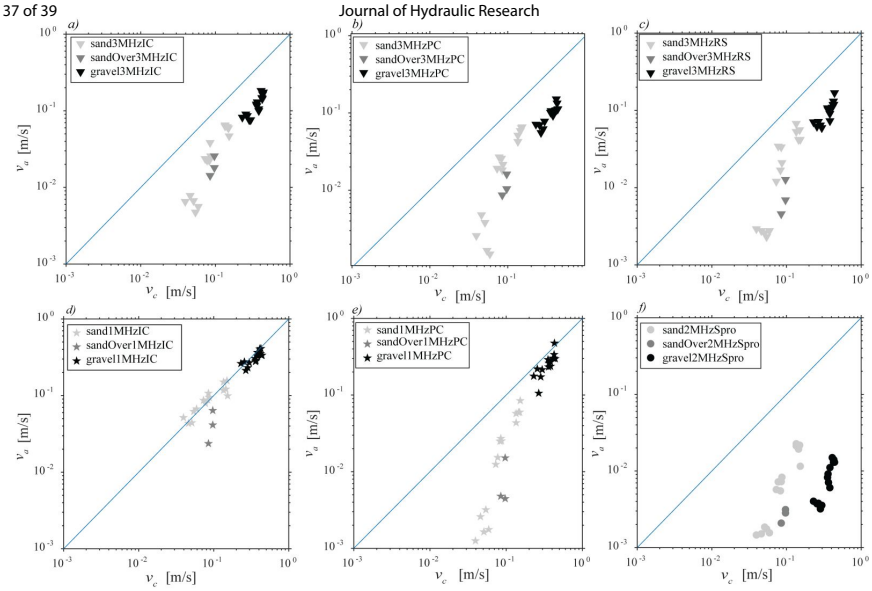

Figure 7 Apparent bedload velocity measured by different instrument and configuration correlated with the bedload velocity estimated by imagery data.

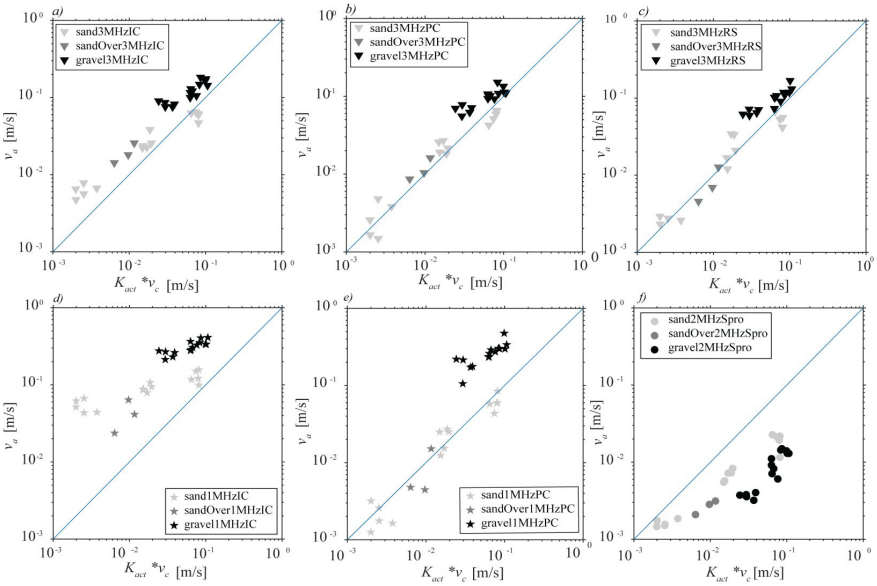

Figure 8 Apparent bedload velocity measured by different instrument and configuration correlated with the normalized bedload velocity estimated by imagery data.

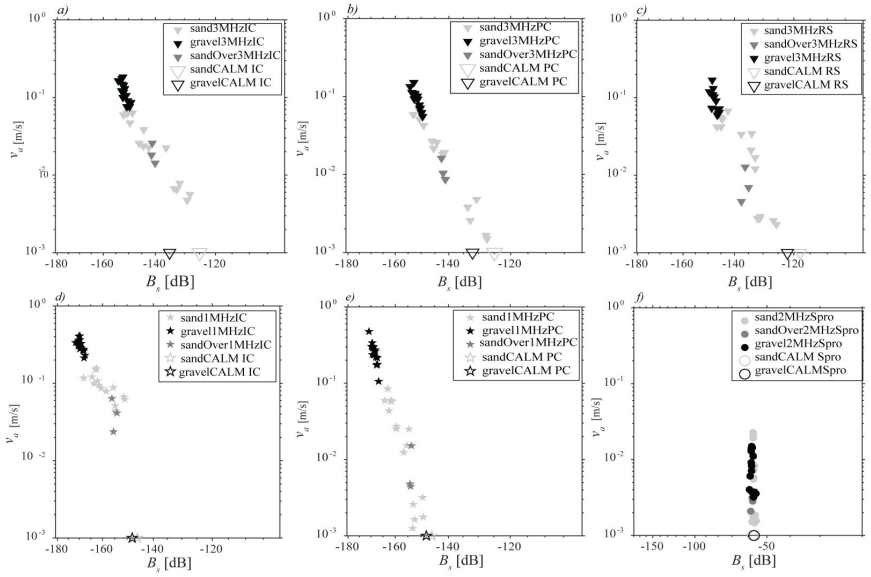

Figure 9 Apparent bedload velocity and the backscattering strength measured by different instrument and configurations.

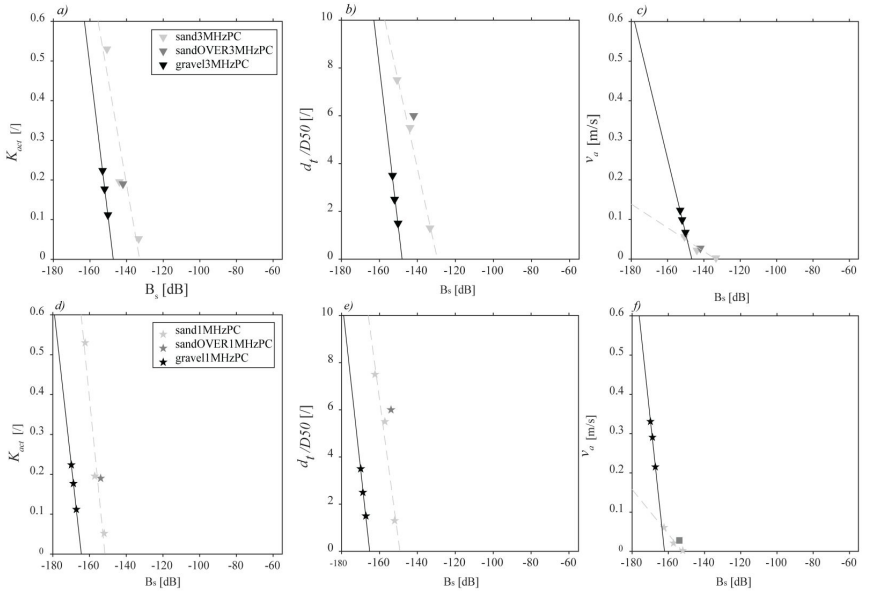

Figure 10 Observations of the average backscattering strength calculated form the all experiments for each sediment material and frequency considering only the PC configuration.

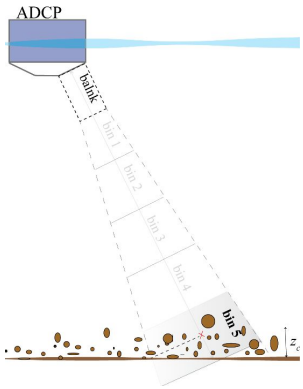

Figure 11 A possible scheme of the echo range-gaging in the procedure of the identifying the bed. The last bin is the bin that determines the bottom echo.

Paper *VI*

Bedload measurements using ultrasound Velocity profilers (UVP) in controlled laboratory conditions

Slaven Conevski, Massimo Guerrero, Marie Burckbuchler, Nils Ruther

PiE 2018, Lisbon

Bedload measurements using ultrasound Velocity profilers (UVP) in controlled laboratory conditions

S.Conevski[1, 2] , N. Ruther[1] , M. Guerrero[2], M. Burckbuchler[3]
[1]Department of Civil and Environmental Engineering, Norwegian University of Science and Technology, Trondheim, Norway. slaven.conevski@ntnu.no; nils.ruther@ntnu.no
[2] Department of Civil, Chemical, Environmental, and Materials Engineering, University of Bologna, Italy. massimo.guerrero@unibo.it; slaven.conevski2@unibo.it
[3] Ubertone, 14, rue du Brochet, Schiltigheim, France. marie.burckbuchler@ubertone.fr

Introduction

Accurate estimation of bedload transport is an engineering challenge since the previous century. Measuring the transport rate, using direct traditional methods (i.e., pressure difference samplers) is a notoriously hard and labor-intensive procedure. The temporal and spatial variability of the bedload, together with the instrument disturbance, can induce stochastic and systematic uncertainties. Very often, this data is considered unreliable and complicates the further elaboration of the sediment transport behavior. On the other hand, statistically valid measurements are essential for the evaluation of the sediment transport masses, especially in large navigable or heavily exploited rivers.

One proposed alternative is the use of hydroacoustic instruments, which provide non-intrusive measurements, are easy-to-deploy, and offer detailed data resolution. Recently, many studies [1, 2, 3] elaborated the use of the bottom tracking (BT) feature of the acoustic Doppler current profilers (ADCP), emerging in a promising technique for evaluating the bedload transport. However, ADCP data do not provide the correct bedload velocity and require field-specific calibration in order to derive the bedload transport rate [4]. Recently, a laboratory study has proved that filtering of the apparent bedload velocity efficiently matched the spatially averaged bedload velocity [5]. Blanckaert et al. [6] in another laboratory experiment found out a strong correlation between the near-bed acoustic signal from a custom made acoustic profiler and the image velocity calculated using the optical flow and PTV methods. These studies show that the acoustic instruments have the potential to measure the bedload average velocity.

Furthermore, the redistribution of the echo from the sediment bed is quite complicated because of variable intensity across the insonified beam width and the bed heterogeneity. Thus, the measured velocity contains many erroneous data and the intensity threshold for the bottom cannot be easily detected, especially during moving bed conditions. This study focuses on identifying and analyzing the acoustic signal from the mobile sediment bed using monostatic ultrasound velocity profilers (UVP) manufactured by Ubertone [7]. Firstly, a simple method for identification of the mobile sediment bed is proposed, then the influence of different frequencies and grazing angles on the backscattered amplitude and the apparent

bedload velocity were analyzed. To confirm the bedload velocity, high-resolution cameras were used to calculate the surface velocity of the bedload.

Methodology

The Echo from the mobile sediment bed

The UVP use monostatic Doppler probes that emit a burst of acoustic pulses at a specified pulse repetition frequency (PRF). This pulse incorporates several periods at a given transducer working frequency. Table 1 presents the deployed frequencies in this campaign of experiments. After emitting the pulse the system switches in receive mode. Each of the incident ultrasound pulses reflects from the riverbed differently, depending on the instrument frequency, the particle size distribution (PSD), and the transport conditions. In mobile bed conditions, it can be assumed that the mobile volume of the bed, or the active layer, could be associated with *volume scattering*. Besides, the immobile surface below the active layer could be defined as a *rough surface scattering*. Assuming that the surface of the immobile particles is acoustically impermeable, the sonar equation of the returned signal formula can be modified for the sediment bed intensity (I_r). If the spreading loss and the attenuation in the water column are negligible (i.e., no sediment suspension and a short distance to the bed), then the slant range R in the attenuation component could be conveniently considered equal to the active layer thickness (R_{at}). The only reason for volume scattering is the sediment concentration in the active layer (Mat). Similarly, for sound attenuation coefficient α_{at}, the active layer concentration should be considered. The final logarithmic form of the corrected sonar equation is:

$$Ir = 10log(I_0 K_p) + 10log(K_s A_r^2 + K_v^2 M_{at}) + 10\log(\frac{c\tau}{2}) - 40R_{at}\alpha_{at}log(e), \quad (1)$$

where I_r is the received signal intensity (the received echo from the riverbed), I_0 is the transmitted intensity K_p is an instrument constant. The coefficient K_v is the volume scattering coefficient that depends on the frequency, and the particle size distribution [8] and K_s accounts for the surface reflection depending on the surface roughness, acoustic frequency, and surface to beam inclination. The A_r^2 term is the variance of the surface of the rough bed which accounts for the phase reinforcement, depending on the acoustic and bottom wavelength irregularities [9]. τ is the pulse duration, c is the speed of sound, $b(\theta,\varphi)$ is a beam coefficient that includes the grazing angle θ , the half beam opening angle (φ) and the beamwidth.

Experimental setup

The experiment was conducted in the hydraulic laboratory at the Norwegian University of Science and Technology (NTNU) in collaboration with Ubertone. In the 60cm wide, glass-sided flume, two hydraulic conditions were performed (Q_1=80 l/s and Q_2=120 l/s) having 40-42 cm water level above the sediment bed. The sediment bed consisted of fine sand with D50= 0.39 mm and D84-D16= 0.22 mm. The water velocities reached 0.3 m/s and 0.5 m/s consequently for the two different discharges.

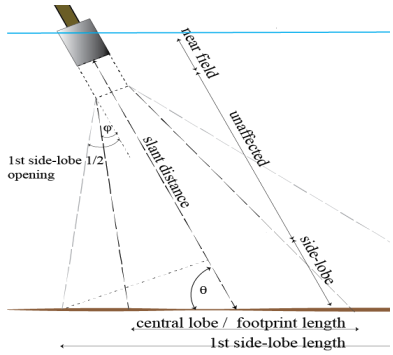

Figure 1. UVP Geometry of the inclined probe

The particle Reynolds number (R_{ep}) is 12.17, and the non-dimensional critical shear stress or the critical Shields number ($\tau*_{cr}$) is 0.045. The dimensionless shear stress ($\tau*$) for the two conditions (0.055 and 0.118) indicated that no sediment suspension would occur [10]. The transducers were mounted 36cm above the sediment bed. Three perpendicular on the sediment bed and three tilted for 65 degrees (θ).

Table 1. UVP acoustic parameters

	f	D_t	λ	ω	φ	Near field	$90-\theta$	R	Cell size	PRF
	MHz	m	m	°	°	m	°	m	m	
inclined	3.0	0.007	0.0005	6.62	2.08	6.62	65	0.39	0.005	1000
	1.5	0.020	0.0010	4.64	1.46	4.64	65	0.39	0.005	500
	0.5	0.015	0.0030	18.54	5.82	18.54	65	0.39	0.011	900
vertical	3.0	0.007	0.0005	6.62	2.08	6.62	90	0.35	0.005	1000
	1.5	0.020	0.0010	4.64	1.46	4.64	90	0.35	0.005	500
	0.5	0.015	0.0030	18.54	5.82	18.54	90	0.35	0.011	900

GoPro Hero6 (3840 x 2160 pixels and 60 frames per second) with a planar field of view was installed over the sampling area of the transducers (Fig.1). Five repetitions of each hydraulic condition were performed; in total, ten experiments were conducted.

Sediment bed echo identification

The bottom identification procedure typically is and internal part of the BT tracking mode of all down looking acoustic Doppler current profilers (ADCPs). The procedure usually involves searching of the strongest echo in acoustic profile over the acoustic beam. The ADCP searches through these depth cells to find the center of the echo and uses the center part to compute the Doppler shift. It also searches backward from beyond the bottom echo to find the echo's trailing edge. The scattered signal from the immobile sediment bed is typically the strongest and results with the highest peak in the received echo cloud. In most of the ultrasound studies, the bottom is analytically considered as surface scattering, and it is the first peak coming after the volume reverberation of the water column above [9]. The sediment used in this experiment has a comparable size with 3MHz wavelength (Tab. 1), but it is smaller than the 1.5MHz and 0.5MHz. It means that the scattering from the particles in saltation or the *volume scattering* will be in the geometric scattering regime for the 3MHz (i.e., stronger backscattering strength) and in the Rayleigh regime for the other two frequencies.

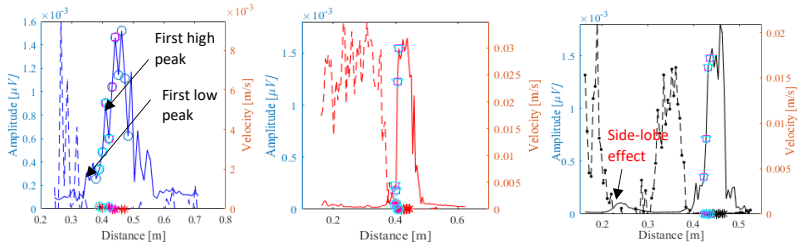

Figure 2. Echo profiles from the inclined transducers (blue-0.5MHz; red-1.5MHz, black-3MHz). The dashed line is the velocity, and it is associated with the right y-axis; the solid lines are the echo amplitudes.

As soon as the signal passes the active layer of the bedload, a *surface scattering* occurs. It is typically stronger (assume specular reflection), and it depends strongly on the grazing angle. Nevertheless, the are several other parameters that influence the shape of the echo and may cause confusion into the identification of the bottom.

The procedure of bottom identification followed several steps: i.) defining of the near field and first side lobe (Tab.1) distances and discarding all the values before these distances; ii.) Identification of the maximum peak; iii.) Identification of the first high peak (Fig1. larger than half the maximum peak); iv.) Identification of the first low peak (larger than the average

water column echo); v.) Extracting the velocity values of the cells that form these peaks. Note that the distance from the sediment bed to the transducers was measured before each measurement. Accordingly, the measured bottom distance was compared with the identified bottom using the UVP data. It should be noted that the internal processing of Ubertone UVPs should give zero values if no Doppler shift is registered in the returned signal. It means that internally filters out some of the erroneous data. The erroneous data produced by the false Doppler shift remained to be filtered out. After extracting the raw velocity data, the velocities with directions opposite of the flow were discarded, in addition to the not valid data registered by the internal processing techniques of Ubertone.

The bottom identification and filtering were implemented in a MatLab script to run the results automatically.

The echo amplitude values that form the first low peak indicate the volume scattering of the active layer, while the first high peak gives the immobile surface scattering. Also, the more intensive hydraulic conditions (Q_2=*120l/s*) showed higher deviations of the results but followed the same pattern. Fig.2 shows that the echo profile of the 0.5MHz frequency contains more spikes and the identification of the bottom is more complicated. This noisy data close to the bottom is associated with the most substantial side-lobe length influence and the size of the transducer. The velocities were measured only in the direction of the flume because the experimental set up allowed considering negligible perpendicular velocities. Apparently, only the inclined probes are to measure the velocities in the flow direction, whereas the perpendicular was used for scattering measurement only.

Camera velocities

The images were preprocessed in order to equalize the light and de-blur the motion effects. After the preprocessing, image-change detection technique was applied to identify the mobile particles. This technique consists of image subtraction of two consecutive frames and kernel filter to smooth the random noise. The identified mobile particles from two consecutive frames are matched using the cross-correlation technique, and the velocities of the displaced particles from one to another frame are identified [11, 5].

Results and discussion

Echo amplitudes comparison

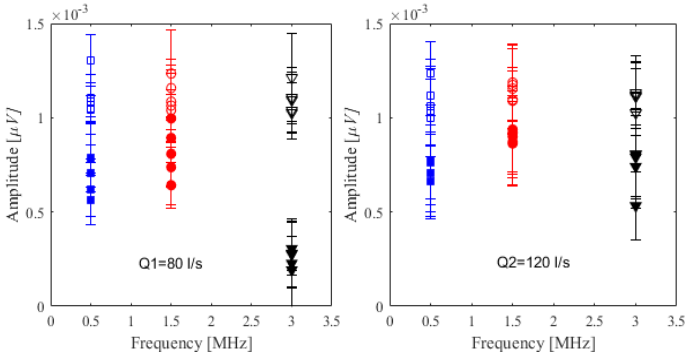

Figure 3. Echo amplitudes variation. The left plot is the weak transport condition (Q_1 = 80 l/s); the right plot is the experiments from the more intensive transport conditions (Q_2 =120 l/s). The solid symbols represent the inclined probes, while the empty symbols are the perpendicular probes.

The average echo amplitudes of each experiment repetition from the vertical and the tilted transducers are plotted in Fig. 3. The amplitudes are the average values of the cells from the low first peak to the high first peak, meaning that they contain the information from the static bottom and the mobile particles of the bedload active layer. The vertical probes (Fig.3 empty symbols) scattered the bottom with almost the same intensity for all the frequencies used in both hydraulic conditions; moreover, it reflects the fact that the bottom surface roughness depends only on the particles. On the other hand, the amplitudes of the inclined probes (Fig.3 filled symbols) increased when passing from 80 to 120 l/s. The difference between the vertical and inclined amplitudes decreased passing from weak to more intensive transport due to an increase of the volume scattering strength in the cells above the immobile bed. The attenuation due to the thicker active layer is relatively small; thus, the echoes from the cells that are fully or partially scattered by the immobile surface did not decrease the total average values given in Fig 3. This amplitude increasing change is more evident for the 3 MHz probe, which falls in the transition scattering regime (i.e., Mie regime); in fact, its wavelength is closer to the mean radius of the used sand particles. It is worth noting that the large size of the acoustic footprint and the side lobes of 0.5 MHz probe contributed to broader distributions of the profiled echoes. In this case, the side lobes at the edge of the acoustic footprint contaminated the received echoes from cells close to the bottom, which made uncertain its detection and the quantification of the corresponding echo amplitude.

UVP Bedload Velocities

The UVP manufactured by Ubertone are pulse-to-pulse coherent Doppler velocity profilers. The velocities were extracted from the cells of the first low peak (i.e., one cell below, the peak cell and one cell above). It should be noted that some of the peak cells also contained velocity data. It is most likely that the cell did not sample the immobile bottom entirely, more precisely the trailing edge did not insonify the immobile bed. The apparent bedload velocities were averaged along with the measured profiles from first low to first high echo peaks to represent the bedload velocity. The data were very noisy, showing a standard deviation more than three times their mean values. Thus, the data was de-spiked using simple local threshold, and temporal averages were calculated from each repetition of the experiments.

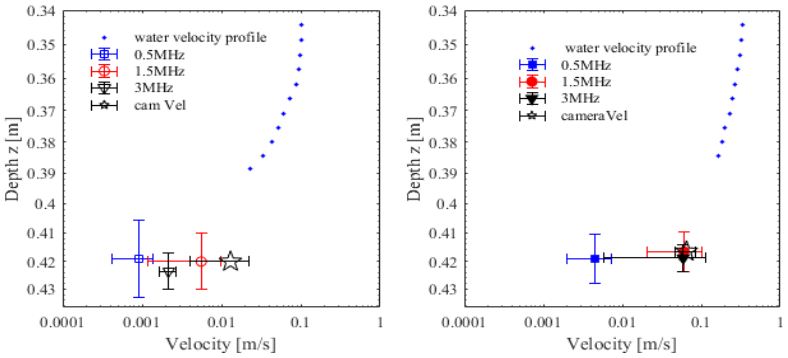

Figure 4. Bedload Velocities. The left plot is the weak transport condition (Q1=80 l/s); the right plot is the experiments from the more intensive transport conditions (Q2=120l/s).

The water velocities taken from the cells in the upper part of the profile were estimated using moving mean averaging. Unfortunately, the few cells above the first low peak gave high deviations; thus, the water velocity profile is not presented for these part if the profile.

Finally, averages and standard deviations among repeated tests represented the expected bedload velocity and the corresponding variation at each hydraulic condition (Fig. 4). The same figure bears out the transition of the water velocities to the bedload velocities. Each transducer had a bit different distance to the bottom, and it varied from one experiment repetition to another that is reflected by the vertical bar. The velocity from 0.5 MHz noticeably underestimates the measured velocities with higher frequencies and the camera during the higher discharge (e.g., blue square, right plot, Fig.4). The 0.5 had double larger cells that made the sampling of the active layer difficult, which was few D50 thick. Besides the longer pulses (i.e., cells) made it easier for the 0.5 to fully sample the immobile bed, adding more information of the rough surface scattering that could be a reason for more erroneous data. The 1.5MHz and 3MHz showed very similarly averaged values but higher

deviations that may be related to turbulence nature of the measuring process. It was expected for the higher frequency UVPs, with the same profiling resolution and the same bed-distance to result in similar Doppler velocity estimations. The results demonstrated that the acoustic sampling of the bottom and selection of the correct cell in the process of identification of the sediment bed play a crucial role in the estimation of the bedload velocity. The higher frequency transducers were able to obtain a finer resolution, closer sampling of the active layer and less influence of the immobile surface; thus, they estimated apparent bedload velocities close to the true particle velocities (i.e., camera velocity)

The underestimation of 0.5 MHz probes can also be ascribed to the side-lobe interference, which deteriorates the received signal from the bottom and in the direction of the Doppler angle. This effect eventually enhanced the received scattering from a direction closer to vertical (i.e., the more intense and closer target at footprint edge) that entailed velocities close to zero, on average. The low discharge experiments gave a higher difference between the camera and the transducers, which appear more similar among them. This is due to the thinner active layer and the prevailing of surface scattering of the immobile bed that entails zero velocity. One should also consider that the very fine particles of sand have velocity very close to the entraining flow (i.e., the slip velocity is minimal).

Conclusions

The Ubertone UVP probes efficiently measured the bedload average velocities. The analyzed echoes have shown a small decrease of the vertical probes amplitudes while increasing the bedload transport conditions but a noticeable increase of the inclined probes amplitudes specifically for the frequency (i.e., 3 MHz) more sensitive to the mobile bed particles transported in the active layer. It suggests the possibility of using the difference among echoes from different grazing angles as an index of particles mobility and active layer thickness. The measured velocities were underestimated especially by the lower frequency (i.e., 0.5 MHz) and for the higher discharge experiment, but the 1.5 and 3.0 MHz probes almost fit the values from the camera. This highlights the importance of profiling acoustic resolution in the acoustic sampling of the sediment bed. The correct methodology that involves the selection of correct pulse length and cell size (profiling resolution) seems to play a crucial role in the estimation of the bedload velocity. Further analysis of lower resolution (0.4 mm per cell) should be performed, and the signal scattered from the active layer should be further elaborated. It would help to develop a standardized methodology for acoustic sampling and profiling of the beam in order to obtain a correct estimation of the apparent bedload velocity.

References

[1] C. Rennie, R. G. Millar and M. A. ,. Church, "Measurement of bedload velocity using an acoustic Doppler current profiler," *Journal of Hydraulic Engineering*, vol. 128(5), p. 473–483, 2002.

[2] D. Gaeuman og R. B. Jacobson, «Acoustic bed velocity and bed load dynamics in a large sand bed river,» *J Geophys Res Earth Surf*, vol. 111(F2), nr. F02005, 2006.

[3] F. G. Latosinski, R. N. zupiany, M. Guerrero, M. L. Amsler og C. Vionnet, «The ADCP's bottom track capability for bedload prediction: Evidence on method reliability from sandy river applications,» *Flow Measurement and Instrumentation*, vol. 54, nr. June 2016, pp. 124-135, 2017.

[4] C. Rennie, D. Vericat, R. Williams, J. Brasington og M. Hicks, «"Calibration of aDcp apparent bedload velocity to bedload transport rate" in Gravel-Bed Rivers,» i *Processes and Disasters*, Tsutsumi, D., and Laronne, J., Wiley., 2017.

[5] S. Conevski, M. Guerrero, N. Ruther og C. Rennie, «ADCP performance of measuring the bedload velocity under changing conditions of particles mobility/bedload transport conditions,» *in submition*, 2018.

[6] Blanckaert K., H. Heyman J. og R. C.D., «Measurments of bedload sediment transport with an Acoustic Doppler Velocity Profiler(ADVP),» *J. Hydraulic Engineering*, October 2017.

[7] Ubertone, «UB-Lab - The versatile ultrasonic profiler,» Ubertone, 2016. [Internett]. Available: http://www.ubertone.com/products-ub-lab.html.

[8] P. Thorne, C. Vincent, H. P. S. Rehman og N. and Pearson, «Measuring suspended sediment concentrations using acoustic backscatter devices,» *Marine Geology*, pp. 7-16, 1991.

[9] R. J. Urick, Principles of Underwater Sound, McGraw-Hill, 1983.

[10] G. Parker, ID SEDIMENT TRANSPORT MORPHODYNAMICS with applications to RIVERS AND TURBIDITY CURRENTS, St. Anthony Falls Laboratory, Mississippi River at 3rd Avenue SE, 2004.

[11] A. Radice, S. Malavasi og F. Bailio, «Solid transport measurements through image processing,» vol. 41, nr. 5, pp. 721-734, 2006.

Appendix

Statements from co-authors

Massimo Guerrero, Nils Ruther, Marie Burckbuchler, Colin D. Rennie, Axel Winterscheid

NTNU

Encl. to application for assessment of PhD thesis

STATEMENT FROM CO-AUTHOR

(cf. section 10.1 in the PhD regulations)

Slaven Conevski applies to have the following thesis assessed:

Bedload monitoring by means of hydro - acoustic techniques

*) The statement is to describe the work process and the sharing of work and approve that the article may be used in the thesis.

*)
Statement from co-author on article: *Laboratory investigation of the apparent bedload velocity measured by ADCPs under different transport conditions; (JHE, 2019)*



Bologna, 04/10/2019
Place, date

Signature co-author

*)
Statement from co-author on article: *Acoustic sampling effects on bedload quantification using acoustic Doppler current profilers; (JHR, under review)*



Bologna, 04/10/2019
Place, date

Signature co-author

*)
Statement from co-author on article: *Laboratory monitoring of bedload transport rates using hydro-acoustic techniques (ADCP); (IAHR, World Congress 2019)*



Bologna, 04/10/2019. Signature co-author
Place, date

*)
Statement from co-author on article: *Evaluation of an acoustic Doppler technique for bed-load transport measurements in sand-bed Rivers;(RiverFlow, Lyon, 2018)*



Bologna, 04/10/2019 Signature co-author
Place, date

*)
Statement from co-author on article: *Towards evaluation of bedload transport characteristics by using velocity and backscatter outputs from ADCPs; (JHR, under review)*



Bologna, 04/10/2019 Signature co-author
Place, date

*)
Statement from co-author on article: *Bedload measurements using ultrasound Velocity profilers (UVP) in controlled laboratory conditions; (Particles in Europe, Lisbon, 2018)*



Bologna, 04/10/2019
Place, date

Signature co-author

NTNU

Encl. to application for assessment of PhD thesis

STATEMENT FROM CO-AUTHOR

(cf. section 10.1 in the PhD regulations)

Slaven Conevski applies to have the following thesis assessed:

Bedload monitoring by means of hydro - acoustic techniques

*) The statement is to describe the work process and the sharing of work and approve that the article may be used in the thesis.

*)
Statement from co-author on article: *Laboratory investigation of the apparent bedload velocity measured by ADCPs under different transport conditions; (JHE, 2019)*

Trondheim, 09.10.2019…….. …..……
Place, date Signature co-author

*)
Statement from co-author on article: *Acoustic sampling effects on bedload quantification using acoustic Doppler current profilers; (JHR, under review)*

Trondheim,09.10.19 …..……
. Place, date Signature co-author

*)
Statement from co-author on article: *Laboratory monitoring of bedload transport rates using hydro-acoustic techniques (ADCP); (IAHR, World Congress 2019)*

Trondheim,09.10.19..
Place, date

…..……
Signature co-author

*)
Statement from co-author on article: *Evaluation of an acoustic Doppler technique for bed-load transport measurements in sand-bed Rivers;(RiverFlow, Lyon, 2018)*

Trondheim,09.10.19
Place, date

……
Signature co-author

*)
Statement from co-author on article: *Towards evaluation of bedload transport characteristics by using velocity and backscatter outputs from ADCPs; (JHR, under review)*

Trondheim,09.10.19
Place, date

…..……
Signature co-author

NTNU

Encl. to application for assessment of PhD thesis

STATEMENT FROM CO-AUTHOR

(cf. section 10.1 in the PhD regulations)

Slaven Conevski applies to have the following thesis assessed:

Bedload monitoring by means of hydro - acoustic techniques

*) The statement is to describe the work process and the sharing of work and approve that the article may be used in the thesis.

*)
Statement from co-author on article: *Bedload measurements using ultrasound Velocity profilers (UVP) in controlled laboratory conditions; (Particles in Europe, Lisbon, 2018)*



Schiltigheim, 01/10/2019
Place, date

Signature co-author

NTNU

Encl. to application for assessment of PhD thesis

STATEMENT FROM CO-AUTHOR

(cf. section 10.1 in the PhD regulations)

Slaven Conevski applies to have the following thesis assessed:

Bedload monitoring by means of hydro - acoustic techniques

*) The statement is to describe the work process and the sharing of work and approve that the article may be used in the thesis.

*)
Statement from co-author on article: *Laboratory investigation of the apparent bedload velocity measured by ADCPs under different transport conditions; (JHE, 2019)*

Ottawa, Canada
Place, date Sep 30 2019

Signature co-author

*)
Statement from co-author on article: *Acoustic sampling effects on bedload quantification using acoustic Doppler current profilers; (JHR, under review)*

Ottawa, Canada
Place, date Sep 30 2019

Signature co-author

*)
Statement from co-author on article: *Laboratory monitoring of bedload transport rates using hydro-acoustic techniques (ADCP); (IAHR, World Congress 2019)*

Ottawa, Canada
Place, date Sep 30 2019

Signature co-author

*)
Statement from co-author on article: *Evaluation of an acoustic Doppler technique for bed-load transport measurements in sand-bed Rivers;(RiverFlow, Lyon, 2018)*

Ottawa, Canada
Place, date Sep 30 2019

Signature co-author

*)
Statement from co-author on article: *Towards evaluation of bedload transport characteristics by using velocity and backscatter outputs from ADCPs; (JHR, under review)*

Ottawa, Canada
Place, date Sep 30 2019

Signature co-author

NTNU

Encl. to application for assessment of PhD thesis

STATEMENT FROM CO-AUTHOR

(cf. section 10.1 in the PhD regulations)

Slaven Conevski applies to have the following thesis assessed:

Bedload monitoring by means of hydro - acoustic techniques

*) The statement is to describe the work process and the sharing of work and approve that the article may be used in the thesis.

*)
Statement from co-author on article: *Acoustic sampling effects on bedload quantification using acoustic Doppler current profilers; (JHR, under review)*

AXEL WINTERSCHEID

KOBLENZ, 2.10.19 ……

Place, date

……

Signature co-author

*)
Statement from co-author on article: *Evaluation of an acoustic Doppler technique for bed-load transport measurements in sand-bed Rivers;(RiverFlow, Lyon, 2018)*

AXEL WINTERSCHEID

KOBLENZ, 2.10.19 ……

Place, date

……

Signature co-author